Targeting mitochondria by mitochondrial fusion, mitochondria-specific peptides and nanotechnology

Dissertation zur Erlangung des Doktorgrades der Naturwissenschaften

(Dr. rer. nat.)

der Fakultät Chemie und Pharmazie

der Universität Regensburg

vorgelegt von

Anne Sabine Heller

aus Markersbach/Erzgebirge

Januar 2013

Anne Sabine Heller

Targeting mitochondria by mitochondrial fusion, mitochondria-specific peptides and nanotechnology

Targeting mitochondria by mitochondrial fusion, mitochondria-specific peptides and nanotechnology

Dissertation zur Erlangung des Doktorgrades der Naturwissenschaften

(Dr. rer. nat.)

der Fakultät Chemie und Pharmazie

der Universität Regensburg

vorgelegt von

Anne Sabine Heller

aus Markersbach/Erzgebirge

Januar 2013

Diese Doktorarbeit entstand in der Zeit von Januar 2008 bis März 2012 am Lehrstuhl für Pharmazeutische Technologie der Universität Regensburg.

Die Arbeit wurde angeleitet von: Prof. Dr. Achim Göpferich.

Promotionsgesuch eingereicht am:	21.01.2013
Datum der mündlichen Prüfung:	08.03.2013
Prüfungsausschuss:	Prof. Dr. S. Elz (Vorsitzender)
	Prof. Dr. A. Göpferich (Erstgutachter)
	Prof. Dr. G. Brockhoff (Zweitgutachter)
	Prof. Dr. J. Schlossmann (Drittprüfer)

Für meine Familie

in Liebe und Dankbarkeit

Ein fester Wille tut überall Wunder.

Joseph von Eichendorff

Table of Contents

Targeting mitochondria by mitochondrial fusion, mitochondria-specific peptides and nanotechnology

Chapter 1

Introduction

1.1

Targeting drugs to mitochondria

European Journal of Pharmaceutics and Biopharmaceutics 82 (2012) 1-18

Abstract

Mitochondria are of increasing interest in pharmaceutical and medical research since it has been reported that dysfunction of these organelles contributes to several diseases with a great diversity of clinical appearance. By the fact that mitochondria are located inside the cell and, in turn, origins of mitochondrial diseases or targets of drugs are located inside mitochondria, a drug molecule has to cross several barriers. This is a severe drawback for the selective accumulation of drug molecules in mitochondria. Therefore, targeting strategies such as direct drug modification or encapsulation into nanocarriers have to be applied to achieve an accumulation of drug molecules in these organelles. In this review, it will be demonstrated how properties and dysfunctions of mitochondria are generating a need for the development of mitochondria specific therapies. Furthermore, intracellular targets of mitochondrial diseases, strategies to utilize mitochondrial specificities and targeting approaches will be discussed. Finally, techniques to investigate mitochondrial characteristics and functionality are reviewed.

Graphical abstract

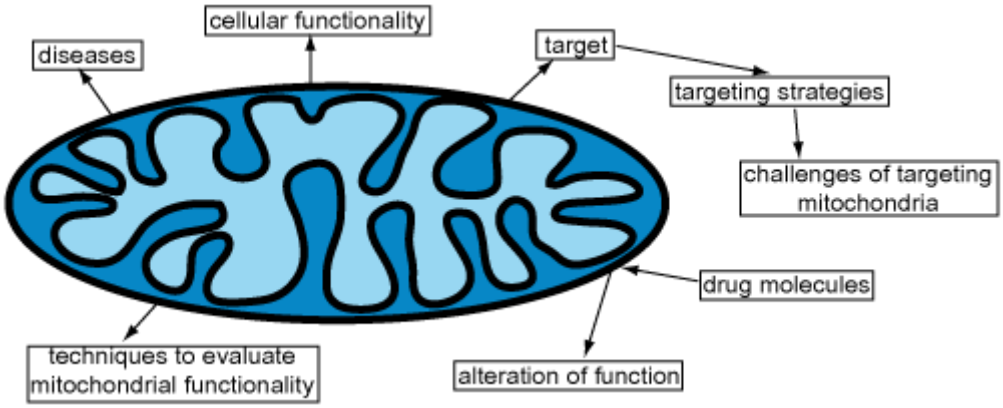

Mitochondria are important for cellular functionality but they are also involved in diseases. Therefore, they are of increasing interest in targeted drug therapy.

Key words

intracellular targeting; mitochondria; drug delivery; targeting strategies; nanocarriers; mitochondrial diseases

Introduction

Mitochondria are intriguing cellular organelles that exhibit numerous structural and functional specificities. They are highly mobile and so are able to distribute the energy that they produce throughout the cell [1]. The production of energy is essential for the maintenance of the functionality of all important cellular processes [2]. In contrast to that, dysfunctions of mitochondria cause disorders. These mitochondrial dysfunctions are mainly related to degenerative diseases affecting tissues that are highly energy dependent on the one hand [3] or malignant diseases on the other hand [4].

It is challenging to treat the cause of a disorder if it is located inside mitochondria, including changes of mitochondrial DNA, mitochondrial proteins or metabolic pathways. Although several substances are known to act on mitochondria [5–7], it is necessary to utilize and develop specific strategies to target them selectively to mitochondria, as this is their site of action.

In general, the physicochemical properties of a drug substance may not be appropriate to overcome biochemical, anatomical or immunological barriers to reach its target [8]. If the target of a substance is located inside of an intracellular compartment such as a mitochondrion, the drug molecule has to penetrate several membranes to find its final destination. The molecule would require very specific physicochemical properties to cross the different barriers. Changing the physicochemical properties of drug molecules is one approach toward overcoming these limitations. D'Souza et al. commented in their review about mitochondria-targeted processes to cancer therapy [9]. They distinguish two processes of targeting in drug therapy: On the one hand the selective interaction between the drug molecule and its target and on the other hand the accumulation of a drug due to its physicochemical properties. Thereby, it can well be that a drug could exert a potent therapeutic effect upon binding to its molecular target but does not exhibit the necessary physicochemical properties to find its way to it. With the help of delivery strategies and delivery technology, such drugs could be better distributed to their site of action [9]. It is thus

possible that the application of targeting strategies could provide us with new applications for the use of well-established drugs.

Over the years, the fields of prodrugs and drug carriers as strategies toward site specific drug delivery have also evolved. There is a number of examples that drugs can be changed to prodrugs with superior physicochemical properties which allow for better site specific delivery. These molecules are then transformed into the active entity at their site of action [10,11]. However, modifications of low molecular weight drug substances to achieve a higher accumulation at their targeted site may also lead to a loss of activity [12].

The idea to synthesize drug carriers that transport the drug molecule to the desired target site evolved more than over 30 years ago. Targeting of a drug substance means to trade the physicochemical properties of drug molecules against that of a carrier to obtain other physicochemical properties that allow for the specific accumulation at the target site. Ringsdorf developed a model for a carrier system that comprises several features. It is based on a polymer that contains different units to influence solubility, to bind a pharmacologically active drug and a transport system that delivers this macromolecule specifically to its site of action by recognizing specific features at the target site (Figure 1.1) [12].

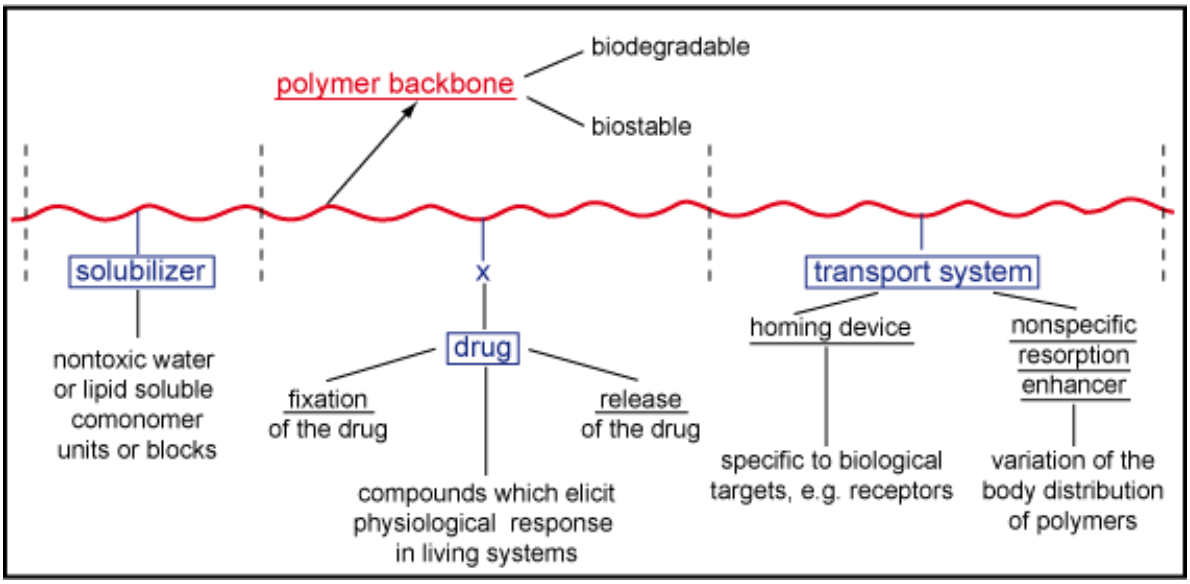

Figure 1.1: Concept of a model drug carrier system according to Ringsdorf [12].

The use of polymers as drug carriers was one of the first approaches toward targeted drug delivery. Over the years, several other drug carriers such as liposomes [13,14], nanoparticles [15,16], and modified polymers such as dendrimers [15,16], polymeric micelles [15–17] or polyplexes [18] followed. Also today, an increasing number of multifunctional nanocarriers that unite targeting, sensing, signaling and drug release properties are emerging [8]. However, the traditional blue print of these carriers suffers from a number of disadvantages. Considering that several barriers may need to be crossed to reach the final site, it may not be sufficient that a carrier system contains only one transport and recognition unit according to the genuine approach by Ringsdorf [12]. Such carrier systems may require several molecular transport and recognition motifs that need to become active, depending on the barrier to be crossed. The more barriers to be overcome, the more transport and recognition moieties would be required, acting one after the other depending on the next type of barrier to be crossed. It is obvious that such a carrier system has a high level of complexity and is, therefore, not easy to develop at all. It also has to be considered that drug carrier systems will undergo the same transformation reactions in the body as low molecular weight substances and that these reactions could change the physicochemical properties and hence the targeting properties of the nanocarriers [8]. If the first targeting moiety is inactivated, for example due to protein adsorption in the blood [8], all subsequent transport and recognition systems will fail, and the drug molecule will not be delivered to its targeted site of action.

In summary, strategies toward targeting are on the one hand highly promising since adverse physicochemical drug properties can be compensated but are on the other hand not simple to realize. This is also true for targeting drugs to mitochondria. Therefore, targeting strategies in drug delivery that have evolved over the years will be reviewed in the following chapter.

General targeting strategies in medical and pharmaceutical research

Advantages of drug targeting

Targeted drug delivery systems may facilitate a better therapeutic outcome as they are supposed to overcome limitations of conventional drug application such as unfavorable biodistribution, low bioavailability, lack of water solubility, low therapeutic response despite high dosages, side effects, drug resistance, toxicity and barriers in the body such as the blood brain barrier [19,20]. Various targeting approaches for the therapy of cancer [21], neurodegenerative diseases e.g. Alzheimer's disease [22], infectious diseases e.g. tuberculosis [23], autoimmune diseases [24] and several other disorders were reported.

Thereby, numerous definitions of "targeting" exist in several areas of research. An overview will show how versatile the use of the term targeting is.

Active and passive targeting

At first, active and passive targeting can be distinguished. Active targeting is defined as the specific recognition of a molecular structure by a target. Passive targeting describes the recognition of a molecule by the reticuloendothelial system (RES or mononuclear phagocyte system) [25] or makes use of the enhanced permeability and retention effect (EPR-effect) in tumor tissue [26]. Passive targeting is achieved when a drug carrier is administered systemically into the blood circulation and gets trapped inside the body on the tissue level mainly based on its size. In fact, it is not feasible to reach targets inside cells like mitochondria by passive targeting [27]. Hence, active targeting strategies such as the recognition by receptors on the surface of the cell [28] and subsequently the targeting of specific structures inside the cell or on intracellular organelles are required to deliver a molecule to its site of action. Active strategies to accomplish an uptake into the cell are mainly studied in cell culture [29–31]. The question remains whether these systems can achieve the same outcome when they are administered in vivo.

As only active targeting is a reasonable strategy to reach mitochondria, passive targeting will not be considered in more detail, but rather the uptake into the cell as well as approaches to intracellular delivery.

Therapy and diagnostics

Beside the therapeutic approach, targeting is also used in diagnostics [32]. Some approaches combine targeted drug therapy and diagnostics, termed *theragnostics* or *theranostics* [33]. Thereby, a diagnostic test that is linked to the application of a specific targeted therapy is supposed to identify responding and non-responding patients [33].

Chemical modification of drugs and encapsulation into nanocarriers

In approaches toward targeting, the chemical modification of a drug or the encapsulation into a drug carrier can be distinguished and will be described in more detail below.

The term “targeting” is used to describe a molecule to which ligands are covalently bound. These ligands such as antibodies [34] or peptides [35] are known to actively bind to a desired target site. Besides this, pure specific antibodies without modification, for which an antigen exhibits a target, are considered targeted therapeutics [36]. It has to be considered that chemical modifications affect the physicochemical properties of the drugs and may also change their pharmacokinetic and pharmacodynamic behavior.

Alternatively, the term “targeting” is used in the context of nanocarriers including liposomes [13], micelles, nanoparticles or dendrimers for the delivery of drug molecules or nucleic acids [15,16]. Liposomes are capable of hosting water soluble drugs in their core or lipophilic drugs in their membrane layers. Micelles are mainly used for the delivery of poorly soluble drugs [14]. An advantage of carriers over chemically modified drugs is that molecules can be encapsulated without changing their molecular structure. Thus, only alterations in pharmacokinetics but not in pharmacodynamics of the respective drug are to be expected. Such nano-sized delivery systems are used to transport low molecular weight substances, peptides, proteins, DNA or siRNA [37–40]. They can be additionally functionalized with

antibodies or receptor specific ligands that recognize a target. Nanocarriers and low molecular weight substances can also be modified by polymers such as polyethylene glycol which is widely used to prolong the blood circulation time. Pharmaceutical nanocarriers are used to increase the stability of the administered drug, to protect it from degradation or inactivation, to improve efficacy and to decrease undesired side effects [8,14]. Another advantage is that they allow for the sustained release of drugs which can improve therapy and compliance. In case of applying a drug without a drug carrier, active control of tissue distribution, uptake into cells and intracellular trafficking may not be sufficient to exhibit a therapeutic activity [41].

"Targeting" specified

To specify a scientific or therapeutic approach, targeting is very often defined more precisely by adding a second term which describes a disease (e.g. cancer), an organ or tissue (e.g. brain) or a structure on the molecular or cellular level (e.g. proteins, genes, receptors and organelles). The latter also involves intracellular targeting which the following will focus on. Nature offers a prominent example for this, a virus which is taken up by selected cells via endocytosis. They release their genome into the cytosol and are able to target their DNA to the nucleus as an organelle. This is an excellent example of intracellular targeting.

Intracellular targeting – interpretations of the term, motivation and challenges

Most approaches of intracellular delivery focus on crossing the cellular membrane without defining a specific intracellular target or controlling the distribution of the drug inside the cell [17,42,43]. In many cases, delivery into the cytosol is hoped to be sufficient, and it is assumed that the drug molecule will find its final subcellular target by simple diffusion and interaction with various structures of the cell. While this may be appropriate for siRNA therapy, an increasing body of evidence has emerged indicating that these simple mechanisms are not sufficient for the majority of targeted drug delivery approaches [17]. It is possible that the dysfunction of a molecular structure which is located inside of an organelle

contributes to a disease and therefore exhibits a target. It is also known that many drugs act on a subcellular localization. Considering this, it is desirable not only to target specific organs or cells but also to efficiently deliver drugs to inner cell compartments and to define this intracellular target specifically. An example is paclitaxel, which directly acts on mitochondria, triggering apoptosis. Mitochondria play a key role in this process [44] but the capacity to induce apoptosis is frequently deficient in cancer cells [45]. Hence, mitochondria exhibit a target for disease and drug action. Other intracellular compartments that can be focused on include mRNA in the cytosol, transgene induction in the nucleus, stimulation or inhibition of apoptosis in mitochondria and in the cytosol, modulation of protein synthesis in the endoplasmic reticulum and Golgi apparatus, certain types of enzyme replacement therapies in endosomes and lysosomes for the therapy of lysosomal storage diseases [46].

Nevertheless, targeting of organelles is extremely challenging as barriers for instance the cell membrane and membrane(s) of organelles have to be penetrated, if the target is located in intracellular compartments. In addition, it is essential to locate intracellular disease related targets, to determine drugs which can act on these targets and to develop suitable methods for the detection of subcellular accumulation.

It is also conceivable to exploit advantages of nanocarriers for intracellular targeting. Such drug delivery systems can be conjugated with organelle specific targeting moieties to deliver an encapsulated drug to a desired subcellular compartment. Targeting moieties for this purpose included peptide sequences that can be recognized by the endoplasmatic reticulum, the nucleus or mitochondria as well as non-peptide molecules that interact with membranes of organelles, in particular mitochondria [47,48]. Considering the challenges that affect intracellular targeting, a major limiting step of nanocarries for intracellular delivery is to escape from endosomes after endocystosis. A drug delivery system decorated with targeting moieties will not be able to target a drug to an organelle of interest if it resides inside an endosome and is not released into the cytosol. Only a small fraction of endosomes degrade spontaneously while the majority of endocytosed material is degraded and not able to reach the cytosol and subsequently the target organelle. Hence, even the delivery into the cytosol

comprises not only the step of cell membrane transfer. Another limitation of intracellular targeting that affects targeting efficiency, is dependent on processes such as the mobility of the system in the cytosol because of the high concentrations of dissolved macromolecules which limit diffusion, the rate of degradation in the cytosol and the rate of uptake into the targeted organelle [17,48]. Therefore, targeting of organelles with nanocarriers is a multi-step process, exhibiting numerous barriers that have to be crossed. Despite all these obstacles, it should become a major goal to develop drug delivery systems which reach subcellular targets specifically to make therapy more efficient and to minimize non-specific side effects.

Targeting drugs to mitochondria – motivation and definitions

Mitochondrial dysfunctions contribute to several diseases that will be considered later in this review, and reaching mitochondrial targets is challenging due to several specifics that will also be reflected in subsequent sections. This review will focus on mitochondria as intracellular targets and specific, active targeting strategies toward mitochondria. Thereby, the term “targeting” will be used to describe the specific, active delivery of drug molecules or drug carriers to the intracellular mitochondrial targets, accomplished by low molecular weight molecules, peptides or nanocarriers with a specific “affinity” to mitochondria. The term “target” will be used as synonym for the specific site of action of drug molecules, mitochondrial metabolic processes and mitochondria, respectively. “Intracellular targeting” will be used in order to describe strategies that overcome intracellular barriers such as mitochondrial membranes to reach a target inside mitochondria.

Mitochondria: functions and properties of a potential target

Before considering mitochondria in relation to diseases, drug therapy and drug targeting, important mitochondrial characteristics and functions are outlined in the following section to provide pertinent insights into this fascinating organelle.

Mitochondrial morphology

Mitochondria exhibit some unique ultrastructural features (Figure 1.2) that differ from other organelles as they are enclosed by a double membrane with an unusual lipid composition [49]. The inner membrane is folded into cristae in order to increase the surface area [50], they have a high membrane potential of 180–200 mV [14,51] and contain their own genome that offers specific characteristics compared to the nuclear genome [50]. The facts, that mitochondria are self-replicating organelles, that they have a lipid composition which is similar to those found in prokaryotes, and that they contain their own DNA and protein synthesis machinery, led to the endosymbiotic hypothesis in the evolution of mitochondria. According to this theory, prokaryotes have been taken up by eukaryotes to form a symbiotic association. Even though this theory is well recognized, and mitochondria and prokaryotes actually share many common features, it is still controversially discussed whether or not mitochondria are indeed originally derived from endosymbiotic prokaryotes [52–54].

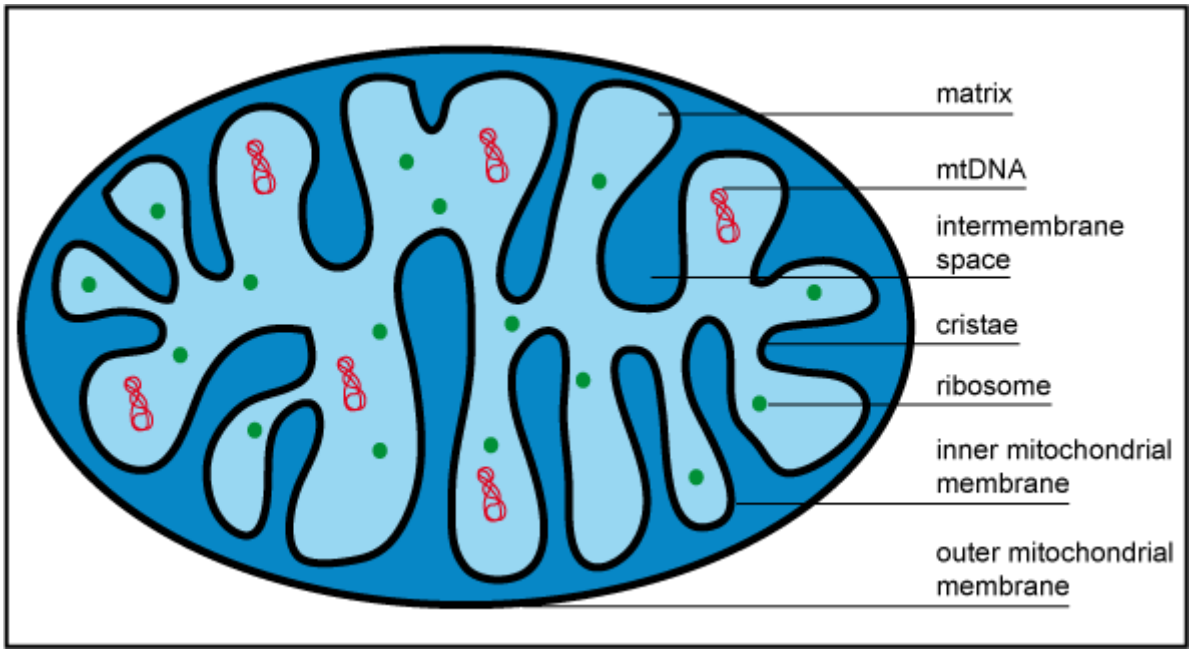

Figure 1.2: Ultrastructure of mitochondria; mitochondrial DNA (mtDNA).

Mitochondria reside in all eukaryotic cells, but the abundance per individual cell depends on the specific energy requirements of the cell and varies dependent on cell type, cell-cycle stage, proliferative state and dysfunction in diseases [55]. Metabolically active organs such

as liver, brain, cardiac and skeletal muscle tissues contain up to several thousands of mitochondria per cell while somatic tissues with low energy demands contain only a few dozen mitochondria [56]. Human oocytes contain up to 100,000 mitochondria while spermatozoa have a constant number of 16 mitochondria which are located in the tail that is cleaved and degraded after fertilization [56]. This phenomenon causes maternal inheritance of these organelles [57]. Mitochondria cannot be formed de novo. During the processes of growth and division of preexisting mitochondria, newly synthesized components such as lipids and proteins have to be introduced into preformed structures [58].

The traditional view on mitochondria as round shaped organelles that produce and supply energy (ATP) has changed [59] since it appeared that they form a network via dynamic processes like fusion and fission, and active transport along microtubules and actin filaments mediated by myosin, dyneins and kinesins to subcellular localization [1,60]. Mitochondrial transport is required to distribute mitochondria throughout the cell. While they move along the cytoskeleton, they can encounter each other and undergo fusion (Figure 1.3), mediated by GTP-dependent fusion proteins in the mitochondrial membranes [61], resulting in the exchange of mitochondrial content. Therefore, mitochondria should not be considered autonomous and static organelles. Shape, length, size and number of mitochondria in a cell are highly variable and can range from small, individual spheres, short rods to long tubules and complex, interconnected, network like structures [50]. Fusion is a protective mechanism that allows mitochondria to tolerate high levels of pathogenic mitochondrial DNA (mtDNA) and is necessary to maintain mtDNA stability and mitochondrial function [62].

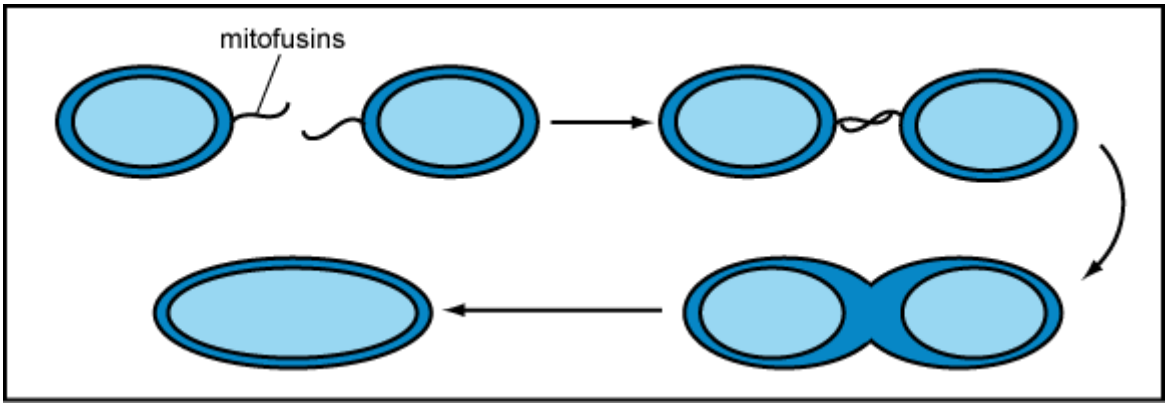

Figure 1.3: Mitochondrial fusion mediated by mitochondrial fusion proteins.

Mitochondrial functionality

Besides the morphological diversity, mitochondria play an essential role in maintaining cellular homeostasis. They exhibit various important functions and metabolic pathways (Figure 1.4) including calcium homeostasis and signaling, thermogenesis, gluconeogenesis, the citric acid cycle, the β-oxidation of fatty acids, the synthesis of heme, amino acids, steroid hormones and Fe-S-clusters, the urea cycle, and the electron transport chain and oxidative phosphorylation (OXPHOS) that end in the production of ATP [2].

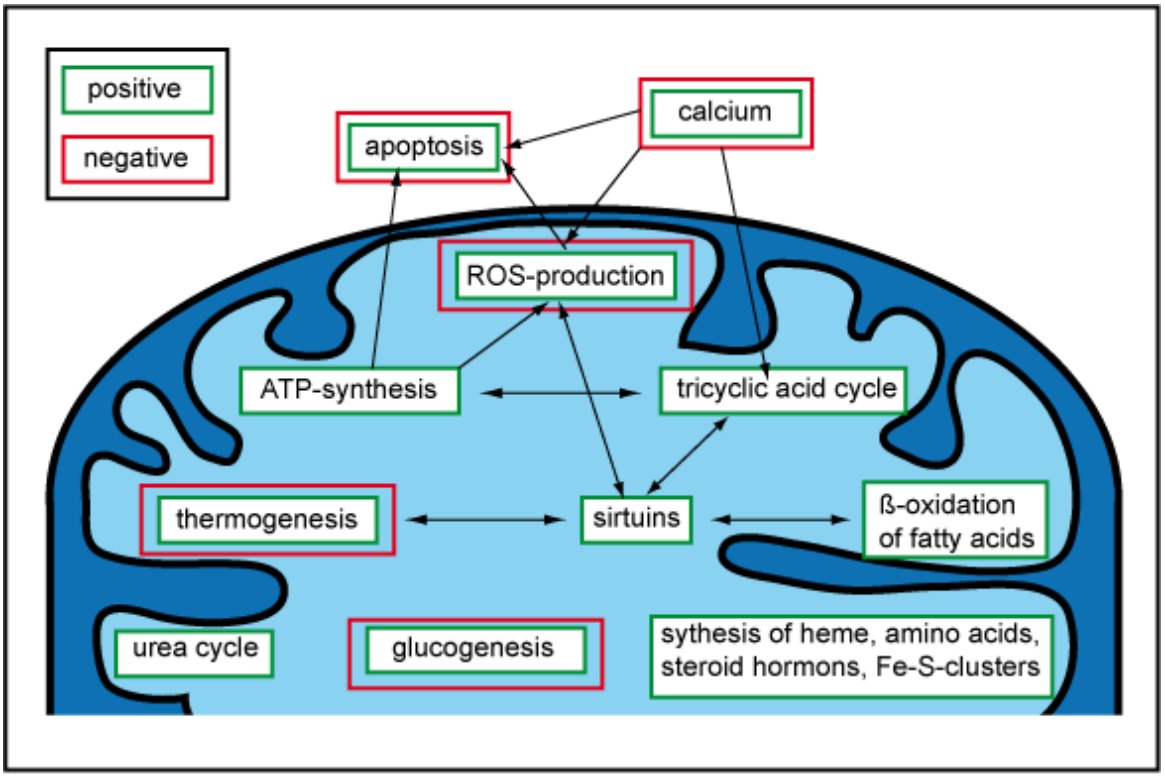

Figure 1.4: Mitochondrial functions and metabolic pathways.

ATP-synthesis is important for all cellular processes but also generates reactive oxygen species (ROS) as byproducts. Early publications suggest that about 2–5 % of oxygen is metabolized into the highly reactive superoxide anion and other radicals [2] whereas more recent studies provide evidence that mitochondria produce one or two orders lower amounts of ROS under normal physiological conditions [63]. Besides this, it is known that an increased calcium influx in mitochondria can lead to the production of reactive oxygen species [64]. ROS play a significant role in the regulation of cell-signaling processes, in

cytoprotection and thus are needed for the survival of the cell [2]. But they are also related to pathological processes when produced in excess. There are mitochondrial and cytosolic enzymes that scavenge ROS [59] as well as non-enzymatic antioxidants, such as glutathione (GSH), vitamin E, vitamin C and ubiquinone to limit the cytotoxicity of reactive oxygen species [63]. But when these cellular antioxidants are depleted, lipid peroxidation, mtDNA damage, OXPHOS dysfunction and damage of Fe-S-containing enzymes occur. The critical limit for the positive and necessary effects of ROS is yet not known, and excessive oxidative stress to nuclear or mitochondrial DNA can cause cellular and mitochondrial dysfunction, mutagenesis and carcinogenesis [2]. These negative and potentially damaging effects of ROS were originally described in the “free radical theory” over 50 years ago. This theory suggested that aging and neurodegenerative diseases could be attributed to the effects of free radicals [65]. Besides the implication in neurodegenerative diseases, it is nowadays discussed that oxidative stress is also related to atherosclerosis, pulmonary fibrosis and cancer [66]. The causes and effects of ROS and ROS related diseases are summarized in Figure 1.5.

Even though mitochondria contain their own genome, the vast majority of mitochondrial proteins are encoded by the nuclear DNA (nDNA). They are synthesized in the cytosol and imported into mitochondria via translocase protein import complexes, the translocase of the outer mitochondrial membrane (TOM-complex) and the translocase of the inner mitochondrial membrane (TIM-complex). These protein import pores recognize specific, positively charged amino-terminal or internal mitochondrial targeting sequences that are also often termed MLS (mitochondrial localization or leading sequence). MLS are short peptide sequences attached to the protein and cleaved after translocation into the mitochondrial matrix or mitochondrial membranes [67]. Mitochondrial DNA itself encodes only 13 of the more than 1000 mitochondrial proteins. All of them are proteins of the respiratory chain [67–69].

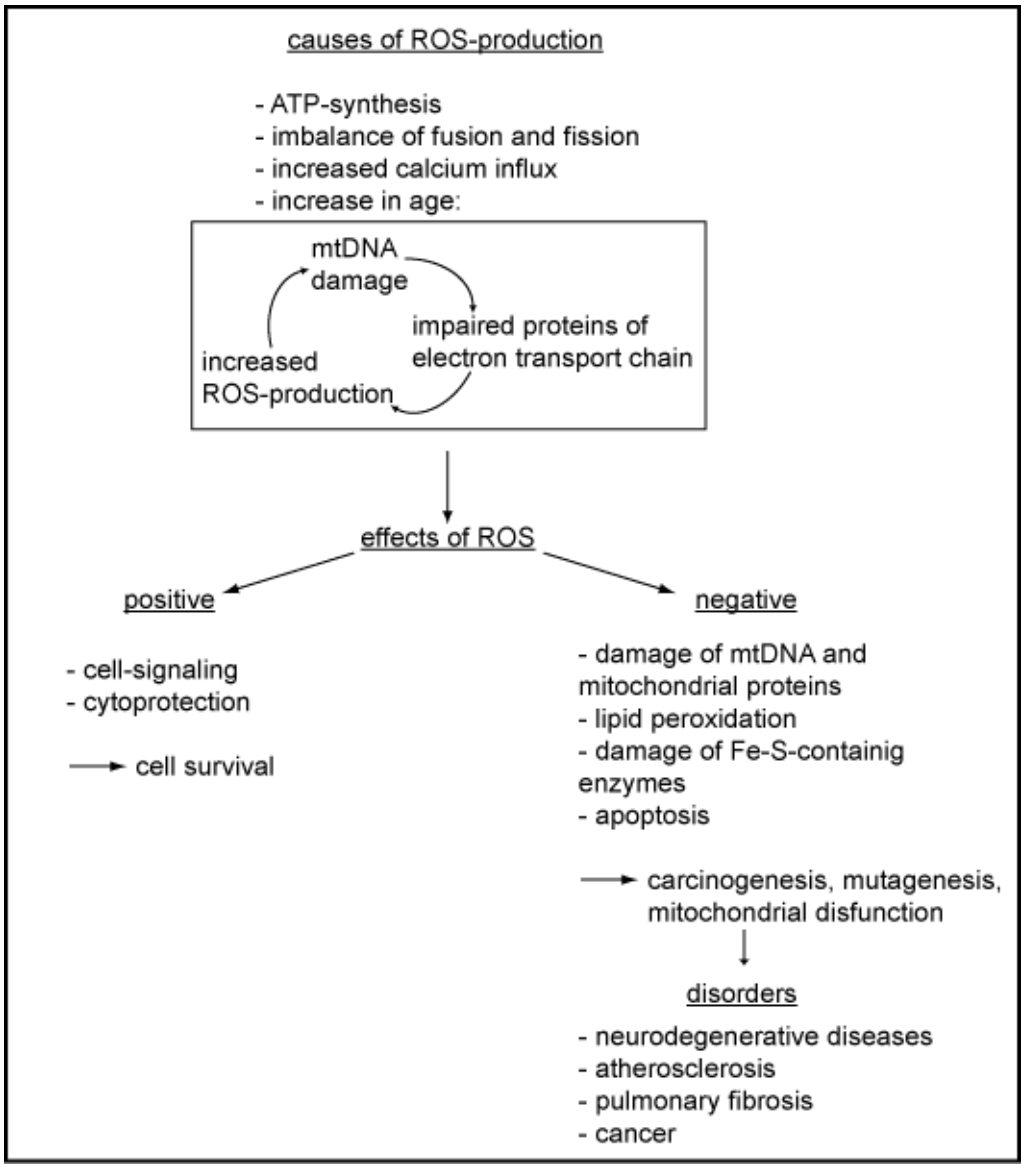

Figure 1.5: Causes and effects of reactive oxygen species (ROS) and ROS related disorders; mitochondrial DNA (mtDNA).

There are some differences between mitochondrial and nuclear DNA. The mitochondrial genetic code differs in four codons from the universal code [70]. Compared to the nuclear genome, mitochondrial DNA lacks histone protection, has no introns and only a weak repair capacity. This in combination with the fact that ROS are generated in mitochondria makes mitochondrial DNA prone to mutations [71]. The fusion and fission machinery allows for the exchange of mutated and wild-type mitochondrial DNA. Mitochondrial DNA copies are organized in protein-associated nucleoids that are motile and can interact with each other. Thereby, recombination of mtDNA has been documented [50]. The exchange of mutated and

wild-type mtDNA as well as recombination prevents the crossing of a critical threshold before a cell expresses a mitochondrial defect. Cells are able to tolerate 70–90 % mutated mtDNA, the so-called “threshold-effect”. The precise value varies from mutation to mutation and from tissue to tissue [3]. But if mutations exceed the critical limit, defects appear even phenotypically [72].

In summary, mitochondrial genetics differ from Mendelian genetics comprising of maternal inheritance, heteroplasmy, the threshold effect and mitotic segregation. Mitochondrial DNA is only inherited maternally because sperm mtDNA is degraded after fertilization. Molecules of mtDNA exist in hundreds or thousands of copies in each cell (polyploid), whereas nuclear genes consist of only one maternal and one paternal allele (diploid). Mutations of mtDNA often do not affect all molecules, and thus, cells may harbor wild-type and mutant mtDNA, an effect called heteroplasmy. A critical number of mutant mtDNA copies must be present before dysfunctions appear phenotypically, termed threshold-effect. The phenomenon mitotic segregation explains the manifestation of different mitochondrial diseases at different stages of patient’s lives: the proportion of mutant mtDNAs in daughter cells can shift which means if the pathogenic threshold is crossed, the phenotype may also change [57,73].

Mitochondria also play a crucial role in the viability of a cell. Various cases of apoptosis are initiated by mitochondria via formation of the mitochondrial permeability transition pore complex (mPTPC) in response to energy deficiency, oxidative stress, increased calcium and other stimuli [2,63]. Apoptosis depends on the release of apoptotic proteins from mitochondria, the disruption of ATP-synthesis and the modification of the cellular redox potential [59]. It is also known that mitochondrial fission plays an important role in apoptosis and can be the onset of the programmed cell death [61]. The mechanisms of all processes that result in apoptosis are not completely understood yet [59].

Last but not least, a particular mitochondrial protein species, so-called sirtuins show intriguing activities. Sirtuins or silent information regulator (Sir) proteins act as key metabolic sensors that directly link environmental signals, such as calorie restriction or cellular stress to metabolic homeostasis and stress response [74]. The field of sirtuin research is quite young,

but it emerges that they play a pivotal role in mitochondrial functionality. A total of seven sirtuins in mammalian cells have been identified. They are localized in diverse cellular compartments, three of them can be found in the nucleus, one is located in the cytosol and another three ones are located in mitochondria. Sirtuins possess a NAD^+-dependent enzymatic activity, catalyzing histone deacetylation and ADP-ribosylation reactions, and targeting multiple substrates. Metabolites of these reactions may be important regulators in physiology. Sirtuins are also involved in various cellular functions, such as metabolism, cell cycle, cell survival, thermogenesis and insulin secretion. They are able to extend replicative lifespan through the delay of mitosis in model organisms like flies, worms and yeast. To this date, it is not clear whether the data gathered regarding the life span of these organisms can be transferred to mammalian organisms. Nevertheless, it is also known that sirtuins enable DNA repair, are involved in chromosome fidelity during meiosis and generally have positive and protective effects in the cell [75]. Several studies revealed a direct linkage between nutrition and activity of sirtuins. The activity of sirtuins is upregulated under calorie restriction and fasting conditions. Calorie restriction also has an increasing effect on mitochondrial function, and it induces the endothelial nitric oxide synthase that results in the activation of mitochondrial biogenesis. Moreover, stress treatments such as heat shock or oxidative damage cause increased sirtuin activity [52,75].

The mitochondrial localization of sirtuins is particularly intriguing because mitochondrial dysfunction is related to aging and diseases. An overexpression of mitochondrial sirtuins increases respiration, while it decreases the production of reactive oxygen species. Furthermore, they affect mitochondrial metabolism, comprising of the citric acid cycle and the synthesis of cholesterol and fatty acids. Sirtuins also regulate the amino-acid stimulated insulin secretion in pancreatic cells [75].

Nuclear sirtuins are considered to act as guardians against cellular oxidative stress and DNA damage. Therefore, they also have an impact on mitochondrial functionality. Nuclear sirtuins regulate physiological and metabolic processes, like insulin secretion, lipolysis, gluconeogenesis, DNA repair and growth via promotion of rRNA transcription. They are

linked to neuronal survival, protection against neurodegenerative disorders such as Alzheimer's disease or Parkinson's disease. In case of neuronal protection, they may act as antiapoptotic factors through the down regulation of proapoptotic factors. Nuclear sirtuins also repress transcription of mitochondrial uncoupling proteins. These uncoupling proteins separate mitochondrial respiration from ATP-production and reduce the proton gradient across the mitochondrial membrane. By preventing this process, sirtuins promote a more efficient energy production [75]. Intracellular levels of ATP are a determinant for apoptosis [76].

The functionality of mitochondria determines cell life, cell death and cellular dysfunction [2]. Therefore, all described features of mitochondria should not be considered independently. In fact, they are closely linked, and an alteration in one function can cause a change of another function or may start a viscous cycle. For example, calcium homeostasis is connected to increased ATP-production followed by the activation of calcium sensitive citric acid cycle enzymes, ROS production, opening of the mitochondrial transition pore and loss of membrane potential which causes apoptosis [5,63,77]. Increased ROS-production can also be generated as a byproduct of the electron transport chain and ATP-production as well as by the dysfunction of these processes. Excessive ROS-production causes mtDNA damage, mitochondrial dysfunction and in turn apoptosis. An imbalance in fusion and fission leads to mitochondrial dysfunction, fragmentation, increased production of ROS and ATP, followed by a decreased membrane potential that can be the starting point of apoptosis [63]. Controlled activity of these processes such as the production of reactive oxygen species, calcium uptake, apoptosis and thermogenesis serves as protective mechanisms against infection and other damages to the cell. Overshooting or alterations of these processes and the resulting dysfunctions of mitochondria are related to aging, senescence and disorders [2,77] that will be reflected in more detail as follows.

Mitochondrial dysfunction and related disorders

By convention, mitochondrial diseases include any disorders that are related to defects or absence of proteins that are localized in mitochondria, independent from their gene locus (nuclear or mitochondrial DNA, mitochondrial tRNAs or rRNAs) [73]. A minimum of about 1 in 8500 individuals is affected by such a disorder [78].

Dysfunctions caused by mutations of nuclear or mitochondrial DNA, inherited or not, mainly affect proteins of the respiratory chain and consequently energy production. This can lead to severe diseases. The group of mitochondrial diseases is highly heterogeneous and includes various clinical appearances [73]. Although mitochondrial function is essential for all cells, mitochondrial disorders do not affect every tissue in the body, tissues and organs that are highly dependent on energy are primarily impaired [3]. Such disorders often exhibit myopathic ("ragged-red fibers") and neurological characteristics [73,79] comprising of ataxia, seizures, stroke-like episodes, dementia, muscle weakness, sensory neuropathy and developmental delay [78,80]. Deafness, exercise intolerance, cardiomyopathy, optic atrophy, lactic acidosis and diabetes mellitus are also well-recognized common clinical phenotypes of mitochondrial diseases [78]. A recent study reported on an inherited mitochondrial disease that causes dysfunction of the mitochondrial lipid metabolism and disturbance of the lipid membranes. The study concluded that this, in turn, impairs mitochondrial energy production and leads to cardiomyopathy, myopathy and lactic acidosis in the phenotypical appearance, mostly without neurological manifestation [81]. Additionally, it is also possible that different mutations have the same clinical phenotype and that the same genetic defect can cause very different clinical phenotypes. Some disorders only affect a single organ, whereas others involve multiple organ systems [3]. Mitochondrial disorders may develop at any age. Until recently, it was generally thought that nuclear DNA abnormalities appear in childhood and mtDNA abnormalities (primary or secondary to a nuclear DNA abnormality) appear in late childhood, or adult life. Recent advances have shown that many mtDNA disorders appear in childhood, and many nuclear genetic mitochondrial disorders appear in adult life [78].

However, disorders, affecting nuclear DNA, often show severe clinical phenotypes that are rapidly progressive, leading to neonatal or infantile death [68].

The transport of mitochondrial proteins that are synthesized in the cytosol and contain specific targeting sequences requires an import machinery consisting of docking proteins, chaperonins that are a class of molecules belonging to chaperones, translocases and proteases to translocate the protein to the right compartment of the mitochondrion and also involves unfolding and refolding processes. Several mutations in targeting sequences have been documented to prevent proteins from being translocated to their desired destination leading to defects related to the function of the protein or the associated protein complex. Only a few genetic defects are known to date that affect the general import machinery because this would impair mitochondrial function severely and would not be compatible with life. At least two disorders have been associated with mutations in components of the transport machinery resulting in neurological and deafness syndromes [73].

The dynamic processes fusion and fission are essential for mammalian development and defects in mitochondrial dynamics cause diseases [50]. The morphology of mitochondria depends on the balance between fusion and fission. Unbalanced fission leads to fragmentation, whereas unbalanced fusion leads to elongation. In normal development, the control of these processes can change the shape of mitochondria to suit a particular developmental or bioenergetic function [61]. In cells that lack fusion proteins or that have defective fusion proteins, mitochondrial function is impaired. Mitochondria become autonomous and cannot exchange mtDNA or proteins to maintain their function [61]. Affected cells grow much more slowly, show heterogeneity in mitochondrial membrane potential and a decreased cellular respiration. Mutations of mitochondrial fusion proteins are mainly related to neurodegenerative diseases such as Alzheimer’s disease [61,82]. The other dynamic process, mitochondrial fission, is related to apoptosis. Fragmentation of mitochondria is a proapoptotic phenomenon in cell death, whereas mitochondrial fusion seems to protect from cell death. Mitochondrial fusion is reduced following induction of apoptosis and overexpression of fusion proteins can reduce the apoptotic capacity [61].

Mitochondrial transport, closely related to the process of mitochondrial fusion, is important to meet the energy requirements of the cell, particularly in cells with high energy demands such as neurons. Mitochondria are rapidly transported to areas of high energy demand, and therefore, this process is important for the development, function and stability of synapses and dendritic spines. Impaired mitochondrial trafficking has been implicated in neurodegenerative disorders including Huntington's disease, Parkinson's disease, Alzheimer's disease and amyotrophic lateral sclerosis [83].

In case of critical illnesses, such as trauma, surgery or sepsis, mitochondria are initially activated. They respond to stress mediators like glucocorticoids or catecholamines by modulating the expression and activity of certain OXPHOS subunits or by increasing their size and number to maintain the increased energy demands of the cell. But prolonged stress and a stress-induced hyperglycemia can then increase the mortality risk by impairing the function of mitochondria caused by cell toxic glucose levels. This leads to disturbance in oxygen use and hence cytopathic hypoxia [2].

The mPTPC is involved in the pathogenesis of necrotic cell death following ischemia-reperfusion. All cellular conditions that promote the formation of the mPTPC such as calcium overload, high phosphate concentrations and oxidative stress also appear during ischemia-reperfusion [56].

It is assumed that alterations in nuclear or mitochondrial DNA and excessive caloric intake contribute to the metabolic syndrome (including visceral obesity, insulin resistance, dyslipidemia, hypertension, proinflammatory and prothrombic syndrome). This leads to an imbalance and to failure of energy metabolism. In turn, the mentioned cardiovascular risk factors accompany with low aerobic capacity and reduced expression of genes that are required for the biogenesis of mitochondria. Caloric restriction reduces the workload of the respiratory chain, improves energy output and decreased oxidative stress [2].

Defects in mitochondrial fatty acid oxidation can lead to the accumulation of metabolites that disrupt insulin signaling and maybe also secretion, causing insulin resistance and hence, type 2 diabetes [2].

Cardiolipin, the major lipid component of the inner mitochondrial membrane, is rich in unsaturated fatty acids and therefore, susceptible to damage caused by ROS. Alterations in the cardiolipin composition can affect the function of the respiratory chain and may also cause disorders [84].

An increased calcium uptake into mitochondria leads to the production of reactive oxygen species and thus is related to neurodegenerative diseases [85].

Dysfunction of mitochondria is also related to cancer. There are differences between normal cells and cancer cells regarding the structure and function of their mitochondria. These differences include metabolic activity, molecular composition and mtDNA sequence [4]. The first association between mitochondrial dysfunction and cancer was made in the 1930s by Otto Warburg. He hypothesized that cancer cells mainly produce ATP by glycolysis as a consequence of impaired mitochondrial respiratory capacity or low oxygen concentrations in tumors. This phenomenon has been called the Warburg-effect. It has been shown that mitochondria in carcinoma cells have a significantly higher membrane potential which is another characteristic that distinguishes them from normal cells. Besides this, numerous other metabolic and functional alterations have been observed in cancer cells, such as acidification caused by the conversion of pyruvate to lactate instead of entering the citric acid cycle [4,6]. Mutations of mtDNA have been reported in a variety of cancers [4]. Dysfunction of programmed cell death caused by mutations in oncogenes or a mutated tumor suppressor gene is another profound characteristic of tumor cells [45,63]. Possible causes of mitochondrial diseases, their effects on the cellular level, affected tissues and clinical appearances are summarized in Table 1.1.

Cause of mitochondrial disease	Effect on cellular level	Affected tissues	Clinical appearance
genetic alterations of nDNA or mtDNA (inherited / acquired)	dysfunction of respiratory chain → reduced energy production	neuronal system, myocardial muscle	ataxia, seizures, stroke-like episodes, dementia, muscle weakness, sensory neuropathy, developmental delay, deafness, optic atrophy, lactic acidosis, diabetes mellitus
	dysfunction of lipid metabolism → reduced energy production	myocardial muscle	lactic acidosis, myopathy
	mutated MLS or translocases → maltranslocation of proteins	neuronal system	deafness, neurological symptoms
	altered metabolic activity (ATP production by glycolysis, acidification) → impaired respiration, impaired apoptosis	all tissues	cancer
	dysfunction of mitochondrial fusion, fission and transport → altered mitochondrial membrane potential, reduced energy production, alterations in apoptosis	neuronal system	neurodegenerative diseases (Alzheimer´s diseases, Huntington´s disease, Parkinson´s disease, amyotrophic lateral sclerosis)
genetic alterations and excessive caloric intake	imbalance and failure of energy metabolism, oxidative stress	cardiovascular system	metabolic syndrome
stress (trauma, surgery, sepsis)	stress mediators (glucocorticoids, catecholamines) activate mitochondria (size, number, energy production); stress induced hyperglycemia induces glucose toxicity	all tissues	cytopathic hypoxia
calcium overload, high phosphate concentrations, oxidative stress	mPTPC formation → apoptosis; oxidation of membrane lipids → reduced energy production	neuronal system, myocardial muscle	necrotic cell death after ischemia reperfusion, neurodegenerative diseases
defects in fatty acid oxidation	accumulation of metabolites that disrupt insulin signaling and secretion	all tissues	diabetes type 2

Table 1.1: Causes of mitochondrial diseases, their effects on the cellular level, affected tissues and clinical appearances; nuclear DNA (nDNA), mitochondrial DNA (mtDNA), mitochondrial leading sequence (MLS), mitochondrial permeability transition pore complex (mPTPC).

The role of mitochondrial dysfunction in aging considers a vicious cycle consisting of accumulation of mtDNA mutations with increasing age and impairment of the respiratory chain, therefore increased production of ROS and further damage of mtDNA and proteins. It is also possible to explain late onset neurodegenerative diseases, such as Parkinson's disease, Huntington's disease and Alzheimer's disease with the age-related increase in ROS [84]. Neurodegenerative diseases are associated with neuronal death and progressive loss of synapses in brain and spinal cord [63]. Additionally, the number of mitochondria is decreased in neurons of patients with Alzheimer's disease [82]. The major effects of neurodegenerative disorders are memory loss, emotional alterations, problems with imbalance and movements [63].

As a result of their physiological functions and their localization in mitochondria, sirtuins and dysfunction in the regulation of the expression of these protective proteins may play a role in aging and certain (age-related) diseases, including cancer, neurodegenerative diseases e.g. Alzheimer's and Parkinson's disease, and metabolic disorders e.g. diabetes and adipositas [75].

The diagnosis of mitochondrial disorders is quite challenging when only one symptom is present. Diagnosis is easier when two or more apparently unrelated symptoms involving more than one organ system are present. If it is possible to identify a known pathogenic mtDNA mutation, investigations can be straightforward [78]. MtDNA or nDNA studies should be accomplished when a classical maternally inherited mitochondrial syndrome or a nuclear DNA-inherited syndrome is present. Difficulties arise when no mtDNA defect is detectable or when the clinical appearance is complex and not easily match those of more common mitochondrial disorders [78]. If the clinical appearance is uncertain but highly suggestive to a mitochondrial disorder, measurement of plasma or cerebrospinal fluid lactic acid concentration, ketone bodies, plasma acylcarnitines, and urinary organic acids should proceed [78]. If these results are abnormal, muscle biopsy and assessment of the respiratory chain enzymes should follow. Neuroimaging (CT or MRI) is indicated in patients with a suspected disease of the central nervous system, electroencephalography (EEG) is indicated

at suspected encephalopathy or seizures, electromyography (EMG) may show myopathic features and nerve conduction velocity (NCV) may show polyneuropathy. Electrocardiography and echocardiography may indicate cardiac involvement [78].

Therapeutic options for mitochondrial dysfunction are currently limited [2], no effective disease-modifying therapy is available, and a careful clinical management is necessary to minimize symptoms of the diseases. The treatment of manifestations and management of mitochondrial disease is largely supportive and may include early diagnosis and treatment of diabetes mellitus, cardiac pacing, ptosis correction, and intraocular lens replacement for cataracts to prevent complications and unnecessary morbidity and mortality [78]. Individuals with complex I and/or complex II deficiency may benefit from oral administration of riboflavin [78]. Food supplements such as ubiquinone are generally well tolerated, and some individuals report a subjective benefit on treatment [78]. Supplementation of other antioxidants, such as vitamins and co-factors, are also usual treatments, but data from controlled clinical studies are absent [86]. Due to the unsatisfying therapeutic options in the treatment of mitochondrial diseases, there is a need for mitochondria-targeted therapies.

Intracellular targets of mitochondrial diseases

At first, it is necessary to identify causes and potential targets that are related to mitochondrial dysfunction. This includes functional alterations in metabolic pathways, proteins and other molecular compositions compared to normal cells. Some mitochondria related diseases exhibit various alterations in function, and it is not possible to treat all causes of the disease. An example is diabetes type 2 that is related to dysfunction of mitochondrial fatty acid oxidation, defects of mitochondrial oxidative phosphorylation and alterations of the mitochondrial genome [2].

Mutations in the mitochondrial or nuclear genome are the cause for most mitochondria-related disorders including respiratory chain defects, mitochondrial fusion defects and malfunction of the protein import machinery. Hence, an overall aim is to reduce the fraction of mutated mtDNA to subthreshold levels. This could be achieved by adding synthetic wild-type

mtDNA, by removing or selective inhibition of mutated mtDNA [3,18]. The mitochondrial genome itself as a target is challenging to influence. To date, it is not possible to treat inherited diseases causally, but it is possible to prevent age-related mutations caused by reactive oxygen species. Scavenging of ROS that are produced in excess is therefore a possible strategy. This also prevents oxidation of cardiolipin in the inner mitochondrial membrane that is related to the function of the respiratory chain [84]. Another option to prevent the accumulation of mtDNA mutations is to increase the DNA repair capacity in mitochondria by transfecting cells with recombinant enzymes that are known to be involved in the repair of oxidative damage to mtDNA [18]. Beyond that, it is conceivable to choose an indirect approach to mitochondria gene therapy also known as allotopic expression. The strategy is to deliver a wild-type mitochondrial gene fused to a sequence that encodes a mitochondrial targeting sequence into the nucleus followed by cytosolic expression and import of the protein into mitochondria [18]. Finally, mitochondrial gene therapy is a promising but challenging approach, and its development is still at an early stage [14].

A target in carcinoma cell mitochondria is the defective programmed cell death due to the overexpression of antiapoptotic proteins contributing to the development and progression of tumors [87]. Induction of apoptosis is a powerful approach in treating malignant diseases [88]. Therefore, mitochondria are nowadays regarded as prime targets for cancer therapy [89]. Other alterations in cancer cells, for example decreased activity of OXPHOS enzymes, modified composition of membrane lipids, alterations in gene expression and mtDNA mutations that differ between the various cancer types, the higher membrane potential compared to normal mitochondria due to metabolic changes, glycolysis, and other metabolic alterations are potential targets although some of them are difficult to manipulate [6,54].

It is also thinkable that calcium signaling can be a target. The increase of mitochondrial calcium concentration can lead to formation of the mitochondrial permeability transition pore complex (mPTPC), loss of membrane potential and hence, apoptosis [61]. The inhibition of calcium channels and reduced calcium influx into tumor cells suppresses tumor cell proliferation, respectively [14,90]. An increased calcium influx also contributes to the

generation of reactive oxygen species and is associated with neurodegenerative diseases [64,84]. Mitochondrial calcium homeostasis is closely related to the mitochondrial membrane potential which is in turn regulated by potassium channels. Mitochondrial potassium channels, therefore, are also a target in therapy [91].

The mPTPC itself plays a central role in apoptosis and presents a target for cytoprotective and cytotoxic therapies [56].

The peripheral benzodiazepine receptor (PBR) that is localized primarily in mitochondrial membranes is thought to be a component or a regulator of mPTPC in apoptosis and therefore exhibits a target for cytotoxicity and cytoprotection [5,6].

The activity of uncoupling proteins in the inner mitochondrial membrane acts in the storage of triglycerides in adipose tissue. Targeting of these proteins may offer new treatment strategies in obesity [56].

Even though the field of sirtuin research is quite young, most studies rely on microorganisms and in spite of the controversial discussion whether sirtuins can really extend lifespan in mammals or not, they seem to be an attractive target in mammals. Due to the correlation of calorie restriction and activation of sirtuin activity, it is possible that in future, new pharmacological agents target and activate sirtuins by mimicking calorie restriction. This may prevent neurodegenerative or metabolic diseases or helps to treat cancer [75]. It has already been shown that the natural product resveratrol can activate sirtuins upon oral administration leading to antidiabetic effects such as improved insulin sensitivity and glucose tolerance as well as decreased fasting glucose levels [92].

Since it is known that mitochondrial fusion has a protective effect on mitochondrial functionality and excessive mitochondrial fragmentation contributes to programmed cell death [61] it is thinkable that the manipulation of mitochondrial dynamics might be a promising therapeutic strategy to improve mitochondrial functionality. Feasible approaches may be the enhancement of mitochondrial fusion or the prevention of mitochondrial fission in cells that exhibit a disequilibrium of both processes. If fragmentation of the mitochondrial network is a consequence of mitochondrial dysfunction, an effective therapeutic approach

cannot be expected by an enhancement of mitochondrial fusion. In contrast, if mitochondrial fragmentation is the cause of dysfunction, the enhancement of mitochondrial fusion can help to normalize and enhance complementation of mitochondrial functionality by redistributing mutated and wild-type mtDNA as well as proteins [93].

Drugs or molecules that affect mitochondrial function

Several low molecular weight substances and macromolecules are known to directly act on mitochondria or to have an influence on their functionality. The therapies with some of these substances would benefit from a specific targeting strategy to exert their action directly on mitochondria, to improve their efficacy, to reduce dosages and side-effects or to apply new indications of approved drugs. Most of these molecules affect mitochondria as they exert ROS scavenging capacity that can be applied in degenerative diseases or they show proapoptotic activity that can be used as an anticancer strategy (Table 1.2). Drugs that have an influence on mitochondria are classified into non-peptide and peptide substances as well as drugs that affect mitochondrial dynamics. Examples from each class will be described in more detail.

drugs	antiapoptotic effects (non-malignant cells)	proapoptotic effects (malignant cells)
antioxidants	ROS-scavenging	
cyclosporin A	prevents mPTPC formation	
SOD-mimicking peptides	ROS-decomposition	
Szeto-Schiller-peptides	ROS-scavenging, prevents mPTPC formation	
resveratrol	stimulation of sirtuins	induction of mPTPC formation
potassium channel openers (diazoxide)	prevents mPTPC formation	inhibition of calcium channels, antiproliferative
vitamine E	ROS-scavenging	triggers apoptosis, suppresses angiogenesis
paclitaxel, "mitocans", PBR-agonists (diazepam analogs), 3-bromopyruvate		induction of mPTPC formation
imexon, menadione, motexafine gadolinium, β-lapachone, mangafodipir, parthenolide, photodynamic substances		oxidative stress / overproduction of ROS
anthracyclines, arsenic trioxide		induction of mPTPC formation and oxidative stress
betulinic acid, dichloroacetate, proapoptotic peptides (mastaparan, $D(KLAKLAK)_2$)		disruption of mitochondrial membrane potential
4-quinolones (ciprofloxacin), nucleoside analogs		mtDNA damage
benzothiazepines		Increasing of calcium influx
cis-Pt		induction of mPTPC formation, inhibition of glycolysis
buthionine sulphoximine, estrogen derivatives		inhibition of endogenous antioxidant system

Table 1.2: Drugs that act on mitochondria; superoxide dismutase (SOD), reactive oxygen species (ROS), mitochondrial permeability transition pore complex (mPTPC), mitochondrial DNA (mtDNA), peripheral benzodiazepine receptor (PBR).

Non-peptide substances

Antioxidants, compounds with free radical scavenging properties are a major group with numerous substances that can influence mitochondrial functionality. Lipoic acid, for example, a coenzyme of mitochondrial enzymes, can readily penetrate the blood brain barrier, and its effects on improving cognition and Alzheimer's disease related pathology have been evaluated in disease models [83]. Lipoic acid can also recycle the endogenous antioxidants vitamin C, vitamin E and glutathione. Coenzyme Q10, also an endogenous coenzyme of electron transport chain proteins, and synthetic derivatives of Coenzyme Q10 such as idebenone can, orally supplemented, attenuate oxidative stress related dysfunctions and are used in the treatment of neurological and neuromuscular diseases [5,83]. The approval for idebenone in the therapy of an inherited mitochondrial optic neuropathy has been submitted recently [94]. Despite their clinical importance, antioxidants show limited therapeutic success when they are not selectively taken up by mitochondria [7]. Antioxidants that only have access to the cytosol have a limited impact on mitochondria. Therefore, it is necessary that antioxidants are delivered into mitochondria to scavenge mitochondrial reactive oxygen species effectively. Such mitochondrial targeted antioxidants have already been developed, and an improved clinical outcome has been shown [7,83]. Two general targeting strategies for antioxidants have been proven to be useful, the conjugation to lipophilic cations and the incorporation into mitochondria targeted peptides [7] which will be described in more detail later in this review. A well-characterized antioxidant, targeted to mitochondria by conjugation to the triphenylphosphonium (TPP) cation, is MitoQ that consists of an ubiquinone moiety linked to a TPP moiety by a ten-carbon alkyl chain. The TPP moiety on MitoQ leads to a rapid uptake across the plasma membrane, driven by the plasma membrane potential, followed by its accumulation in mitochondria. MitoQ is continually converted to the active ubiquinol antioxidant by respiratory complex II inside mitochondria, and it has been shown to have protective capacity in a large number of cell models of mitochondrial oxidative stress [7].

Vitamins and coenzymes of respiratory chain proteins contribute to the function of these mitochondrial proteins. In diseases that are related to dysfunction of these proteins, the oral administration of coenzymes such as vitamin B_1 or B_2, succinic acid and coenzyme Q, and ATP itself can, to some extent, compensate mitochondrial dysfunction, resulting in positive therapeutic effects [41].

Many clinically approved drugs directly act on mitochondria triggering apoptosis including paclitaxel [14,44]. Although it is largely believed that paclitaxel exerts its action by stabilizing microtubules of the cell, it has been shown that it induces the formation of the mPTPC and hence apoptosis [17]. Interestingly, in studies with intact cells that have been treated with paclitaxel, a 24 h delay of apoptosis was observed compared to studies with isolated mitochondria. This delay has been attributed to the interaction with several sites inside the cell, making only a fraction of the drug molecules available for mitochondria. Hence, paclitaxel appears to be a molecule whose action and efficiency may be significantly improved by specific subcellular delivery to the mitochondrion [17]. It has been shown that the encapsulation of paclitaxel in liposomes from dequalinium (DQAsomes) improved efficacy [17]. Similarly to paclitaxel, doxorubicin and cisplatin are also known for different mechanisms of action, but were shown to induce the formation of the mPTPC as well [87].

The anticancer activity of anthracyclines such as doxorubicin is mainly attributed to their DNA intercalation. However, the cytotoxic side effects of the widely used anthracyclines adriamycin and daunomycin have been associated with mitochondrial dysfunction. Interaction of these drugs with mitochondria appears to follow complex mechanisms, including major membrane disruption caused by the high affinity of anthracyclines to cardiolipin, and the redox activity of the quinone moiety which results in oxidative damage of proteins [5].

A group of anticancer agents called “mitocans”, an acronym for “mitochondrially targeted, apoptosis-inducing anticancer compounds”, usually cause mitochondrial destabilization of tumor cells through the activation of mitochondrial mediators of apoptosis including the proapoptotic proteins and the formation of the mPTPC [5,95]. These agents have been

classified and reviewed by Ralph and Neuzil [95]. Some of them are among the following agents that will be discussed below.

Arsenic trioxide (Trisenox™) has been commercialized for the treatment of acute promyelocytic leukemia. As_2O_3 has undoubtedly multiple biological targets, but the most common mechanism of action seems to be its interaction with sulfhydryl groups, especially those of mPTPC members, leading to the production of ROS and subsequent apoptosis [5]. Other substances that target mitochondrial permeability transition by depleting inhibitors of mPTPC such as glucose, ATP, creatine phosphate, glutathione or by increasing calcium or by stimulating the production of ROS include lonidamine, bisphosphonate clodronate and retinoid-related compounds [6]. Lonidamine also inhibits oxygen consumption and blocks energy metabolism which results in the loss of the membrane potential and apoptosis [87].

Imexon, an aziridine-containing iminopyrrolidone and isothiocyanates bind to thiols (GSH, cysteine), causing an accumulation of ROS and mitochondrial swelling, and that leads to apoptosis. Imexon is currently being evaluated for the treatment of pancreatic and lung cancers [5,6]. Other compounds that induce the overproduction of ROS offer potential strategies to cancer therapy such as menadione, motexafine gadolinium and β-lapachone or substances that inhibit the endogenous antioxidant systems such as buthionine sulphoximine which inhibits glutathione synthesis. Mangafodipir increases ROS in cancer cells and some estrogen derivatives inhibit ROS-scavenging enzymes [6].

Gamitrinibs, geldanamycin mitochondrial matrix inhibitors, that contain geldanamycin conjugated to a cyclic guanidium moiety which acts as a mitochondrial targeting signal, selectively target a heat shock protein in cancerous mitochondria inducing rapid tumor cell death [96].

As it was revealed that ceramides show an antiproliferative and proapoptotic activity in tumor cells, specific targeted liposomal carrier were formulated to deliver ceramides to mitochondria [97,98]. These specific carrier systems are another example of the improvement of drug efficacy by targeted drug delivery systems.

A variety of chemical agents cause depletion of mitochondrial DNA and could theoretically be used in cancer therapy. Examples are 4-quinolone drugs such as ciprofloxacin which cause loss of mtDNA and consequently loss of mitochondrial function and other substances such as the intercalating agent ditercalinium or antiviral nucleoside analogs [87].

The peripheral benzodiazepine receptor (PBR) as a component or a regulator of mPTPC in apoptosis can be addressed by PBR agonists such as diazepam analogs that act as proapoptotic antitumor agents and PBR antagonists such as isoquinoline derivatives that act as antiapoptotic agents, respectively [5,6].

Other approaches to cancer therapy are the targeting of the altered mitochondrial metabolism, such as the inhibition of glycolysis which increases the toxicity of cisplatin, the downregulation of the high membrane potential by dichloroacetate, the inhibition of the fatty acid synthesis by soraphen A resulting in reduced phospholipid content, growth inhibition and enhanced cell death, the promotion of mPTPC formation by 3-bromopyruvate or methyl jasmonate or the inhibition of lactate dehydrogenase A which converts pyruvate to lactate leading to acidification [6]. Targeting and inhibition of a cancer specific heat shock protein by shepherdin results in tumor growth inhibition. Betulinic acid triggers mitochondrial apoptosis in cancer cells by disrupting the membrane potential. Resveratrol improves mitochondrial function of non-malignant cells by the stimulation of sirtuins and contributes to cell death induction by inhibition of ATP synthesis and triggering of mPTPC in cancer cells as well. Vitamin E analogs trigger apoptosis in cancer cells and suppress angiogenesis. The sesquiterpene lactone parthenolide shows cytotoxic effects involving ROS-overproduction [6].

Mitochondrial potassium channels (mitoK_{ATP}) can be blocked by antidiabetic sulfonylureas such as glibenclamide or activated by potassium channel openers such as diazoxide. Potassium channel openers exert a cardioprotective action via the prevention of mPTPC formation and are therefore a potential therapeutic application in the treatment of myocardial infarction and stroke [5]. Diazoxide also affects the activity of uncoupling proteins and can

prevent cell death [99]. In another study, diazoxide was shown to inhibit calcium channels and to reduce calcium influx into tumor cells, suppressing tumor cell proliferation [14,90].

Benzothiazepines were shown to inhibit the mitochondrial Na^{+}-Ca^{2+}-exchange resulting in an increase in mitochondrial Ca^{2+}-concentration and subsequent ATP production. These findings suggest that deficiencies in respiratory chain complexes are associated with altered cytosolic Ca^{2+}-homeostasis [5]. The manipulation of mitochondrial associated calcium signaling provides an anticancer strategy as diazoxide was shown to inhibit calcium channels suppressing tumor cell proliferation [14,90].

Nucleoside analogs used as antiviral drugs, such as zidovudine, can cause mitochondrial damage through two mechanisms. The short-term mechanism directly affects the activity of mitochondrial enzymes, *via* the competitive inhibition of the ADP/ATP antiport and of the nucleoside diphosphate kinase. The long-term mechanism alters the mtDNA, *via* oxidative damage to mtDNA and inhibition of the polymerase responsible for mtDNA replication [5]. Non-steroidal anti-inflammatory drugs (NSAIDs) can inhibit the β-oxidation of fatty acids and cause the uncoupling of respiratory chain and ATP synthesis, partly due to induction of the formation of the mPTPC [5]. Local anesthetics also uncouple respiratory chain and ATP synthesis and also inhibit mitochondrial ATPase and respiratory chain enzymes [5]. Hence, besides possible new applications of approved drugs like nucleoside analogs, NSAIDs or local anesthetics, late-stage adverse drug toxicity events are related to mitochondrial toxicity [5].

In the growing group of photosensitizers for photodynamic therapy, there are substances known that accumulate in mitochondria causing ultrastructural and functional alterations that can be utilized in the therapy of cancer [100].

Peptide substances

Besides non-peptide-based agents that act on mitochondria, there are also peptide- and amino acid-based molecules modulating mitochondrial functionality.

Proapoptotic peptides are capable of disrupting mitochondria and triggering apoptosis. They are typically derived from the sequences of membrane-disrupting antimicrobial peptides. Since they can be easily fused to tissue- or tumor-specific peptides or antibodies, they may be attractive as new targeted anticancer agents. However, they usually suffer from low potencies, thereby limiting their clinical utility. Mitochondrial localization and membrane-disrupting activity of the widely used cationic amphipathic α-helical killer peptide D-$(KLAKLAK)_2$ could be improved by increasing its hydrophobicity via the exchange of amino acids. Thereby, a dramatic increase in potency could be achieved [5]. Mastoparan is a toxic peptide that targets the membrane potential promoting apoptosis [87].

Cyclosporin A (CsA), a cyclic peptide, was shown to inhibit the formation of the mPTPC and prevents or delays cell death caused by oxidative stress, protecting the heart and the brain from ischemia-reperfusion injury. Despite the potential of CsA as an anti-ischemic drug, there are other targets of CsA in the cell, this makes it difficult to predict concentrations of CsA in mitochondria. The therapy with CsA would benefit from a mitochondria-specific drug carrier system [56].

Manganese metalloporphyrin oligopeptide conjugates are a new class of mitochondria targeted superoxiddismutase (SOD)-mimics that consist of manganese metallopophyrin conjugated to a mitochondrial targeting sequence peptide. The natural SOD as well as the oligopeptide conjugates decompose highly reactive oxygen species and protect cells from oxidative stress [5].

Szeto-Schiller-peptides are not only a suitable targeting strategy for mitochondrial targeting (this will be reflected upon later), but some of them show an intrinsic antioxidant capacity as an additional feature [7,101]. The free radical scavenging abilities of these peptides are likely to originate from their tyrosine residues. They can reduce intracellular ROS production and apoptosis and prevent mitochondrial depolarization, formation of the mPTPC and Ca^{2+}-induced swelling [102]. Hence, such mitochondria-targeted antioxidants represent a promising approach in the therapy of neurodegenerative diseases [5].

The tripeptide glutathione (GSH) plays an important role in protecting cells against oxidants and electrophiles. When donating an electron to unstable molecules such as ROS, two GSHs react to form glutathione disulfide (GSSG). Increasing mitochondrial glutathione and other thiol-based antioxidants can be an effective strategy to prevent mitochondrial oxidative stress. Using a similar approach as with the TPP conjugated antioxidants, choline esters of glutathione and of its analog *N*-acetyl-L-cysteine were shown to target mitochondria and to protect against oxidative damage [5].

The possibility of gramicidin as a potential targeting strategy has been proven by the tethering of a hemi-gramicidin S pentapeptide sequence to a stable free radical. Thereby, the gramicidine peptide acts as the targeting moiety, and the conjugated free radical acts as the ROS scavenging drug. The major advantage of sterically hindered free radicals is their electron acceptor/donor nature depending on the redox potential of the environment. By accepting one electron, they become reduced and can act as direct radical scavengers. Afterward, they are converted back into nitroxides. In other words, these compounds undergo redox recycling. Nitroxides also possess superoxide dismutase and catalase mimetic activities, thus offering additional protective benefits against oxidative cellular damage [5].

Substances that influence on mitochondrial dynamics

In strategies toward influencing mitochondrial dynamics, genetic experiments have shown that inhibition of fusion shifts the equilibrium to fission and vice versa. A pharmacological agent that inhibits fission was shown to increase the proportion of fused mitochondria in cells that contain fragmented mitochondria. The quinazolinone derivative binds to fission-mediating proteins, inhibiting their activity and thus, promoting fusion via the prevention of mitochondrial fragmentation. This compound could therefore be a therapeutic approach to a group of neurodegenerative diseases that result from aberrant mitochondrial fusion [93]. Pharmacological agents that induce the mitochondrial fusion by directly influencing the fusion machinery are currently unknown.

Although the list of compounds that can act on or interact with mitochondria is long, it certainly does not raise a claim to completeness. In addition, it remains unclear to what extent these molecules selectively accumulate at the desired target [9]. Targeting strategies that were shown to achieve a selective accumulation in mitochondria will be described in detail later in this review. They may help to find a suitable targeting approach for the mentioned drug molecules. Before mitochondrial targeting strategies are evaluated in detail, the next two chapters will reflect on structural characteristics that make targeting of mitochondria very challenging and will also give ideas about how barriers can be crossed by utilization of mitochondrial specificities.

Challenges of targeting mitochondria and of working with isolated mitochondria

Although mitochondria play a central role in various important pathologies, they have been a neglected target. This is in partly due to the difficulty of selectively targeting molecules to this organelle *in vivo [7]*.

General challenges of intracellular targeting, concerning drug molecules as well as drug carriers, are to cross the cellular membrane that prevents large molecules from spontaneously entering the cell and to escape the endosomes and reach the cytosol without degradation, in case of endocytosis of larger drug molecules, DNA or nanocarriers [14,48]. There is a need to develop strategies that bypass the endocytotic pathway and that achieve a sufficient intracellular transport [14].

To avoid the obstacles of drug delivery, namely the cell membrane as a transport barrier, endocytotic and lysosomal or cytosolic degradation processes before a drug reaches mitochondria, or to avoid invasive techniques that help to cross the cellular membrane such as microinjection or electroporation, it can be advantageous to work with isolated mitochondria. Isolation of mitochondria from tissues or cells is still a standard method to monitor mitochondrial bioenergetics and physiology. Experimental conditions can be precisely controlled and modified to accomplish the requirements of the scientific approach

by supplementation of substrates, inhibiting or uncoupling substances. Oxygen kinetics can only be analyzed on isolated mitochondria. Preparations of isolated mitochondria are also required to study and separate different mitochondrial subpopulations [103]. They are further required for investigations on the molecular level, such as enzyme activity, analytics of proteins, protein import and DNA or as a subsequent method after the application of molecules or carriers to intact cells, to determine site and extent of their subcellular accumulation [104,105]. Disadvantages that are associated with the isolation of mitochondria include separating mitochondria from their natural environment and signaling processes, the temporarily limited metabolic activity, the risk of damaging mitochondrial membranes due to shear forces during the isolation process and the risk that mitochondrial networks might be disrupted. Isolated mitochondria may not behave as they would do in their natural environment [106]. Working with isolated mitochondria is therefore controversially considered. Approaches with intact cells are preferred in many subjects, and it has to be emphasized that for purposes in which the cellular context contributes to the experimental outcome, it is essential to work with intact cells rather than with isolated mitochondria [106]. Studies that have investigated the influence of paclitaxel on mitochondria have shown a different outcome for intact cells compared to isolated mitochondria [17]. However, one can argue that even intact cells lack the true in vivo complexity of cell-cell interactions of tissues or organisms. Advantages and disadvantages of working with isolated mitochondria compared to intact cells have been recently summarized by Brand and Nicholls [107]. For the isolation of mitochondria, numerous protocols that are making use of fast methods, such as differential centrifugation [108,109], more time-consuming gradient-purification procedures [105,110], or antibody-based approaches [111] have been established over the years. The choice of the method depends on the source of mitochondria and the respective research goal. The isolation process itself can be challenging as large amounts of cells are required to obtain enough mitochondria for further studies. This means, in the case of mammalian cells that grow as monolayers, a large number of cell culture flasks have to be cultivated and processed for the isolation procedure. Purification steps after isolation can lead to the dilution

of the preparation and loss of mitochondria. Therefore, their application is not always practicable. Despite all challenges and disadvantages that are associated with isolated mitochondria, the first approaches in targeting mitochondria are widely investigated with isolated mitochondria to provide a basis of knowledge. However, to understand the relation of mitochondria to other aspects of cell physiology and to understand how other cell functions respond to changes in mitochondrial function, it is necessary to proceed with studies in intact cells [112].

The challenge of targeting mitochondria by itself is to transfer the drug or drug carrier across two membranes in the case of mitochondrial matrix targeting. In targeting of the intermembrane space, it is sufficient to pass the outer mitochondrial membrane, but almost all potential targets are located in the mitochondrial matrix. Therefore, it is necessary to overcome both mitochondrial membranes which have only small pores and a highly lipophilic inner membrane. Theoretically, membrane impermeable probes can enter mitochondria through protein import pores (TOM- and TIM-complex), the pore protein porin, also referred to as the voltage dependent anion channel (VDAC), the mitochondrial permeability transition pore complexes (mPTPCs), through mitochondrial apoptosis-related channels and through apoptosis-related ceramide pores. But only the VDAC and the protein import pores are relevant in normal mitochondrial function. The others are related to apoptosis and dysfunction and are localized in the outer but not the inner mitochondrial membrane [113]. Except a few membrane-permeable lipophilic compounds, such as molecular oxygen, acetaldehyde and short fatty acids, all metabolites that enter and leave mitochondria must cross the outer mitochondrial membrane through the VDAC [113] which is also the most abundant protein in the outer mitochondrial membrane [69]. The protein import pores in the outer mitochondrial membrane (TOM-complex) have a dimension of about 2–2.6 nm. The pores of the inner mitochondrial membrane (TIM-complex) are even smaller with a pore size of about 1.3 nm [114,115]. The size of the VDAC, only localized in the outer mitochondrial membrane, was determined to have a dimension of 3–6 nm with silver-enhanced gold nanoparticles in electron microscopy studies [113,116].

Therefore, targeting of mitochondria is limited to molecules and very small-sized nanocarriers.

Utilization of mitochondrial properties for targeting

Due to the fact that mitochondria exhibit some features that differ from other cellular compartments and in turn some of these features vary between normal and diseased mitochondria, these properties can be utilized for the targeting strategies that are reflected in the next section.

The first property that can be utilized for targeting is the mitochondrial membrane potential. The electron transport chain and ATP synthesis via oxidative phosphorylation create a transmembrane electrochemical gradient that leads to a high membrane potential, negative inside and a pH difference, acidic outside. Therefore, positively charged molecules are attracted to mitochondria and selectively accumulate in the mitochondrial matrix in response to their membrane potential [2,14]. Carcinoma cell mitochondria show an even higher membrane potential due to metabolic changes. It is approximately 60mV higher than in normal mitochondria. This difference accounts for a tenfold greater accumulation of a positively charged compound in carcinoma mitochondria than in control mitochondria [54]. Therefore, cationic molecules are preferentially taken up by tumor cells leaving non-tumor cells unaffected [54].

The inner mitochondrial membrane that has to be crossed for the delivery of substances into the mitochondrial matrix exhibits a lipid composition that differs from other membranes. Cardiolipin is a major lipid component of the inner mitochondrial membrane and is very lipophilic. Therefore, lipophilic molecules or rather lipophilic and positively charged molecules that take advantage of the membrane potential accumulate in mitochondria [117].

In utilizing mitochondrial membrane pores, it is more appropriate to target the protein import pores than to target the VDAC because specific targeting sequences are known for the protein import pores, and they are present in both membranes, whereas the VDAC is only present in the outer mitochondrial membrane and cannot be targeted specifically.

An approach in mitochondrial targeting that has not been considered until now is the utilization of the mitochondrial fusion process. It might be a suitable approach to make use of mitochondrial fusion in order to deliver drug carriers to mitochondria that are too large to pass the mitochondrial protein import pores. Even though most pharmaceutical drug carriers have a size in the nano-range, they are too large for the 2.6 nm pores. It can be hypothesized that a pharmaceutical drug carrier which is decorated with moieties, peptidic or non-peptidic ones, that are attracted by mitochondria and accomplish a close binding of the carrier to the organelle, can be taken up by mitochondrial fusion subsequently to binding at the outer mitochondrial membrane.

In the following, targeting strategies which make use of the described properties of mitochondria will be reflected in more detail.

Targeting strategies for mitochondria

It has been mostly presumed that molecules which exhibit a positive charge are attracted to mitochondria in response to the highly negative membrane potential. However, compounds that exhibit a positive charge cannot enter the mitochondrial matrix because the inner mitochondrial membrane is impermeable to polar molecules. Additional physicochemical properties are necessary to achieve a mitochondrial targeting [14]. Although it has been widely implied that mitochondrial targeting molecules should comprise the features positive charge and lipophilicity/amphiphilicity, there are still controversies regarding this idea [5]. A study that evaluated the characteristics of a large number of mitochondria targeting substances classified only one third as lipophilic cations. One third represented acids and anions, and another third were neutral compounds. Two thirds of the investigated substances were lipophilic and one third was hydrophilic. Therefore, a general correlation between physicochemical properties and extent of accumulation in mitochondria could not be verified [117]. However, several strategies toward mitochondrial targeting that were shown to selectively deliver drugs or molecules into mitochondria will be reflected in the following. The

targeting approaches comprise of non-peptide and peptide moieties as well as nanocarrieres and invasive or biological techniques.

Non-peptide targeting strategies

Delocalized lipophilic cations can easily pass the lipid bilayers of the plasma membrane and the mitochondrial membranes because the charge of the cation is effectively distributed over a large and hydrophobic surface area, thereby lowering the activation energy for their movement across the membrane [7]. The ability of these cations to move through membranes enables their accumulation in the mitochondrial matrix, in response to the large mitochondrial membrane potential that is negative inside [7]. Lipophilic cations do not require a specific import mechanism. The Nernst equation indicates that the uptake of lipophilic cations in the mitochondrial matrix that is only driven by the membrane potential increases 10-fold for every 61.5 mV [7]. The mitochondrial membrane potential is about 180–200 mV which is the maximum a bilayer can sustain and simultaneously maintain integrity [14]. This leads to a 200–400 fold higher accumulation of lipophilic cations in the mitochondrial matrix. Uptake into cells is also driven by the membrane potential of the plasma membrane that is 30–60 mV, negative inside [7]. Therefore, the accumulation of these compounds in mitochondria relative to the extracellular environment can be up to several thousand-fold higher according to the Nernst equation [7]. The best characterized and most widely used delocalized lipophilic cation for delivery to mitochondria is the triphenylphosphonium (TPP) cation, which was originally used to assess the mitochondrial membrane potential [5,7,118]. The TPP cation has been conjugated to a range of antioxidants in order to target them to mitochondria. There are a number of advantages of using the TPP cation approach as its uptake into mitochondria is well established and it is relatively straightforward to introduce this functionality into a compound late in the chemical synthesis scheme, typically by displacing a leaving group with triphenylphosphine [7]. A wide range of antioxidants have been targeted to mitochondria by conjugation to the TPP lipophilic cation, including vitamin E, ebselen, lipoic acid, plastoquinone, nitroxides, nitrones and Mito Q [7]. It is also possible

to conjugate DNA analogs like peptide nucleic acids to TPP for mitochondrial targeting in order to inhibit the replication of mutated mtDNA [18].

Peptide-based targeting strategies

Another approach in targeting substances to mitochondria is the use of small, positively charged peptides, called Szeto-Schiller (SS)-peptides that are composed of four alternating aromatic and basic amino acids [7,101,102]. Szeto-Schiller-peptides exhibit three positive charges at physiological pH, and studies with isolated cells showed their rapid uptake through the plasma membrane and accumulation in mitochondria, where they bind to the inner membrane [7,102]. Despite their positive charge, the uptake of Szeto-Schiller-peptides into mitochondria does not seem to occur in response to the membrane potential. The mechanism that underlies their selective uptake by mitochondria is currently not clear [7,101].

More recently, it has been shown that peptides with a similar structure are taken up by mitochondria within cells due to the influence of the mitochondrial membrane potential on the positively charged peptides [7]. These so called mitochondria-penetrating peptides (MPPs) consist of four or eight alternating positively charged and hydrophobic, partly unnatural, amino acids. They are a very promising targeting approach as delivery vectors for selective and effective mitochondrial transport [119]. In a subsequent study, it has been shown that MPPs are able to deliver small molecules, biotin and trolox, a water soluble analog of vitamin E, into mitochondria [120]. The unanswered question is whether or not MPP are also able to deliver larger cargos such as DNA for gene delivery or nanocarriers into mitochondria.

Approaches to target mitochondria with synthetic peptides are comparatively new. They followed up the targeting of cells with cell penetrating peptides and mitochondrial targeting with natural mitochondrial targeting peptides. Cell penetrating peptides are larger compared to SS-peptides or MPPs and consist of up to 30 only positively charged or alternating positively charged and hydrophobic amino acids. They can enter the cell membrane and are able to transport cargoes with a much higher molecular weight than their own ones [121]. It

has been shown that a wide range of molecules such as peptides, nucleic acids, proteins, and even nanoparticles and liposomes can be delivered in this way into cells [122].

Natural mitochondrial leading sequences (MLSs), derived from mitochondrial proteins that are synthesized in the cytosol, are able to deliver molecules into mitochondria. All proteins synthesized in the cytosol must carry such an amino-terminal pre-protein to be translocated to their final mitochondrial destination. Mitochondrial targeting sequences have a typical size of about 10–80 amino acids with many positively charged, hydrophobic and hydroxylated amino acids. An important feature of these sequences is their ability to form an amphiphatic α-helix that presents one positively charged surface and one hydrophobic surface. These structural characteristics are important for the recognition by the mitochondrial protein import pores. When an MLS is attached to a non-mitochondrial protein, it can specifically direct the protein into mitochondria [69]. The utilization of the mitochondrial protein import pathway was used for the first demonstration of DNA delivery into mitochondria. A mitochondrial leading sequence peptide has been conjugated to oligonucleotides up to 322 bp and specifically introduced exogenous DNA into mitochondria [18]. These targeting sequences can also be coupled to drug molecules or drug carries to achieve a mitochondrial targeting.

An alternative concept in mitochondrial targeting by peptides is based on the affinity of certain natural antibiotics to microbial cell membranes. Due to the close evolutionary relationship between bacterial membranes and the components of the inner mitochondrial membrane, in particular their lipid composition, the antibacterial membrane disruptor gramicidin S is hypothesized to serve as a template for mitochondrial targeting. It was shown that a hemi-gramicidin S pentapeptide sequence can target ROS scavengers to mitochondria [5].

Nanocarriers

In the field of nanocarriers for mitochondrial drug targeting, approaches are mainly based on cationic liposomes prepared from trimethyl aminoethane carbamoyl cholesterol iodide (TMAEC-Chol) or dequalinium, as well as branched PEI to deliver peptide-DNA conjugates

[18] or micelles [17]. Liposomes are able to fuse with mitochondrial membranes delivering their cargo into mitochondria which is especially intriguing for the delivery of larger molecules. This approach takes advantage of the known fact that mitochondria are able to fuse with one another [123]. One of the first mitochondria targeted drug delivery systems that were able to deliver drugs and DNA has been self-assembling liposomes from dequalinium, called DQAsomes [18,124]. Dequalinium is an amphiphilic compound that is able to enter the mitochondrial membranes. DQAsomes are able to bind or to entrap drugs such as paclitaxel and DNA and transport them to mitochondria [14,17,56]. Other cationic liposomes composed of DOPE (1,2-dioleoyl-sn-glycero-3-phosphoethanolamine) and DOTAP (dioleoyl-1,2-diacyl-3-trimethylammoniumpropane) were shown to deliver the propaoptotic peptide D-$(KLAKLAK)_2$ together with an antisense oligonucleotide into mitochondria in order to treat cancer [125]. A liposomal carrier system with octaarginine modifications at the surface that stimulate internalization into cells via macropinocytosis rather than clathrin-endocytosis, called MITO-Porter, promotes fusion with mitochondrial membranes and was shown to selectively deliver cargos into mitochondria [17,126]. Another gene delivery system that permits efficient and simple packaging of macromolecules is the multifunctional envelope-type nano-device (MEND). It consists of a condensed core of plasmid DNA, proteins or other substances and a lipid envelope equipped with various functional devices to mimic envelope-type viruses [104]. A further strategy to mitochondria specific drug carriers is the utilization of water soluble fullerene derivatives that accumulate in mitochondria as well [14,127].

Combinations of nanocarrier based strategies and targeting moieties, peptidic or non-peptidic ones are also useful approaches to mitochondrial drug targeting. A TPP modified fatty acid, stearyl triphenyl phosphonium (STPP), incorporated into liposomes that were composed of a phospholipid and cholesterol was shown to deliver molecules into mitochondria [17,128] and to improve the efficacy of ceramide as an antitumor agent [97,98]. Thereby, a proof of concept has been established which shows that targeted organelle specific drug delivery can reduce the dosage of a drug [17]. Conjugates of TPP to gold nanoparticles are under investigation, and it has to be shown, if they are also a suitable targeted delivery approach

[17]. By a study with quantum dots that are enfolded in micelles and conjugated to a mitochondrial targeting peptide, it could be demonstrated that these particles selectively accumulate in mitochondria when they are applied to intact cells [129].

Invasive and biological approaches to mitochondrial targeting

Completely different approaches to mitochondrial targeting comprise physical methods like electroporation or biolistic bombardment with DNA-coated heavy metal particles. These methods have been described to introduce DNA into mitochondria but are restricted to isolated organelles and are therefore hardly applicable in clinical treatments. It has also been reported that healthy isolated mitochondria can be endocytosed by cells, or they can be directly transferred into cells by physical methods such as microinjection or by biological methods like ovum transplantation and cytoplast fusion. In more recent methods, E. coli is used to transfer DNA into isolated mitochondria by conjugation of DNA-transformed E. coli and mitochondria [18].

Advances and techniques to probe the properties of mitochondria

The methods to study mitochondrial function can be distinguished in two principle groups. One is the analysis of mitochondria in the cellular environment, and the other one is the analysis of isolated mitochondria [106].

The methods, described in the following, allow for the investigation of mitochondrial morphology, metabolism, calcium homeostasis, membrane potential, apoptosis, respiratory activity, mitochondrial dynamics, ROS production and accumulation of substances [56,105,106].

Methods to investigate mitochondria inside cells

Approaches to study mitochondria in the cellular environment include confocal/fluorescence and electron microscopy, X-ray analysis, optical trapping, patch-clamp and flow cytometry [106]. Fluorescence based microscopy methods are applied to investigate the

permeabilization of the mitochondrial membranes induced by substances. For example, cells transfected with a mitochondrial targeted green fluorescent protein (GFP) show GFP fluorescence outside mitochondria after mitochondrial membrane permeabilization. With this method, it is also possible to detect alterations in mitochondrial membrane potential by using transmembrane potential sensitive dyes that accumulate in functional mitochondria. Agents that lead to the dissipation of the mitochondrial membrane potential alter the accumulation or the emission wavelength of the fluorescent dyes. Such studies allow detecting early stages of apoptosis that accompany with alterations in membrane potential [6,130]. Furthermore, confocal and fluorescence microscopy have been applied to investigate mitochondrial morphology, calcium uptake, ROS and mitochondrial connectivity using fluorescence recovery after photobleaching (FRAP) techniques [106]. Electron microscopy is applied to study mitochondrial morphology, membrane structure and for cytochemical determinations of mitochondrial enzymes to map metabolic activity [106]. X-ray microanalysis allows the determination of the elemental composition in mitochondria, such as calcium, iron, sodium, potassium and chloride, when a small diameter electron beam is focused on individual mitochondria [106]. Optical trapping is used to investigate the force of motion of mitochondria along microtubules, and the patch-clamping is applied to study mitochondrial membrane conductance [106]. Flow cytometry is a well-established technique to analyze mitochondria within whole cells [106]. It allows the examination of ROS production, mitochondrial cytochrome c release in apoptosis and mitochondrial transmembrane potentials [56,131–133].

Methods to investigate isolated mitochondria

Advances to study isolated mitochondria also include microscopy techniques as well as patch-clamping, optical trapping, capillary electrophoresis with laser induced fluorescence detection, functionality measurements and flow cytometry [106]. Electron microscopy allows for ultrastructural analysis, and fluorescence microscopy can be applied to determine membrane potential alterations [106]. Patch clamping monitors the electrophysiological

behavior of ion channels in membranes using a pipette electrode that is gently touched to the membrane surface. This method is suitable to study all events that are related to the opening of the mPTPC [106]. Optical trapping uses the force of laser beams and allows the analysis of only a few mitochondria. It has also been applied to measure the force with which a single mitochondrion moves along microtubules [106]. Capillary electrophoresis with laser-induced fluorescence detection has been shown to successfully separate and detect mitochondria [106]. Due to surface charges of the outer mitochondrial membrane, individual mitochondria can be separated electrophoretically. Post-column fluorescence detection then allows for the analysis of several mitochondrial features [106,134].

To determine the functionality of isolated mitochondria, it is common practice to measure oxygen consumption and phosphorylating activities of isolated mitochondria with Clark electrodes [108,135].

Flow cytometry was introduced to analyze isolated mitochondria in 1986 [136]. The advantages of flow cytometry are the capability for high throughput screening analysis [106], that it is applicable to analyze highly diluted samples and thus does not consume large amounts of isolated mitochondria. A disadvantage of this technique is that the size of mitochondria is at the lower limit of size related resolution [136]. Additionally, it is difficult to distinguish between different populations of mitochondria dependent on the size or to exclude double mitochondria from analysis. Therefore, most assays of isolated mitochondria analysis by flow cytometry are based on fluorescence measurements that allow for the analysis of individual mitochondria [137]. Alterations in membrane potential as a result of various treatments can be detected with transmembrane potential sensitive fluorescence dyes [106]. Flow cytometry further enables to measure reactive oxygen species with fluorescence dyes that react with ROS [135,138] and mitochondrial related changes during apoptosis can also be analyzed [139,140]. Fluorescently labeled antibodies can be used to determine the localization of proteins [106]. Further, the accumulation of substances or nanocarriers in mitochondria can be detected with this technique [9,47,141]. Flow cytometry has also been applied to separate individual mitochondria via a sorting device for

mitochondrial genome analysis after a following PCR amplification [106,142]. Until recently, a not described but possible application of flow cytometry is the analysis of mitochondrial dynamics, in particular mitochondrial fusion, a process that has been imitated and observed in vitro with GFP- and dsRed-transfected isolated mitochondria and analysis by microscopy techniques [143]. Flow cytometry also allows for the analysis of two and more fluorescent dyes simultaneously, i.e. multiparametric analysis, and therefore, it is thinkable that studies of mitochondrial fusion in vitro may also be carried out by flow cytometry. An even higher number of mitochondria can be investigated compared to microscopy techniques that accompany with time consuming counting of a comparatively low sample number.

Conclusions

Due to the facts that mitochondria play a crucial role in various metabolic processes of the cell, that they exhibit a lot of structural and functional features which differ from other cellular compartments and that mitochondrial dysfunction is related to several diseases, these organelles went into the focus of drug and drug delivery research. But even though mitochondria exhibit a lot of potential targets and the knowledge about functional characteristics in relation to diseases and drug action increases continuously, the field of mitochondrial research, in particular regarding drug delivery, is still in its infancy. This is certainly due to the barriers that have to be crossed to achieve a selective targeting and accumulation in mitochondria. Even though several approaches to mitochondrial drug delivery have already been accomplished, there is still a demand for more selective targeting to improve drug efficiency and the therapeutic outcome in various diseases. Thereby, applicable analytics to assure drug accumulation and their physiological effects on mitochondria are required as well.

1.2 Goals of the thesis

This thesis was focused on mitochondria as an intracellular target for drug delivery. The main idea was to accomplish targeting of mitochondria with nanomaterials by utilization of the mitochondrial fusion process instead of the mitochondrial protein import pores. To achieve recognition by mitochondria, the nanomaterials were conjugated to mitochondrial targeting peptides that are known to be recognized by mitochondria and in particular, by the mitochondrial protein import pores. This means, the goal was to combine targeting strategies by using specific targeting peptides and utilization of mitochondrial fusion to accomplish an uptake of nanomaterials into mitochondria. The challenge was to establish methods that are able to follow the individual steps of this process.

First, a protocol for the isolation of mitochondria was developed (Chapter 2). Furthermore, methods to characterize these preparations in order to demonstrate integrity and functionality of mitochondria by making use of a membrane integrity assay, staining with a potential dependent dye und analysis of mitochondrial ultrastructure by transmission electron microscopy are described.

A method, established to monitor long time functionality of isolated mitochondria in terms of their oxygen consumption, is described in Chapter 3. Analytical techniques to image isolated mitochondria and making them accessible to fluorescence microscopy and flow cytometry are described in Chapter 4.

Chapter 5 summarizes protocols to accomplish and detect mitochondrial fusion in vitro. Mitochondrial fusion in vitro was detected qualitatively by confocal laser scanning microscopy that detects merged colors of fluorescent labels and transmission electron microscopy that reveals fusion intermediates of mitochondria with distinct inner membranes and fused outer membranes. Finally, mitochondrial fusion in vitro was determined quantitatively by establishing a protocol based on flow cytometry.

The targeting of mitochondria with nanoparticles by utilization of mitochondrial fusion and several approaches to affect mitochondrial fusion itself are summarized in Chapter 6. Based on the successful in the presence of PEG, the idea evolved to affect mitochondrial fusion in

vitro specifically by other PEG derivatives and nanomaterials that carry targeting peptides which are known to be recognized by mitochondria. For this set of experiments, two different targeting peptides, a natural mitochondrial targeting sequence (MLS) and a mitochondria penetrating peptide (MPP) were conjugated to 8arm PEGs, dendrimers, a polyetheramine and quantum dots. The efficiency of these additives on mitochondrial fusion in vitro was evaluated using flow cytometry.

As a consequence of the results of affecting mitochondrial fusion efficiency in vitro, the binding behavior of the mitochondrial targeting peptides, MLS and MPP, to isolated mitochondria was investigated, described in Chapter 7. Therefore, the MLS was labeled with quantum dots and fluorescent dyes to determine binding by flow cytometry. MLS capped gold nanoparticles were synthesized for a transmission electron microscopy study. The binding behavior of the MPP was determined by a photoconversion method in transmission electron microscopy using an 8armPEG modified with MPP and a fluorescent dye.

1.3 References

[1] P.J. Hollenbeck, W. Saxton, The axonal transport of mitochondria, Journal of Cell Science 118 (2005) 5411–5419.

[2] I. Manoli, S. Alesci, G. Chrousos, Mitochondria, in: G. Fink (Ed.), Encyclopedia of stress, 2nd ed., Academic Press, San Diego, 2007, pp. 754–761.

[3] P.F. Chinnery, E.A. Schon, Mitochondria, Journal of Neurology, Neurosurgery & Psychiatry 74 (2003) 1188–1199.

[4] J.S. Modica-Napolitano, K.K. Singh, Mitochondrial dysfunction in cancer, Mitochondrion 4 (2004) 755–762.

[5] M.-C. Frantz, P. Wipf, Mitochondria as a target in treatment, Environ. Mol. Mutagen 51 (2010) 462–475.

[6] S. Fulda, L. Galluzzi, G. Kroemer, Targeting mitochondria for cancer therapy, Nat Rev Drug Discov 9 (2010) 447–464.

[7] R.A.J. Smith, M.P. Murphy, Mitochondria-targeted antioxidants as therapies, Discov Med 11 (2011) 106–114.

[8] S. Moghimi, A. Hunter, T. Andresen, Factors Controlling Nanoparticle Pharmacokinetics: An Integrated Analysis and Perspective, Annu. Rev. Pharmacol. Toxicol 52 (2012) 481–503.

[9] G.G. D'Souza, M.A. Wagle, V. Saxena, A. Shah, Approaches for targeting mitochondria in cancer therapy, Biochimica et Biophysica Acta (BBA) - Bioenergetics 1807 (2011) 689–696.

[10] V.J. Stella, W.N. Charman, V.H. Naringrekar, Prodrugs. Do they have advantages in clinical practice?, Drugs 29 (1985) 455–473.

[11] J.H. Lin, A.Y. Lu, Role of pharmacokinetics and metabolism in drug discovery and development, Pharmacol. Rev 49 (1997) 403–449.

[12] H. Ringsdorf, Structure and properties of pharmacologically active polymers, J. polym. sci., C Polym. symp 51 (1975) 135–153.

[13] M.L. Immordino, F. Dosio, L. Cattel, Stealth liposomes: review of the basic science, rationale, and clinical applications, existing and potential, Int J Nanomedicine 1 (2006) 297–315.

[14] V.P. Torchilin, Recent Approaches to Intracellular Delivery of Drugs and DNA and Organelle Targeting, Annu. Rev. Biomed. Eng 8 (2006) 343–375.

[15] E. Blanco, A. Hsiao, A.P. Mann, M.G. Landry, F. Meric-Bernstam, M. Ferrari, Nanomedicine in cancer therapy: Innovative trends and prospects, Cancer Science 102 (2011) 1247–1252.

[16] D.R. Lewis, K. Kamisoglu, A.W. York, P.V. Moghe, Polymer-based therapeutics: nanoassemblies and nanoparticles for management of atherosclerosis, WIREs Nanomed Nanobiotechnol 3 (2011) 400–420.

[17] G.G.M. D'Souza, V. Weissig, Subcellular targeting: a new frontier for drug-loaded pharmaceutical nanocarriers and the concept of the magic bullet, Expert Opin. Drug Deliv 6 (2009) 1135–1148.

[18] G.G.M. D'Souza, S.V. Boddapati, V. Weissig, Gene Therapy of the Other Genome: The Challenges of Treating Mitochondrial DNA Defects, Pharm Res 24 (2007) 228–238.

[19] K. Cho, X. Wang, S. Nie, Z. Chen, D.M. Shin, Therapeutic Nanoparticles for Drug Delivery in Cancer, Clinical Cancer Research 14 (2008) 1310–1316.

[20] A.Z. Wang, F. Gu, L. Zhang, J.M. Chan, A. Radovic-Moreno, M.R. Shaikh, O.C. Farokhzad, Biofunctionalized targeted nanoparticles for therapeutic applications, Expert Opin Biol Ther 8 (2008) 1063–1070.

[21] E. Voltz, H. Gronemeyer, A new era of cancer therapy: Cancer cell targeted therapies are coming of age, The International Journal of Biochemistry & Cell Biology 40 (2008) 1–8.

[22] F. Mangialasche, A. Solomon, B. Winblad, P. Mecocci, M. Kivipelto, Alzheimer's disease: clinical trials and drug development, The Lancet Neurology 9 (2010) 702–716.

[23] A. Sosnik, Á.M. Carcaboso, R.J. Glisoni, M.A. Moretton, D.A. Chiappetta, New old challenges in tuberculosis: Potentially effective nanotechnologies in drug delivery, Advanced Drug Delivery Reviews 62 (2010) 547–559.

[24] J. Sun, Z. Lin, J. Feng, Y. Li, B. Shen, BAFF-targeting therapy, a promising strategy for treating autoimmune diseases, European Journal of Pharmacology 597 (2008) 1–5.

[25] S. Kunjachan, S. Gupta, A.K. Dwivedi, A. Dube, M.K. Chourasia, Chitosan-based macrophage-mediated drug targeting for the treatment of experimental visceral leishmaniasis, Journal of Microencapsulation 28 (2011) 301–310.

[26] V.P. Torchilin, Passive and active drug targeting: drug delivery to tumors as an example, in: M. Schäfer-Korting (Ed.), Drug Delivery, 2010, pp. 3–53.

[27] D. Peer, J.M. Karp, S. Hong, O.C. Farokhzad, R. Margalit, R. Langer, Nanocarriers as an emerging platform for cancer therapy, Nature Nanotech 2 (2007) 751–760.

[28] S.A. Kularatne, P.S. Low, Targeting of Nanoparticles: Folate Receptor, in: S.R. Grobmyer, B.M. Moudgil (Eds.), Methods in Molecular Biology, Humana Press, Totowa, NJ, 2010, pp. 249–265.

[29] P. Kocbek, N. Obermajer, M. Cegnar, J. Kos, J. Kristl, Targeting cancer cells using PLGA nanoparticles surface modified with monoclonal antibody, Journal of Controlled Release 120 (2007) 18–26.

[30] Y. Teow, S. Valiyaveettil, Active targeting of cancer cells using folic acid-conjugated platinum nanoparticles, Nanoscale 2 (2010) 2607.

[31] J. You, X. Li, F. de Cui, Y.-Z. Du, H. Yuan, F.q. Hu, Folate-conjugated polymer micelles for active targeting to cancer cells: preparation, in vitro evaluation of targeting ability and cytotoxicity, Nanotechnology 19 (2008) 45102.

[32] M. Talekar, J. Kendall, W. Denny, S. Garg, Targeting of nanoparticles in cancer, Anti-Cancer Drugs 22 (2011) 949–962.

[33] F. Pene, E. Courtine, A. Cariou, J.-P. Mira, Toward theragnostics, Critical Care Medicine 37 (2009) S50–58.

[34] V.H.J. van der Velden, J.G. te Marvelde, P.G. Hoogeveen, I.D. Bernstein, A.B. Houtsmuller, M.S. Berger, J.J.M. van Dongen, Targeting of the CD33-calicheamicin immunoconjugate Mylotarg (CMA-676) in acute myeloid leukemia: in vivo and in vitro saturation and internalization by leukemic and normal myeloid cells, Blood 97 (2001) 3197–3204.

[35] C. Rousselle, P. Clair, J.M. Lefauconnier, M. Kaczorek, J.M. Scherrmann, J. Temsamani, New advances in the transport of doxorubicin through the blood-brain barrier by a peptide vector-mediated strategy, Mol. Pharmacol 57 (2000) 679–686.

[36] J.C.W. Edwards, L. Szczepanski, J. Szechinski, A. Filipowicz-Sosnowska, P. Emery, D.R. Close, R.M. Stevens, T. Shaw, Efficacy of B-cell-targeted therapy with rituximab in patients with rheumatoid arthritis, N. Engl. J. Med 350 (2004) 2572–2581.

[37] P. Kan, C.-W. Tsao, A.-J. Wang, W.-C. Su, H.-F. Liang, A Liposomal Formulation Able to Incorporate a High Content of Paclitaxel and Exert Promising Anticancer Effect, Journal of Drug Delivery 2011 (2011) 1–9.

[38] S. Martins, B. Sarmento, D.C. Ferreira, E.B. Souto, Lipid-based colloidal carriers for peptide and protein delivery--liposomes versus lipid nanoparticles, Int J Nanomedicine 2 (2007) 595–607.

[39] D.J. Bharali, I. Klejbor, E.K. Stachowiak, P. Dutta, I. Roy, N. Kaur, E.J. Bergey, P.N. Prasad, M.K. Stachowiak, Organically modified silica nanoparticles: A nonviral vector for in vivo gene delivery and expression in the brain, Proceedings of the National Academy of Sciences 102 (2005) 11539–11544.

[40] Y. Patil, J. Panyam, Polymeric nanoparticles for siRNA delivery and gene silencing, International Journal of Pharmaceutics 367 (2009) 195–203.

[41] Y. Yamada, H. Akita, K. Kogure, H. Kamiya, H. Harashima, Mitochondrial drug delivery and mitochondrial disease therapy--an approach to liposome-based delivery targeted to mitochondria, Mitochondrion 7 (2007) 63–71.

[42] J. Ding, F. Shi, C. Xiao, L. Lin, L. Chen, C. He, X. Zhuang, X. Chen, One-step preparation of reduction-responsive poly(ethylene glycol)-poly(amino acid)s nanogels as efficient intracellular drug delivery platforms, Polym. Chem 2 (2011) 2857–2864.

[43] J. das Neves, J. Michiels, K.K. Ariën, G. Vanham, M. Amiji, M.F. Bahia, B. Sarmento, Polymeric Nanoparticles Affect the Intracellular Delivery, Antiretroviral Activity and Cytotoxicity of the Microbicide Drug Candidate Dapivirine, Pham Res (2011), http://www.ncbi.nlm.nih.gov/pubmed/22072053.

[44] P. Costantini, E. Jacotot, D. Decaudin, G. Kroemer, Mitochondrion as a Novel Target of Anticancer Chemotherapy, J. Natl. Cancer Inst 92 (2000) 1042–1053.

[45] S.W. Lowe, A.W. Lin, Apoptosis in cancer, Carcinogenesis 21 (2000) 485–495.

[46] V. Weissig, G.G.M. D'Souza, Organelle-specific pharmaceutical nanotechnology, Wiley, Hoboken, NJ, 2010.

[47] H. Sneh-Edri, D. Likhtenshtein, D. Stepensky, Intracellular Targeting of PLGA Nanoparticles Encapsulating Antigenic Peptide to the Endoplasmic Reticulum of Dendritic Cells and Its Effect on Antigen Cross-Presentation in Vitro, Mol. Pharmaceutics 8 (2011) 1266–1275.

[48] D. Stepensky, Quantitative Aspects of Intracellularly-Targeted Drug Delivery, Pharm Res 27 (2010) 2776–2780.

[49] S. Fleischer, G. Rouser, B. Fleischer, A. Casu, G. Kritchevsky, Lipid composition of mitochondria from bovine heart, liver, and kidney, J. Lipid Res 8 (1967) 170–180.

[50] S.A. Detmer, D.C. Chan, Functions and dysfunctions of mitochondrial dynamics, Nat Rev Mol Cell Biol 8 (2007) 870–879.

[51] L.B. Chen, Mitochondrial Membrane Potential in Living Cells, Annu. Rev. Cell. Biol 4 (1988) 155–181.

[52] J.-Y. Huang, M.D. Hirschey, T. Shimazu, L. Ho, E. Verdin, Mitochondrial sirtuins, Biochimica et Biophysica Acta (BBA) - Proteins & Proteomics 1804 (2010) 1645–1651.

[53] M.W. Gray, W.F. Doolittle, Has the endosymbiont hypothesis been proven?, Microbiol. Rev 46 (1982) 1–42.

[54] J.S. Modica-Napolitano, K.K. Singh, Mitochondria as targets for detection and treatment of cancer, Expert Rev Mol Med 4 (2002) 1–19.

[55] Invitrogen - Molecular Probes - The Handbook, Probes for Mitochondria—Section 12.2, http://de-de.invitrogen.com/site/de/de/home/References/Molecular-Probes-The-Handbook/Probes-for-Organelles/Probes-for-Mitochondria.html.

[56] V. Weissig, Mitochondrial-targeted drug and DNA delivery, Crit Rev Ther Drug Carrier Syst 20 (2003) 1–62.

[57] S. DiMauro, E.A. Schon, Mitochondrial DNA mutations in human disease, Am. J. Med. Genet 106 (2001) 18–26.

[58] F. Hartl, N. Pfanner, D.W. Nicholson, W. Neupert, Mitochondrial protein import, Biochimica et Biophysica Acta (BBA) - Reviews on Biomembranes 988 (1989) 1–45.

[59] B.V. Chernyak, O.Y. Pletjushkina, D.S. Izyumov, K.G. Lyamzaev, A.V. Avetisyan, Bioenergetics and death, Biochemistry (Moscow) 70 (2005) 240–245.

[60] I.R. Boldogh, L.A. Pon, Mitochondria on the move, Trends in Cell Biology 17 (2007) 502–510.

[61] D.C. Chan, Mitochondrial Fusion and Fission in Mammals, Annu. Rev. Cell Dev. Biol 22 (2006) 79–99.

[62] H. Chen, M. Vermulst, Y.E. Wang, A. Chomyn, T.A. Prolla, J.M. McCaffery, D.C. Chan, Mitochondrial Fusion Is Required for mtDNA Stability in Skeletal Muscle and Tolerance of mtDNA Mutations, Cell 141 (2010) 280–289.

[63] M.B. de Moura, L.S. dos Santos, B. van Houten, Mitochondrial dysfunction in neurodegenerative diseases and cancer, Environ. Mol. Mutagen 51 (2010) 391–405.

[64] C. Chinopoulos, V. Adam-Vizi, Calcium, mitochondria and oxidative stress in neuronal pathology: Novel aspects of an enduring theme, FEBS Journal 273 (2006) 433–450.

[65] D. Harman, Aging: a theory based on free radical and radiation chemistry, J Gerontol 11 (1956) 298–300.

[66] V.J. Thannickal, B.L. Fanburg, Reactive oxygen species in cell signaling, Am. J. Physiol. Lung Cell Mol. Physiol 279 (2000) L1005-1028.

[67] N. Pfanner, M. Meijer, Mitochondrial biogenesis: The Tom and Tim machine, Current Biology 7 (1997) R100–103.

[68] P.F. Chinnery, Searching for nuclear-mitochondrial genes, Trends in Genetics 19 (2003) 60–62.

[69] N. Pfanner, A. Geissler, Versatility of the mitochondrial protein import machinery, Nat. Rev. Mol. Cell Biol 2 (2001) 339–349.

[70] V. Weissig, V.P. Torchilin, Towards mitochondrial gene therapy: DQAsomes as a strategy, J Drug Target 9 (2001) 1–13.

[71] J.S. Carew, Y. Zhou, M. Albitar, J.D. Carew, M.J. Keating, P. Huang, Mitochondrial DNA mutations in primary leukemia cells after chemotherapy: clinical significance and therapeutic implications, Leukemia 17 (2003) 1437–1447.

[72] P.F. Chinnery, N. Howell, R.N. Lightowlers, D.M. Turnbull, MELAS and MERRF. The relationship between maternal mutation load and the frequency of clinically affected offspring, Brain 121 (Pt 10) (1998) 1889–1894.

[73] S. DiMauro, Mitochondrial diseases, Biochimica et Biophysica Acta (BBA) - Bioenergetics 1658 (2004) 80–88.

[74] X. Li, N. Kazgan, Mammalian Sirtuins and Energy Metabolism, Int. J. Biol. Sci 7 (2011) 575–587.

[75] M.C. Haigis, L.P. Guarente, Mammalian sirtuins-emerging roles in physiology, aging, and calorie restriction, Genes & Development 20 (2006) 2913–2921.

[76] Y. Tsujimoto, Apoptosis and necrosis: intracellular ATP level as a determinant for cell death modes, Cell Death Differ 4 (1997) 429–434.

[77] J. Santo-Domingo, N. Demaurex, Calcium uptake mechanisms of mitochondria, Biochimica et Biophysica Acta (BBA) - Bioenergetics 1797 (2010) 907–912.

[78] P.F. Chinnery, Gene Reviews: Mitochondrial Disorders Overview. Mitochondrial Encephalomyopathies, Mitochondrial Myopathies, Oxidative Phosphorylation Disorders, Respiratory Chain Disorders, http://www.ncbi.nlm.nih.gov/books/NBK1224/.

[79] D.C. Wallace, Mitochondrial diseases in man and mouse, Science 283 (1999) 1482–1488.

[80] I.J. Holt, A.E. Harding, R.K. Petty, J.A. Morgan-Hughes, A new mitochondrial disease associated with mitochondrial DNA heteroplasmy, Am. J. Hum. Genet 46 (1990) 428–433.

[81] J.A. Mayr, T.B. Haack, E. Graf, F.A. Zimmermann, T. Wieland, B. Haberberger, A. Superti-Furga, J. Kirschner, B. Steinmann, M.R. Baumgartner, I. Moroni, E. Lamantea, M. Zeviani, R.J. Rodenburg, J. Smeitink, T.M. Strom, T. Meitinger, W. Sperl, H. Prokisch, Lack of the Mitochondrial Protein Acylglycerol Kinase Causes Sengers Syndrome, The American Journal of Human Genetics 90 (2012) 314–320.

[82] X. Wang, B. Su, H.-g. Lee, X. Li, G. Perry, M.A. Smith, X. Zhu, Impaired balance of mitochondrial fission and fusion in Alzheimer's disease, J. Neurosci 29 (2009) 9090–9103.

[83] J.E. Selfridge, E. Lezi, J. Lu, R.H. Swerdlow, Role of mitochondrial homeostasis and dynamics in Alzheimer's disease, http://www.ncbi.nlm.nih.gov/pubmed/22266017.

[84] S. DiMauro, K. Tanji, E. Bonilla, F. Pallotti, E.A. Schon, Mitochondrial abnormalities in muscle and other aging cells: Classification, causes, and effects, Muscle Nerve 26 (2002) 597–607.

[85] J.N. Keller, G.W. Glazner, Mitochondrial oxidative stress and metabolic alterations in neurodegenerative disorders, in: M.P. Mattson (Ed.), Advances in Cell Aging and Gerontology: Interorganelle Signaling in Age-Related diseases, 2001, pp. 205–237.

[86] P.F. Chinnery, D.M. Turnbull, Mitochondrial DNA mutations in the pathogenesis of human disease, Mol Med Today 6 (2000) 425–432.

[87] J.S. Armstrong, Mitochondria: a target for cancer therapy, Br. J. Pharmacol 147 (2006) 239–248.

[88] S. Kasibhatla, B. Tseng, Why target apoptosis in cancer treatment?, Mol. Cancer Ther 2 (2003) 573–580.

[89] V. Weissig, From Serendipity to Mitochondria-Targeted Nanocarriers, Pharm Res 28 (2011) 2657–2668.

[90] E. Holmuhamedov, L. Lewis, M. Bienengraeber, M. Holmuhamedova, A. Jahangir, A. Terzic, Suppression of human tumor cell proliferation through mitochondrial targeting, FASEB J 16 (2002) 1010–1016.

[91] D. Morin, T. Hauet, M. Spedding, J.-P. Tillement, Mitochondria as target for antiischemic drugs, Adv. Drug Deliv. Rev 49 (2001) 151–174.

[92] M. Lagouge, C. Argmann, Z. Gerhart-Hines, H. Meziane, C. Lerin, F. Daussin, N. Messadeq, J. Milne, P. Lambert, P. Elliott, B. Geny, M. Laakso, P. Puigserver, J. Auwerx, Resveratrol Improves Mitochondrial Function and Protects against Metabolic Disease by Activating SIRT1 and PGC-1α, Cell 127 (2006) 1109–1122.

[93] E.A. Schon, S. DiMauro, M. Hirano, R.W. Gilkerson, Therapeutic prospects for mitochondrial disease, Trends in Molecular Medicine 16 (2010) 268–276.

[94] Santhera Pharmaceuticals Holding AG, Santhera's Marketing Authorization Application for Idebenone in LHON Accepted for Review by European Medicines Agency, 2011, http://hugin.info/137261/R/1532611/466727.pdf.

[95] S.J. Ralph, J. Neuzil, Mitochondria as targets for cancer therapy, Mol. Nutr. Food Res 53 (2009) 9–28.

[96] L. Rajendran, H.-J. Knölker, K. Simons, Subcellular targeting strategies for drug design and delivery, Nat Rev Drug Discov 9 (2010) 29–42.

[97] T.C. Stover, A. Sharma, G.P. Robertson, M. Kester, Systemic Delivery of Liposomal Short-Chain Ceramide Limits Solid Tumor Growth in Murine Models of Breast Adenocarcinoma, Clinical Cancer Research 11 (2005) 3465–3474.

[98] S.V. Boddapati, G.G.M. D'Souza, S. Erdogan, V.P. Torchilin, V. Weissig, Organelle-Targeted Nanocarriers: Specific Delivery of Liposomal Ceramide to Mitochondria Enhances Its Cytotoxicity in Vitro and in Vivo, Nano Lett. 8 (2008) 2559–2563.

[99] M.P. Mattson, G. Kroemer, Mitochondria in cell death: novel targets for neuroprotection and cardioprotection, Trends in Molecular Medicine 9 (2003) 196–205.

[100] J. Morgan, A.R. Oseroff, Mitochondria-based photodynamic anti-cancer therapy, Adv. Drug Deliv. Rev 49 (2001) 71–86.

[101] H.H. Szeto, Mitochondria-targeted peptide antioxidants: Novel neuroprotective agents, AAPS J 8 (2006) E277–283.

[102] K. Zhao, G.-M. Zhao, D. Wu, Y. Soong, A.V. Birk, P.W. Schiller, H.H. Szeto, Cell-permeable Peptide Antioxidants Targeted to Inner Mitochondrial Membrane inhibit Mitochondrial Swelling, Oxidative Cell Death, and Reperfusion Injury, Journal of Biological Chemistry 279 (2004) 34682–34690.

[103] E. Gnaiger, Isolated Mitochondria or Permeabilized tissues and Cells, http://www.oroboros.at/fileadmin/user_upload/Protocols/MiPNet11.05_Mitos-PermeabilizedCells.pdf.

[104] Y. Yamada, H. Harashima, Mitochondrial drug delivery systems for macromolecule and their therapeutic application to mitochondrial diseases☆, Advanced Drug Delivery Reviews 60 (2008) 1439–1462.

[105] M. Duvvuri, W. Feng, A. Mathis, J.P. Krise, A Cell Fractionation Approach for the Quantitative Analysis of Subcellular Drug Disposition, Pharm Res 21 (2004) 26–32.

[106] K.M. Fuller, E.A. Arriaga, Advances in the analysis of single mitochondria, Curr. Opin. Biotechnol 14 (2003) 35–41.

[107] M.D. Brand, D.G. Nicholls, Assessing mitochondrial dysfunction in cells, Biochem. J 435 (2011) 297–312.

[108] C. Frezza, S. Cipolat, L. Scorrano, Organelle isolation: functional mitochondria from mouse liver, muscle and cultured filroblasts, Nat Protoc 2 (2007) 287–295.

[109] E. Fernández-Vizarra, G. Ferrín, A. Pérez-Martos, P. Fernández-Silva, M. Zeviani, J.A. Enríquez, Isolation of mitochondria for biogenetical studies: An update, Mitochondrion 10 (2010) 253–262.

[110] N.R. Sims, M.F. Anderson, Isolation of mitochondria from rat brain using Percoll density gradient centrifugation, Nat Protoc 3 (2008) 1228–1239.

[111] H.-T. Hornig-Do, G. Günther, M. Bust, P. Lehnartz, A. Bosio, R.J. Wiesner, Isolation of functional pure mitochondria by superparamagnetic microbeads, Analytical Biochemistry 389 (2009) 1–5.

[112] M.R. Duchen, Roles of Mitochondria in Health and Disease, Diabetes 53 (2004) S96–102.

[113] V. Salnikov, Y. Lukyánenko, C. Frederick, W. Lederer, V. Lukyánenko, Probing the Outer Mitochondrial Membrane in Cardiac Mitochondria with Nanoparticles, Biophysical Journal 92 (2007) 1058–1071.

[114] M.P. Schwartz, A. Matouschek, The dimensions of the protein import channels in the outer and inner mitochondrial membranes, PNAS 96 (1999) 13086–13090.

[115] N. Pfanner, K.N. Truscott, Powering mitochondrial protein import, Nat. Struct Biol 9 (2002) 234–236.

[116] A. Parfenov, V. Salnikov, W. Lederer, V. Lukyánenko, Aqueous Diffusion Pathways as a Part of the Ventricular Cell Ultrastructure, Biophysical Journal 90 (2006) 1107–1119.

[117] R.W. Horobin, S. Trapp, V. Weissig, Mitochondriotropics: A review of their mode of action, and their applications for drug and DNA delivery to mammalian mitochondria, Journal of Controlled Release 121 (2007) 125–136.

[118] E. Liberman, V. Skulachev, Conversion of biomembrane-produced energy into electric form. IV. General discussion, Biochimica et Biophysica Acta (BBA) - Bioenergetics 216 (1970) 30–42.

[119] K.L. Horton, K.M. Stewart, S.B. Fonseca, Q. Guo, S.O. Kelley, Mitochondria-Penetrating Peptides, Chemistry & Biology 15 (2008) 375–382.

[120] L.F. Yousif, K.M. Stewart, K.L. Horton, S.O. Kelley, Mitochondria-Penetrating Peptides: Sequence Effects and Model Cargo Transport, ChemBioChem 10 (2009) 2081–2088.

[121] V. Sebbage, Cell-penetrating peptides and their therapeutic applications, Bioscience Horizons 2 (2009) 64–72.

[122] J.P. Richard, K. Melikov, E. Vives, C. Ramos, B. Verbeure, M.J. Gait, L.V. Chernomordik, B. Lebleu, Cell-penetrating Peptides. A Reevaluation of the Mechanism of Cellular Uptake, Journal of Biological Chemistry 278 (2002) 585–590.

[123] A. Muratovska, R.N. Lightowlers, R.W. Taylor, J.A. Wilce, M.P. Murphy, Targeting large molecules to mitochondria, Adv. Drug Deliv. Rev 49 (2001) 189–198.

[124] V. Weissig, J. Lasch, G. Erdos, H.W. Meyer, T.C. Rowe, J. Hughes, DQAsomes: a novel potential drug and gene delivery system made from Dequalinium, Pharm. Res 15 (1998) 334–337.

[125] Y.T. Ko, C. Falcao, V.P. Torchilin, Cationic liposomes loaded with proapoptotic peptide D-(KLAKLAK)(2) and Bcl-2 antisense oligodeoxynucleotide G3139 for enhanced anticancer therapy, Mol. Pharm 6 (2009) 971–977.

[126] Y. Yamada, H. Akita, H. Kamiya, K. Kogure, T. Yamamoto, Y. Shinohara, K. Yamashita, H. Kobayashi, H. Kikuchi, H. Harashima, MITO-Porter: A liposome-based carrier system for delivery of macromolecules into mitochondria via membrane fusion, Biochimica et Biophysica Acta (BBA) - Biomembranes 1778 (2008) 423–432.

[127] S. Foley, C. Crowley, M. Smaihi, C. Bonfils, B.F. Erlanger, P. Seta, C. Larroque, Cellular localisation of a water-soluble fullerene derivative, Biochem. Biophys. Res. Commun 294 (2002) 116–119.

[128] S.V. Boddapati, P. Tongcharoensirikul, R.N. Hanson, G.G.M. D'Souza, V.P. Torchilin, V. Weissig, Mitochondriotropic liposomes, J Liposome Res 15 (2005) 49–58.

[129] A. Hoshino, K. Fujioka, T. Oku, S. Nakamura, M. Suga, Y. Yamaguchi, K. Suzuki, M. Yasuhara, K. Yamamoto, Quantum dots targeted to the assigned organelle in living cells, Microbiol. Immunol 48 (2004) 985–994.

[130] D.C. Joshi, J.C. Bakowska, Determination of Mitochondrial Membrane Potential and Reactive Oxygen Species in Live Rat Cortical Neurons, Journal of Viszualized Experiments (2011) 1–4.

[131] D. Cassart, T. Fett, M. Sarlet, E. Baise, F. Coignoul, D. Desmecht, Flow cytometric probing of mitochondrial function in equine peripheral blood mononuclear cells, BMC Vet Res 3 (2007) 1–7.

[132] M. Poot, R.H. Pierce, Analysis of mitochondria by flow cytometry, Methods Cell Biol 64 (2001) 117–128.

[133] G. Lamm, P. Steinlein, M. Cotten, G. Christofori, A rapid, quantitative and inexpensive method for detecting apoptosis by flow cytometry in transiently transfected cells, Nucleic Acids Research 25 (1997) 4855–4857.

[134] B.G. Poe, M. Navratil, E.A. Arriaga, Analysis of subcellular sized particles, Journal of Chromatography A 1137 (2006) 249–255.

[135] T. Wakabayashi, M.A. Teranishi, M. Karbowski, Y. Nishizawa, J. Usukura, C. Kurono, T. Soji, Functional aspects of megamitochondria isolated from hydrazine- and ethanol-treated rat livers, Pathol. Int 50 (2000) 20–33.

[136] P. Petit, P. Diolez, P. Muller, S.C. Brown, Binding of concanavalin A to the outer membrane of potato tuber mitochondria detected by flow cytometry, FEBS Letters 196 (1986) 65–70.

[137] J.M. Medina, C. López-Mediavilla, A. Orfao, Flow cytometry of isolated mitochondria during development and under some pathological conditions, FEBS Letters 510 (2002) 127–132.

[138] P. Mukhopadhyay, M. Rajesh, K. Yoshihiro, G. Haskó, P. Pacher, Simple quantitative detection of mitochondrial superoxide production in live cells, Biochemical and Biophysical Research Communications 358 (2007) 203–208.

[139] R.A. Gottlieb, D.J. Granville, Analyzing mitochondrial changes during apoptosis, Methods 26 (2002) 341–347.

[140] B.H. Kang, M.D. Siegelin, J. Plescia, C.M. Raskett, D.S. Garlick, T. Dohi, J.B. Lian, G.S. Stein, L.R. Languino, D.C. Altieri, Preclinical Characterization of Mitochondria-Targeted Small Molecule Hsp90 Inhibitors, Gamitrinibs, in Advanced Prostate Cancer, Clinical Cancer Research 16 (2010) 4779–4788.

[141] N. Zheng, H.N. Tsai, X. Zhang, G.R. Rosania, The Subcellular Distribution of Small Molecules: From Pharmacokinetics to Synthetic Biology, Mol. Pharmaceutics 8 (2011) 1619–1628.

[142] L. Cavelier, A. Johannisson, U. Gyllensten, Analysis of mtDNA copy number and composition of single mitochondrial particles using flow cytometry and PCR, Exp. Cell Res 259 (2000) 79–85.

[143] S. Meeusen, J.M. McCaffery, J. Nunnari, Mitochondrial Fusion Intermediates Revealed in Vitro, Science 305 (2004) 1747–1752.

Chapter 2

Isolation of mitochondria and characterization of isolated mitochondria preparations

Abstract

A protocol for the isolation of mitochondria from CHO-K1 cells based on differential centrifugation in an isotonic isolation buffer was established. Several purification procedures were evaluated regarding to their applicability for the preparative separation of isolated mitochondria from cell fragments. The protein concentration of the crude isolated mitochondrial fraction was determined using a Bradford-Assay. Integrity of the outer mitochondrial membranes was evaluated by Cytochrome c Oxidase Assay, revealing that more than 90 % of mitochondria were intact immediately after isolation. Furthermore, the accumulation of the membrane potential sensitive fluorescent dye JC-1 in isolated mitochondria indicated intactness of mitochondrial membranes and hence, functionality of mitochondria. The characterization of isolated mitochondria by transmission electron microscopy (TEM) revealed typical features of mitochondria such as the double membrane that is folded into cristae. The size of isolated mitochondria was also determined by TEM and photon correlation spectroscopy.

2.1 Introduction

The isolation of mitochondria can be a necessary procedure for many purposes [1]. It can be the step prior to the purification of mitochondrial subcomponents such as proteins or nucleic acids, the performance of metabolic measurements such as respiratory activity measurements or enzymatic assays and the performance of metabolic analyses on biogenetic activity [1,2]. Isolation of mitochondria can also be utilized as a subsequent step following the application of molecules or nanocarriers to intact cells, to determine site and extent of their subcellular accumulation [3,4]. It can also be used as the primary step in such targeting approaches to bypass the cellular membrane and to prevent endocytosis and lysosomal or cytosolic degradation of the molecules or carriers that are intended to target mitochondria. Although working with isolated mitochondria is controversially discussed and exhibits disadvantages such as the lack of signaling processes and the risk of damaging mitochondria [5,6] it can be helpful in first approaches toward targeting mitochondria in which the organelle and not overcoming the cellular membrane is primary goal of the investigations.

Over the years, numerous isolation procedures with several modifications depending on the differences in tissues or cells have evolved. Most of them comprise the basic steps of rupturing cells or homogenizing tissues and differential centrifugation with a first centrifugation step at low speed to pelletize nuclei und unbroken cells and a second centrifugation step at higher speed to pelletize mitochondria [1]. These steps are usually carried out in a special isolation buffer. The composition of such buffers varies between different protocols but they usually contain sugars or sugar alcohols to adjust the osmolarity, buffering agents such as Tris or HEPES to adjust the pH and EDTA to chelate divalent cations which can act as uncouplers by inhibition of the coupling between respiratory chain and oxidative phosphorylation followed by impaired mitochondrial metabolic activity. Additionally, other salts can be added to isolation buffers for special requirements of further investigations. Some protocols make use of hypotonic buffers that cause swelling of the cells and ease rupturing. But such buffers may also cause swelling and damage of mitochondria

that is why isotonic buffers should be preferred. Usually all steps of the isolation procedures are carried out on ice to reduce enzymatic activity and to prevent degradation processes. There are different methods to break cells or to rupture tissues such as Dounce-type glass homogenizers with loose- or tight-fitting glass pestles or Elvehjem-type glass potters with motor-driven Teflon pestles that break cells due to liquid shear forces [1,7]. Nitrogen cavitation, sonication and mechanical homogenization by the Ultra-Turrax® are other methods to rupture cells [7]. Beside differential centrifugation following the rupture of cells, other methods to separate mitochondria are antibody-based immunoisolation approaches [7,8] and separation by electrophoresis [7]. Especially the differential centrifugation procedures result in crude mitochondrial preparations with several contaminants such as fragments of the cell membrane and other organelles. Working with these crude mitochondrial fractions can be sufficient but in case of isolation of mitochondrial components such as proteins or nucleic acid further purification steps might be required [1].

Purification methods make use of density gradients and ultracentrifugation. Gradient media vary from polyhydric alcohols such as sucrose, glycerol or sorbitol, to polysaccharides such as dextran and Ficoll®, and Percoll® that consists of colloidal silica [7,9]. Different gradient types can be distinguished: discontinuous gradients formed by layering techniques, continuous gradients and self-generating gradients. Percoll® is easy to handle as it consists of polydispers silica particles that are able to form a continuous density gradient by themselves via ultracentrifugation without time-consuming layering techniques. It is usable to separate populations of cell organelles based in their density [4]. All gradient media and gradient types have advantages and disadvantages and hence limitations [7,10]. For example, a limit of sucrose, glycerol and sorbitol gradients is the high osmolarity that can cause damage of the osmotically active mitochondria [7,10]. Therefore, the purification method has to be carefully selected with respect to the source of mitochondria and requirements of further investigations. Another method to purify isolated mitochondria is the utilization of size exclusion chromatography [11]. General disadvantageous of all purification methods are that they are time consuming and lower the already limited metabolic activity of

isolated mitochondria. They also lead to dilution of the mitochondrial fraction and loss of material. Therefore, purification steps should only be applied when they are reasonable.

To characterize and standardize or rather determine the yield of the mitochondrial preparation, it is common practice to determine the protein content of the mitochondrial fraction or to assess mitochondrial enzyme activity [1,12]. A standard method to determine protein concentrations is the Bradford assay, a colorimetric assay that is based on the absorbance shift of coomassie blue from 495 nm to 595 nm after binding to proteins [13]. It has to be considered that contaminants in the mitochondrial preparation can adulterate the results when using unpurified mitochondrial fractions.

The determination of mitochondrial functionality and integrity includes the measurement of the activity of various mitochondrial enzymes, the determination of the mitochondrial membrane potential, the evaluation of mitochondrial respiratory activity and the analysis of the mitochondrial ultrastructure [1,7,14,15].

The assessment of the outer mitochondrial membrane integrity is necessary due to risk of outer membrane damage during isolation [7] leading to loss of functionality. The loss of outer mitochondrial membrane integrity inside the cell and the release of cytochrome c into the cytosol lead to apoptosis [16]. Therefore, the determination of cytochrome c oxidase activity is a useful tool to determine the extent of mitochondrial outer membrane damage of isolated mitochondria [17]. It is a rapid and convenient method assaying the rate of oxidation of exogenous, reduced cytochrome c. Exogenous cytochrome c cannot penetrate the outer mitochondria membrane and is only oxidized when it has access to the cytochrome c oxidase in the inner mitochondrial membrane due to damage of the outer mitochondrial membrane. The more exogenous cytochrome c is oxidized, the more damaged mitochondria are present in the preparation. Disruption of mitochondria with a suitable detergent unmasks complete cytochrome c activity and is set as a reference value in comparison to intact mitochondria [7].

JC-1 (5,5',6,6'-tetrachloro-1,1',3,3'-tetraethylbenzimidazolylcarbocyanine iodide) is a fluorescent dye that accumulates in a membrane potential dependent manner in

mitochondria followed by a fluorescence shift from green (529 nm) in the cytosol to red (590 nm) in mitochondria by the formation of so called J-aggregates. It can be used as an indicator of the mitochondrial membrane potential in intact cells as well as isolated mitochondria and as an indicator for early stages of apoptosis [17].

The determination of mitochondrial ultrastructure and extent of possible damages can be directly assessed by using electron microscopy although this technique allows only qualitative investigations, is time consuming and particularly not convenient [7].

In this study, the establishment of a differential centrifugation method for the isolation of mitochondria will be described as well as approaches toward purification by Percoll® gradients, ultrafiltration and size exclusion chromatography.

The characterization methods for isolated mitochondria focus on the determination of the protein concentration, mitochondrial outer membrane integrity, mitochondrial membrane potential, mitochondrial ultrastructure, mitochondrial fusion competence and respiratory activity.

2.2 Materials and methods

2.2.1 Materials

HAM F-12 nutrient mixture and fetal calf serum (FCS) were purchased from Sigma-Aldrich (Steinheim, Germany). Trypsin-EDTA 0.25 % was obtained from Gibco-Invitrogen (Karlsruhe, Germany). Purified water was obtained by using a Milli-Q water purification system from Millipore (Schwalbach, Germany). All cell culture materials were purchased from Corning (Bodenheim, Germany).

Isolation buffer consisted of 250 mM sucrose (Merck, Darmstadt, Germany), 10 mM Tris (USB Corporation, Cleveland, OH USA), 10 mM KCl (Merck, Darmstadt, Germany), 1 mM Na_2EDTA (Merck, Darmstadt, Germany) and 0.1 % bovine serum albumin (BSA) (Sigma-Aldrich, Steinheim, Germany). Percoll® was obtained from Sigma-Aldrich (Steinheim, Germany). Ultrafree-MC centrifugal filter units with microporous Durapore membrane (PVDF) and a pore size of 0.45 µm were purchased from Millipore (Schwalbach, Germany). PD-10 columns filled with Sephadex G-25 medium and Sephacryl™ S-1000 were obtained from GE Healthcare (Freiburg, Germany). Bradford-reagent was prepared by dissolving 100 mg Coomassie Brilliant Blue G250 (Sigma-Aldrich, Steinheim, Germany) in 50 ml ethanol 95 %, 100 ml ortho-phosphoric acid 85 % (Merck, Darmstadt, Germany) and subsequent addition of purified water to 1000 ml. The mixture was filtrated through a folded filter afterwards and stored in the dark. The Cytochrome c Oxidase Assay Kit was purchased from Sigma-Aldrich (Steinheim, Germany). JC-1 was obtained from Invitrogen (Karlsruhe, Germany). Antimycin A was purchased from Sigma-Aldrich (Steinheim, Germany). DPBS without calcium and magnesium was obtained from Gibco-Invitrogen (Karlsruhe, Germany).

0.1 M cacodylate fixation buffer consisted of 100 mM sodium cacodylate (Roth, Karlsruhe, Germany), 2 mM magnesium chloride hexahydrate (Merck, Darmstadt, Germany), 1 mM calcium chloride dihydrate (Merck, Darmstadt, Germany), 40 mM sodium chloride (Merck, Darmstadt, Germany) and 2 % glutaraldehyde (Serva, Heidelberg, Germany). 0.1 M cacodylate washing buffer consisted of 100 mM sodium cacodylate (Roth, Karlsruhe, Germany), 2 mM magnesium chloride hexahydrate (Merck, Darmstadt, Germany), 1 mM

calcium chloride dihydrate (Merck, Darmstadt, Germany) and 40 mM sodium chloride (Merck, Darmstadt, Germany). Osmium tetroxide (ScienceServices, Munich, Germany) was dissolved to 1 % in 0.1 M cacodylate buffer that consisted of 100 mM sodium cacodylate (Roth, Karlsruhe, Germany), 2 mM magnesium chloride hexahydrate (Merck, Darmstadt, Germany), 1 mM calcium chloride dihydrate (Merck, Darmstadt, Germany) and 40 mM sodium chloride (Merck, Darmstadt, Germany). Agarose was purchased from Biozym (Hessisch Oldendorf, Germany). Embedding in Epon was carried out with an Epoxy Embedding Medium Kit (Fluka by Sigma-Aldrich, Steinheim, Germany). Propylen oxide was purchased from Sigma-Aldrich (Steinheim, Germany). Uranyl acetate was obtained from Roth (Karlsruhe, Germany). Lead citrate by Reynolds consisted of lead nitrate (Merck, Darmstadt, Germany) and tri-sodium citrate dihydrate (Merck, Darmstadt, Germany).

2.2.2 Establishment of a protocol for the isolation of mitochondria

CHO-K1 cells were cultured in HAM-F12 nutrient mixture containing 10 % FCS in 150 cm^2 culture flasks until confluency, harvested by Trypsin-EDTA 0.25 % and washed with isolation buffer. The centrifugation steps for the washing steps of the cells were carried out in a GS-15R centrifuge (Beckman, Krefeld, Germany). Afterwards, cells from one culture flask were suspended in 250 µl isolation buffer. Then, cells from four flasks were pooled and the resulting one milliliter of cell suspension was transferred into a cooled 2-ml Dounce glass homogenizer (Sigma-Aldrich, Steinheim, Germany) where the cells were disrupted by 25 strokes. The suspension was transferred into a 2-ml safe-lock tube (Eppendorf, Hamburg, Germany) and centrifuged at 1500 g at 4 °C for 10 min a type 5415 R centrifuge (Eppendorf, Hamburg, Germany) to pelletize nuclei as well as remaining intact cells. The first supernatant was kept on ice, while the pellet was resuspended in isolation buffer and homogenized by 25 Dounce strokes for a second time to break remaining intact cells. A second centrifugation step at 1500 g at 4 °C for 10 min yielded a pellet that was the nuclei enriched fraction. The first and the second supernatant were mixed and centrifuged at 16000 g at 4 °C for 15 min to obtain a pellet that was the mitochondria enriched fraction. The supernatant of this last

centrifugation step was considered an organelle-free soluble fraction. The isolation process is depicted in Figure 2.1. The amount of cells used for the isolation of mitochondria depended on the required amount for the different experiments.

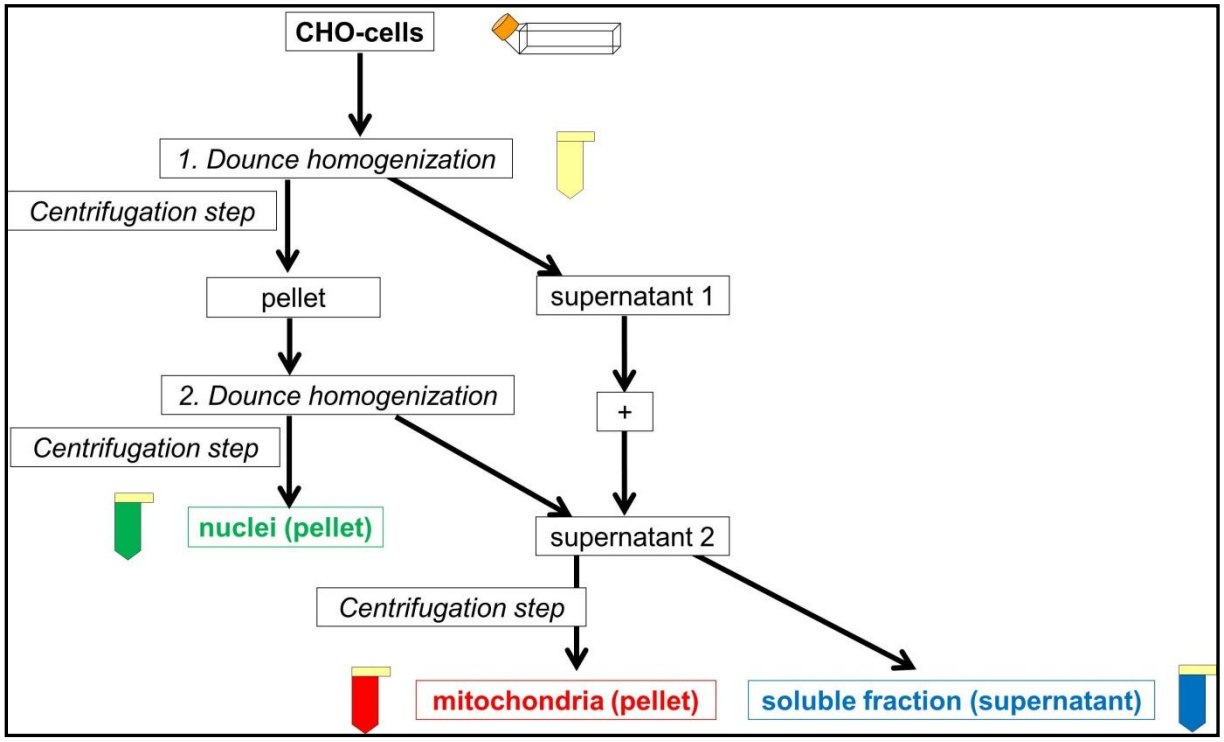

Figure 2.1: Isolation of mitochondria from CHO-cells by differential centrifugation.

2.2.3 Purification of isolated mitochondria

Cells were cultured and mitochondria were isolated as described previously. For purification of isolated mitochondria by a Percoll® gradient, the Percoll® solution was diluted to different initial densities according to the provider´s instruction [18]. The pH of the initial solution was adjusted to 7.4 with 0.1 N HCl and the osmolarity was adjusted to 280 mosmol/l by a 2.5 M sucrose solution. The volume of the initial solution for each gradient was 10 ml. Various gradients were formed via ultracentrifugation in a TFT70.13 rotor. After ultracentrifugation, each gradient was separated into 12 fractions with 800 µl each. The density range of the gradients was determined by refractive index and calculated according to Pertoft [19]. Three different initial densities were tested: an initial density of 1.04 g/ml, ultracentrifuged at 27100 rpm = 50000 g that resulted in a gradient of 1.15 g/ml – 1.1 g/ml, an initial density of 1.09 g/ml, ultracentrifuged at 27200 rpm = 50132 g that formed a gradient of 1.19 g/ml –

1.08 g/ml and an initial density of 1.1 g/ml, ultracentrifuged at 20000 rpm = 27104 g that resulted in a gradient of 1.19 g/ml – 1.11 g/ml. The fractions of the gradients were stained with JC-1 2.5 µg/ml and fluorescence was determined with a fluorescence spectrometer LS55 (Perkin-Elmer, Rodgau, Germany).

Purification of isolated mitochondria by ultrafiltration was carried out in centrifugal filter units with a pore size of 0.45 µm at 4°C and 12000 g for 5 min in a type 5415 R centrifuge (Eppendorf, Hamburg, Germany) to separate cell fragments with a size lower than 0.45 µm and to obtain purified isolated mitochondria as the filtration residue. The size of separated mitochondria and particles was determined by photon correlation spectroscopy (PCS).

Purification of isolated mitochondria by size exclusion chromatography was carried out in PD-10 columns filled with Sephadex G-25 medium. 20 fractions with 1 ml each were collected and the size of separated mitochondria and particles was determined by PCS. As a second gel filtration medium, Sephacryl™ S-1000 was filled into a 10 ml syringe to obtain a gel filtration column. Isolated mitochondria were layered on top and 20 fractions with each 1 ml were collected. The size of separated mitochondria and particles was determined by photon correlation spectroscopy (PCS).

2.2.4 Characterization of mitochondrial protein concentration (Bradford-Assay)

Cells were cultured and mitochondria were isolated as described previously. For the determination of mitochondrial protein concentration, a calibration curve with 1, 2, 4, 6, 8 and 10 µg/µl BSA was recorded to calculate the protein concentration of the mitochondrial fraction. Each sample of the calibration curve and the mitochondrial fraction was diluted to 100 µl with purified water in micro-cuvettes. Then, 1 ml of Bradford-reagent was added, mixed and incubated at room temperature in the dark for 10 min. Afterwards, absorption of the coomassie-protein-complexes at 595 nm was determined by a Kontron Instruments Uvikon 900 spectrophotometer (Goebel Instrumentelle Analytik, Hallertau, Germany).

2.2.5 Characterization of mitochondrial outer membrane integrity (Cytochrome c Oxidase Assay)

Cells were cultured and mitochondria were isolated as described previously. The principle of the Cytochrome c Oxidase Assay is based on the impermeability of the outer mitochondrial membrane to exogenous cytochrome c. The cytochrome c oxidase is located at the inner mitochondrial membrane. If the outer mitochondrial membrane is intact, added ferrocytochrome c cannot be oxidized to ferricytochrome c by the cytochrome c oxidase. In case of outer mitochondrial membrane damage, the exogenous substrate has access to the enzyme and can be oxidized, resulting in a decrease of absorbance of ferrocytochrome c at 550 nm. For the determination of mitochondrial membrane integrity, ferrocytochrome c was added to a sample of isolated mitochondria and absorption of ferrocytochome c at 550 nm was measured to determine the cytochrome c oxidase activity of intact mitochondria. To calculate the amount of undamaged mitochondria according to the provider´s instruction [20], it was also necessary to determine the total cytochrome c oxidase activity. Therefore, the outer mitochondrial membrane of an isolated mitochondria sample was lysed by the detergent n-dodecyl-β-D-maltoside and absorption of added ferrocytochrome c was also measured at 550 nm. The concentration of mitochondrial protein was determined by Bradford-assay [13]. Isolated mitochondria were diluted to a concentration of 0.2 mg/ml and 2 µg of mitochondrial protein were used for each sample. All absorption measurements were carried out at a Kontron Instruments Uvikon 900 spectrophotometer (Goebel Instrumentelle Analytik, Hallertau, Germany) immediately after isolation and 1 h, 2 h, 4 h and 5 h after isolation.

2.2.6 Determination of mitochondrial membrane potential (JC-1)

Cells were cultured and mitochondria were isolated as described previously. The carbocyanine dye JC-1 forms red fluorescent J-aggregates with an emission wave length maximum of 590 nm when it is taken up into the mitochondrial matrix compared to green fluorescent monomers with an emission wave length maximum of 529 nm. Isolated

mitochondria were stained with 2.5 µg/ml JC-1. Additionally, isolated mitochondria were treated with 10 µM antimycin A for 30 min. Fluorescence was determined by the fluorescence spectrometer LS55 (Perkin-Elmer, Rodgau, Germany).

2.2.7 Characterization of mitochondrial ultrastructure (transmission electron microscopy – TEM)

Cells were cultured and mitochondria were isolated as described previously. Isolated mitochondria were fixed in cacodylate fixation buffer at room temperature for 5 min and on ice overnight. Afterwards, mitochondria were washed by five washing steps, each of them in cacodylate washing buffer for 2 min. Then, isolated mitochondria were pelletized in a 1 % agarose solution that was heated up to 40 °C. All centrifugation steps were carried out in a himac CT15RE (VWR Leuven, Belgium by Hitachi Koki Co. Ltd.). After gelation of the agarose, the gel block was cut and fixed with osmium tetroxide solution overnight. Then, the samples were washed in DPBS four times for 15 min. Afterwards, the samples were dehydrated in a graded series of ethanol: 50 %, 70 %, 80 %, 90 % and 100 %. Each dehydration step was carried out two times for 15 min. Then, the samples were treated in an equal mixture of acetone or propylene oxide and ethanol for 20 min and two times in acetone or propylene oxide for 20 min. Afterwards, the samples were treated with a mixture of acetone or propylene oxide and Epon (2:1) for 2 h, then, in a mixture of acetone or propylene oxide and Epon (1:1) for 2 h and subsequently in a mixture of acetone or propylene oxide and Epon (1:2) in an open vial overnight. Then, the samples were embedded and hardened in Epon at room temperature for 1 h, at 30 °C for 2 h and at 60 °C for 2 days.

Epon blocks were cut into sections of 50 nm with a microtome Leica EM UC6 (Leica, Vienna, Austria) and transferred to copper slot grids with a 1.5 % hyaloform foil. They were examined either unstained or stained with uranyl acetate and lead citrate in a transmission electron microscope Zeiss EM 902 (Carl Zeiss, Oberkochen, Germany), operating at 80kV. Digital images were recorded by a slow scan CCD camera (TRS Typ 7888, Serial No. 321/08).

2.2.8 Characterization of mitochondrial size

Cells were cultured and mitochondria were isolated as described previously. Measurements of the hydrodynamic diameter of isolated mitochondria by photon correlation spectroscopy (PCS) were carried out with a Zetasizer nano ZS (Malvern, Herrenberg, Germany). All size measurements were carried out in isolation buffer at 25 °C.

2.3 Results and discussion

An isolation procedure comprising homogenization by a Dounce-type homogenizer and differential centrifugation was established. It was essential to start with an appropriate amount of cultured cells to obtain a visible and experimentally manageable pellet of the mitochondrial fraction. Thereby, the amount of cells that were cultured prior to the isolation procedure varied from 12 to 24 150 cm^2 culture flasks, or sometimes more, depending on the sample size of the study. The final protocol for the isolation of mitochondria that was used for all studies with isolated mitochondria is described in the materials and methods section.

The mitochondrial fraction was purified by Percoll®-gradients, by ultrafiltration and by size exclusion chromatography. The Percoll®-gradients were separated into 12 fractions and the presence of isolated mitochondria was determined by measuring the fluorescence intensity of JC-1, with which isolated mitochondria were stained prior to the purification procedure. Various initial densities of the Percoll® suspension and different centrifugation conditions were investigated. All of them led to a high dilution of the mitochondrial fraction with almost no more detectable fluorescence of JC-1 in the Percoll®-fractions (Figure 2.2).

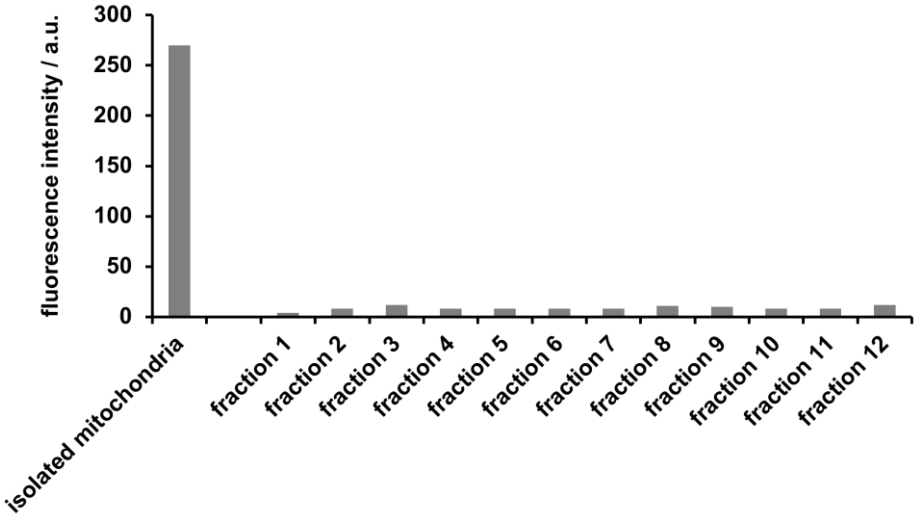

Figure 2.2: Fluorescence intensity of isolated mitochondria and isolated mitochondria after separation into 12 Percoll® fractions. Isolated mitochondria and Percoll® fractions were stained with 2.5 µl/ml JC-1. JC-1 was excited at 490 nm and emission of J-aggregates was detected at 590 nm.

It was also not possible to separate isolated mitochondria from the Percoll®-fractions preparatively. For the purification of isolated mitochondria by ultrafiltration, ultrafiltration units with a cut-off of 0.45 µm were used to separate cell fragments that were smaller than 0.45 µm from isolated mitochondria. The size of the cell fragments and isolated mitochondria in the filtrate and filter residue was determined by photon correlation spectroscopy. Before ultrafiltration, the mitochondrial fraction contained one population of particles with a size of 500-600 nm which approximately corresponds to the size of isolated mitochondria [21]. After ultrafiltration, one population of particles with a size of 190 nm was detected in the filtrate and two populations of particles with a size of 100 nm (90 %) and 500-600 nm (10 %) were detected in the filter residue. Hence, it was possible to separate fragments with a size lower than isolated mitochondria but the mitochondrial fraction was divided into two populations with a high amount of small fragments compared to a low amount of particles that were in the size-range of isolated mitochondria. Maybe, isolated mitochondria were disrupted during the ultrafiltration process leading to this high amount of small fragments in the filter residue. Therefore, ultrafiltration was not a suitable method for the purification of isolated mitochondria. For the purification of isolated mitochondria by size exclusion chromatography, two gel filtration media were investigated. 20 fractions 1 ml each were collected and the size of the fragments and isolated mitochondria was determined by photon correlation spectroscopy. Before gel filtration, the mitochondrial fraction contained one population of particles with a size of 500-600 nm. After gel filtration through a Sephadex G 25 column, two populations of particles, 100 nm (90 %) and 500-600 nm (6-10 %) were detected in the fractions 8-12. After gel filtration through the Sephacyrl medium, particles of 200-300 nm were detected in all fractions. Hence, it seemed that isolated mitochondria were disrupted by both gel filtration media. Beside this, the preparation became highly diluted and it was not possible to separate isolated mitochondria from the fractions preparatively. Therefore, size exclusion chromatography was also not a suitable method for the purification of isolated mitochondria and all studies were carried out with the crude isolated mitochondrial fraction.

For standardization and to determine the yield of the mitochondrial preparation, the protein concentration of each isolated mitochondrial preparation was determined. Therefore, a Bradford-assay [13] was applied after isolation and prior to entering into further experiments. The protein concentration was calculated by a calibration curve that was recorded at the beginning of each assay. One example is shown in Figure 2.3.

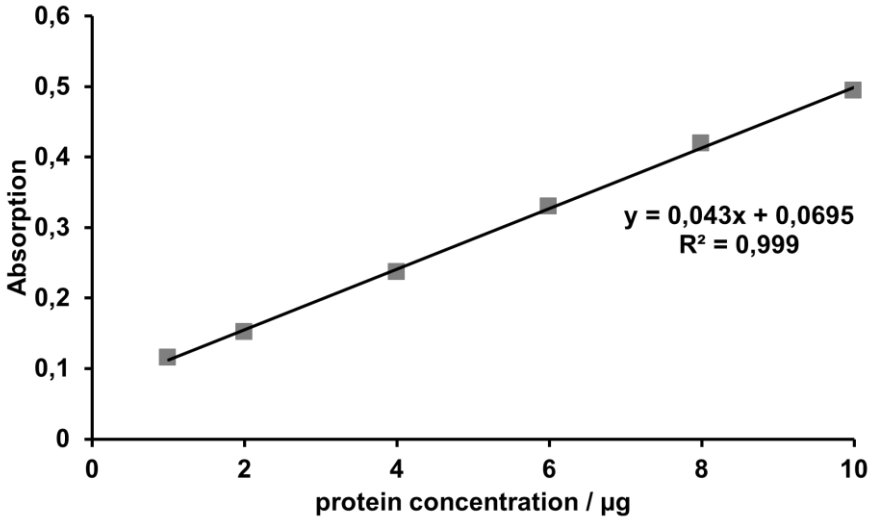

Figure 2.3: Calibration curve of a Bradford Assay determined by UV-Vis absorption at 595 nm.

One 150 cm^2 culture flask with approximately 25 million cells yielded 61 ± 16 µg mitochondrial protein (mean of 20 measurements ± standard deviation).

Beside the yield of the mitochondrial preparation, the integrity of the isolated mitochondria preparation was determined as only intact mitochondria are functional. Therefore, the integrity of the outer mitochondrial membrane was examined by the Cytochrome c Oxidase assay [20]. The established differential centrifugation protocol for the isolation of mitochondria yielded in an amount of 91.9 ± 0.6 % undamaged mitochondria (mean of three individual isolated mitochondria preparations ± standard deviation). This value gave evidence that the used isolation procedure did not disrupt the majority of isolated mitochondria and was comparable to data from literature that report on 8-44 % damaged mitochondria that were isolated from various tissues [22]. Additionally, the integrity of the outer membrane and the amount of intact mitochondria was determined over a period of 5 h as most of the studies with isolated mitochondria described in this thesis took over a period of several hours.

Figure 2.4 shows that the amount of intact mitochondria decreased over time but even after 4 h, over 80 % of mitochondria were intact. After 5 h, the standard deviation increased indicating the loss of integrity after this period of time.

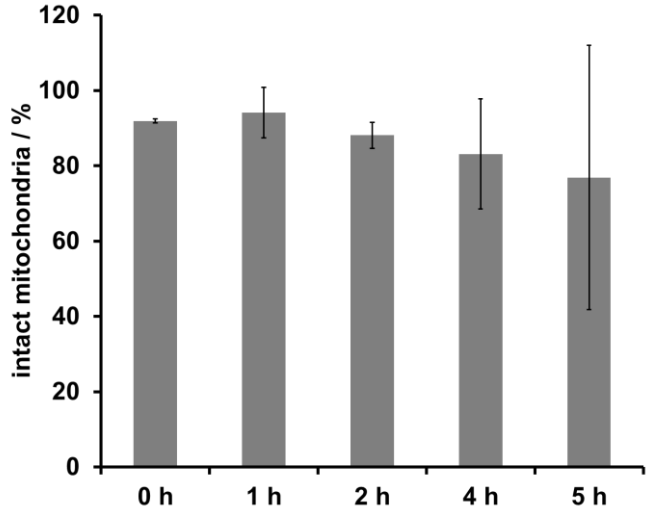

Figure 2.4: Determination of the amount of intact mitochondria immediately after isolation and 1 h, 2 h, 4 h, and 5 h after isolation by Cytochrome c Oxidase Assay [20]. Data are expressed as means of three measurements ± standard deviations (SD).

The membrane potential was also an indicator for the intactness and functionality of isolated mitochondria. If isolated mitochondria were intact and functional, the membrane potential could be determined by the accumulation of JC-1 in mitochondria and the formation of J-aggregates that showed fluorescence at 590 nm. Figure 2.5 shows the fluorescence intensity of JC-1 stained isolated mitochondria at 590 nm compared to isolated mitochondria that were treated with antimycin A, an inhibitor of the respiratory chain. Isolated mitochondria treated with antimycin A showed almost no more fluorescence intensity because the membrane potential was disrupted.

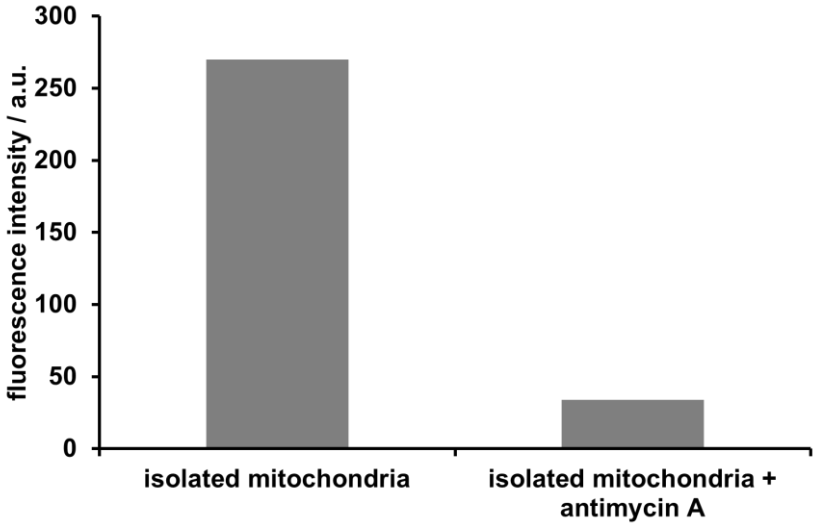

Figure 2.5: Determination of the fluorescence intensity of isolated mitochondria and isolated mitochondria treated with antimycin A after staining with 2.5 µg/ml JC-1. JC-1 was excited at 490 nm and emission of J-aggregates was detected at 590 nm.

The investigation of the ultrastructure of isolated mitochondria was another method to study the integrity of isolated mitochondrial membranes. Figure 2.6, 2.7 and 2.8 show transmission electron microscopy (TEM) images of an isolated mitochondrial preparation. The figures gave evidence that the applied isolation procedure led to a crude mitochondrial fraction containing intact isolated mitochondria but also a lot of cell fragments. The images also show that isolated mitochondria had a size of approximately 500-1000 nm.

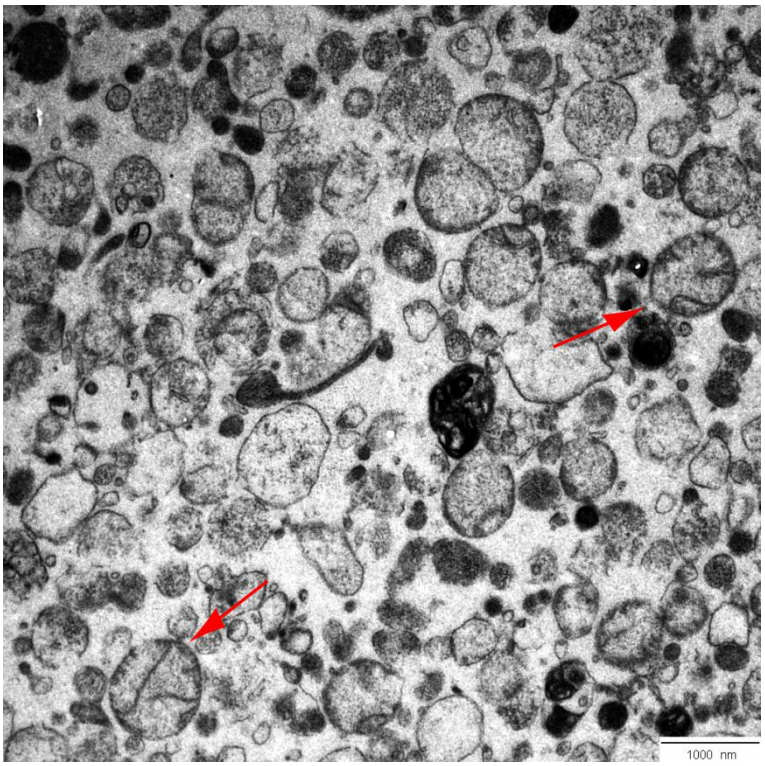

Figure 2.6: TEM image of an isolated mitochondria preparation, 7000x magnification, red arrows indicate intact isolated mitochondria.

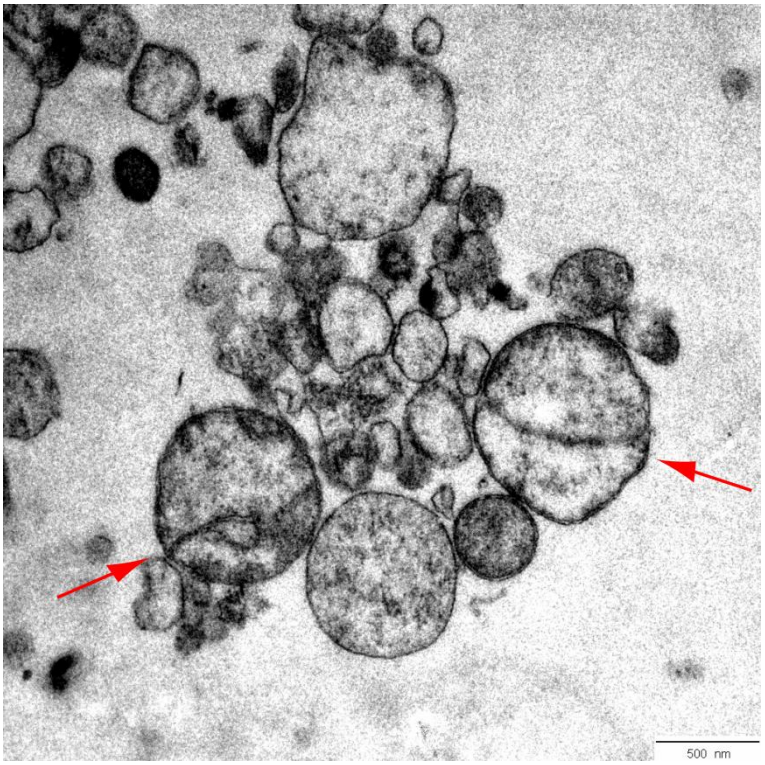

Figure 2.7: TEM image of an isolated mitochondria preparation, 12000x magnification, red arrows indicate intact isolated mitochondria.

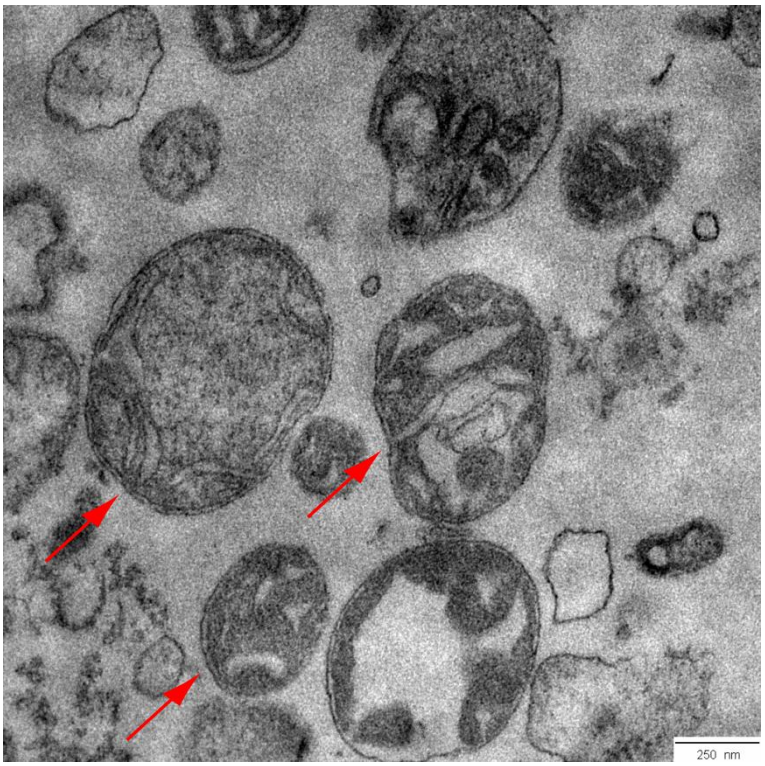

Figure 2.8: TEM image of an isolated mitochondria preparation, 20000x magnification, red arrows indicate intact isolated mitochondria.

Beside the determination of the size of isolated mitochondria by TEM images, the size was also determined by photon correlation spectroscopy. This method was also applied for the characterization of purified isolated mitochondrial samples, described previously. Furthermore, the size was determined over a period of several hours. Immediately after isolation, one population with a size of 500-600 nm was found. After 2.5 h, the size of the population increased up to 600-700 nm indicating a swelling of mitochondria. Beside the 600-700 nm population, a population of 100 nm fragments was detectable after 5 h, indicating disrupture of mitochondria. These results corresponded to the results of the Cytochrome c Oxidase assay.

2.4 Conclusions

The goals of this study were to establish a suitable protocol for the isolation of mitochondria from cultured cells and to characterize these isolated mitochondria. An isolation procedure can be either quick or time consuming especially when purification steps follow the isolation process. All investigated purification methods were time consuming, led to dilution of the samples and therefore, were not applicable for preparative purposes. Additionally, ultrafiltration and gel filtration led to disrupture of isolated mitochondria. As it depends on the requirements of the subsequent studies, it should be decided as the case arises whether purification steps are reasonable or not. In case of the studies presented in this thesis, it was essential to obtain intact and functional mitochondria that showed functionality over several hours. Therefore, a quick isolation protocol without further purification steps was established. It led to a crude mitochondrial fraction containing intact isolated mitochondria and cell fragments as the TEM studies showed. Staining with the potential sensitive dye JC-1 showed intactness of isolated mitochondria by the presence of the mitochondrial membrane potential. The Cytochrome c Oxidase assay showed that a high amount of isolated mitochondria was intact after isolation with the established protocol, indicating that the isolation procedure was very gentle. It was also shown that mitochondria were intact for up to 4 h after isolation which means that all studies with isolated mitochondria should be accomplished within 4 h.

.

2.5 References

[1] E. Fernández-Vizarra, P. Fernández-Silva, J.A. Enríquez, Isolation of Mitochondria from Mammalian Tissues and Cultured Cells, in: J.E. Celis (Ed.), Cell biology: A Laboratory Handbook, Acad. Press, San Diego, Calif, 2006, pp. 69–77.

[2] E. Fernández-Vizarra, G. Ferrín, A. Pérez-Martos, P. Fernández-Silva, M. Zeviani, J.A. Enríquez, Isolation of mitochondria for biogenetical studies: An update, Mitochondrion 10 (2010) 253–262.

[3] Y. Yamada, H. Harashima, Mitochondrial drug delivery systems for macromolecule and their therapeutic application to mitochondrial diseases☆, Advanced Drug Delivery Reviews 60 (2008) 1439–1462.

[4] M. Duvvuri, W. Feng, A. Mathis, J.P. Krise, A cell fractionation approach for the quantitative analysis of subcellular drug disposition, Pharm. Res 21 (2004) 26–32.

[5] M.D. Brand, D.G. Nicholls, Assessing mitochondrial dysfunction in cells, Biochem. J 435 (2011) 297–312.

[6] K.M. Fuller, E.A. Arriaga, Advances in the analysis of single mitochondria, Curr. Opin. Biotechnol 14 (2003) 35–41.

[7] J.M. Graham, D. Rickwood, Subcellar fractionation: A practical approach, IRL press, Oxford, op. 1997.

[8] H.-T. Hornig-Do, G. Günther, M. Bust, P. Lehnartz, A. Bosio, R.J. Wiesner, Isolation of functional pure mitochondria by superparamagnetic microbeads, Analytical Biochemistry 389 (2009) 1–5.

[9] N.R. Sims, M.F. Anderson, Isolation of mitochondria from rat brain using Percoll density gradient centrifugation, Nat Protoc 3 (2008) 1228–1239.

[10] J.M. Graham, D. Rickwood, Biological centrifugation, Bios, Oxford, 2001.

[11] J.L. Harley, M.K. Black, R.T. Wedding, Preparation of plant mitochondria using gel filtration columns, New Phytol 81 (1978) 223–231.

[12] C. Frezza, S. Cipolat, L. Scorrano, Organelle isolation: functional mitochondria from mouse liver, muscle and cultured filroblasts, Nat Protoc 2 (2007) 287–295.

[13] M.M. Bradford, A rapid and sensitive method for the quantitation of microgram quantities of protein utilizing the principle of protein-dye binding, Analytical Biochemistry 72 (1976) 248–254.

[14] S. Hauptmann, I. Scherping, S. Dröse, U. Brandt, K.L. Schulz, M. Jendrach, K. Leuner, A. Eckert, W.E. Müller, Mitochondrial dysfunction: an early event in Alzheimer pathology accumulates with age in AD transgenic mice, Neurobiol. Aging 30 (2009) 1574–1586.

[15] A. Pecinová, Z. Drahota, H. Nůsková, P. Pecina, J. Houštěk, Evaluation of basic mitochondrial functions using rat tissue homogenates, Mitochondrion 11 (2011) 722–728.

[16] S. Pervin, R. Singh, G. Chaudhuri, Nitric-oxide-induced Bax integration into the mitochondrial membrane commits MDA-MB-468 cells to apoptosis: essential role of Akt, Cancer Res 63 (2003) 5470–5479.

[17] D. Sareen, P.R. van Ginkel, J.C. Takach, A. Mohiuddin, S.R. Darjatmoko, D.M. Albert, A.S. Polans, Mitochondria as the Primary Target of Resveratrol-Induced Apoptosis in Human Retinoblastoma Cells, Investigative Ophthalmology & Visual Science 47 (2006) 3708–3716.

[18] Sigma, Product Information Percoll.

[19] H. Pertoft, Fractionation of cells and subcellular particles with Percoll, J. Biochem. Biophys. Methods 44 (2000) 1–30.

[20] Sigma, Product Information Cytochrome c Oxidase Assay.

[21] M.H. Burgos, A. Aoki, F.L. Sacerdote, Ultrastructure of isolated kidney mitochondria treated with phlorizin and ATP, J. Cell Biol. 23 (1964) 207–215.

[22] L. Wojtczak, H. Zaluska, A. Wroniszewska, A.B. Wojtczak, Assay for the intactness of the outer membrane in isolated mitochondria, Acta Biochim. Pol. 19 (1972) 227–234.

Chapter 3

Long time monitoring of the respiratory activity of isolated mitochondria

Experimental Cell Research 318 (2012) 1667–1672

Abstract

We have investigated the ability of optical oxygen sensors incorporated in a microplate to determine the respiratory activity of cell fractions. Different cell fractions were monitored, in particular to evaluate the long term functionality of isolated mitochondria. It is possible to continuously sense respiratory activity of isolated mitochondria over time. We found that they are functional for three hours but stop respiring at a critical limit of 20 % air saturation in the system. Furthermore, inhibition and enhancement of respiratory activity were detected. In conclusion, oxygen sensors are a powerful tool to evaluate the functionality of isolated mitochondria.

Keywords

Isolated mitochondria, respiratory activity, optical oxygen sensor, high throughput screening

3.1 Introduction

Due to the emergence of evidence that mitochondria are involved in diseases [1] such as cancer [2,3], neurodegenerative diseases [4–6] and diabetes [7,8] mitochondria have become an increasingly important target of contemporary cellular research [9–12].

Studies with isolated mitochondria are thereby common practice and have been applied to several aspects of mitochondrial research, such as mitochondrial physiology [13], altered mitochondrial function in diseases [14], biogenetical activities like mtDNA expression, tRNA aminoacylation, protein synthesis and protein import [15]. In addition, the influence of substances on mitochondrial respiratory competence [16], the accumulation of drugs [17] and drug carriers [18] have also been reported.

Isolated mitochondria are advantageous in that experimental conditions can be precisely controlled and adapted to the requirements of the scientific approach by supplementation of substrates, inhibiting and uncoupling substances. Hence, isolation of mitochondria is a widely used procedure in mitochondrial research. Numerous protocols have evolved over the years, making use of fast methods, such as differential centrifugation [19], more time-consuming gradient-purification procedures [17,20] and antibody-based approaches [21]. The choice of the method depends on the source of mitochondria and the respective research goal.

The ultimate goal of a preparation of isolated mitochondria is to obtain the organelles as functional as possible. Therefore, it is common practice to measure the functionality of isolated mitochondria in terms of their oxygen consumption [19]. Amperometry is the standard method for the determination of oxygen partial pressure in aqueous solutions by using Clark electrodes. Even though they are sensitive, Clark electrodes suffer from a number of drawbacks in that they are difficult to miniaturize, consume oxygen, are limited to discrete measurements and difficult to use in high throughput applications [22]. Measurements with such oxygen electrodes are carried out over a short period of time and can, therefore, only be used on respiring mitochondria that have been obtained prior to entering into further experiments. Optical sensors and microplate based systems can overcome these limitations [22] allowing the possibility to work with moderate sample

volumes, hence limiting the wastage of the majority of the preparation and making it possible to measure over long periods of time [23]. The quantification of dissolved oxygen with such systems was first described for cytotoxicity and proliferation assays of living cells [23–26] and more recently for isolated mitochondria. The influence of cisplatin on the respiratory activity of isolated mitochondria [27] and a high throughput method [28] have been reported.

The advantages of optical oxygen sensors compared to standard amperometry methods led us to the establishment of a method that monitors the oxygen consumption of cell fractions (in particular isolated mitochondria) over a long period of time, consumes only a small part of the preparation, is easy to handle and allows for automation in high throughput assays. Applications of this method in various biological, medical and pharmacological experiments should be conceivable.

A 96 well microplate with optical oxygen sensors was integrated in a polymer film in the bottom of each well (OxoPlate®) and served to determine oxygen depletion by monitoring the oxygen concentration in the surrounding medium continuously over a period of four hours. Different cell fractions obtained from CHO-K1 cells were monitored and particular attention was paid to the respiratory competence of the mitochondria-enriched fraction. The sensitivity of isolated mitochondria to respiration inhibiting and uncoupling substances was also studied.

3.2 Materials and methods

3.2.1 Materials

The isolation buffer consisted of 250 mM sucrose (Merck, Darmstadt, Germany), 10 mM Tris (USB Corporation, Cleveland, OH USA), 10 mM KCl (Merck, Darmstadt, Germany), 1 mM Na_2EDTA (Merck, Darmstadt, Germany) and 0.1 % BSA (Sigma-Aldrich, Steinheim, Germany). The respiration buffer consisted of 250 mM sucrose (Merck, Darmstadt, Germany), 10 mM Tris (USB Corporation, Cleveland, OH USA), 2 mM K_2HPO_4 (Merck, Darmstadt, Germany), 5 mM succinic acid (Sigma-Aldrich, Steinheim, Germany), 1 mM Na_2EDTA (Merck, Darmstadt, Germany) and 0.4 mM ADP (Sigma-Aldrich, Steinheim, Germany). Antimycin A and carbonyl cyanide 4-(trifluoromethoxy)phenylhydrazone (FCCP) were purchased from Sigma-Aldrich (Steinheim, Germany). The microtiter plate with integrated optical sensos for oxygen (OxoPlate®) was obtained from PreSens (Regensburg, Germany) and paraffin oil was purchased from Caelo (Hilden, Germany).

3.2.2 Preparation of cell fractions

Three cell fractions: the mitochondria enriched fraction, the nuclei enriched fraction and the organelle-free soluble fraction were obtained using a modified differential centrifugation procedure based on methods that were reviewed by Fernández-Vizarra [15]. In brief, CHO-K1 cells were cultured until confluency in culture flasks of 150 cm^2, then harvested and washed with isolation buffer. Cells from one culture flask were suspended in 250 µl isolation buffer. Then, cells were pooled from four flasks and the resulting one milliliter cell suspension was transferred into a 2-ml Dounce glass homogenizer (Sigma-Aldrich, Steinheim, Germany), where the cells were disrupted by 25 strokes. The suspension was transferred into a 2-ml safe-lock tube (Eppendorf, Hamburg, Germany) and centrifuged at 1500 g and 4 °C for 10 min in a type 5415 R centrifuge (Eppendorf, Hamburg, Germany) to pelletize nuclei as well as remaining intact cells. The first supernatant was kept on ice, while the pellet was resuspended in isolation buffer and homogenized by 25 Dounce strokes for a second time to break the cells. A second centrifugation step at 1500 g and 4 °C for 10 min yielded a pellet

containing the nuclei enriched fraction. It was resuspended in respiration buffer for the oxygen consumption measurements. The pellet that contained nuclei from four cell culture flasks was resuspended in one milliliter of respiration buffer and an amount of 25 µl was used for the measurement of oxygen consumption.

The first and the second supernatant were mixed and centrifuged at 16000 g and 4 °C for 15 min to obtain a pellet. This gave the mitochondria enriched fraction and was also resuspended in respiration buffer for the measurements of oxygen consumption. The supernatant of this last centrifugation step is considered an organelle-free soluble fraction. We used about 40 µg of isolated mitochondria resuspended in 25 µl respiration buffer per individual sample which approximately corresponds to mitochondria from confluently grown cells in one 150 cm^2 cell culture flask. A Bradford-assay was applied to determine the amount of isolated mitochondria.

3.2.3 Determination of oxygen consumption

The measurement of the oxygen concentration was based on an optical sensing scheme. The fluorescent probe Pt(II)-pentafluorophenylporphyrin was incorporated into polystyrene microparticles which in turn were contained in a thin film of a polymer that was deposited on the bottom of the well of a conventional microtiter plate. The red fluorescence of the probe (indicator dye) in the sensor film was photoexcited at 544 nm and its intensity was dynamically quenched by molecular oxygen [29]. An inert reference dye (sulforhodamine) was also contained in the sensor film and could be excited at the same wavelength as the indicator dye, yielding a yellow reference signal that was independent of the partial pressure of oxygen (pO_2) [30]. The oxygen partial pressure (pO_2) was then calculated by the plate reader via the Stern–Volmer equation after a two-point calibration [31]. The determined oxygen concentration was indicated as the percentage of air saturation (% air saturation), a relative measure for the amount of dissolved oxygen in a medium related to the oxygen concentration in ambient air. Completely air saturated medium was defined as 100 %.

Resuspended cell fractions (25 µl of each) and buffer as a control were pipetted into the microplate wells, and each sample was then covered with approximately 100 µl of paraffin oil to prevent oxygen in the air from diffusing into the samples. The functionality of the mitochondria enriched fraction was evaluated by monitoring the oxygen depletion of the surrounding buffer and by investigating the effect of substances that inhibit or enhance respiration. Antimycin A and FCCP (each in 10 µM concentration) were applied to inhibit respiration, while a 1 µM concentration of FCCP was used to enhance respiration. Standards with oxygen-free and oxygen-saturated water were also measured and used for the calculation of oxygen concentrations. The measurements started 1 h after the preparation of cell fractions. Oxygen concentrations in each well were determined over 4 h in 5 min intervals. The optical sensors were read out through the optically transparent bottom of the plate by a commercially available fluorescence intensity microplate reader (Thermo Fisher Scientific Fluoroskan Ascent Microplate Reader, Waltham, MA USA). Fluorescence of each well was measured in a dual kinetic mode to detect the fluorescence of the indicator (at 544/650 nm) and the reference dye (at 544/590 nm). Analysis of the raw data and calculation of the oxygen concentration was carried out as described [24].

3.2.4 Statistical analysis

Data are expressed as means of five measurements ± standard deviations (SD).

3.3 Results and discussion

3.3.1 Differences of oxygen consumption in cell fractions

We first measured the oxygen concentration of all cell fractions obtained by differential centrifugation over a period of 4 h (Figure 1). The mitochondria enriched fraction (Figure 1A) showed a high depletion of oxygen with a minimum of about 20 % air saturation after approximately 100 min. In contrast the organelle-free soluble fraction (Figure 1C) showed no oxygen consumption because these fractions contained no oxygen consuming cell components.

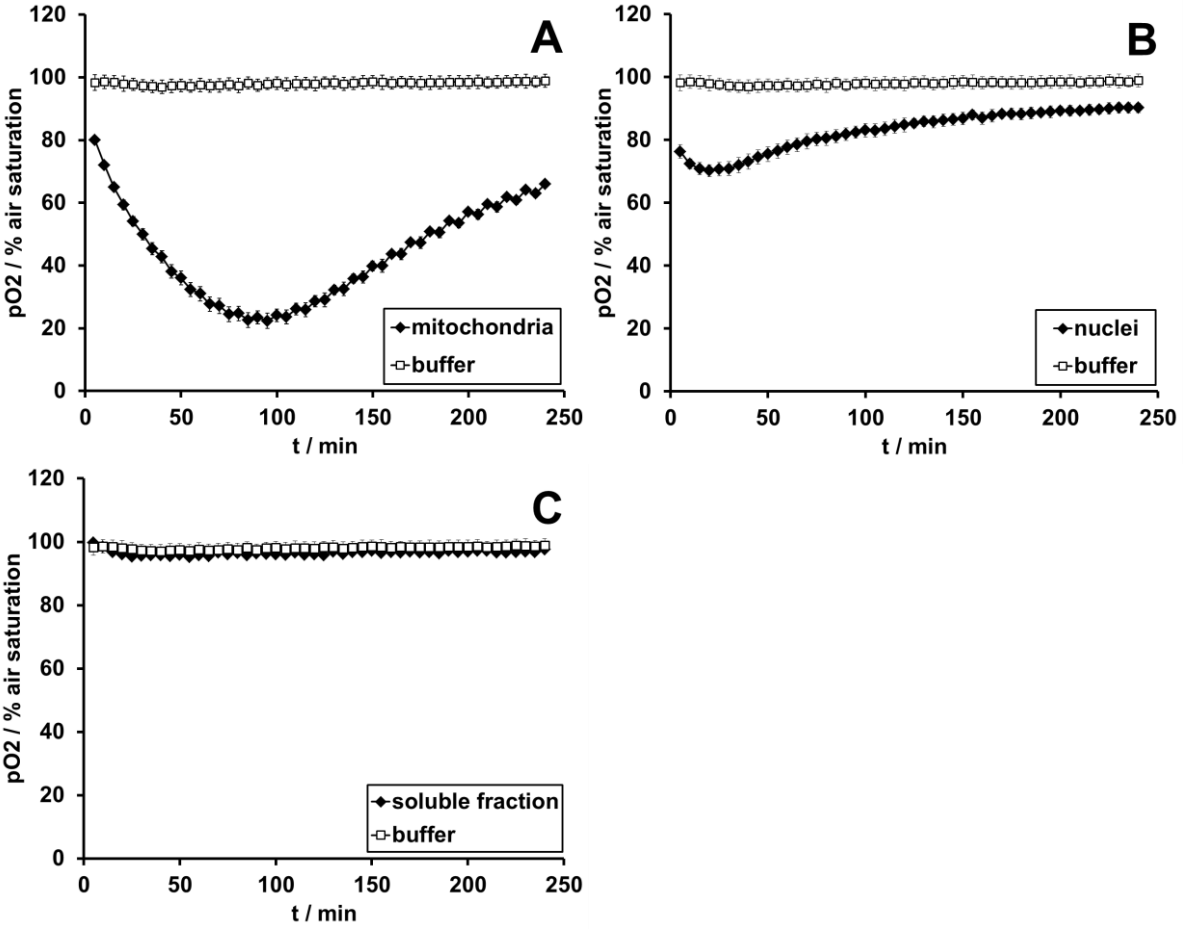

Figure 3.1: Oxygen consumption of (A) mitochondria enriched fraction (black rhombs) compared to buffer (gray squares), (B) nuclei enriched fraction (black rhombs) compared to buffer (gray squares) and (C) soluble fraction (black rhombs) compared to buffer (gray squares). The mitochondria enriched fraction shows a high depletion of oxygen whereas the nuclei enriched fraction and the soluble fraction show only marginal or no oxygen consumption compared to buffer.

The mitochondria enriched fraction showed a maximum oxygen consumption of about 60 % air saturation. After approximately 100 min at a concentration of about 20 % air saturation in the surrounding medium, the mitochondria stopped respiring. Considering that there was a 1 h delay between isolation and starting of the measurements, mitochondria respired for approximately 3 h. The continuous increase of oxygen concentration in the mitochondria-enriched fraction after approximately 100 min occurred due to the diffusion of oxygen from the environment. This occurred permanently but is only detectable after the mitochondria stopped respiring. The paraffin cover could not completely prevent diffusion of oxygen from ambient air and hence partly compensated oxygen consumption [32]. The same effect was observed for bacteria under treatment of bactericidal compounds: once the bacteria stopped respiring after they were killed by antibiotics, the oxygen concentration caused by oxygen diffusion from the environment increased [24].

The nuclei enriched fraction (Figure 1B) shows an oxygen consumption of about 10 % air saturation during the first 20 min of the measurements. Among others, this effect can be explained by the contamination of the nuclei enriched fraction with mitochondria. The organelle containing cell fractions are defined as enriched fractions, nuclei and mitochondria enriched fraction, but it has to be considered that they were obtained by a quick isolation procedure without purification. Therefore, it is likely that all cell fractions contained contaminants. Beside contamination of the nuclei enriched fraction with mitochondria, intranuclear mitochondria that can be functional have also been reported [33–36]. Both phenomena, contamination of the nuclei enriched fraction and intranuclear mitochondria, are responsible for the marginal oxygen consumption in the nuclei enriched fraction.

3.3.2 Effect of respiration inhibiting substances on the consumption of oxygen by the mitochondria enriched fraction

After having established a measurement protocol, we evaluated, if the effect of substances that inhibit mitochondrial function can be detected. We, therefore, blocked the respiratory chain using antimycin A (an inhibitor of complex III) or stopped the oxidative phosphorylation

using FCCP at high concentration (10 µM). Both substances interrupted the respiratory chain and consequently decreased oxygen consumption. Figure 2 shows that it is possible to detect the inhibition of mitochondrial respiration under the applied experimental conditions. Antimycin A seems to have inhibited respiration more efficiently than FCCP since both substances were added to the same molar concentration half an hour prior to the measurement started. Antimycin A led to almost no oxygen depletion, while mitochondria under a 10 µM FCCP treatment still consumed oxygen of about 20 % air saturation over 45 min. Hence, it is possible to detect time-dependent differences in the toxicity of substances. FCCP required more than 1 h of incubation time to show a toxic effect whereas mitochondria had already stopped respiring after half an hour at the antimycin A treatment. After mitochondria had stopped respiring under a 10 µM FCCP treatment, the effect of increasing oxygen concentration due to oxygen diffusion from the environment was also detectable.

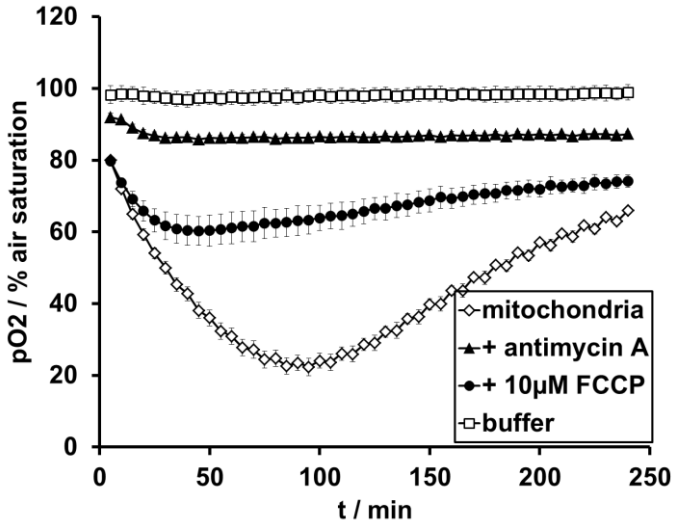

Figure 3.2: Inhibition of mitochondrial respiration with antimycin A (black triangles) and FCCP (black circles) at concentrations of 10 µM compared to respiration of mitochondria under normal conditions (gray rhombs) and buffer (gray squares). Mitochondria completely stopped respiring under antimycin A treatment while half an hour preincubation with 10 µM FCCP was not enough to inhibit respiration entirely. They stop respiring after additionally 45 min incubation time.

3.3.3 Effect of a respiration enhancing substance on the consumption of oxygen by the mitochondria enriched fraction

We also tested if an increase of oxygen consumption that is known to follow the supplementation with low concentrations of FCCP that thereby acts as an uncoupling agent is detectable [37]. To this end, we added FCCP to a 1 µM concentration which uncouples the respiratory chain and oxidative phosphorylation and hence leads to increased oxygen consumption. Figure 3 shows that an increase in the consumption of oxygen under a 1 µM FCCP treatment was indeed detectable. The starting point of the FCCP curve at 60 % air saturation is related to the time delay between adding FCCP to the sample, pipetting into the well-plate, covering with paraffin and starting the experiment. During this time mitochondria had already consumed oxygen of about 20 % air saturation compared to the sample without FCCP 1 µM. Uncoupled mitochondria stopped respiring at concentrations of about 20 % air saturation. This occurred approximately after 50 min. This means that uncoupled mitochondria respired of half the time compared to untreated mitochondria. Again, after mitochondria had stopped respiring, oxygen concentration increased due to the diffusion of oxygen from the environment.

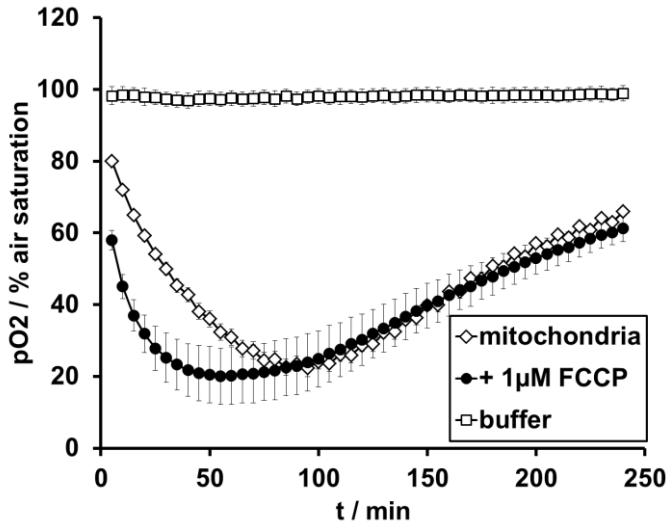

Figure 3.3: Enhancement of mitochondrial respiration with low concentration (1µM) of FCCP (black circles) compared to respiration of mitochondria under normal conditions (gray rhombs) and buffer (gray squares). The respiration rate under 1 µM FCCP treatment is higher than under normal conditions. In both cases mitochondria stop respiring at about 20 % air saturation but under FCCP treatment they reach this value in half the time.

It is likely that an oxygen concentration of about 20 % air saturation in the surrounding medium is a critical limit below which mitochondrial death is induced. It is also possible that a change in respiratory states which depends on the availability of substrates occurred. Five respiratory states of isolated mitochondria can be distinguished according to Chance and Williams [38]. State 1 is indicated by high oxygen levels, low ADP and low substrate levels. State 2 shows high oxygen and high ADP levels but almost no substrate. In state 3, all components are available in excess. State 4 indicates high oxygen and high substrate levels but low ADP levels and state 5 shows high substrate and ADP levels but no oxygen.

It is likely that an oxygen concentration of about 20 % air saturation in the surrounding medium is a critical limit below which mitochondrial death is induced. It is also possible that a change in respiratory states which depends on the availability of substrates occurred. Five respiratory states of isolated mitochondria can be distinguished according to Chance and Williams [38]. State 1 is indicated by high oxygen levels, low ADP and low substrate levels. State 2 shows high oxygen and high ADP levels but almost no substrate. In state 3, all components are available in excess. State 4 indicates high oxygen and high substrate levels but low ADP levels and state 5 shows high substrate and ADP levels but no oxygen.

The applied experimental conditions are related to state 3 when the measurement started. This means that all components were available in excess and enzymes of the respiratory chain worked at the highest level when ADP, substrates such as succinate and oxygen were available in excess. In this case, the respiration rate was high. While mitochondria were respiring, oxygen was consumed and became a respiration rate limiting component moving the system into respiratory state 5 with no respiration activity. Succinate and ADP were also metabolized but they were added in excess. If the concentration of succinate or ADP reduced to a critical limit, the respiration rate would slow down but not reach zero like in state 5.

Respiration came to an end at an oxygen concentration of approximately 20 % air saturation which gives evidence that this concentration is a critical limit for mitochondrial respiration and oxygen is the respiration rate limiting substance.

3.4 Conclusions

We are presenting a tool to monitor the functionality of mitochondrial preparations over several hours. Typical features include the need of only a few microliters of isolated mitochondria, the possibility of using microplate sensor technology which allows for the high throughput screening of large sample numbers. The duration of the measurements can be extended easily without any additional experimental effort. With the data from the oxygen consumption measurements a user of this setup can subsequently control the functionality of a mitochondrial preparation at each step of an experiment under different experimental conditions, for example varying buffers or additives. The system is finally able to detect whether substances act directly on mitochondrial respiratory competence.

Acknowledgments

We thank Dr. Sarina Arain at PreSens for providing the OxoPlates®.

3.5 References

[1] S. DiMauro, Mitochondrial diseases, Biochimica et Biophysica Acta (BBA) - Bioenergetics 1658 (2004) 80–88.

[2] A. Chatterjee, S. Dasgupta, D. Sidransky, Mitochondrial Subversion in Cancer, Cancer Prevention Research 4 (2011) 638–654.

[3] V. Gogvadze, S. Orrenius, B. Zhivotovsky, Mitochondria as targets for cancer chemotherapy, Seminars in Cancer Biology 19 (2009) 57–66.

[4] J.L. Chou, D.V. Shenoy, N. Thomas, P.K. Choudhary, F.M. LaFerla, S.R. Goodman, G.A. Breen, Early dysregulation of the mitochondrial proteome in a mouse model of Alzheimer's disease, Journal of Proteomics 74 (2011) 466–479.

[5] R. McFarland, R.W. Taylor, D.M. Turnbull, A neurological perspective on mitochondrial disease, Lancet Neurol 9 (2010) 829–840.

[6] E. Schon, S. Przedborski, Mitochondria: The Next (Neurode)Generation, Neuron 70 (2011) 1033–1053.

[7] J.L. Rains, S.K. Jain, Oxidative stress, insulin signaling, and diabetes, Free Radical Biology and Medicine 50 (2011) 567–575.

[8] J. Szendroedi, E. Phielix, M. Roden, The role of mitochondria in insulin resistance and type 2 diabetes mellitus, Nat Rev Endocrinol (2011) 1–12.

[9] A. Ghosh, K. Chandran, S.V. Kalivendi, J. Joseph, W.E. Antholine, C.J. Hillard, A. Kanthasamy, A. Kanthasamy, B. Kalyanaraman, Neuroprotection by a mitochondria-targeted drug in a Parkinson's disease model, Free Radical Biology and Medicine 49 (2010) 1674–1684.

[10] V.E. Kagan, P. Wipf, D. Stoyanovsky, J.S. Greenberger, G. Borisenko, N.A. Belikova, N. Yanamala, A.K. Samhan Arias, M.A. Tungekar, J. Jiang, Y.Y. Tyurina, J. Ji, J. Klein-Seetharaman, B.R. Pitt, A.A. Shvedova, H. Bayir, Mitochondrial targeting of electron scavenging antioxidants: Regulation of selective oxidation vs random chain reactions, Advanced Drug Delivery Reviews 61 (2009) 1375–1385.

[11] D. Park, P.J. Dilda, Mitochondria as targets in angiogenesis inhibition, Molecular Aspects of Medicine 31 (2010) 113–131.

[12] F. Wang, M.A. Ogasawara, P. Huang, Small mitochondria-targeting molecules as anti-cancer agents, Molecular Aspects of Medicine 31 (2010) 75–92.

[13] M.W. Mather, J.M. Morrisey, A.B. Vaidya, Hemozoin-free Plasmodium falciparum mitochondria for physiological and drug susceptibility studies, Molecular and Biochemical Parasitology 174 (2010) 150–153.

[14] C.S. Caspersen, A. Sosunov, I. Utkina-Sosunova, V.I. Ratner, A.A. Starkov, V.S. Ten, An Isolation Method for Assessment of Brain Mitochondria Function in Neonatal Mice with Hypoxic-Ischemic Brain Injury, Dev Neurosci 30 (2008) 319–324.

[15] E. Fernández-Vizarra, G. Ferrín, A. Pérez-Martos, P. Fernández-Silva, M. Zeviani, J.A. Enríquez, Isolation of mitochondria for biogenetical studies: An update, Mitochondrion 10 (2010) 253–262.

[16] W.P. Mao, N.N. Zhang, F.Y. Zhou, W.X. Li, H.Y. Liu, J. Feng, L. Zhou, C.J. Wei, Y.B. Pan, Z.J. He, Cadmium directly induced mitochondrial dysfunction of human embryonic kidney cells, Human & Experimental Toxicology 30 (2011) 920–929.

[17] M. Duvvuri, W. Feng, A. Mathis, J.P. Krise, A Cell Fractionation Approach for the Quantitative Analysis of Subcellular Drug Disposition, Pharm Res 21 (2004) 26–32.

[18] S. Biswas, N.S. Dodwadkar, R.R. Sawant, A. Koshkaryev, V.P. Torchilin, Surface modification of liposomes with rhodamine-123-conjugated polymer results in enhanced mitochondrial targeting, Journal of Drug Targeting 19 (2011) 552–561.

[19] C. Frezza, S. Cipolat, L. Scorrano, Organelle isolation: functional mitochondria from mouse liver, muscle and cultured filroblasts, Nat Protoc 2 (2007) 287–295.

[20] N.R. Sims, M.F. Anderson, Isolation of mitochondria from rat brain using Percoll density gradient centrifugation, Nat Protoc 3 (2008) 1228–1239.

[21] H.-T. Hornig-Do, G. Günther, M. Bust, P. Lehnartz, A. Bosio, R.J. Wiesner, Isolation of functional pure mitochondria by superparamagnetic microbeads, Analytical Biochemistry 389 (2009) 1–5.

[22] S. Nagl, C. Baleizão, S. Borisov, M. Schäferling, M. Berberan-Santos, O. Wolfbeis, Optical Sensing and Imaging of Trace Oxygen with Record Response, Angew. Chem. Int. Ed 46 (2007) 2317–2319.

[23] D.T. Stitt, M.S. Nagar, T.A. Haq, M.R. Timmins, Determination of growth rate of microorganisms in broth from oxygen-sensitive fluorescence plate reader measurements, BioTechniques 32 (2002) 684, 686, 688-9.

[24] B. Hutter, G.T. John, Evaluation of OxoPlate for Real-Time Assessment of Antibacterial Activities, Current Microbiology 48 (2004) 57–61.

[25] W. Wang, L. Upshaw, D.M. Strong, R.P. Robertson, J. Reems, Increased oxygen consumption rates in response to high glucose detected by a novel oxygen biosensor system in non-human primate and human islets, Journal of Endocrinology 185 (2005) 445–455.

[26] M. Wodnicka, R.D. Guarino, J.J. Hemperly, M.R. Timmins, D. Stitt, J.B. Pitner, Novel fluorescent technology platform for high throughput cytotoxicity and proliferation assays, J Biomol Screen 5 (2000) 141–152.

[27] H. Alborzinia, S. Can, P. Holenya, C. Scholl, E. Lederer, I. Kitanovic, S. Wölfl, Real-Time Monitoring of Cisplatin-Induced Cell Death, PLoS ONE 6 (2011) e19714.

[28] G.W. Rogers, M.D. Brand, S. Petrosyan, D. Ashok, A.A. Elorza, D.A. Ferrick, A.N. Murphy, High Throughput Microplate Respiratory Measurements Using Minimal Quantities Of Isolated Mitochondria, PLoS ONE 6 (2011) e21746.

[29] O.S. Wolfbeis, Sensor Paints, Adv. Mater 20 (2008) 3759–3763.

[30] S. Arain, G.T. John, C. Krause, J. Gerlach, O.S. Wolfbeis, I. Klimant, Characterization of microtiterplates with integrated optical sensors for oxygen and pH, and their applications to enzyme activity screening, respirometry, and toxicological assays, Sensors and Actuators B: Chemical 113 (2006) 639–648.

[31] O.S. Wolfbeis, I. Oehme, N. Papkovskaya, I. Klimant, Sol–gel based glucose biosensors employing optical oxygen transducers, and a method for compensating for variable oxygen background, Biosensors and Bioelectronics 15 (2000) 69–76.

[32] S. Arain, S. Weiss, E. Heinzle, G.T. John, C. Krause, I. Klimant, Gas sensing in microplates with optodes: Influence of oxygen exchange between sample, air, and plate material, Biotechnol. Bioeng 90 (2005) 271–280.

[33] H. Jensen, H. Engedal, T.S. Saetersdal, Ultrastructure of mitochondria-containing nuclei in human myocardial cells, Virchows Archiv B Cell Pathology Zell-pathologie 21 (1976) 1–12.

[34] M. Matsuyama, H. Suzuki, Seizing mechanism and fate of intranuclear mitochondria, Cellular and Molecular Life Sciences 28 (1972) 1347–1348.

[35] G. Takemura, Y. Takatsu, H. Sakaguchi, H. Fujiwara, Intranuclear mitochondria in human myocardial cells, Pathol. Res. Pract. 193 (1997) 305–311.

[36] J.W. Shay, H. Werbin, New evidence for the insertion of mitochondrial DNA into the human genome: significance for cancer and aging, Mutation Research/DNAging 275 (1992) 227–235.

[37] J.P. Brennan, R. Southworth, R.A. Medina, S.M. Davidson, M.R. Duchen, M.J. Shattock, Mitochondrial uncoupling, with low concentration FCCP, induces ROS-dependent cardioprotection independent of KATP channel activation, Cardiovascular Research 72 (2006) 313–321.

[38] B. Chance, G.R. Williams, Respiratory enzymes in oxidative phosphorylation. I. Kinetics of oxygen utilization, J. Biol. Chem 217 (1955) 383–393.

Chapter 4

Permanent labeling of isolated mitochondria

Abstract

Isolated mitochondria were labeled with fluorescent dyes and fluorescent proteins to make them accessible for fluorescence based analytical methods. The study revealed that staining with fluorescent dyes (JC-1 and MitoTracker® Deep Red) was only temporary as the dyes washed out. In contrast to that, mitochondria were labeled permanently with fluorescent proteins. Therefore, cells were transfected using plasmid vectors that encode fluorescent proteins. After transfection, fluorescing cells were separated from cells that did not carry fluorescent proteins by antibiotic selection and flow cytometry sorting. Thereby, stable cells lines containing different mitochondrial fluorescent proteins were obtained. The cell lines either carried a mitochondria targeted green fluorescent protein (mtGFP) or a mitochondria targeted red fluorescent protein (mtRFP). Additionally, cells that already contained a mitochondria targeted aequorin were transfected with mtGFP to detect green fluorescence of the mtGFP without excitation by a laser but by excitation due to Förster resonance energy transfer (FRET) from aequorin to GFP.

4.1 Introduction

A permanent fluorescent labeling of isolated mitochondria is essential to make them accessible to fluorescence based analytical methods such as fluorescence microscopy and flow cytometry to study, for example, mitochondrial fusion. Thereby, it is possible to tag unlabeled isolated mitochondria or to label mitochondria inside cells and to isolate them afterwards. There are various possibilities to label mitochondria. Among these, there are numerous organic dyes that are lipophilic, positively charged and that accumulate potential dependent in mitochondria or that are sensitive to oxidation in mitochondria [1,2]. They are mainly used to stain mitochondria in cells but some of them can also be used to stain isolated mitochondria. Other methods to label mitochondria make use of fluorescent proteins that contain a mitochondrial targeting sequence and label mitochondria independently of their function as well as antibodies that bind to mitochondrial proteins and that can be detected by a secondary fluorescently labeled antibody [1].

In the following, imaging of mitochondria by fluorescent dyes, fluorescent proteins and the natural Förster resonance energy transfer (FRET) pair of the photoprotein aequorin and the green fluorescent protein (GFP) are compared. The two fluorescent dyes that have been chosen are JC-1 and the MitoTracker® Deep Red FM. MitoTracker® probes are mitochondria selective dyes with a mildly thiol reactive chloromethyl moiety that appears to be responsible for keeping the dye associated with mitochondria even after fixation [3,4]. The MitoTracker® Deep Red FM is a far red fluorescent dye that exhibits an absorption maximum at 644 nm and an emission maximum at 665 nm [5,6]. The green-fluorescent JC-1 dye (5,5',6,6'-tetrachloro-1,1',3,3'-tetraethylbenzimidazolylcarbocyanine iodide) exists as a monomer at low concentrations or at low membrane potential and emits light of approximately 529 nm. At higher concentrations or higher potentials it accumulates potential dependent in mitochondria and forms red-fluorescent J-aggregates with an emission maximum at approximately 590 nm. Thus, the emission of this cyanine dye and the ratio red/green can be used as an indicator of mitochondrial membrane potential and mitochondrial depolarization at early stages of apoptosis [3,7–9]. Various types of ratio measurements are possible by combining

signals from the green-fluorescent JC-1 monomer and the J-aggregate. Thereby, the ratio of red-to-green JC-1 fluorescence is only dependent on the membrane potential and not on other factors that may influence single-component fluorescence signals, such as mitochondrial size, shape and density. Both forms of the dye can be effectively excited at 488 nm [3].

Another method to label mitochondria fluorescently is the transfection with fluorescent proteins. Thereby, expression vectors that encode fluorescent proteins fused to a mitochondrial targeting sequence [10] are delivered into cells by baculoviruses [11,12] or transfection reagents such as Lipofectamine® [13,14]. The genes of the plasmid are transcribed in the nucleus and the proteins are expressed in the cytosol. After their expression, they are translocated into mitochondria due to the mitochondrial targeting sequence and there, they can exhibit their fluorescence. In this study, cells were transfected with a mitochondria targeted green fluorescent protein (mtGFP) or a mitochondria targeted red fluorescent protein (mtRFP).

Imaging of mitochondria by the natural FRET pair aequorin and GFP is an additional method that was applied, in particular as a possibility to detect mitochondrial fusion in a further study. Aequorin is a luminescent photoprotein of the jellyfish *Aequorea victoria* that emits light of approximately 470 nm when it binds to its prosthetic group coelenterazine and calcium. The jellyfish shows green luminescence due to the energy transfer to GFP [15]. Recombinant aequorin is mainly used in sensing intracellular calcium signals [16]. The idea was to detect mitochondrial fusion of isolated mitochondria in vitro by mixing isolated mitochondria that contain mitochondria targeted aequorin and isolated mitochondria that contain mitochondria targeted GFP [17]. After mitochondrial fusion, the green fluorescence of GFP should be detectable only by excitation of aequorin after supplementation of calcium and coelenterazine.

4.2 Materials and methods

4.2.1 Materials

HAM F-12 nutrient mixture and fetal calf serum (FCS) were purchased from Sigma-Aldrich (Steinheim, Germany). Trypsin-EDTA 0.25 % was obtained from Gibco-Invitrogen (Karlsruhe, Germany). Purified water was obtained by using a Milli-Q water purification system from Millipore (Schwalbach, Germany). All cell culture materials were purchased from Corning (Bodenheim, Germany). Imaging plates 24 CG, sample cover glass, were obtained from Zell-Kontakt (Nörten-Hardenberg, Germany).

Isolation buffer consisted of 250 mM sucrose (Merck, Darmstadt, Germany), 10 mM Tris (USB Corporation, Cleveland, OH USA), 10 mM KCl (Merck, Darmstadt, Germany), 1 mM Na_2EDTA (Merck, Darmstadt, Germany) and 0.1 % bovine serum albumin (BSA) (Sigma-Aldrich, Steinheim, Germany). JC-1 and MitoTracker® Deep Red FM were obtained from Invitrogen (Karlsruhe, Germany) and dissolved in DMSO (Sigma-Aldrich, Steinheim, Germany). pShooter™ pCMV/myc/mito and pCMV/myc/mito/GFP were purchased from Invitrogen (Karlsruhe, Germany) and pTurboRFP-mito was obtained from BioCat (Heidelberg, Germany). The pDsRed2-N1 plasmid was purchased from Takara Bio Europe/Clontech (Saint-Germain-en-Laye, France). Opti-MEM® I Reduced Serum Medium, Lipofectamine® 2000 and Zeocin Selection Reagent were purchased from Invitrogen (Karlsruhe, Germany). G418 was obtained from Sigma-Aldrich (Steinheim, Germany) and dissolved in DPBS without calcium and magnesium from Gibco-Invitrogen (Karlsruhe, Germany). Hygromycin B and coelenterazine h were purchased from Sigma-Aldrich (Steinheim, Germany) and calcium chloride dihydrate was obtained from Merck (Darmstadt, Germany). Digitonin was purchased from Calbiochem/Merck (Darmstadt, Germany) and NPY was kindly provided by Prof. Buschauer (Department of Pharmaceutical/Medicinal Chemistry II, University of Regensburg, Germany).

Restriction enzymes Not I and Xho I, antarctic phosphatase, BSA, NEBuffers, T4 DNA ligase and T4 DNA ligase buffer with 10mM ATP were purchased from New England Biolabs (Frankfurt, Germany). Sodium acetate trihydrate was obtained from Merck (Darmstadt,

Germany). The QIAquick Gel Extraction Kit and the QIAGEN Plasmid Purification Maxi Kit were purchased from Qiagen (Hilden, Germany). Agarose was obtained from Bio-Rad (Munich, Germany). Tris acetate EDTA (TAE)-buffer was purchased from Sigma-Aldrich (Steinheim, Germany). The DNA ladder TrackIt 100 bp was obtained from Invitrogen (Karlsruhe, Germany). Competent E. coli JM 109 were purchased from Promega (Mannheim, Germany). Ampicillin was obtained from Sigma-Aldrich (Steinheim, Germany). LB-medium consisted of 10 g Bacto Yeast Extract (BD Bioscience, Heidelberg, Germany), 5 g Bacto Tryptone (BD Bioscience, Heidelberg, Germany), 5 g sodium chloride (Merck, Darmstadt, Germany) in 1000 ml purified water, pH-value was adjusted by 10 N NaOH to 7.5 and sterilized by autoclave. Standard nutrient agar was obtained from Merck (Darmstadt, Germany). SOC-medium consisted of 2 g Bacto Yeast Extract (BD Bioscience, Heidelberg, Germany), 0.5 g Bacto Tryptone (BD Bioscience, Heidelberg, Germany), 10 mM sodium chloride (Merck, Darmstadt, Germany), 2.5 mM potassium chloride (Merck, Darmstadt, Germany), 20 mM magnesium chloride hexahydrate (Merck, Darmstadt, Germany) and magnesium sulfate heptahydrate (Merck, Darmstadt, Germany) and 20 mM glucose (Sigma-Aldrich, Steinheim, Germany) in 100 ml purified water and sterilized by autoclave. CHO-K1 cells transfected with mitochondrial aequorin (CHO-hY2-k9-qi5-k9-mtAEQ-A7) were a kind gift from Prof. Bernhardt (Department of Pharmaceutical/Medicinal Chemistry II, University of Regensburg, Germany).

4.2.2 Staining mitochondria with fluorescent dyes

CHO-K1 cells were cultured in HAM-F12 nutrient mixture containing 10 % FCS in 150 cm^2 culture flasks until confluency, harvested by Trypsin-EDTA 0.25 % and washed with isolation buffer. The centrifugation steps for the washing steps of the cells were carried out in a GS-15R centrifuge (Beckman, Krefeld, Germany). Afterwards, cells from one culture flask were suspended in 250 µl isolation buffer. Then, cells from four flasks were pooled and the resulting one milliliter of cell suspension was transferred into a cooled 2-ml Dounce glass homogenizer (Sigma-Aldrich, Steinheim, Germany) where the cells were disrupted by 25

strokes. The suspension was transferred into a 2-ml safe-lock tube (Eppendorf, Hamburg, Germany) and centrifuged at 1500 g at 4 °C for 10 min a type 5415 R centrifuge (Eppendorf, Hamburg, Germany) to pelletize nuclei as well as remaining intact cells. The first supernatant was kept on ice, while the pellet was resuspended in isolation buffer and homogenized by 25 Dounce strokes for a second time to break remaining intact cells. A second centrifugation step at 1500 g at 4 °C for 10 min yielded a pellet that was the nuclei enriched fraction. The first and the second supernatant were mixed and centrifuged at 16000 g at 4 °C for 15 min to obtain a pellet enriched with isolated mitochondria.

Isolated mitochondria were stained with either 2.5 µg/ml (~3.8 nmol/ml) JC-1 or 2 µg/ml (~3.8 nmol/ml) MitoTracker® Deep Red FM, incubated for 15 min on ice and washed with isolation buffer three times. Afterwards, isolated mitochondria were analyzed by confocal laser scanning microscopy (CLSM) with a Zeiss Axiovert LSM 510 (Carl Zeiss, Oberkochen, Germany) and an AxioCam HRc (Carl Zeiss, Oberkochen, Germany). Thereby, JC-1 was excited at 488 nm and detected at 560–615 nm whereas the MitoTracker® Deep Red FM was excited at 633 nm and detected with a 650 nm long pass filter. In samples containing both dyes, a multitrack scan mode was applied. Flow cytometry of JC-1- and MitoTracker®-stained samples was carried out with a FACSCalibur™ (BD Bioscience, Heidelberg, Germany). Thereby, JC-1 was excited at 488 nm and detected at 564–606 nm whereas the MitoTracker® Deep Red FM was excited at 633 nm and detected with a 670 nm long pass filter.

4.2.3 Cloning of DsRed into pCMV/myc/mito

The plasmid vector pShooter™ pCMV/myc/mito encoded a mitochondrial targeting sequence to translocate proteins to mitochondria. It expressed proteins fused to the mitochondrial targeting sequence [18]. The multiple cloning site (MCS) of the pShooter was cleaved by the restriction enzymes Xho I and Not I. The sequence that encoded DsRed in the pDsRed2-N1 plasmid was also separated by Xho I and Not I. Therefore, both plasmids were incubated with Xho I and Not I in NEB3 and BSA at 37 °C for 1 h. Afterwards, DNA was precipitated by

sodium acetate and ethanol at -20 °C for 15 min and at 4 °C centrifugation at 16000 g for 15 min. The pellet was washed with ethanol 70 % and dried at 37 °C for 10 min. Then, the pellet was dissolved in purified water at room temperature for 10 min and on ice for 30-60 min. To prevent self-ligation, the pShooter was additionally treated with antarctic phosphatase for dephosphorylation at 37 °C for 1 h and at 65 °C for 10 min. Afterwards, electrophoresis was applied for both plasmids at 120 V for 30 min to separate the fragments that were obtained by restriction. Electrophoresis of the agarose gel was carried out in TAE-buffer with ethidium bromide. A loading buffer containing bromphenol blue and xylene cyanole was added to both plasmids. A DNA ladder was also separated to evaluate the size of the fragments. The large fragment of the pShooter and the small fragment of the pDsRed2-N1 were detected by UV excitation, cut from the gel and extracted by the QIAquick Gel Extraction Kit. Afterwards, ligation of the pShooter and DsRed insert was conducted by T4 ligase in ligase buffer containing ATP at 16 °C overnight. Then, the clonal plasmid was transformed into E. coli. Therefore, the clonal plasmid DNA was added to E. coli, incubated on ice for 20 min, treated at 42 °C for 45-50 s and incubated on ice for 2 min again. Afterwards, SOC-medium was added and incubated at 37 °C on a shaker for 1 h. Then, E. coli were plated on LB-agar plates with 100 µg/ml ampicillin to select transformants containing the plasmid as the pShooter vector contains a resistance gene for ampicillin. The plates were incubated at 37 °C overnight with a maximum of 12-16 h. Afterwards, transformants were picked, transferred into LB-medium containing 100 µg/ml ampicillin and incubated at 37 °C on a shaker overnight. On the next day, glycerol stocks of E. coli were prepared for long-term storage. Afterwards, plasmid DNA was extracted from E. coli by a QIAGEN Plasmid Purification Maxi Kit. DNA was resuspended in water and the concentration was determined photometrically.

4.2.4 Transfection of fluorescent proteins into CHO-cells

For transfection of CHO-K1 cells, 38.000 cells per well were seeded into 24 well plates on the day before transfection and cells were cultured in HAM-F12 nutrient mixture containing 10 % FCS. Cells were transfected with 0.5 µg, 1 µg or 2 µg plasmid DNA (pDNA) of pShooter™ pCMV/myc/mito/GFP and pTurboRFP-mito. A pDNA to Lipofectamin™ 2000 transfection reagent ratio of 1:2 or 1:3 was applied. Therefore, both pDNA and Lipofectamin™ 2000 were diluted in Opti-MEM® I Reduced Serum Medium separately. Afterwards, the Lipofectamine solution was added to the pDNA solution, gently mixed and incubated at room temperature for 20 min. During the incubation and formation of the polyplexes, the medium of the cells was exchanged to serum-free HAM-F12 medium after washing the cells with DPBS. Then, the pDNA-Lipofectamine solution was added to the cells and incubated for 4 h. Afterwards, the medium of the cells was exchanged to HAM-F12 containing 10 % FCS. After 24-48 h, mitochondrial fluorescence of the cells was detected by CLSM with a Zeiss Axiovert LSM 510 (Carl Zeiss, Oberkochen, Germany) and pictures were recorded with an AxioCam HRc (Carl Zeiss, Oberkochen, Germany). Thereby, GFP was excited at 488 nm and detected at 505–530 nm whereas RFP was excited at 488 nm and detected at 530–600 nm. For stable transfection, transfected cells were split 1:10 into fresh medium and after 24 h the medium was changed to selection medium, HAM-F12 containing 10 % FCS and 400 µg/ml G418, an aminoglycoside antibiotic. As the used plasmids contain a resistance factor to G418, only transfected cells should survive the selection antibiotic. After 3–4 h incubation in the selection medium transfected cells were sorted by flow cytometry with a FACSCalibur™ (BD Bioscience, Heidelberg, Germany) to separate fluorescent cells from non-fluorescent cells and to obtain stably transfected, fluorescent cell lines with either mitochondrial GFP or mitochondrial RFP. Thereby, GFP was excited a 488 nm and detected at 515–545 nm whereas RFP was excited at 488 nm and detected at 564–606 nm. Stably transfected CHO-mtGFP and CHO-mtRFP cell lines were cultured in HAM-F12 containing 10 % FCS and 400 µg/ml G418.

4.2.5 Imaging with natural FRET-pair aequorin-GFP

As a positive control for an approach to detect mitochondrial fusion in vitro with aequorin containing and GFP containing mitochondria, CHO-cells that contained mitochondrial aequorin were co-transfected with GFP as described previously. CHO-AEQ-GPF cells were cultured in selection medium HAM-F12 containing 10 % FCS and 400 µg/ml G418, 400µg/ml hygromycin B and 250 µg/ml zeocin. Aequorin emits light of 470 nm after binding to coelenterazine and calcium. The energy transfer of aequorin to GFP and the following fluorescence of GFP in intact cells was induced by the addition of 2 or 5 µM coelenterazine h and incubation for 2 h to reconstitute the holoenzyme. Afterwards, 150 µM or 1.5 mM of Ca^{2+} was added as a co-factor of aequorin leading to conformational changes and luminescence of aequorin (Figure 4.1).

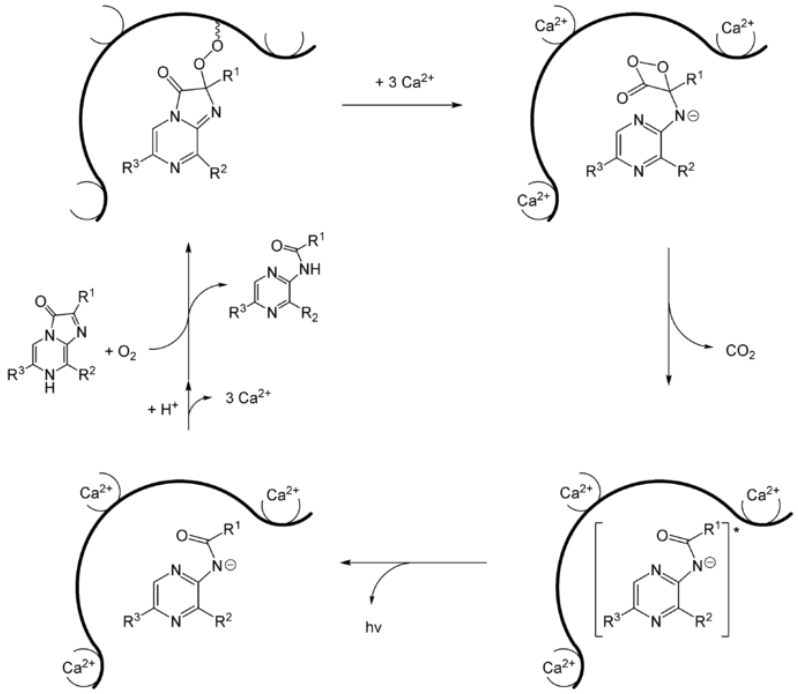

Figure 4.1: Conformational changes of aequorin after binding of coelenterazine and calcium [19]. Coelenterazine is bound to aequorin via a peroxide linkage and aequorin has three binding sites for calcium. After binding of calcium, the conformation of aequorin changes and the intramolecular reaction of coelenterazine starts. Thereby, an instable dioxetanone reacts to coeleteramide after decarboxylation. After relaxation into the ground state, a photon of 470 nm is emitted.

Fluorescence of GFP after fluorescence resonance energy transfer (FRET) and excitation by aequorin in adherent cells was observed by a CLSM Zeiss Axiovert LSM 510 (Carl Zeiss, Oberkochen, Germany) with an AxioCam HRc (Carl Zeiss, Oberkochen, Germany). Luminescence of aequorin in intact cells and isolated mitochondria was determined with a GENios Pro plate reader (Tecan, Salzburg, Austria). Therefore, adherent cells were detached by trypsin to obtain suspended cells and mitochondria were isolated as described previously. Coelenterazine h was added to suspended cells and isolated mitochondria and incubated for 2 h. Luminescence of aequorin in cells was stimulated by addition of 1.5 mM Ca^{2+} after cell membrane permeabilization with 50 µM digitonin or by intracellular calcium release after binding of an agonist (NPY) to a G-protein coupled receptor (GPCR). The measurement started 2 h after addition of digitonin or rather immediately after addition of the agonist. Luminesence of aequorin in isolated mitochondria was stimulated by the addition of 150 µM or 1.5 mM Ca^{2+}. The measurement started 2 h after the addition of calcium.

4.3 Results and discussion

The principle of mitochondrial fusion experiments in vitro, described in a further study [20], was based on differently labeled isolated mitochondria. The hypothesis was to mix differently labeled isolated mitochondria and to detect both labels in one mitochondrion after two differently labeled mitochondria had fused. For labeling with fluorescent dyes, isolated mitochondria were stained either with the fluorescent dyes JC-1 or MitoTracker® Deep Red. Staining intact cells, JC-1 exists as a green monomer in the cytosol and forms orange J-aggregated as it accumulates potential dependent in mitochondria (Figure 4.2) [21].

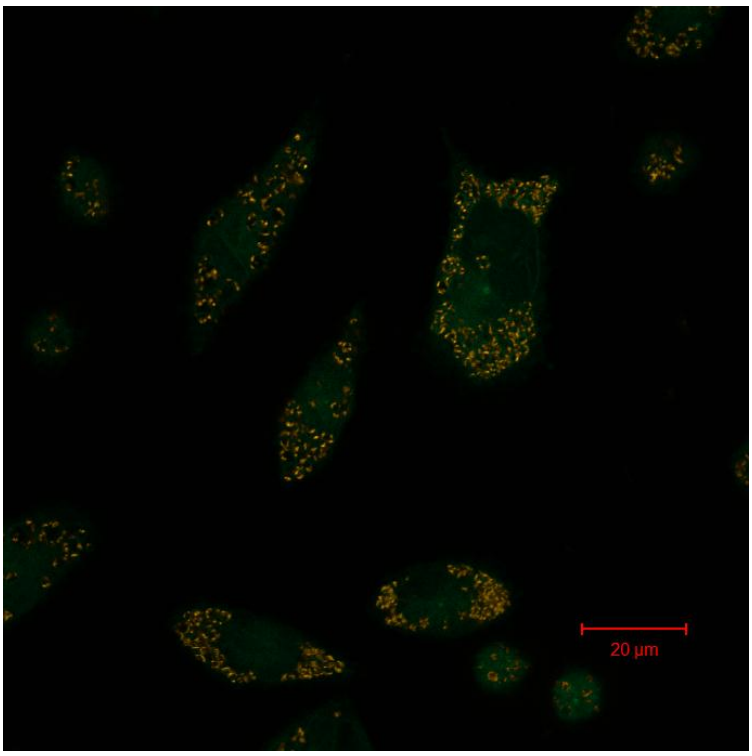

Figure 4.2: CLSM image of JC-1 stained cells showing green fluorescent dye monomers in the cytosol and orange fluorescent J-aggregates in mitochondria.

Staining isolated mitochondria with JC-1, only orange J-aggregates were detected (Figure 4.3) indicating that isolated mitochondria were intact and the membrane potential was still existent [8]. Isolated mitochondria stained with Mito Tracker® Deep Red are shown in Figure 4.4.

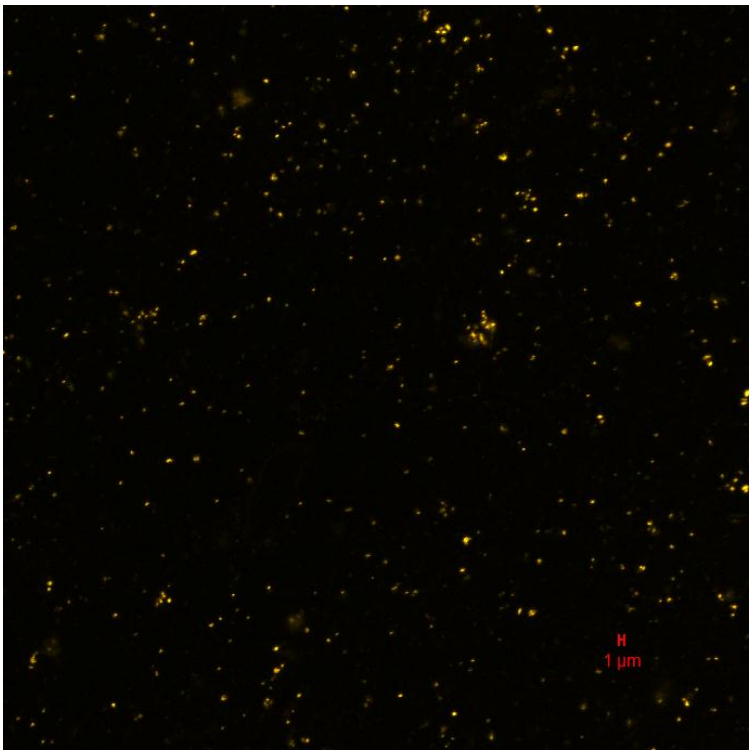

Figure 4.3: CLSM image of JC-1 stained isolated mitochondria.

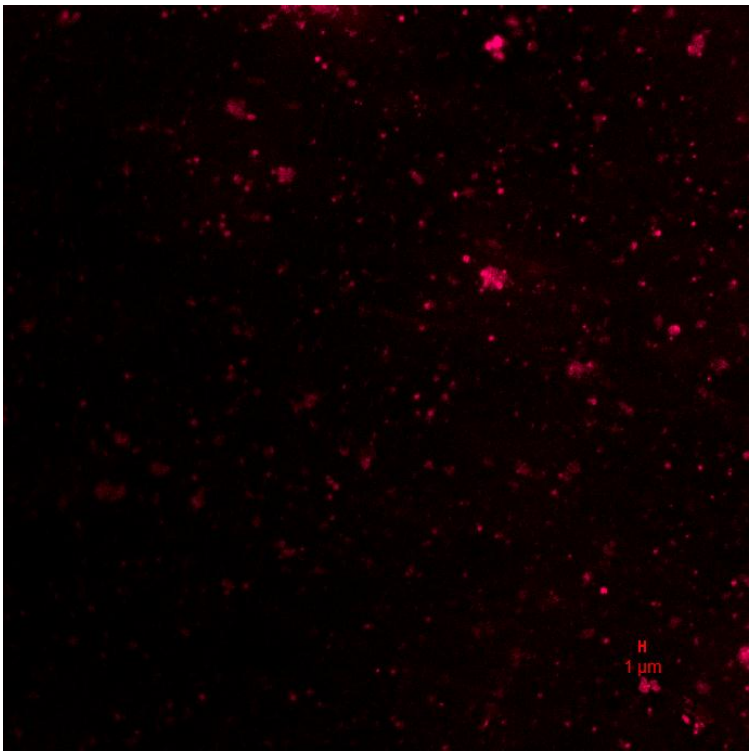

Figure 4.4: CLSM image of MitoTracker® Deep Red stained isolated mitochondria.

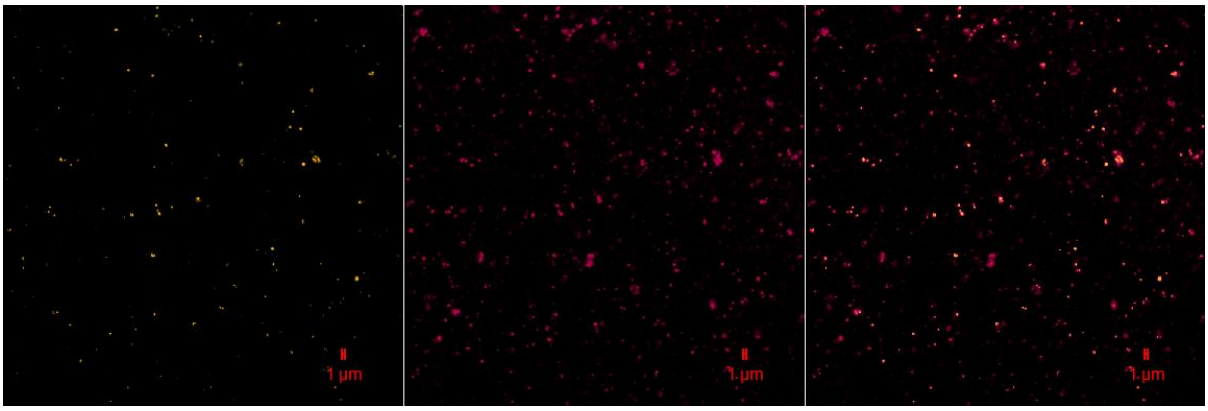

Figure 4.5: CLSM image of a mixture of JC-1 and MitoTracker® Deep Red stained isolated mitochondria, the left image shows fluorescence of JC-1, the image in the middle shows fluorescence of MitoTracker® Deep Red and the right image shows both fluorescence channels.

It was hypothesized that JC-1 and MitoTracker® Deep Red could only be detected in one isolated mitochondrion after two differently labeled isolated mitochondria, one stained with JC-1 and the other one stained with MitoTracker® Deep Red, had fused. Isolated mitochondria did not undergo mitochondrial fusion in vitro. Additional conditions had to be applied to induce mitochondrial fusion of isolated mitochondria in vitro [22]. Therefore, it was expected that isolated mitochondria containing JC-1 or MitoTracker® Deep Red could be detected individually labeled side by side when samples of isolated mitochondria stained with JC-1 and samples of isolated mitochondria stained with Mito Tracker® Deep Red were simply mixed without the application of conditions that induce mitochondrial fusion in vitro. But the merged image of the CLSM study showed that most of the isolated mitochondria carried both fluorescent dyes (Figure 4.5). Therefore, the hypothesis that two different labels can only be detected in one mitochondrion after two differently labeled mitochondria had fused was not appropriate. This can be explained by distribution effects. The dyes were not only inside mitochondria, but there were still free dye molecules in the surrounding medium that accumulated in the oppositely stained mitochondria when the samples were mixed. This problem could not be solved by extensive washing of the single-stained samples. As a consequence, fluorescent dyes were not applicable for the imaging of mitochondrial fusion in vitro.

As an alternative, mitochondria were labeled with fluorescent proteins by transfection of CHO-cells with different mitochondria targeted fluorescent proteins. At first, CHO-cells were transfected with a commercially available plasmid that expressed a mitochondria targeted green fluorescent protein (mtGFP). Only a few cells showed green fluorescence 24 h after transfection (Figure 4.6). Then, cells were selected with a G418 containing medium as the plasmid also carried a resistance gene against the antibiotic G418. After selection with G418, more but yet not all cells showed green fluorescence (Figure 4.7).

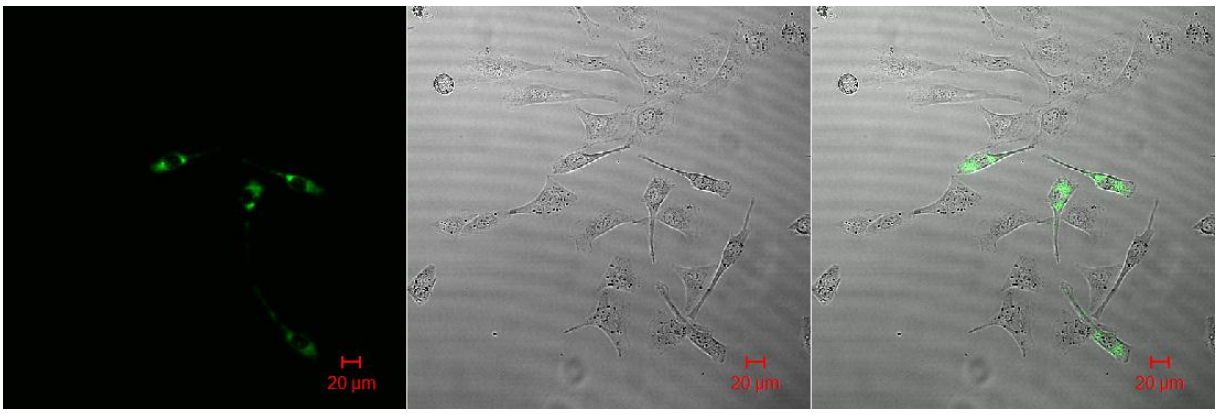

Figure 4.6: CLSM images showing cells transfected with mitochondria targeted GFP 24 h after transfection, the left image shows fluorescence of GFP, the image in the middle shows the bright field image and the right panel shows the merged image. Only some cells show GFP fluorescence.

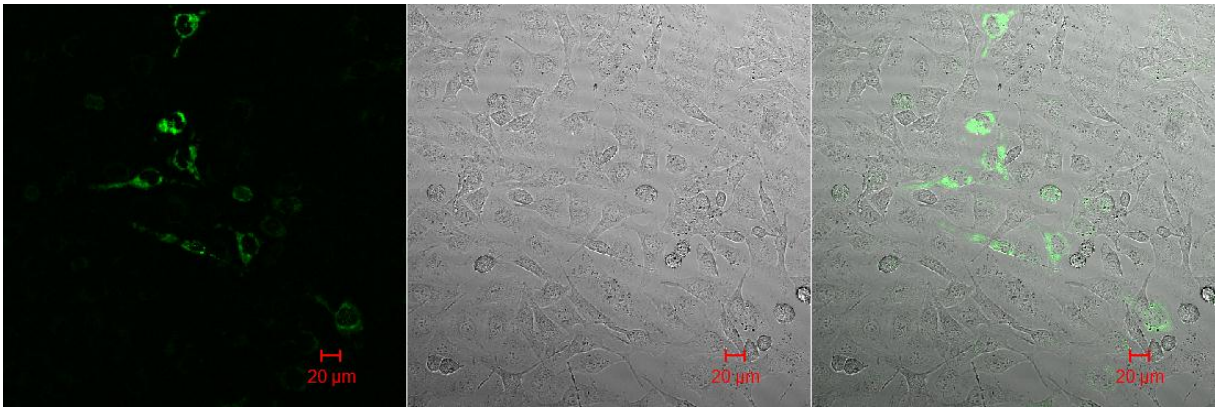

Figure 4.7: CLSM images showing cells transfected with mitochondria targeted GFP after G418 selection, the left image shows fluorescence of GFP, the image in the middle shows the bright field image and the right panel shows the merged image. Not all cells show GFP fluorescence.

Because selection with G418 was not sufficient, cells were sorted by flow cytometry. Only strong fluorescing cells were selected, resulting in a stable transfected cell line in which all cells showed green fluorescence (Figure 4.8). Figure 4.9 shows in more detail that the GFP resided in mitochondria.

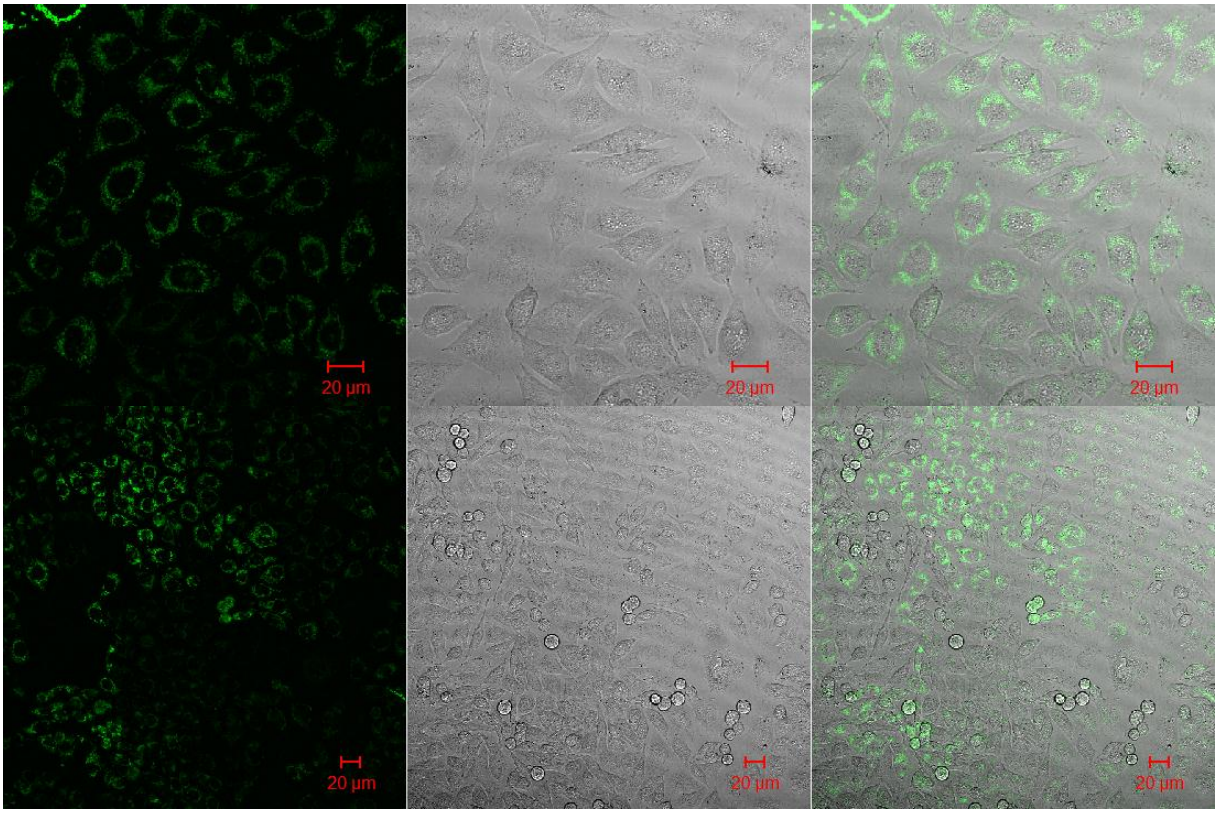

Figure 4.8: CLSM images showing cells transfected with mitochondria targeted GFP after sorting by flow cytometry, the left images show fluorescence of GFP, the images in the middle show the bright field images and the right panels show the merged images. All cells show GFP fluorescence.

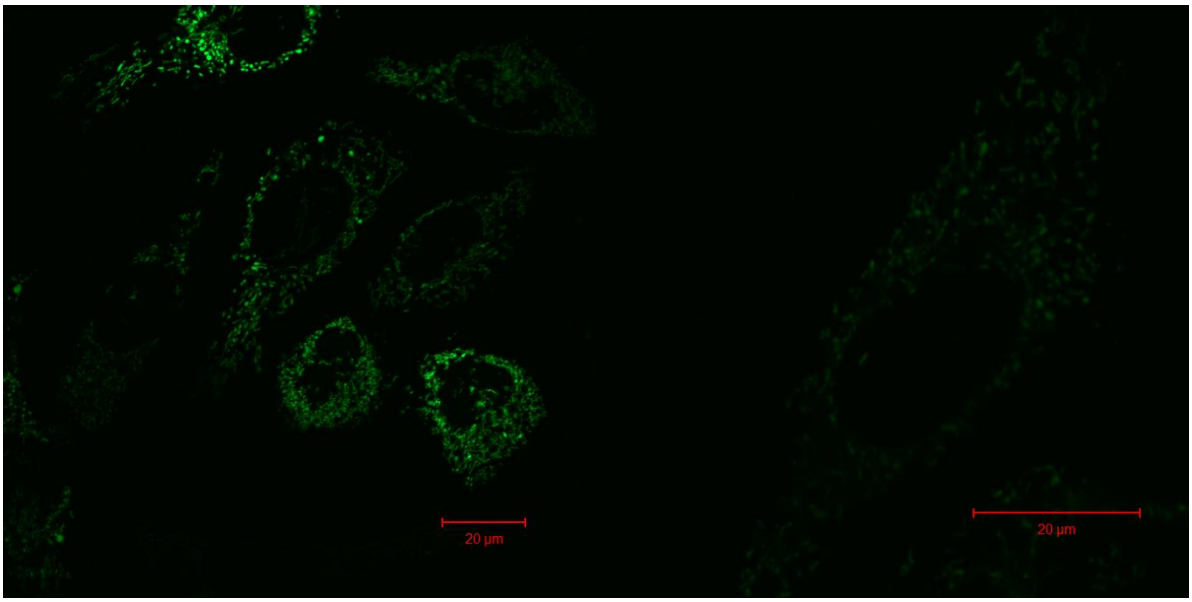

Figure 4.9: CLSM images showing cells transfected with mitochondria targeted GFP.

DsRed was chosen as second label for isolated mitochondria. Therefore, the sequence that encoded DsRed was cloned into the plasmid vector that expressed the mitochondria targeted GFP, resulting in the expression of a mitochondria targeted DsRed. After successful cloning and isolation of the plasmid from E. coli, CHO cells were transfected with the mitochondria targeted DsRed. Some of the cells showed orange fluorescence 24 h after transfection (Figure 4.10). Unfortunately, the fluorescence of the DsRed was weak and the cells lost the plasmid after more than 24 h and after selection with G418. It was not possible to produce a stable transfected cell line with mitochondria targeted DsRed.

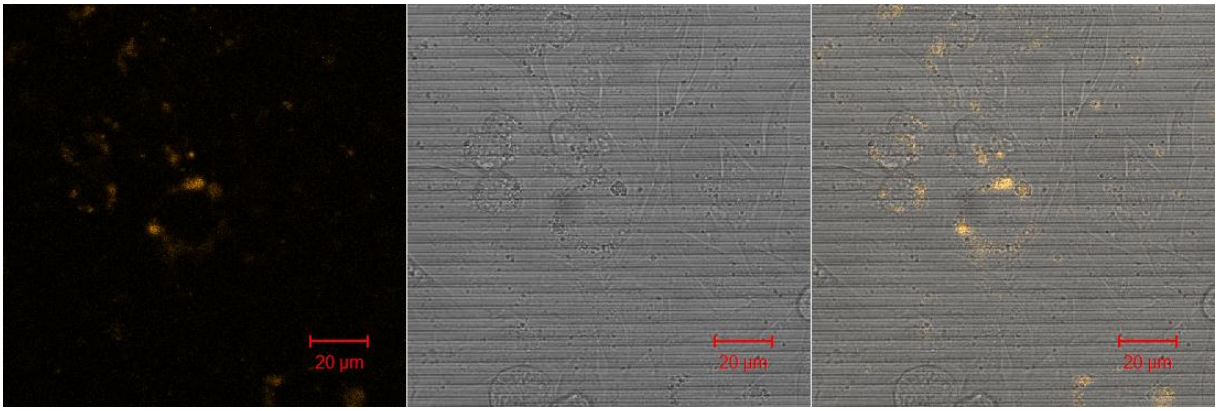

Figure 4.10: CLSM images showing cells transfected with mitochondria targeted DsRed 24 h after transfection, the left image shows fluorescence of DsRed, the image in the middle shows the bright field image and the right panel shows the merged image.

As an alternative to the fluorescent protein pair GFP – DsRed, the natural FRET-pair GFP – aequorin was chosen. The idea was to use isolated mitochondria that carry aequorin and isolated mitochondria that carry GFP for the detection of mitochondrial fusion in vitro. The hypothesis was that the FRET of aequorin to GFP could be detected after two mitochondria, one carrying aequorin and one carrying GFP, had mixed their contents after fusion. To proof that the FRET of aequorin to GFP is effective in mitochondria, cells that carried a mitochondria targeted aequorin were co-transfected with the mitochondria targeted GFP. Transfection with GFP was detected by laser excitation of GFP. After antibiotic and flow cytometry selection, a stable transfected cell line with mitochondria targeted aequorin and mitochondria targeted GFP was obtained (Figure 4.11).

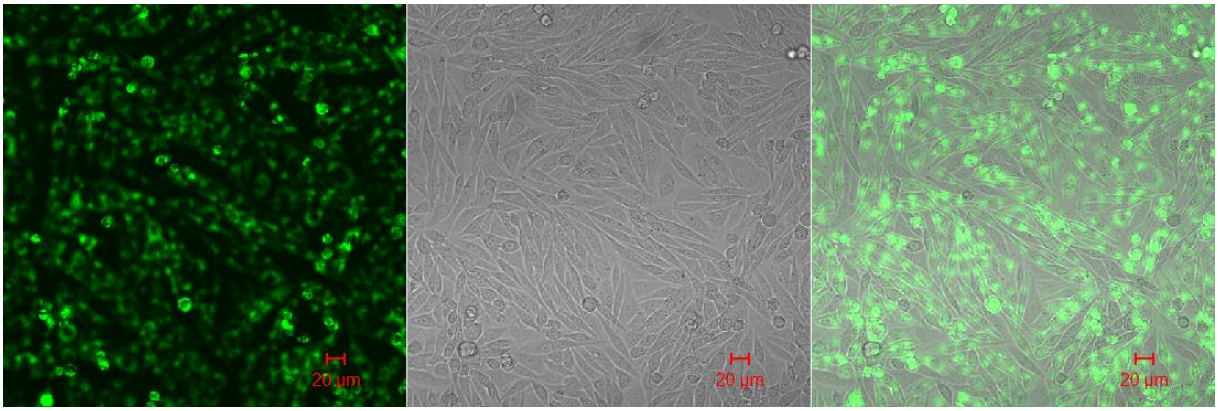

Figure 4.11: CLSM images showing cells transfected with mitochondria targeted aequorin and mitochondria targeted GFP, the left image shows the laser excited fluorescence of GFP, the image in the middle shows the bright field image and the right panel shows the merged image.

After stimulation of aequorin by coelenterazine h and calcium, the excitation of GFP by FRET from aequorin to GFP was not detectable and no green fluorescence of GFP was visible by microscopy. Therefore, the luminescence of aequorin was assessed. Intact cells and isolated were incubated with coelenterazine h. In intact cells, luminescence was stimulated by calcium after cell permeabilization with digitonin or by intracellular release of calcium after binding of NPY to a G-protein coupled receptor. In isolated mitochondria, luminescence was stimulated by the addition of calcium (Figure 4.12).

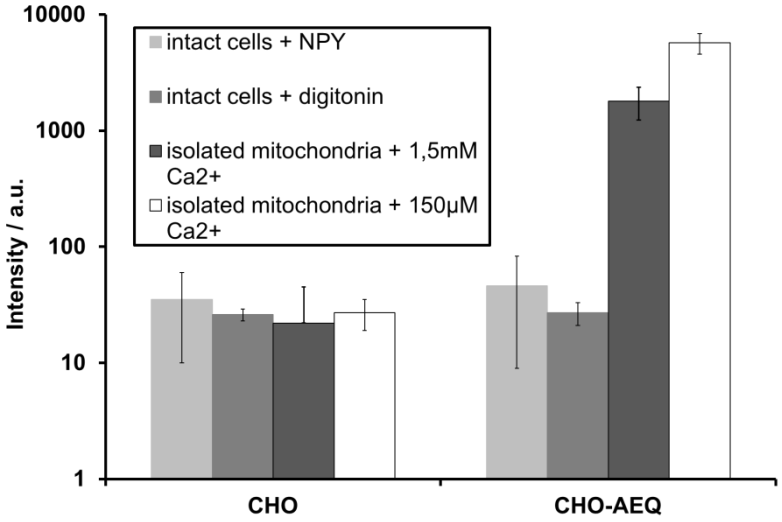

Figure 4.12: Luminescence intensity of aequorin of CHO cells (CHO) and CHO cells transfected with mitochondria targeted aequorin (CHO-AEQ). Luminescence was stimulated by NPY or calcium after permeabilization with digitonin in intact cells and with calcium in isolated mitochondria.

In intact cells carrying aequorin, no luminescence was detectable as well as in cells that did not carry aequorin, neither immediately after stimulation nor 2 h after stimulation. It seemed that luminescence decayed too fast. In contrast to that, luminescence of aequorin in isolated mitochondria was detectable even 2 h after stimulation by calcium. This indicated that aequorin was functional. Therefore, the failure of the FRET from aequorin to GFP could not be attributed to the functionality of aequorin as aequorin showed as strong and long lasting luminescence but the failure may be attributed to the concentrations of GFP and aequorin in mitochondria. The concentrations of both proteins were eventually too low for allowing a FRET effect.

Because DsRed and aequorin were not usable as counterparts to GFP, mitochondria were labeled with a red fluorescent protein (RFP). Therefore, cells were transfected with a commercially available plasmid that expressed a mitochondria targeted RFP (mtRFP). Only a few cells showed red fluorescence 24 h after transfection (Figure 4.13). Then, cells were selected with a G418 containing medium as the plasmid also carried a resistance gene against the antibiotic G418. After selection with G418, more but yet not all cells showed red fluorescence (Figure 4.14).

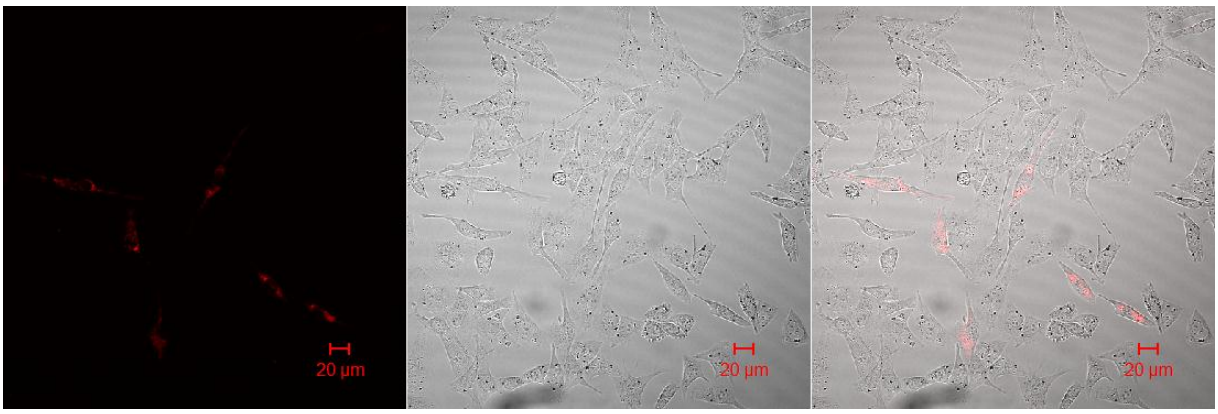

Figure 4.13: CLSM images showing cells transfected with mitochondria targeted RFP 24 h after transfection, the left image shows fluorescence of RFP, the image in the middle shows the bright field image and the right panel shows the merged image. Only some cells show RFP fluorescence.

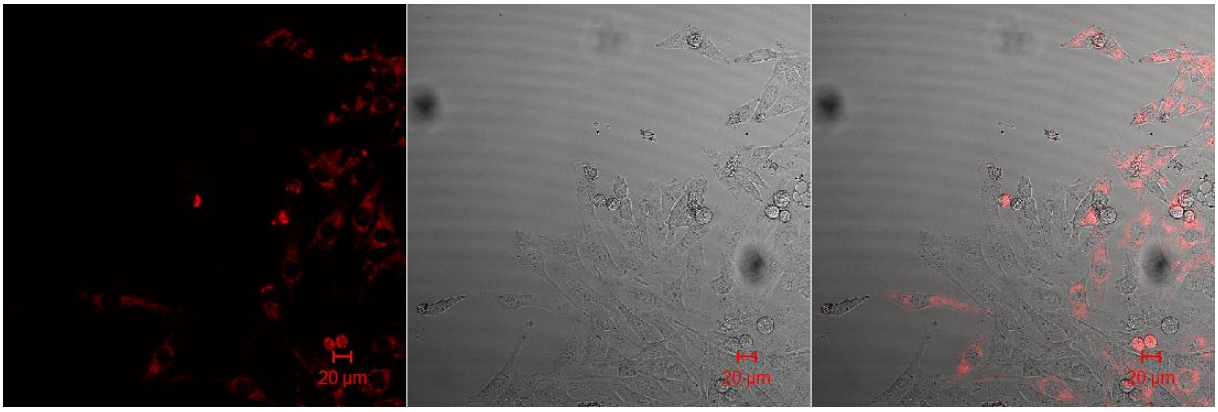

Figure 4.14: CLSM images showing cells transfected with mitochondria targeted RFP after G418 selection, the left image shows fluorescence of RFP, the image in the middle shows the bright field image and the right panel shows the merged image. Not all cells show RFP fluorescence.

Because selection with G418 was not sufficient, cells were again sorted by flow cytometry. Only strong fluorescing cells were selected, resulting in a stable transfected cell line in which all cells showed red fluorescence (Figure 4.15).

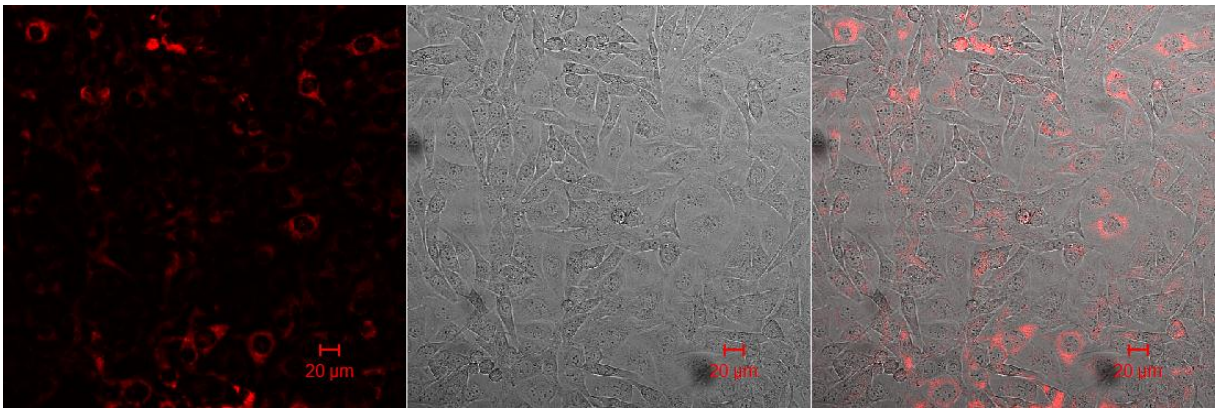

Figure 4.15: CLSM images showing cells transfected with mitochondria targeted RFP after sorting by flow cytometry, the left image shows fluorescence of RFP, the image in the middle shows the bright field image and the right panel shows the merged image. All cells show RFP fluorescence.

When isolated mitochondria containing GFP were mixed with isolated mitochondria containing RFP, only single-labeled mitochondria were detected (Figure 4.16) as fluorescent proteins did not wash out and labeled isolated mitochondria permanently.

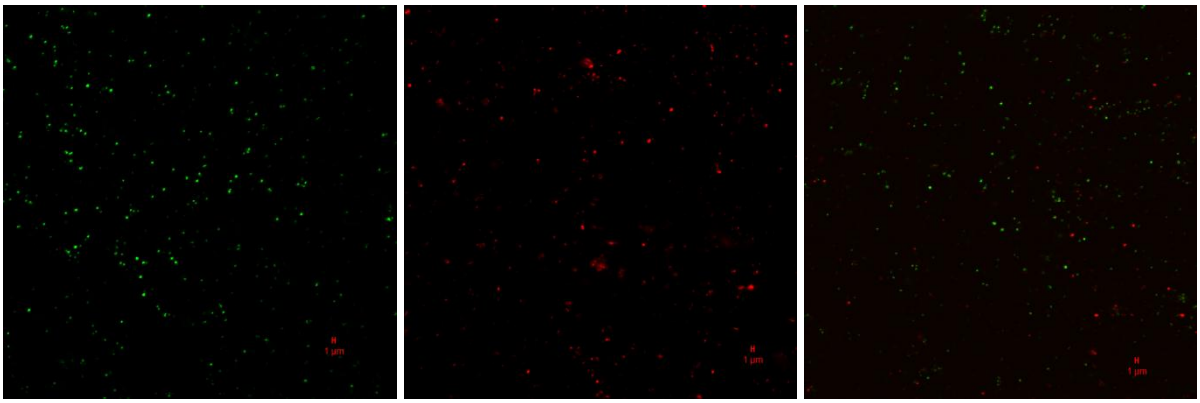

Figure 4.16: CLSM image of isolated mitochondria containing GFP on the left image, isolated mitochondria containing RFP in the middle and a mixture of GFP and RFP containing mitochondria on the right image.

4.4 Conclusions

The goal was to tag isolated mitochondria with two different labels to detect mitochondrial fusion in vitro in further studies. It was possible to label isolated mitochondria with mitochondria specific fluorescent dyes which was a quick and comfortable method. Additionally, intactness of isolated mitochondria was shown by the potential sensitive dye JC-1. But when samples of differently stained isolated mitochondria were mixed, the samples stained each other due to washing out of the fluorescent dyes. Therefore, it emerged that fluorescent dyes were not applicable for mitochondrial fusion studies in vitro. Alternatively, mitochondria targeted fluorescent proteins were chosen. Transfection of cells with commercially available plasmids was successful even though several selection cycles with an antibiotic were not sufficient to obtain a stable cell line. After sorting cells by flow cytometry, stable cell lines were obtained. In contrast to the commercially available plasmids, cloning of DsRed into a plasmid that carried a mitochondrial targeting sequence was a time consuming process. It was successful at last but the transfection efficiency of the cloned plasmid was low, the fluorescence of the DsRed was low and the cells lost the plasmid within a short period of time. It was not possible to create a stable cell line with DsRed containing mitochondria. It was also not possible to use the natural FRET pair aequorin – GFP for the detection of mitochondrial fusion in vitro as the positive control, a co-transfection of aequorin and GFP, failed. The aequorin was active after stimulation but it was likely that the concentrations of both proteins were too low and hence, the distance between both proteins was too far. Because transfection with mitochondria targeted GFP and RFP was successful and stable, GFP- and RFP-labeled mitochondria were used in further studies of mitochondrial fusion in vitro.

4.5 References

[1] Invitrogen, Fluorescent detection reagents for imaging mitochondria and lysosomes, http://de-de.invitrogen.com/site/de/de/home/References/Molecular-Probes-The-Handbook/tables/Fluorescent-detection-reagents-for-imaging-mitochondria-and-lysosomes.html.

[2] Invitrogen, Molecular Probes fluorescent organelle stains, http://de-de.invitrogen.com/site/de/de/home/References/Molecular-Probes-The-Handbook/tables/Molecular-Probes-organelle-selective-probes.html.

[3] Invitrogen, Probes for Mitochondria—Section 12.2, http://de-de.invitrogen.com/site/de/de/home/References/Molecular-Probes-The-Handbook/Probes-for-Organelles/Probes-for-Mitochondria.html.

[4] Invitrogen, Spectral characteristics of the MitoTracker probes—Table 12.2, http://de-de.invitrogen.com/site/de/de/home/References/Molecular-Probes-The-Handbook/tables/Spectral-characteristics-of-the-MitoTracker-probes.html.

[5] Invitrogen, MitoTracker® Deep Red 633, http://products.invitrogen.com/ivgn/product/M22426.

[6] E.R. Dabkowski, C.L. Williamson, V.C. Bukowski, R.S. Chapman, S.S. Leonard, C.J. Peer, P.S. Callery, J.M. Hollander, Diabetic cardiomyopathy-associated dysfunction in spatially distinct mitochondrial subpopulations, Am. J. Physiol. Heart Circ. Physiol 296 (2009) H359-69.

[7] Invitrogen, JC-1, http://products.invitrogen.com/ivgn/product/T3168.

[8] S.-H. Yang, S.N. Sarkar, R. Liu, E.J. Perez, X. Wang, Y. Wen, L.-J. Yan, J.W. Simpkins, Estrogen Receptor as a Mitochondrial Vulnerability Factor, Journal of Biological Chemistry 284 (2009) 9540–9548.

[9] S.S. Winter, D.M. Lovato, H.M. Khawaja, B.S. Edwards, I.D. Steele, S.M. Young, T.I. Oprea, L.A. Sklar, R.S. Larson, High-throughput screening for daunorubicin-mediated drug resistance identifies mometasone furoate as a novel ABCB1-reversal agent, J Biomol Screen 13 (2008) 185–193.

[10] F. Fuchs, H. Prokisch, W. Neupert, B. Westermann, Interaction of mitochondria with microtubules in the filamentous fungus Neurospora crassa, J. Cell. Sci 115 (2002) 1931–1937.

[11] Invitrogen, Baculovirus-Mediated Transduction of Mammalian Cells, http://de-de.invitrogen.com/site/de/de/home/References/Molecular-Probes-The-Handbook/Technical-Notes-and-Product-Highlights/BacMam-Gene-Delivery-Technology.html.

[12] F. Distelmaier, W.J.H. Koopman, E.R. Testa, A.S. de Jong, H.G. Swarts, E. Mayatepek, J.A.M. Smeitink, P.H.G.M. Willems, Life cell quantification of mitochondrial membrane potential at the single organelle level, Cytometry A 73 (2008) 129–138.

[13] Invitrogen, Lipofectamine™, http://de-de.invitrogen.com/site/de/de/home/brands/Product-Brand/lipofectamine.html.

[14] N. Hirota, D. Yasuda, T. Hashidate, T. Yamamoto, S. Yamaguchi, T. Nagamune, T. Nagase, T. Shimizu, M. Nakamura, Amino acid residues critical for endoplasmic reticulum export and trafficking of platelet-activating factor receptor, J. Biol. Chem 285 (2010) 5931–5940.

[15] A. Chiesa, E. Rapizzi, V. Tosello, P. Pinton, M. de Virgilio, K.E. Fogarty, R. Rizzuto, Recombinant aequorin and green fluorescent protein as valuable tools in the study of cell signalling, Biochem. J 355 (2001) 1–12.

[16] M. Brini, Calcium-sensitive photoproteins, Methods 46 (2008) 160–166.

[17] F. de Giorgi, M. Brini, C. Bastianutto, R. Marsault, M. Montero, P. Pizzo, R. Rossi, R. Rizzuto, Targeting aequorin and green fluorescent protein to intracellular organelles, Gene 173 (1996) 113–117.

[18] Invitrogen, pShooter, http://tools.invitrogen.com/content/sfs/manuals/pshooter_pcmv_man.pdf.

[19] Wikipedia, Luciferin, http://de.wikipedia.org/wiki/Luciferin.

[20] A. Heller, Chapter 5: Mitochondrial fusion in vitro, in: A. Heller (Ed.), Targeting mitochondria by mitochondrial fusion, mitochondria-specific peptides and nanotechnology: Dissertation.

[21] N.M. Mhaidat, Y. Wang, K.A. Kiejda, X.D. Zhang, P. Hersey, Docetaxel-induced apoptosis in melanoma cells is dependent on activation of caspase-2, Molecular Cancer Therapeutics 6 (2007) 752–761.

[22] S. Meeusen, J.M. McCaffery, J. Nunnari, Mitochondrial Fusion Intermediates Revealed in Vitro, Science 305 (2004) 1747–1752.

Chapter 5

Mitochondrial fusion in vitro

Abstract

Mitochondrial fusion is an important process in cellular physiology. A protocol for fusion of isolated mitochondria from mammalian CHO-K1 cells was established. Mitochondrial fusion efficiency was evaluated qualitatively by microscopic methods and quantitatively by flow cytometry. Transmission electron microscopy revealed fusion intermediates, mitochondria with fused outer membranes but separated inner membranes detected by the ultrastructure whereas confocal light scanning microscopy revealed completely fused mitochondria with mixed matrices detected by the mixed yellow color of the mitochondrial green and red fluorescent proteins. A flow cytometry protocol for the quantitative analysis of mitochondrial fusion in vitro was established. It involved control samples to exclude mitochondria that stick together from fused mitochondria. A fusion efficiency of about 25 % was determined with this method.

5.1 Introduction

Mitochondria are dynamic organelles that move along the cytoskeleton inside cells [1] and that form dynamic networks via continuous elapsing fusion and fission processes [2]. Fusion and fission regulate mitochondrial morphology, distribution, activity and result in exchange of mitochondrial content [2,3]. They are a protective mechanism as the exchange of mitochondrial DNA (mtDNA) and proteins facilitates the redistribution of dysfunctional proteins and mutated mtDNA to maintain mitochondrial functionality and stability of the mitochondrial genome [4]. Mitochondrial fusion is mediated by GTPases in the mitochondrial membranes. Mitofusin (Mfn) 1 and 2 are located in the outer membrane of mammalian mitochondria and OPA 1 is the fusion GTPase of the inner membrane [2,5]. The N- and C-terminal regions of the mitofusins protrude into the cytosol forming a U-shaped transmembrane domain. The N-terminal domain contains a GTPase and a heptad repeat region, HR1 whereas the C-terminus contains a second heptad repeat region, HR2. The interaction of mitofusions on adjacent mitochondria is mediated by these HR2 regions forming an antiparallel coiled coil that results in tethering of mitochondria [2,6]. OPA1 is located within the intermembrane space and is associated with the inner membrane. Fusion of the inner membrane is also an energy dependent process mediated by the GTPase domain of OPA1 [2].

Components of the mitochondrial fission machinery are the dynamin related protein (Drp) 1 and Fis1. Drp1 contains a GTPase domain and is one key component of the fission machinery. It is mainly localized in the cytosol. Fis1, the other key component of the fission machinery is localized in the outer mitochondria membrane and does not contain a GTPase domain [2].

Defects in mitochondrial fusion are related to several diseases. Dysfunction of mitochondrial fusion due to absence or defective fusion proteins results in fragmentation of mitochondria and affects cell growth and development, membrane potential, cellular respiration and plays a proapoptotic role [2,7]. Although it is known that mitochondrial fusion plays an important role in cellular development, the mechanisms that occur during this event have not been

revealed in detail yet. A step towards the understanding of mitochondrial fusion has been the establishment of a protocol that captured this process in vitro by Meeusen et al. [8]. It relies on studies with yeast mitochondria and has been the initial point for the fusion experiments of mitochondria isolated from mammalian cells, described in this study as well as in further studies.

This study focusses on the establishment of a fusion protocol for mammalian mitochondria and the methods to detect mitochondrial fusion in vitro. The protocols described in this study are based on the imaging methods for isolated mitochondria. To detect mitochondrial fusion in vitro, it is necessary to start with two differently labeled populations of isolated mitochondria. The behavior of populations, individually labeled with fluorescent proteins, has been investigated. Applied detection methods have been confocal laser scanning microscopy (CLSM), flow cytometry and transmission electron microscopy (TEM). Both microscopic methods allow for the qualitative analysis of mitochondrial fusion in vitro whereas flow cytometry has been used for the quantitative determination of mitochondrial fusion efficiency in vitro.

5.2 Materials and methods

5.2.1 Materials

HAM F-12 nutrient mixture and fetal calf serum (FCS) were purchased from Sigma-Aldrich (Steinheim, Germany). Trypsin-EDTA 0.25 % was obtained from Gibco-Invitrogen (Karlsruhe, Germany). G418 was purchased from Sigma-Aldrich (Steinheim, Germany). Purified water was obtained by using a Milli-Q water purification system from Millipore (Schwalbach, Germany). All cell culture materials were purchased from Corning (Bodenheim, Germany).

Isolation buffer consisted of 250 mM sucrose (Merck, Darmstadt, Germany), 10 mM Tris (USB Corporation, Cleveland, OH USA), 10 mM KCl (Merck, Darmstadt, Germany), 1 mM Na_2EDTA (Merck, Darmstadt, Germany) and 0.1 % bovine serum albumin (BSA) (Sigma-Aldrich, Steinheim, Germany). Antimycin A was purchased from Sigma-Aldrich (Steinheim, Germany). Fusion buffer consisted of 600 mM sorbitol (Sigma-Aldrich, Steinheim, Germany), 20 mM Tris (USB Corporation, Cleveland, OH USA), 150 mM potassium acetate (Merck, Darmstadt, Germany), 5 mM magnesium acetate tetrahydrate (Merck, Darmstadt, Germany), 0.1 % BSA (Sigma-Aldrich, Steinheim, Germany), 0.5 mM GTP (Sigma-Aldrich, Steinheim, Germany), 1mM ATP (Sigma-Aldrich, Steinheim, Germany), 40mM creatine phosphate (Sigma-Aldrich, Steinheim, Germany) and 30 units/ml creatine phosphokinase (Sigma-Aldrich, Steinheim, Germany). DPBS without calcium and magnesium was obtained from Gibco-Invitrogen (Karlsruhe, Germany).

0.1 M cacodylate fixation buffer consisted of 100 mM sodium cacodylate (Roth, Karlsruhe, Germany), 2 mM magnesium chloride hexahydrate (Merck, Darmstadt, Germany), 1 mM calcium chloride dihydrate (Merck, Darmstadt, Germany), 40 mM sodium chloride (Merck, Darmstadt, Germany) and 2 % glutaraldehyde (Serva, Heidelberg, Germany). 0.1 M cacodylate washing buffer consisted of 100 mM sodium cacodylate (Roth, Karlsruhe, Germany), 2 mM magnesium chloride hexahydrate (Merck, Darmstadt, Germany), 1 mM calcium chloride dihydrate (Merck, Darmstadt, Germany) and 40 mM sodium chloride (Merck, Darmstadt, Germany). Osmium tetroxide (ScienceServices, Munich, Germany) was

dissolved to 1 % in 0.1 M cacodylate buffer that consisted of 100 mM sodium cacodylate (Roth, Karlsruhe, Germany), 2 mM magnesium chloride hexahydrate (Merck, Darmstadt, Germany), 1 mM calcium chloride dihydrate (Merck, Darmstadt, Germany) and 40 mM sodium chloride (Merck, Darmstadt, Germany). Agarose was purchased from Biozym (Hessisch Oldendorf, Germany). Embedding in Epon was carried out with an Epoxy Embedding Medium Kit (Fluka by Sigma-Aldrich, Steinheim, Germany). Propylen oxide was purchased from Sigma-Aldrich (Steinheim, Germany). Uranyl acetate was obtained from Roth (Karlsruhe, Germany). Lead citrate by Reynolds consisted of lead nitrate (Merck, Darmstadt, Germany) and tri-sodium citrate dihydrate (Merck, Darmstadt, Germany).

5.2.2 Mitochondrial fusion in vitro

Long-time cultivation of CHO-cell lines that were stably transfected with mitochondria targeted green fluorescent protein (mtGFP) and mitochondria targeted red fluorescent protein (mtRFP) was carried out in selection medium HAM-F12 containing 10 % FCS and 400 µg/ml G418. The last cultivation step of CHO-mtGFP and CHO-mtRFP cells prior to fusion experiments was carried out in G418-free medium because the cells did not lose the plasmid within one week. Cells were cultured in HAM-F12 nutrient mixture containing 10 % FCS in 150 cm^2 culture flasks until confluency, harvested by Trypsin-EDTA 0.25 % and washed with isolation buffer. The centrifugation steps for the washing steps of the cells were carried out in a GS-15R centrifuge (Beckman, Krefeld, Germany). Afterwards, mtGFP- or mtRFP-containing cells from one culture flask were suspended in 250 µl isolation buffer. Then, cells from four flasks were pooled and the resulting one milliliter of cell suspension was transferred into a cooled 2-ml Dounce glass homogenizer (Sigma-Aldrich, Steinheim, Germany) where the cells were disrupted by 25 strokes. The suspension was transferred into a 2-ml safe-lock tube (Eppendorf, Hamburg, Germany) and centrifuged at 1500 g at 4 °C for 10 min a type 5415 R centrifuge (Eppendorf, Hamburg, Germany) to pelletize nuclei as well as remaining intact cells. The first supernatant was kept on ice, while the pellet was resuspended in isolation buffer and homogenized by 25 Dounce strokes for a second time to

break remaining intact cells. A second centrifugation step at 1500 g at 4 °C for 10 min yielded a pellet that was the nuclei enriched fraction. The first and the second supernatant were mixed and centrifuged at 16000 g at 4 °C for 15 min to obtain a pellet enriched with GFP- or RFP-containing isolated mitochondria. The amount of cells used for the isolation of mitochondria depended on the required amount for the different experiments. Mitochondrial protein concentration was determined by Bradford-Assay [9].

Mitochondrial fusion was carried out according to Meeusen et al. [8]. Thereby, equal amounts of GFP- and RFP-containing isolated mitochondria regarding to the mitochondrial protein concentration were mixed and centrifuged at 16000 g, 4 °C for 10 min. The pellet was incubated on ice for 10 min and was resuspended in fusion buffer, 40 µl for 500 µg total mitochondrial protein. After incubation at room temperature for 1 h, the fusion samples were analyzed by CLSM, TEM or flow cytometry. Isolated mitochondria of the control samples (G+R) were treated in the same manner like isolated mitochondria for mitochondrial fusion in vitro (F), except the fusion buffer that was exchanged by isolation buffer.

5.2.3 Qualitative characterization of mitochondrial fusion in vitro by CLSM

Fluorescence of the fusion samples was analyzed by CLSM with a Zeiss Axiovert LSM 510 (Carl Zeiss, Oberkochen, Germany) and an AxioCam HRc (Carl Zeiss, Oberkochen, Germany). Thereby, GFP was excited a 488 nm and detected at 505–530 nm and RFP was excited at 488 nm and detected at 530–600 nm. In samples containing both fluorescent proteins, a multitrack scan mode was applied.

5.2.4 Qualitative characterization of mitochondrial fusion in vitro by TEM

For qualitative analysis by TEM, unlabeled isolated mitochondria were used instead of GFP- and RFP-containing isolated mitochondria. Isolation and mitochondrial fusion in vitro were accomplished as described previously. Fusion samples were fixed in cacodylate fixation buffer at room temperature for 5 min and on ice overnight. Afterwards, mitochondria were washed by five washing steps, each of them in cacodylate washing buffer for 2 min. Then,

isolated mitochondria were pelletized in a 1 % agarose solution that was heated up to 40 °C. All centrifugation steps were carried out in a himac CT15RE centrifuge (VWR Leuven, Belgium by Hitachi Koki Co. Ltd.). After gelation of the agarose, the gel block was cut and fixed with osmium tetroxide solution overnight. The samples were washed in DPBS four times for 15 min. Afterwards, the samples were dehydrated in a graded series of ethanol: 50 %, 70 %, 80 %, 90 % and 100 %. Each dehydration step was carried out two times for 15 min. Then, the samples were treated in an equal mixture of acetone or propylene oxide and ethanol for 20 min and two times in acetone or propylene oxide for 20 min. Afterwards, the samples were treated with a mixture of acetone or propylene oxide and Epon (2:1) for 2 h, followed by in a mixture of acetone or propylene oxide and Epon (1:1) for 2 h and subsequently in a mixture of acetone or propylene oxide and Epon (1:2) in an open vial overnight. Then, the samples were embedded and hardened in Epon at room temperature for 1 h, at 30 °C for 2 h and at 60 °C for 2 days. Epon blocks were cut into sections of 50 nm with a Leica EM UC6 microtome (Leica, Vienna, Austria) and transferred to copper slot grids with a 1.5 % hyaloform foil. They were examined either unstained or stained with uranyl acetate and lead citrate in an EM 902 transmission electron microscope from Zeiss (Carl Zeiss, Oberkochen, Germany), operated at 80kV. Digital images were recorded by a slow scan CCD camera (TRS Typ 7888, Serial No. 321/08).

5.2.5 Quantitative characterization of mitochondrial fusion efficiency in vitro by flow cytometry

For the quantitative evaluation of mitochondrial fusion efficiency in vitro by flow cytometry, control samples, treated similar to the fusion samples, were analyzed. Therefore, GFP- and RFP-containing isolated mitochondria were mixed and centrifuged at 16000 g, 4 °C for 10 min. The pellet was incubated on ice for 10 min and resuspended in isolation buffer, 40 µl for 500 µg total mitochondrial protein. After incubation at room temperature for 1 h, the control samples (G+R) were analyzed in the same way like the fusion samples (F). That means

treatment of fusion and control sample was similar, only the influence of fusion buffer was evaluated as it was exchanged by isolation buffer in the control sample (G+R).

Quantitative analysis of mitochondrial fusion in vitro of GFP- and RFP-containing samples was carried out by flow cytometry with a FACSCanto™ (BD Bioscience, Heidelberg, Germany). Therefore, the samples were diluted to not exceed the critical count rate of the flow cytometer. GFP and RFP were excited by a 488 nm blue laser. GFP was detected at 515–545 nm and RFP was detected at 564–606 nm. Single labeled isolated mitochondria with either GFP or RFP were used to define GFP- and RFP-positive quadrants and to separate fluorescent mitochondria from non-fluorescent cell fragments. For the analysis of mitochondrial fusion in vitro, plots that indicated fluorescence of GFP on the x-axis and fluorescence of RFP on the y-axis were created. Quadrants of the plots were defined as follows: the lower left quadrant (LL) indicated non fluorescent cell fragments, the upper left quadrant (UL) was determined by single-labeled RFP-mitochondria, the lower right quadrant (LR) was determined by single-labeled GFP-mitochondria and the upper right quadrant (UR) was positive for GFP and RFP showing mitochondria that contain both fluorescent proteins, either by fusing or by sticking together (Figure 5.1).

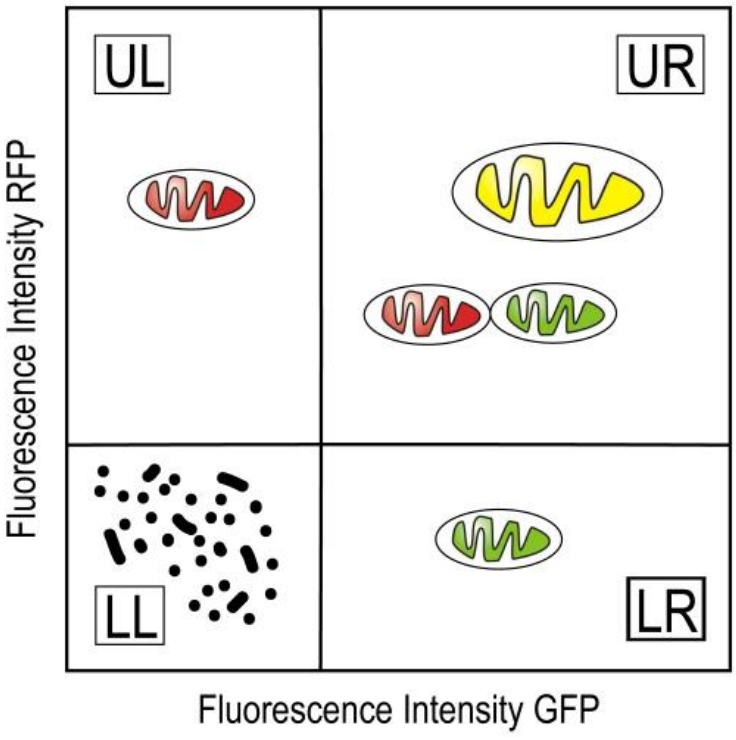

Figure 5.1: Flow cytometry plot for the analysis of mitochondrial fusion.

Because mitochondria (UL, UR and LR quadrant) could be easily distinguished from cell fragments (LL quadrant) by this method, the amount of double positive, GFP- and RFP-containing mitochondria of all mitochondria (single GFP, single RFP and double GFP-RFP) was calculated for the fusion sample, defined as (F raw) and for the control sample, defined as (G+R), as follows:

$$(F\ raw) or\ (G+R) = \frac{UR}{UR+UL+LR}.$$

The flow cytometer could not distinguish between fused mitochondria and mitochondria that simply stick together. Therefore, the calculated amount of double positive results for RFP and GFP in the control sample (G+R) that did not contain fused mitochondria but that could contain mitochondria which stick together, was subtracted from the amount of double positive results for RFP and GFP in the fusion sample (F raw) resulting in a value that indicated only fused mitochondria, defined as F:

$$(F) = (F\ raw) - (G+R).$$

These calculations are illustrated in Figure 5.2. Thereby, it was assumed that the amounts of mitochondria that stick together without fusing were similar in the fusion sample (F raw) and in the control sample (G+R) because both samples were treated in the same way. It has to be considered that the fusion sample (F) can contain mitochondria in which both membranes were fused and mitochondria in which only the outer membrane was fused.

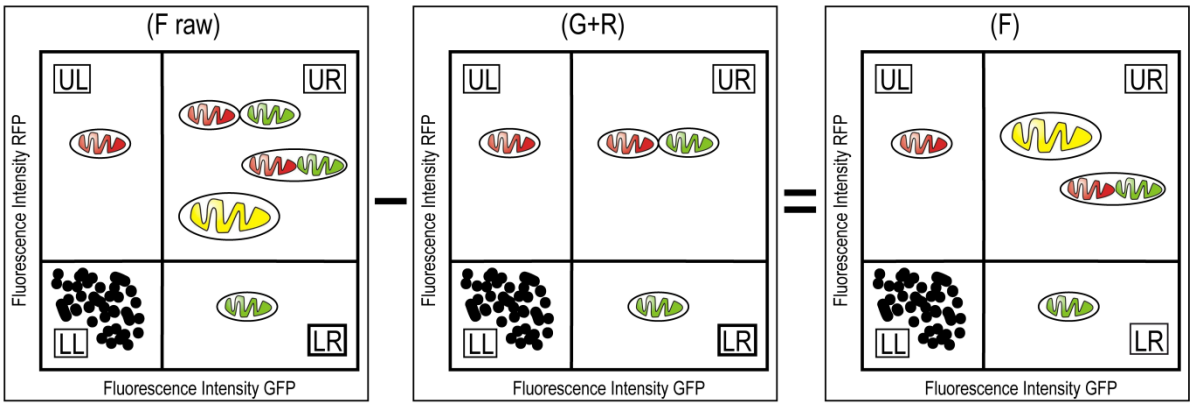

Figure 5.2: Flow cytometry plots of the quantitative analysis of mitochondrial fusion.

G+R samples were evaluated in every flow cytometry experiment and this value was subtracted from all fusion samples that were analyzed in the same experiment.

5.2.6 Statistical analysis

Results were expressed as means ± standard deviation (SD).

5.3 Results and discussion

A protocol for mitochondrial fusion in vitro of isolated mitochondria from mammalian cells was established according to a protocol for yeast mitochondria that was published by Meeusen et al. [8]. For detection of mitochondrial fusion in vitro with fluorescence based methods such as confocal light scanning microscopy or flow cytometry, it was essential to work with permanently labeled isolated mitochondria. As it emerged that fluorescence dyes were not applicable for studying mitochondrial fusion in vitro due to washing out of the dyes [10], the studies were accomplished with fluorescence proteins expressed in mitochondria that labeled isolated mitochondria permanently. Equal amounts of red and green fluorescent isolated mitochondria were mixed. The mixture was centrifuged to bring isolated mitochondria in close contact and then, they were resuspended in a fusion buffer that provided the required energy for mitochondrial fusion. In the control samples, only individually labeled green or red mitochondria were detected (Figure 5.3).

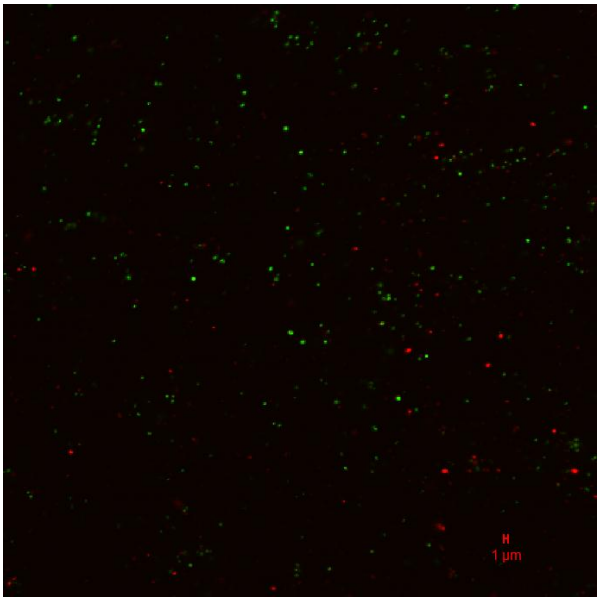

Figure 5.3: CLSM image of the control sample (G+R) containing a mixture of GFP and RFP mitochondria that was treated in the same way like the fusion sample (F). Only single labeled mitochondria were detected. No mitochondrion contained both fluorescent proteins.

In the fusion samples (F), yellow mitochondria containing a mixture of green and red fluorescent proteins were detected (Figure 5.4). The yellow color indicated that the matrices

of differently labeled mitochondria had mixed due to fusion of outer and inner mitochondrial membranes. Beside the mixed-colored mitochondria, also individually labeled green and red mitochondria were detected. Individually labeled mitochondria could either be non-fused mitochondria or mitochondria that had fused with a mitochondrion of the same color (green-green or red-red) which could not be detected by this method.

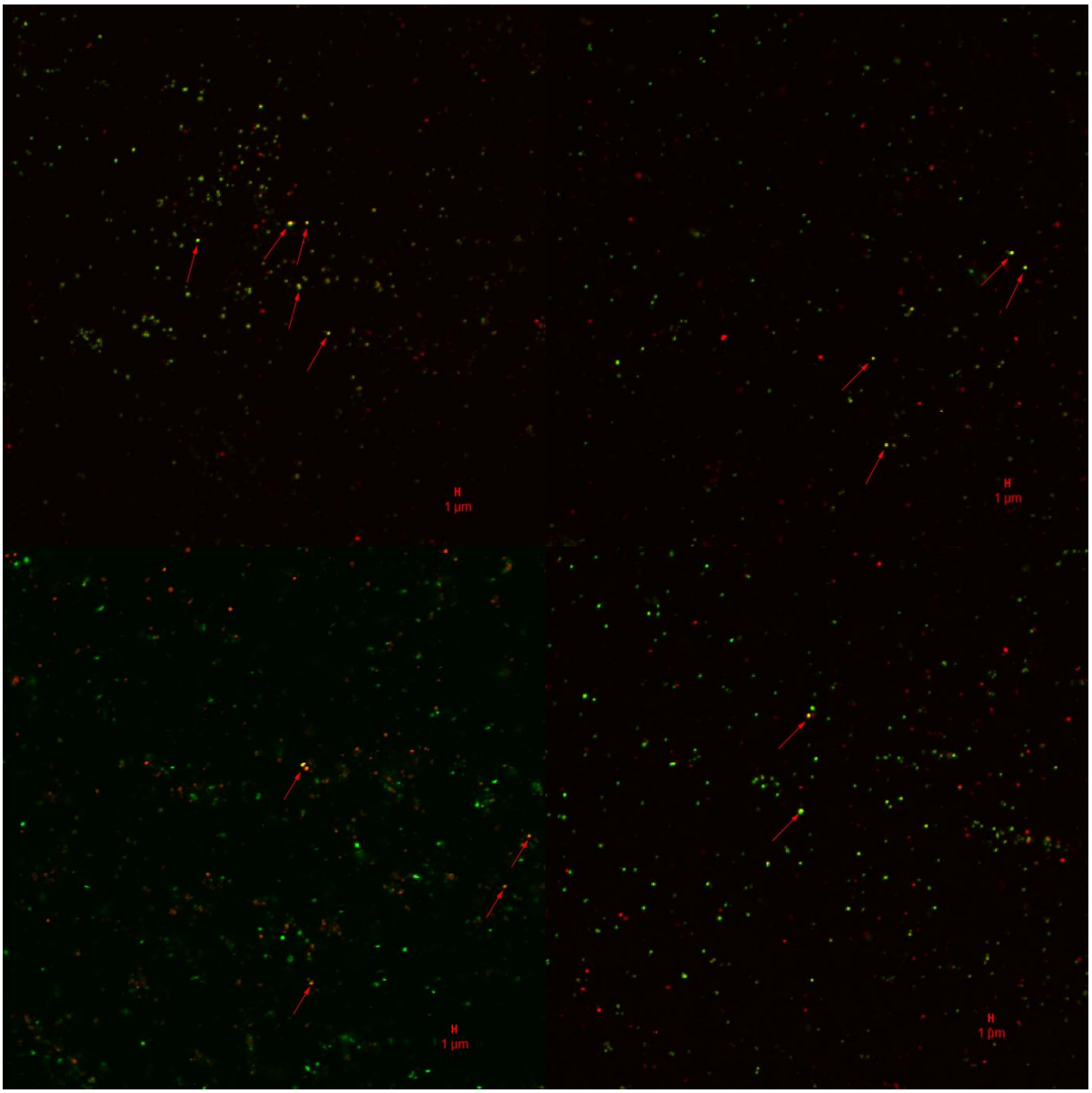

Figure 5.4: CLSM images of fusion samples (F). Single labeled mitochondria and mitochondria containing a mixture of GFP and RFP are visible as yellow dots. These fused mitochondria are indicated by red arrows.

For the quantitative analysis of mitochondrial fusion efficiency in vitro, a flow cytometry protocol was established. Flow cytometry has been used for the analysis of isolated mitochondria since 1986 [11]. It allowed for the simultaneous analysis of two and more fluorescent dyes, was capable for high throughput analysis [12] and was applicable for the analysis of highly diluted samples that did not consume large amounts of isolated mitochondria. Therefore, it was the method of choice for the evaluation of mitochondrial fusion efficiency in vitro. Thereby, mitochondria containing both fluorescent proteins due to fusion of outer or of both membranes were detected and the amount of fused isolated mitochondria among all analyzed isolated mitochondria was calculated and expressed as fusion efficiency. Mitochondria that were treated with antimycin A, an inhibitor of the respiratory chain that interrupted mitochondrial functionality and integrity, were not fusion competent anymore (Figure 5.5)

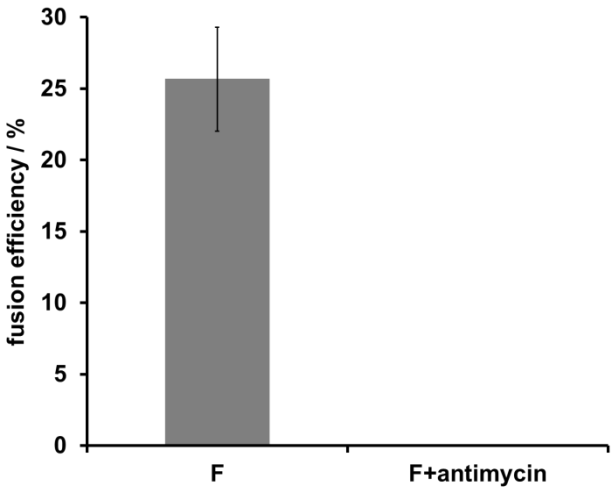

Figure 5.5: Quantitative evaluation of fusion efficiency in vitro by flow cytometry in comparison to fusion efficiency after pre-treatment of isolated mitochondria with antimycin A. Data are expressed as means of three measurements ± standard deviations (SD).

A disadvantage of the method was the limitation to size related resolution as the size of mitochondria was at the lower size resolution limit. Therefore, only fluorescence based analysis was applied.

The analysis of the fusion samples by TEM revealed fusion intermediates with fused outer and separated adjacent inner membranes (Figure 5.6, 5.7 and 5.8). Completely fused mitochondria with fused outer and inner membrane could not be detected with this transmission electron microscopy method. It was rather rare to detect such fusion intermediates as the change of mitochondrial morphology and mitochondrial fusion were very rapid elapsing processes [8]. It is known that mitochondria can form 15-20 different shapes in 10 min [13]. No fusion intermediates were detected in samples with isolated mitochondria that were not treated according to the fusion protocol.

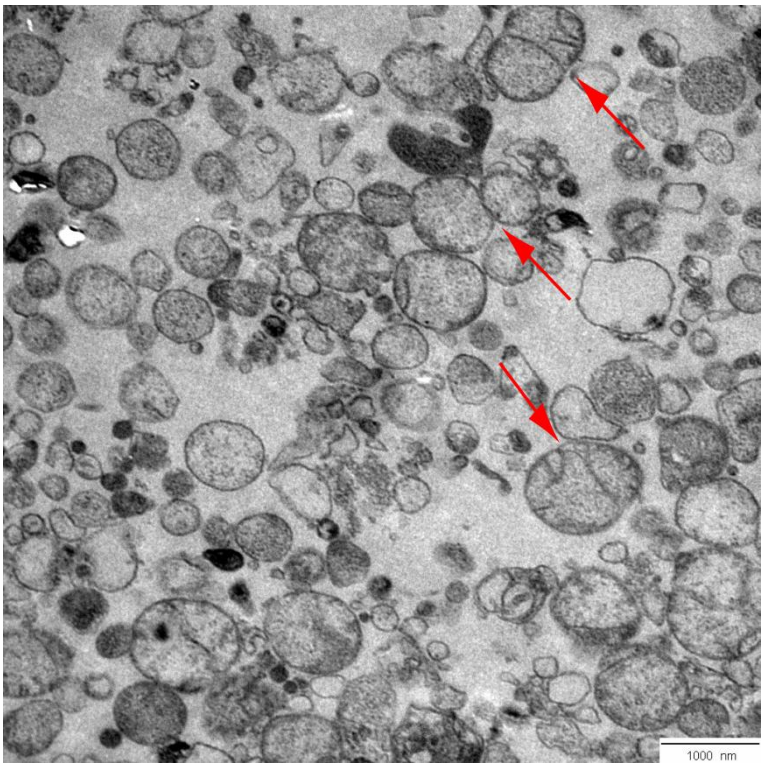

Figure 5.6: TEM image of the fusion sample (F), 7000x magnification. Fusion intermediates of mitochondria with separated inner membranes and fused outer membrane are indicated by red arrows.

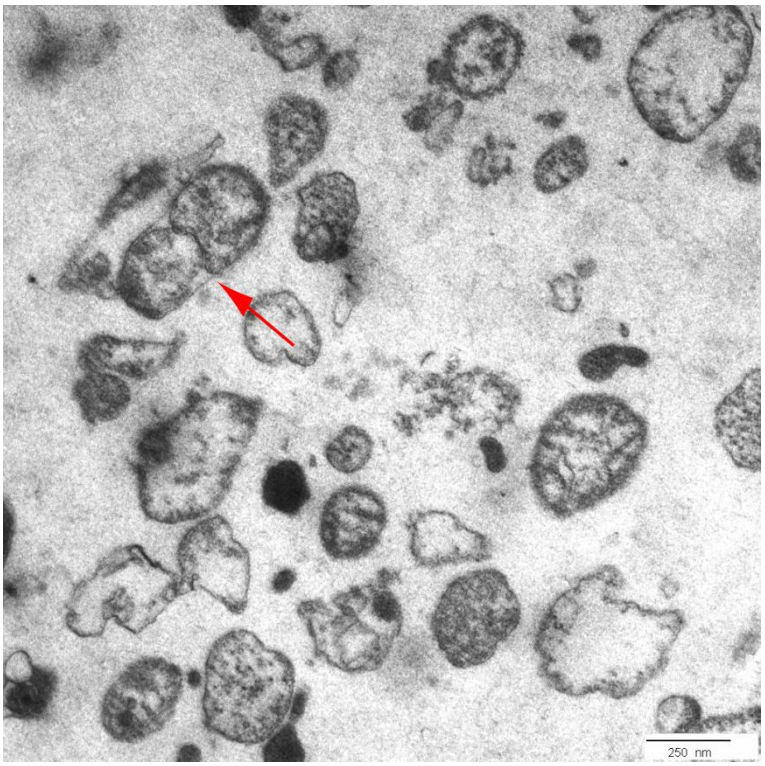

Figure 5.7: TEM image of the fusion sample (F), 12000x magnification. The fusion intermediate with separated inner membranes and fused outer membrane is indicated by a red arrow.

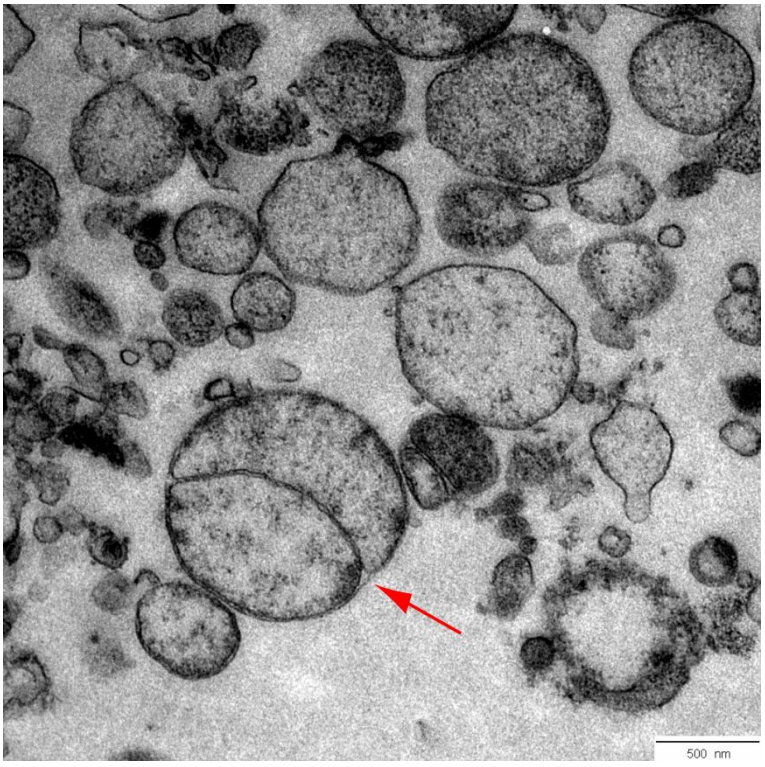

Figure 5.8: TEM image of the fusion sample (F), 12000x magnification. The fusion intermediate with separated inner membranes and fused outer membrane is indicated by a red arrow.

5.4 Conclusions

According to mitochondrial fusion in vitro of yeast mitochondria [8], successful mitochondrial fusion in vitro of mitochondria from mammalian cells was shown. The occurrence of mitochondrial fusion in vitro was detected qualitatively with microscopic methods. Thereby, the analysis by CLSM revealed fused mitochondria with fused outer and inner mitochondrial membranes due to mixed-colored fluorescent mitochondrial matrices whereas the analysis by TEM revealed fusion intermediates with fused outer, but separated inner membrane. Flow cytometry was the method of choice for quantification and evaluation of mitochondrial fusion efficiency due to several advantages such as the capability for high throughput analysis, the possibility to analyze highly diluted samples that did not consume large amounts of isolated mitochondria and an even higher number of mitochondria that could be investigated compared to microscopy techniques that would accompany with time consuming counting of a comparatively low number of mitochondria. Thereby, a protocol for the determination and calculation of mitochondrial fusion efficiency was established.

5.5 References

[1] P.J. Hollenbeck, M. Saxton, The axonal transport of mitochondria, Journal of Cell Science 118 (2005) 5411–5419.

[2] D.C. Chan, Mitochondrial Fusion and Fission in Mammals, Annu. Rev. Cell Dev. Biol 22 (2006) 79–99.

[3] K.L. Cerveny, Y. Tamura, Z. Zhang, R.E. Jensen, H. Sesaki, Regulation of mitochondrial fusion and division, Trends in Cell Biology 17 (2007) 563–569.

[4] H. Chen, M. Vermulst, Y.E. Wang, A. Chomyn, T.A. Prolla, J.M. McCaffery, D.C. Chan, Mitochondrial Fusion Is Required for mtDNA Stability in Skeletal Muscle and Tolerance of mtDNA Mutations, Cell 141 (2010) 280–289.

[5] B. Westermann, Molecular Machinery of Mitochondrial Fusion and Fission, Journal of Biological Chemistry 283 (2008) 13501–13505.

[6] T. Koshiba, S.A. Detmer, J.T. Kaiser, H. Chen, J.M. McCaffery, D.C. Chan, Structural Basis of Mitochondrial Tethering by Mitofusin Complexes, Science 305 (2004) 858–862.

[7] S.A. Detmer, D.C. Chan, Functions and dysfunctions of mitochondrial dynamics, Nat Rev Mol Cell Biol 8 (2007) 870–879.

[8] S. Meeusen, J.M. McCaffery, J. Nunnari, Mitochondrial Fusion Intermediates Revealed in Vitro, Science 305 (2004) 1747–1752.

[9] M.M. Bradford, A rapid and sensitive method for the quantitation of microgram quantities of protein utilizing the principle of protein-dye binding, Analytical Biochemistry 72 (1976) 248–254.

[10] A. Heller, Chapter 4: Permanent labeling of isolated mitochondria, in: A. Heller (Ed.), Targeting mitochondria by mitochondrial fusion, mitochondria-specific peptides and nanotechnology: Dissertation.

[11] P. Petit, P. Diolez, P. Muller, S.C. Brown, Binding of concanavalin A to the outer membrane of potato tuber mitochondria detected by flow cytometry, FEBS Letters 196 (1986) 65–70.

[12] K.M. Fuller, E.A. Arriaga, Advances in the analysis of single mitochondria, Curr. Opin. Biotechnol 14 (2003) 35–41.

[13] L.B. Chen, Fluorescent Labeling of Mitochondria, in: Wang Y.-L., D.L. Taylor, K.W. Jeon (Eds.), Methods in Cell Biology: Fluorescence Microscopy of Living Cells in Culture Part A Fluorescent Analogs, Labeling Cells, and Basic Microscopy, Elsevier, 1988, pp. 103–123.

Chapter 6

Affecting mitochondrial fusion efficiency in vitro

Abstract

The influence of several polymers such as PEGs and 8arm PEGs, nanocarriers such as dendrimers or quantum dots, and targeting peptides on mitochondrial fusion in vitro was evaluated. Mitochondrial fusion was affected unspecifically by highly concentrated polymer solutions and specifically by polymers and nanocarriers that were modified with mitochondria specific targeting peptides. Thereby, a natural mitochondrial targeting sequence (MLS) and a synthetic mitochondria penetrating peptide (MPP) were investigated. Highly concentrated PEG solutions increased mitochondrial fusion efficacy unspecifically due to physical effects. MPP-modified polymers and dendrimers increased fusion efficiency specifically whereas MLS-modified polymers and nanocarriers did not increase mitochondrial fusion efficiency in vitro.

6.1 Introduction

Due to the fact that mitochondrial fusion deficiencies are involved in diseases [1,2] and the imbalance towards mitochondrial fragmentation contributes to programmed cell death [3], manipulation of mitochondrial fusion can be a promising strategy to improve mitochondrial functionality [4]. Beside the approach of affecting mitochondrial fusion, specific targeting of mitochondria is another goal. But targeting of mitochondria is challenging due to the enclosure by two membranes and only small pores in these membranes [5,6]. To achieve a mitochondria specific targeting, it is not possible to utilize all different pore complexes that can be found in the mitochondrial membranes. It is only feasible to utilize the mitochondrial protein import pores that recognize specific targeting sequences [7,8].

Therefore, this study focuses on strategies that combine the utilization of the mitochondrial fusion machinery and the utilization of mitochondrial protein import machinery with the goals to enhance mitochondrial fusion and to achieve a specific targeting of mitochondria. All investigations described in this study are based on protocols for mitochondrial fusion of isolated mammalian mitochondria in vitro and established protocols for the detection of mitochondrial fusion in vitro as well as the quantitative determination of mitochondrial fusion efficiency in vitro, described in a previous study [9].

It is known that polyethylene glycol (PEG) with molecular weights from 400-6000 Da at concentrations of 50-55 % can induce cell fusion [10] in which the detail mechanisms that underlie PEG-mediated, artificial cell fusion are not known [11]. Dehydration due to the water binding properties of PEG in solutions of 35 % or higher may play a role in PEG-mediated fusion [12]. Therefore, the initial step towards the specific manipulation of mitochondrial fusion in vitro by using targeting strategies was the unspecific enhancement of mitochondrial fusion in vitro by using PEG 1500 at a concentration of 50 %.

Specific targeting strategies that have been applied were a natural mitochondrial leading sequence (MLS) derived from a mitochondrial protein [7] and a mitochondria penetrating peptide (MPP) [13,14] that has been shown to deliver cargos selectively into mitochondria. The used MLS consists of 17 amino acids derived from the targeting sequence of the

saccharomyces cerevisiae protein cytochrome c oxidase subunit IV (CoxIV) plus an additional cysteine at the C-terminus to make use of the thiol group for the covalent attachment to other molecules. This targeting sequence has been shown to have a high binding affinity to the translocator complexes in the mitochondrial membranes [15–17]. An important feature, that applies to all mitochondrial targeting sequences, is the high content of basic and hydrophobic amino acids with the ability to form an amphiphatic α-helix that presents one positively charged surface and one hydrophobic surface that are necessary for the recognition by the mitochondrial protein import pores [7]. Natural mitochondrial targeting sequences are also known to deliver non-protein cargos into mitochondria [18]. The used MPP consists of 6 amino acids according to MPPs described by Horton et al. [13]. As a sixth amino acid, cysteine has been attached to the C-terminus for reasons of chemical reactivity. The amino acid sequence and properties of the MLS and the MPP are shown in the Appendix of this thesis.

The nanomaterials that have been used for specific enhancement of mitochondrial fusion in vitro were dendritic polymers: 8arm PEGs of 20 and 40 kDa molecular weight and PAMAM-dendrimers G4-G7, as well as a polyetheramine (Jeffamine®) of 2 kDa and quantum dots. All these materials have been modified with either the MLS or the MPP and their influence on mitochondrial fusion at different concentrations has been investigated in comparison to the same nanomaterials modified in a non-targeting manner by conjugating them to β-mercaptoethanol and cysteine. According to the unspecific PEG-mediated cell fusion, the influence of all unconjugated nanomaterials and both targeting moieties on mitochondrial fusion in vitro has also been investigated. The dendritic polymers (8arm PEGs and dendrimers) have been chosen as they contain several arms that can be modified with multiple targeting moieties. In particular, the 8arm PEGs have been chosen to eventually utilize the effects of PEG-mediated cell fusion transferring these effects to mitochondrial fusion and specifying the mechanisms by conjugation of targeting moieties. Dendrimers have been chosen because they are known as effective carriers for anticancer agents [19] and the specific delivery of anticancer agents to mitochondria may be desirable goal to improve

therapy [20]. Polyamidoamine (PAMAM) dendrimers, in particular, are known to affect mitochondria [21]. Jeffamine® was chosen because of the lower molecular weight compared to the 8arm PEGs to investigate the effects of a polymer with a molecular weight in the range of PEG for PEG-mediated cell fusion. Quantum dots (Qdots) have been chosen because of their fluorescent properties to establish a detectable system with respect to achieve and detect a specific targeting and uptake into mitochondria mediated by mitochondrial fusion.

6.2 Materials and methods

6.2.1 Materials

HAM F-12 nutrient mixture and fetal calf serum (FCS) were purchased from Sigma-Aldrich (Steinheim, Germany). Trypsin-EDTA 0.25 % was obtained from Gibco-Invitrogen (Karlsruhe, Germany). G418 was purchased from Sigma-Aldrich (Steinheim, Germany). Purified water was obtained by using a Milli-Q water purification system from Millipore (Schwalbach, Germany). All cell culture materials were purchased from Corning (Bodenheim, Germany).

Isolation buffer consisted of 250 mM sucrose (Merck, Darmstadt, Germany), 10 mM Tris (USB Corporation, Cleveland, OH USA), 10 mM KCl (Merck, Darmstadt, Germany), 1 mM Na_2EDTA (Merck, Darmstadt, Germany) and 0.1 % bovine serum albumin (BSA) (Sigma-Aldrich, Steinheim, Germany). Fusion buffer consisted of 600 mM sorbitol (Sigma-Aldrich, Steinheim, Germany), 20 mM Tris (USB Corporation, Cleveland, OH USA), 150 mM potassium acetate (Merck, Darmstadt, Germany), 5 mM magnesium acetate tetrahydrate (Merck, Darmstadt, Germany), 0.1 % BSA (Sigma-Aldrich, Steinheim, Germany), 0.5 mM GTP (Sigma-Aldrich, Steinheim, Germany), 1mM ATP (Sigma-Aldrich, Steinheim, Germany), 40mM creatine phosphate (Sigma-Aldrich, Steinheim, Germany) and 30 units/ml creatine phosphokinase (Sigma-Aldrich, Steinheim, Germany).

PEG 1500, 4000 and 10000 were obtained from Hoechst (Frankfurt, Germany). 8arm PEG-maleimide 20 kDa and 40 kDa were purchased from Nanocs Inc. (New York, NY, USA). The Polyetheramine (Jeffamine® ED-2003) with a molecular weight of 2000 Da was obtained from Huntsman (Everberg, Belgium). The PAMAM Dendrimer Kit generation 4-7 was purchased from Sigma-Aldrich (Steinheim, Germany). Qdot 655 ITK amino (PEG) quantum dots were obtained from Invitrogen (Karlsruhe, Germany). Sulfo-SMCC was purchased from Thermo Fisher Scientific (Bonn, Germany). β-mercaptoethanol and L-cysteine hydrochloride monohydrate were obtained from Sigma-Aldrich (Steinheim, Germany).

Sodium phosphate/sodium chloride buffer consisted of 0.1 M disodium hydrogenphosphate dihydrate (Merck, Darmstadt, Germany) and 0.15 M sodium chloride (Merck, Darmstadt,

Germany). The pH-value was adjusted to 7.2 by TitriPUR® 1 N hydrochloric acid (Merck, Darmstadt, Germany).

MLS and MPP peptides were synthesized by GeneCust (Dudelange, Luxembourg) and were reduced prior to use by TCEP Reducing Gel (Thermo Fisher Scientific, Bonn, Germany) or TCEP (Sigma-Aldrich, Steinheim, Germany) in sodium phosphate/sodium chloride buffer. Amicon® Ultra-4 centrifugal filter unit 10 kDa and 100 kDa (Millipore, Schwalbach, Germany) were used for purification by ultrafiltration. The dialysis tube was obtained from Sigma-Aldrich (Steinheim, Germany). DPBS without calcium and magnesium was obtained from Gibco-Invitrogen (Karlsruhe, Germany).

0.1 M cacodylate fixation buffer consisted of 100 mM sodium cacodylate (Roth, Karlsruhe, Germany), 2 mM magnesium chloride hexahydrate (Merck, Darmstadt, Germany), 1 mM calcium chloride dihydrate (Merck, Darmstadt, Germany), 40 mM sodium chloride (Merck, Darmstadt, Germany) and 2 % glutaraldehyde (Serva, Heidelberg, Germany). 0.1 M cacodylate washing buffer consisted of 100 mM sodium cacodylate (Roth, Karlsruhe, Germany), 2 mM magnesium chloride hexahydrate (Merck, Darmstadt, Germany), 1 mM calcium chloride dihydrate (Merck, Darmstadt, Germany) and 40 mM sodium chloride (Merck, Darmstadt, Germany). BODIPY® FL L-cystine was obtained from Invitrogen (Karlsruhe, Germany). Diaminobenzidine was purchased from Sigma-Aldrich (Steinheim, Germany) and agarose was obtained from Biozym (Hessisch Oldendorf, Germany). Osmium tetroxide (ScienceServices, Munich, Germany) was dissolved to 1 % in 0.1 M cacodylate buffer that consisted of 100 mM sodium cacodylate (Roth, Karlsruhe, Germany), 2 mM magnesium chloride hexahydrate (Merck, Darmstadt, Germany), 1 mM calcium chloride dihydrate (Merck, Darmstadt, Germany) and 40 mM sodium chloride (Merck, Darmstadt, Germany). The freeze substitution medium for the fixation by high pressure freezing/freeze substitution (HPF/FS) consisted of 2 % osmium tetroxide (ScienceServices, Munich, Germany), 5 % hydrogen peroxide (Merck, Darmstadt, Germany) and 0.25 % uranyl acetate (Roth, Karlsruhe, Germany). Agarose was purchased from Biozym (Hessisch Oldendorf, Germany). Embedding in Epon was carried out with an Epoxy Embedding Medium Kit (Fluka by Sigma-

Aldrich, Steinheim, Germany). Propylen oxide was purchased from Sigma-Aldrich (Steinheim, Germany).

6.2.2 Unspecific manipulation of mitochondrial fusion in vitro

Cell culture

Long-time cultivation of CHO-cell lines that were stably transfected with mitochondria targeted green fluorescent protein (mtGFP) and mitochondria targeted red fluorescent protein (mtRFP) was carried out in selection medium HAM-F12 containing 10 % FCS and 400 µg/ml G418, an antibiotic for the selection of plasmid containing cells. The last cultivation step of CHO-mtGFP and CHO-mtRFP cells before fusion experiments was carried out in G418-free medium because the cells did not lose the plasmid within one week. Cells were cultured in HAM-F12 nutrient mixture containing 10 % FCS in 150 cm^2 culture flasks until confluency, harvested by Trypsin-EDTA 0.25 % and washed with isolation buffer. The centrifugation steps during washing of cells were carried out in a GS-15R centrifuge (Beckman, Krefeld, Germany).

Isolation of mitochondria

MtGFP- or mtRFP-containing cells from one culture flask were suspended in 250 µl isolation buffer. Cells from four flasks were pooled and the resulting one milliliter cell suspension was transferred into a cooled 2-ml Dounce glass homogenizer (Sigma-Aldrich, Steinheim, Germany) where the cells were disrupted by 25 strokes. The suspension was transferred into a 2-ml safe-lock tube (Eppendorf, Hamburg, Germany) and centrifuged at 1500 g at 4 °C for 10 min a type 5415 R centrifuge (Eppendorf, Hamburg, Germany) to pelletize nuclei as well as remaining intact cells. The first supernatant was kept on ice, while the pellet was resuspended in isolation buffer and homogenized by 25 Dounce strokes for a second time to break remaining intact cells. A second centrifugation step at 1500 g at 4 °C for 10 min yielded a pellet that was the nuclei enriched fraction. The first and the second supernatant were mixed and centrifuged at 16000 g at 4 °C for 15 min to obtain a pellet enriched with

mtGFP- or mtRFP-containing isolated mitochondria. The amount of cells used for the isolation of mitochondria depended on the required amount for the different experiments. Mitochondrial protein concentration was determined by a Bradford-Assay [22].

Mitochondrial fusion in vitro and unspecific manipulation of mitochondrial fusion in vitro

Mitochondrial fusion was carried out according to Meeusen et al. [23]. Thereby, equal amounts of mtGFP- and mtRFP-containing mitochondria regarding to the mitochondrial protein concentration were mixed and centrifuged at 16000 g, 4 °C for 10 min. The pellet was incubated on ice for 10 min and was resuspended in 40 µl fusion buffer for 500 µg total mitochondrial protein. After incubation at room temperature for 1 h, the fusion samples were centrifuged at 16000 g, 4°C for 5min. Then, the pellet was covered with a 50 % PEG 1500 solution in isolation buffer and incubated at room temperature for 60 s. Afterwards, the pellet was washed three times with isolation buffer and resuspended in isolation buffer.

Fusion efficiency of mitochondria in vitro was also evaluated for treatment with 50% PEG 4000, 50% PEG 10000, 100µM and 1mM PEG 1500, 25% 8arm PEGs 20k Da and 8arm PEG 40 kDa, 5% PAMAM dendrimers G4-G7 and 50% Jeffamine®. These studies were carried out as described previously for 50% PEG 1500.

Qualitative analysis of mitochondrial fusion by CLSM

Qualitative analysis of mitochondrial fusion in vitro was carried out by confocal laser scanning microscopy (CLSM). Fluorescence of the fusion samples was analyzed with a Zeiss Axiovert LSM 510 (Carl Zeiss, Oberkochen, Germany) and an AxioCam HRc (Carl Zeiss, Oberkochen, Germany). Thereby, GFP was excited a 488 nm and detected at 505–530 nm whereas RFP was excited at 488 nm and detected at 530–600 nm. In samples containing both fluorescent proteins, a multitrack scan mode was applied.

Qualitative analysis mitochondrial fusion in vitro by TEM

Qualitative analysis of mitochondrial fusion in vitro was also carried out by transmission electron microscopy (TEM) in which fixation was accomplished by high pressure freezing (HPF) and freeze substitution (FS). The high pressure freezing was carried out in a Leica EM PACT2 high pressure freezer (Leica, Vienna, Austria) and freeze substitution was accomplished in a freeze substitution processor Leica EM AFS2 (Leica, Vienna, Austria). The samples were treated with an osmium tetroxide containing medium at -90 °C for 8 h, heated from -90 °C – -60 °C for 2 h, left at -60 °C for 6 h, heated from -60 °C – -30 °C for 2 h, left at -30 °C for 8 h, heated from -30 °C – 0 °C for 2 h and left at 0 °C for 8 h. Then, the mixture was treated three times with acetone at 0 °C for 1 h. Afterwards, the samples were treated with a mixture of acetone and Epon (2:1) for 30 min and heated from 0 °C to room temperature. Then, the samples were transferred to a mixture of acetone and Epon (2:1) at room temperature for 30 min. Subsequently, they were treated in a mixture of acetone and Epon (1:1) at room temperature for 2 h. Afterwards, the samples were left in a mixture of acetone and Epon (1:2) in an open vial overnight. Then, the samples were embedded and hardened in Epon at 30 °C for 2 h and at 60 °C for 2 days. Epon blocks were cut into sections of 50 nm with a microtome Leica EM UC6 (Leica, Vienna, Austria) and transferred to copper slot grids with a 1.5 % hyaloform foil. They were examined either unstained or stained with uranyl acetate and lead citrate in a transmission electron microscope Zeiss EM 902 (Carl Zeiss, Oberkochen, Germany), operating at 80kV. Digital images were recorded by a slow scan CCD camera (TRS Typ 7888, Serial No. 321/08).

Quantitative analysis of mitochondrial fusion efficiency by flow cytometry

Quantitative analysis of mitochondrial fusion efficiency in vitro was accomplished by flow cytometry with a FACSCanto™ (BD Bioscience, Heidelberg, Germany) as described previously [9]. Data in the graphs of quantitative fusion efficiency were normalized to the data of untreated fusion samples (F = 1) for reasons of relative comparison of the fusion efficiency

of untreated fusion samples (F = 1) and fusion efficiency after unspecific manipulation (F = 1 ± xy).

6.2.3 Specific manipulation of mitochondrial fusion in vitro

Modification of 8arm PEGs

8arm PEG-maleimides 20 kDa and two batches of 40 kDa were modified with a twentyfold molar excess of MLS, MPP, cysteine and β-mercaptoethanol. Therefore, 8arm PEGs were dissolved in sodium phosphate/sodium chloride buffer to concentrations of 100 µM or 1 mM. Prior to use, MLS, MPP and cysteine were dissolved in purified water and reduced by a thirtyfold molar excess of TCEP in the dark for 30 min. Reduced MLS, MPP or cysteine solutions as well as β-mercaptoethanol diluted in sodium phosphate/sodium chloride buffer were added to the 8arm PEG solutions in a twentyfold molar excess. Reactions were carried out at 4 °C overnight. Afterwards, β-mercaptoethanol was added in excess to react with unmodified maleimides. The modified 8arm PEGs were purified by three ultrafiltration steps in ultrafiltration units with a cut-off of 10 kDa and sodium phosphate/sodium chloride buffer. Unmodified 8arm PEGs in concentrations of 100 µM and 1 mM were also purified by ultrafiltration to obtain equal concentrations for the comparison of unmodified and modified 8arm PEGs.

Modification of quantum dots

Quantum dots were modified with a twentyfold molar excess of MLS, MPP, cysteine and β-mercaptoethanol. Therefore, the buffer of the quantum dots was exchanged to sodium phosphate/sodium chloride buffer by ultrafiltration in ultrafiltration units with a cut-off of 10 kDa. Afterwards, 10 nM and 100 nM quantum dots that carried an amino-PEG shell were activated by a 1000-fold molar excess of sulfo-SMCC. The reaction was carried out at room temperature in the dark on a shaker for 30 min. Activated quantum dots were purified by three ultrafiltration steps in ultrafiltration units with a cut-off of 10 kDa and sodium phosphate/sodium chloride buffer. Before use, MLS, MPP and cysteine were dissolved in

purified water and reduced by a thirtyfold molar excess of TCEP in the dark for 30 min. Reduced MLS, MPP or cysteine solutions as well as β-mercaptoethanol diluted in sodium phosphate/sodium chloride buffer were added to the quantum dots in a twentyfold molar excess. Reactions were carried out at 4 °C overnight. Afterwards, β-mercaptoethanol was added in excess to react with unmodified maleimides. The modified quantum dots were purified by three ultrafiltration steps in ultrafiltration units with a cut-off of 10 kDa and sodium phosphate/sodium chloride buffer. Unmodified quantum dots in concentrations of 10 nM and 100 nM were also purified by ultrafiltration to obtain equal concentrations for the comparison of unmodified and modified quantum dots. Quantum dots were stored in low-bind cups, likewise all reactions were carried out in low-bind cups (Eppendorf, Hamburg, Germany).

Modification of dendrimers

Dendrimers were activated and modified similar to the quantum dots. The amount of amine groups on the surface depended on the generation of the dendrimer. G4 dendrimers contained 64 amine groups, G5 dendrimers contained 128 amine groups, G6 dendrimers contained 256 amine groups and G7 dendrimers contained 512 amine groups. G4 – G7 dendrimers were modified at a concentration of 1 µM with a twentyfold molar excess of MLS, MPP, cysteine or β-mercaptoethanol as well as with equal and double molar concentrations of MLS or MPP according to the amine groups on the surface. That means for equal concentrations of MLS or MPP according to the amine groups (1:1), a 64-fold molar excess of peptide was added to G4 dendrimers, a 128-fold molar excess of peptide was added to G5 dendrimers, a 256-fold molar excess of peptide was added to G6 dendrimers and a 512-fold molar excess of peptide was added to G7 dendrimers. For double concentrations of MLS or MPP according to the amine groups (1:2), a 128-fold molar excess of peptide was added to G4 dendrimers, a 256-fold molar excess of peptide was added to G5 dendrimers, a 512-fold molar excess of peptide was added to G6 dendrimers and a 1024-fold molar excess of peptide was added to G7 dendrimers. G4 and G5 dendrimers were modified at a concentration of 100 µM with a twentyfold molar excess of MLS, MPP, cysteine or β-

mercaptoethanol as well as with an equal molar concentration of MLS or MPP according to the amine groups on the surface. That means for equal concentrations of MLS or MPP according to the amine groups (1:1), a 64-fold molar excess of peptide was added to G4 dendrimers and a 128-fold molar excess of peptide was added to G5 dendrimers. Unmodified dendrimers in concentrations of 1 µM and 100 µM were also purified by ultrafiltration to obtain equal concentrations for the comparison of unmodified and modified dendrimers.

Modification of Jeffamine®

The polyetheramine Jeffamine® was activated and modified similar to the quantum dots and dendrimers. Jeffamine® in concentrations of 100 µM and 1 mM was modified with a twentyfold molar excess of MLS, MPP, cysteine and β-mercaptoethanol. Purification steps were carried out by dialysis instead of ultrafiltration. Unmodified Jeffamine® in concentrations of 100 µM and 1 mM was also purified by dialysis to obtain equal concentrations for the comparison of unmodified and modified Jeffamine®.

Targeting peptides

For studying the efficacy of the targeting peptides MLS and MPP without carrier, concentrations of 10 nM, 100 nM, 100 µM and 1 mM, reduced on a TCEP-gel or not reduced, were investigated.

Cell culture

Long-time cultivation of stably transfected CHO-mtGFP and CHO-mtRFP cell lines was carried out as described previously.

Isolation of mitochondria

Isolation of mitochondria was carried out as described previously.

Mitochondrial fusion in vitro and specific manipulation of mitochondrial fusion in vitro

Mitochondrial fusion was carried out according to Meeusen et al. [23]. Thereby, equal amounts of mtGFP- and mtRFP-containing mitochondria regarding to the mitochondrial protein concentration were mixed and defined amounts of MLS, reduced or not reduced; MLS-modified 8arm PEGs, quantum dots, dendrimers or Jeffamine®; MPP, reduced or not reduced or MPP-modified 8arm PEGs, quantum dots, dendrimers or Jeffamine® as well as cysteine- and β-mercaptoethanol-modified 8arm PEGs, quantum dots, dendrimers and Jeffamine® were added. Each mixture was centrifuged at 16000 g, 4 °C for 10 min. Then, the pellet was incubated on ice for 10 min and was resuspended in fusion buffer, 40 µl for 500 µg total mitochondrial protein. The mixture was incubated at room temperature for 1 h.

Quantitative analysis of mitochondrial fusion in vitro by flow cytometry

Mitochondrial fusion efficiency was evaluated by flow cytometry with a FACSCanto™ (BD Bioscience, Heidelberg, Germany) as described in a previous study [9]. Data in the graphs of quantitative fusion efficiency were normalized to the data of untreated fusion samples (F = 1) for reasons of relative comparison of the fusion efficiency of untreated fusion samples (F = 1) and fusion efficiency after specific manipulation (F = 1 ± xy).

Qualitative analysis of mitochondrial fusion in vitro by TEM after photooxidation

It is possible to visualize a fluorescence dye for TEM by photooxidation of diaminobenzidine. Thereby, the fluorescent dye is excited and bleaches, in which diaminobenzidine is oxidized to an insoluble polymer that can be stained by osmium tetroxide and appears in black. Therefore, the 8arm PEG 40 kDa 1mM was labeled with BODIPY® FL L-cystine and modified with MPP or β-mercaptoethanol. Therefore, the BODIPY® FL L-cystine was reduced by TCEP and was added in an equal molar concentration to the 8arm PEG. Before use, the MPP was reduced by a thirtyfold molar excess of TCEP in the dark for 30 min. The reduced MPP was added to the 8arm PEG solution in a tenfold molar excess. The reaction was carried out at 4 °C overnight. Afterwards, β-mercaptoethanol was added in excess to react

with unmodified maleimids. The modified 8arm PEGs were purified by six ultrafiltration steps in ultrafiltration units with a cut-off of 10 kDa and sodium phosphate/sodium chloride buffer. Mitochondrial fusion in vitro was carried out as described previously and was evaluated by photooxidation and TEM. Therefore, isolated mitochondria were fixed in cacodylate fixation buffer with glutaraldehyde at room temperature for 5 min and on ice overnight. Afterwards, mitochondria were washed by five washing steps, each of them in cacodylate washing buffer for 2 min. Then, the buffer solution was exchanged by diaminobenzide in cacodylate buffer 0.1 M and photooxidation was carried out at an Axiovert 200 (Carl Zeiss, Göttingen, Germany) with an excitation wave length of 488 nm and an emission wave length of 515 nm. Afterwards, the diaminobenzidine solution was exchange by cacodylate buffer 0.1 M. Then, isolated mitochondria were pelletized in a 1 % agarose solution that was heated up to 40 °C. All centrifugation steps were carried out in a himac CT15RE (VWR Leuven, Belgium by Hitachi Koki Co. Ltd.). After gelation of the agarose, the gel block was cut and fixed with osmium tetroxide solution overnight. The samples were washed in DPBS four times for 15 min. Afterwards, the samples were dehydrated in a graded series of ethanol: 50 %, 70 %, 80 %, 90 % and 100 %. Each dehydration step was carried out two times for 15 min.

Then, the samples were treated in an equal mixture of acetone or propylene oxide and ethanol for 20 min and two times in acetone or propylene oxide for 20 min. Afterwards, the samples were treated with a mixture of acetone or propylene oxide and Epon (2:1) for 2 h, then, in a mixture of acetone or propylene oxide and Epon (1:1) for 2 h and subsequently in a mixture of acetone or propylene oxide and Epon (1:2) in an open vial overnight. The samples were subsequently embedded and hardened in Epon at room temperature for 1 h, at 30 °C for 2 h and at 60 °C for 2 days. Epon blocks were cut into sections of 50 nm with a Leica EM UC6 microtome (Leica, Vienna, Austria) and transferred to copper slot grids with a 1.5 % hyaloform foil. They were examined either unstained or stained with uranyl acetate and lead citrate in a transmission electron microscope Zeiss EM 902 (Carl Zeiss, Oberkochen, Germany), operating at 80kV. Digital images were recorded by a slow scan CCD camera (TRS Typ 7888, Serial No. 321/08).

6.2.4 Statistical analysis

Results were expressed as means ± standard deviations. Statistical analysis was performed using SigmaPlot 12.0 one-way analysis of variance (ANOVA) with subsequent Holm-Sidak test to assess the significance of differences between groups. The acceptance level of significance was $p < 0.05$, denoted by (°) or $p < 0.01$, denoted by (*). Before analysis, a normality test was conducted. In case of failure of the normality test, analysis of variance on ranks was conducted (Kruskal Wallis analysis of variance on ranks with subsequent Dunnett test).

6.2.5 Characterization of MLS-conjugates

For characterization of the unmodified and modified 8arm PEGs, UV measurements and ^{1}H-NMR measurements were conducted. UV-spectra of the samples were recorded by a Kontron Instruments Uvikon 900 spectrophotometer (Goebel Instrumentelle Analytik, Hallertau, Germany). For ^{1}H-NMR measurements, 20 mg of the samples were dissolved in 1 ml deuterated chloroform or deuterated DMSO. ^{1}H-NMR spectra were recorded at 300 MHz with an Avance 300 NMR spectrometer (Bruker BioSpin, Ettlingen, Germany).

6.3 Results and discussion

Characterization of MLS-conjugates

For verification that conjugation of the MLS, cysteine and β-mercaptoethanol to the 8arm PEGs was successful, UV-spectra and ^{1}H-NMR measurements were conducted. A first hint that conjugation was successful was the non-toxicity of the conjugated 8arm PEGs compared to the toxicity of the unconjugated 8arm PEGs (see Figure 6.14).

The maleimide of the 8arm PEGs showed an absorption band at 215-240 nm (Figure 6.1).

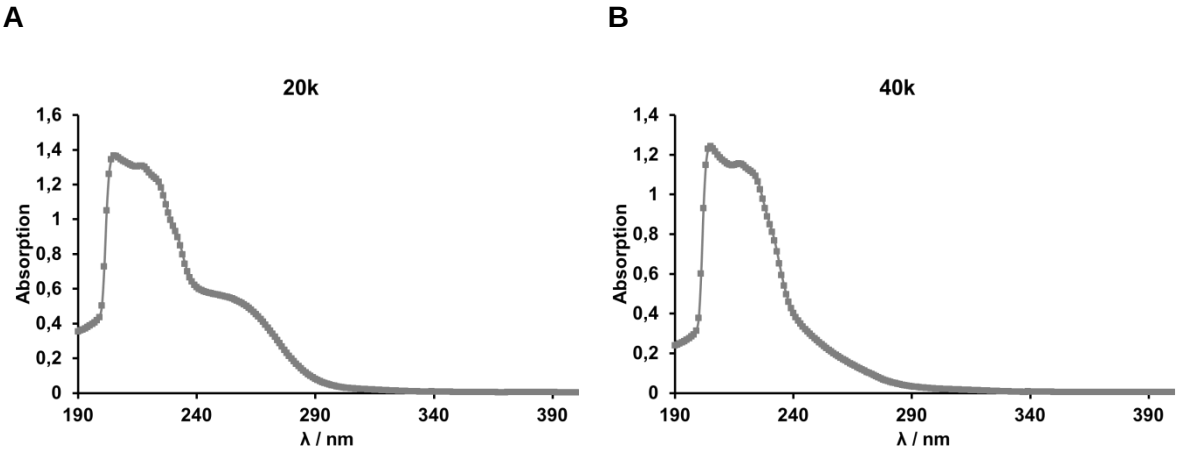

Figure 6.1: UV-spectra of **20 kDa 8arm PEG** (A) and **40 kDa 8arm PEG** (B).

After conjugation of MLS and cysteine, the absorption band of the maleimide disappeared which indicated that conjugation was successful and that cysteine could be used as a model molecule for conjugation studies (Figure 6.2).

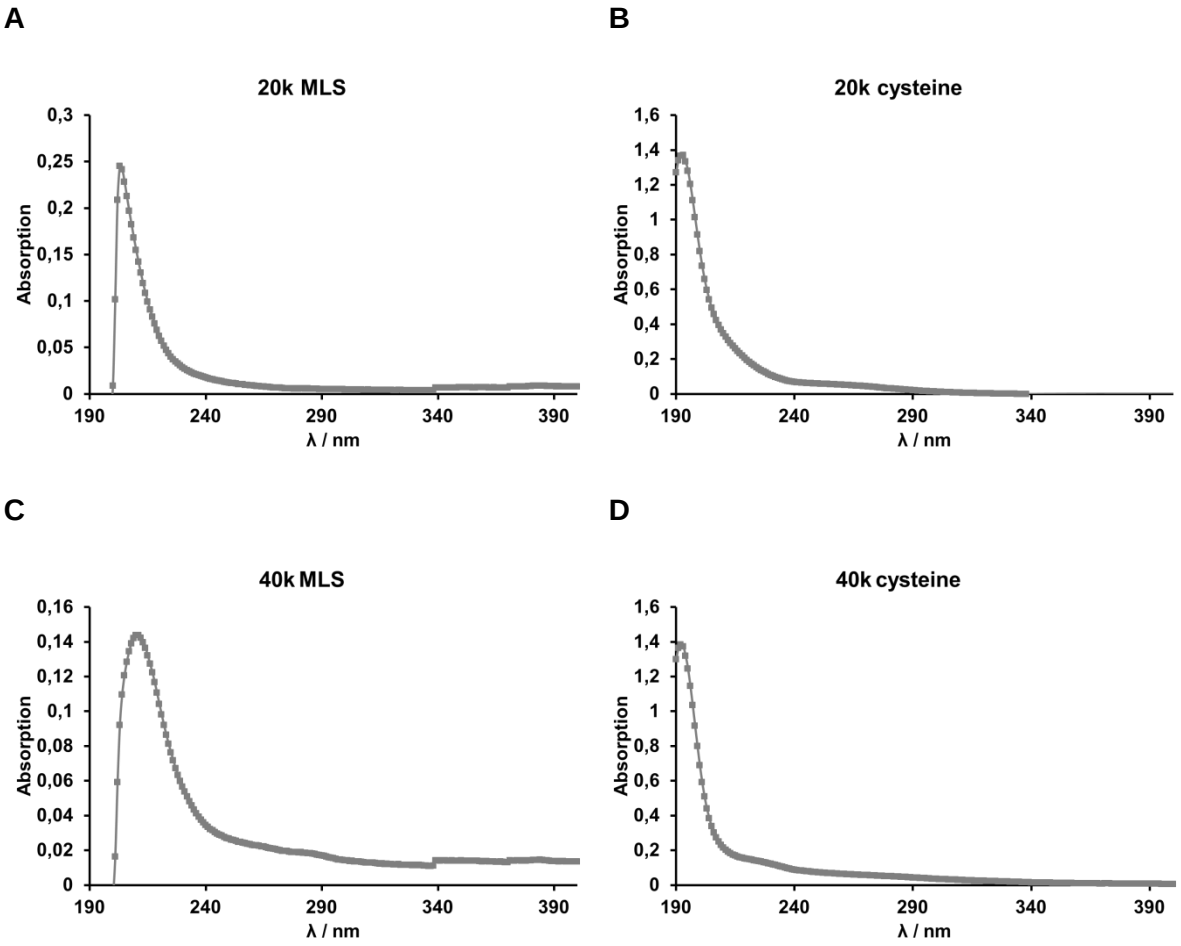

Figure 6.2: UV-spectra of **20 kDa 8arm PEG** conjugated with **MLS** (A) and **cysteine** (B) and UV-spectra of **40 kDa 8arm PEG** conjugated with **MLS** (C) and **cysteine** (D).

It emerged that β-mercaptoethanol was not suitable for UV-related characterization of conjugation to maleimides as the UV-spectrum of β-mercaptoethanol also showed a strong absorption at 215-240 nm (Figure 6.3).

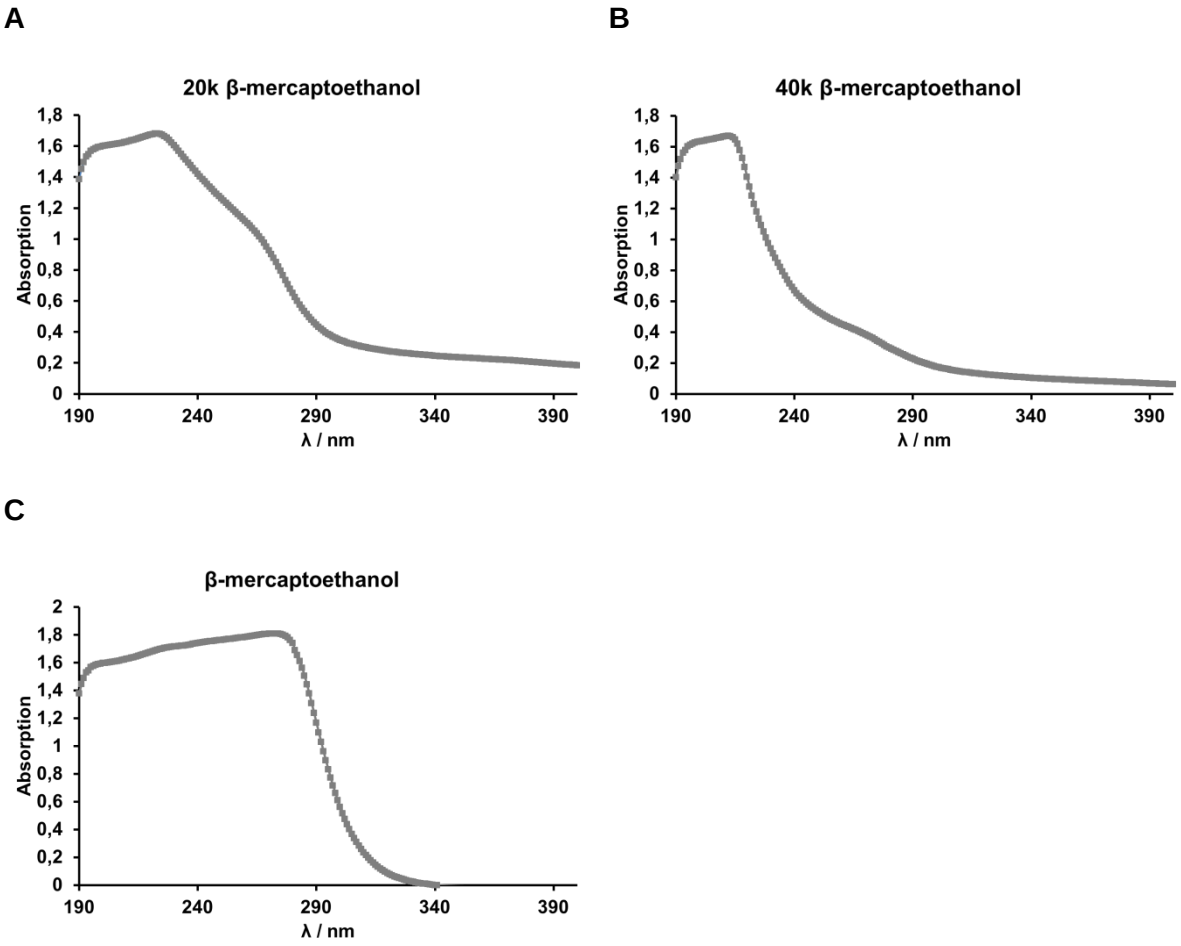

Figure 6.3: UV-spectra of **20 kDa 8arm PEG** conjugated with **β-mecaptoethanol** (A) and **40 kDa 8arm PEG** conjugated with **β-mecaptoethanol** (B) and UV-spectrum of **β-mecaptoethanol** (C).

The ^{1}H-NMR spectra of the native 8arm PEGs showed a peak for PEG at 3.3-3.9 ppm and a peak for the maleimide at 6.7 ppm (Figure 6.4 and Figure 6.5). In the ^{1}H-NMR spectra of the β-mecaptoethanol conjugated 8arm PEGs, the peak for PEG was detectable at 3.3-3.9 ppm whereas the peak for the maleimid disappeared (Figure 6.4 and Figure 6.5). This indicated that conjugation of β-mecaptoethanol to the 8arm PEGs was successful and that β-mecaptoethanol could be used as a model molucule for conjugation. The ^{1}H-NMR spectra of cysteine conjugates did not show the characteristic peak for PEG at 3.3-3.9 ppm as the cysteine conjugated did not solve in $CDCl_3$.

A

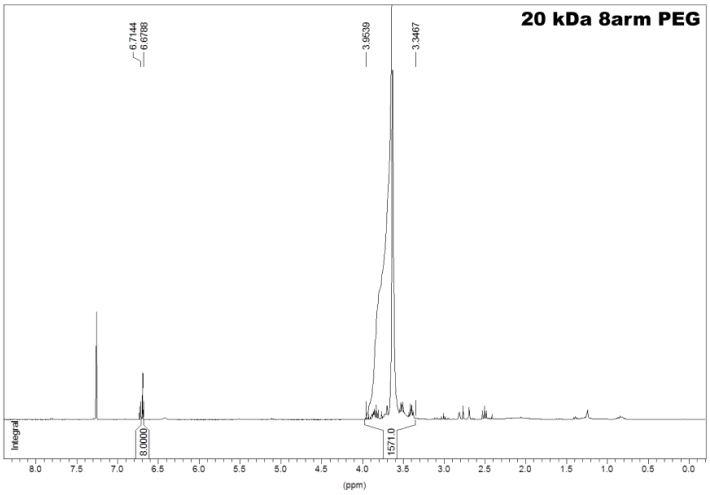

B

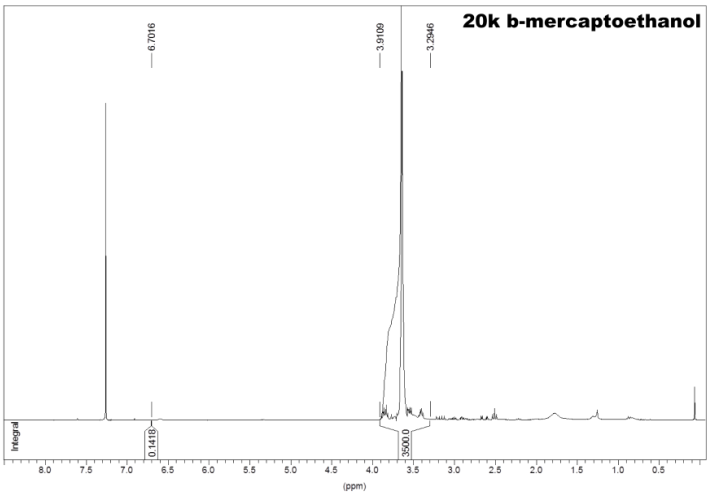

C

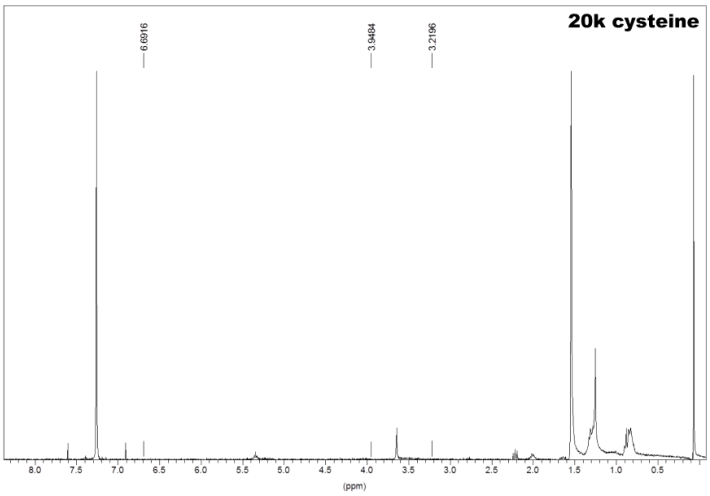

Figure 6.4: NMR spectra of **20 kDa 8arm PEG** (A), **20 kDa 8arm PEG-β-mercaptoethanol conjugate** (B) and **20 kDa 8arm PEG-cysteine conjugate** (C).

A

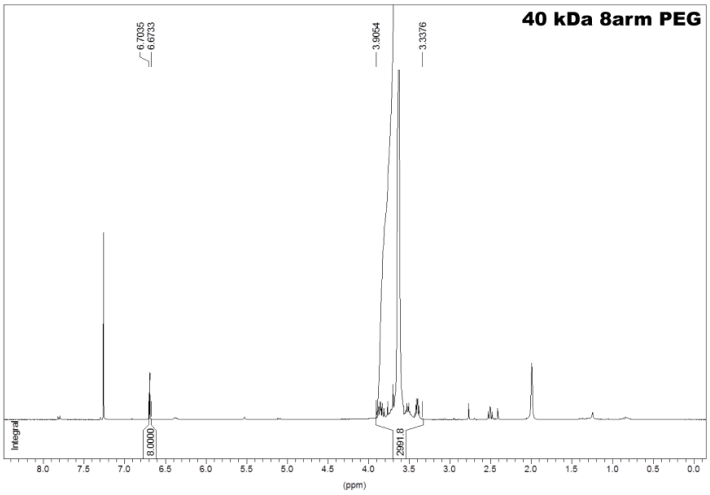

B

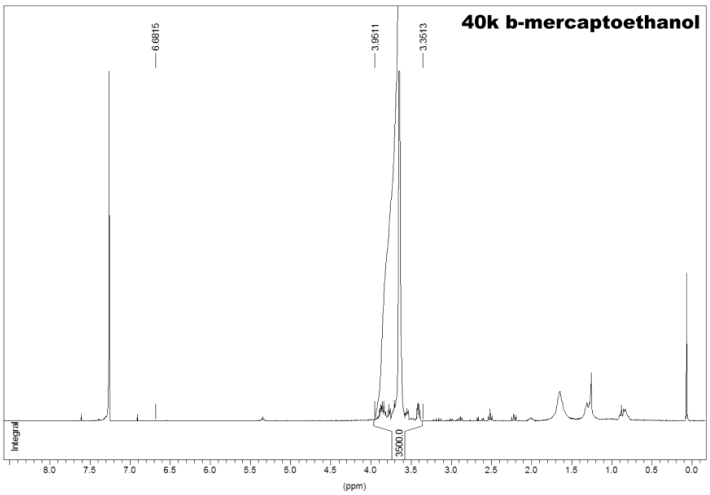

C

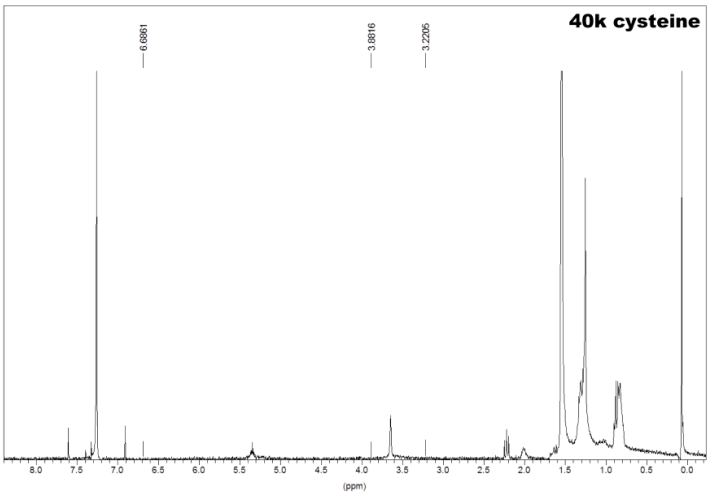

Figure 6.5: NMR spectra of **40 kDa 8arm PEG** (A), **40 kDa 8arm PEG-β-mercaptoethanol conjugate** (B) and **40 kDa 8arm PEG-cysteine conjugate** (C).

Unspecific manipulation of mitochondrial fusion in vitro

A first step towards an enhancement of mitochondrial fusion in vitro was the treatment with a 50 % PEG 1500 solution to stimulate mitochondrial fusion unspecifically. PEG 1500 treated fusion samples were analyzed qualitatively by CLSM (Figure 6.7) in comparison to conventional mitochondrial fusion without manipulation (Figure 6.6). In both cases yellow mitochondria containing both fluorescent dyes that indicated mitochondrial fusion as well as individually labeled green and red mitochondria were detected. This method did not give evidence that mitochondrial fusion was enhanced by PEG 1500.

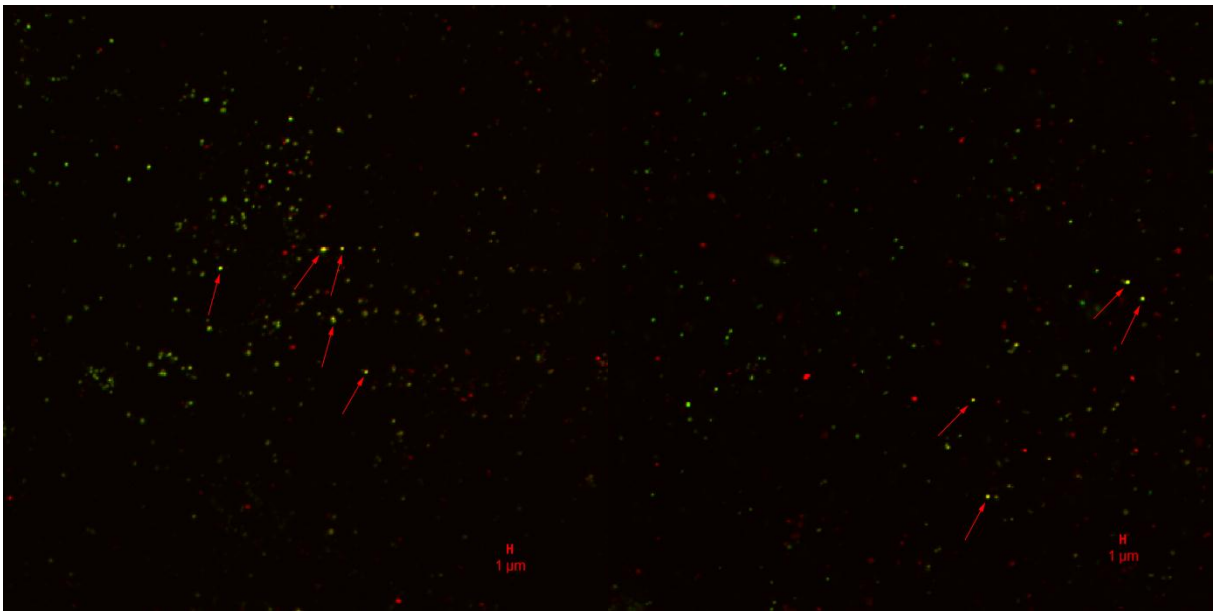

Figure 6.6: CLSM images of fusion without PEG 1500. Single labeled red and green mitochondria and mitochondria containing a mixture of GFP and RFP are visible as yellow dots. These fused mitochondria are indicated by red arrows.

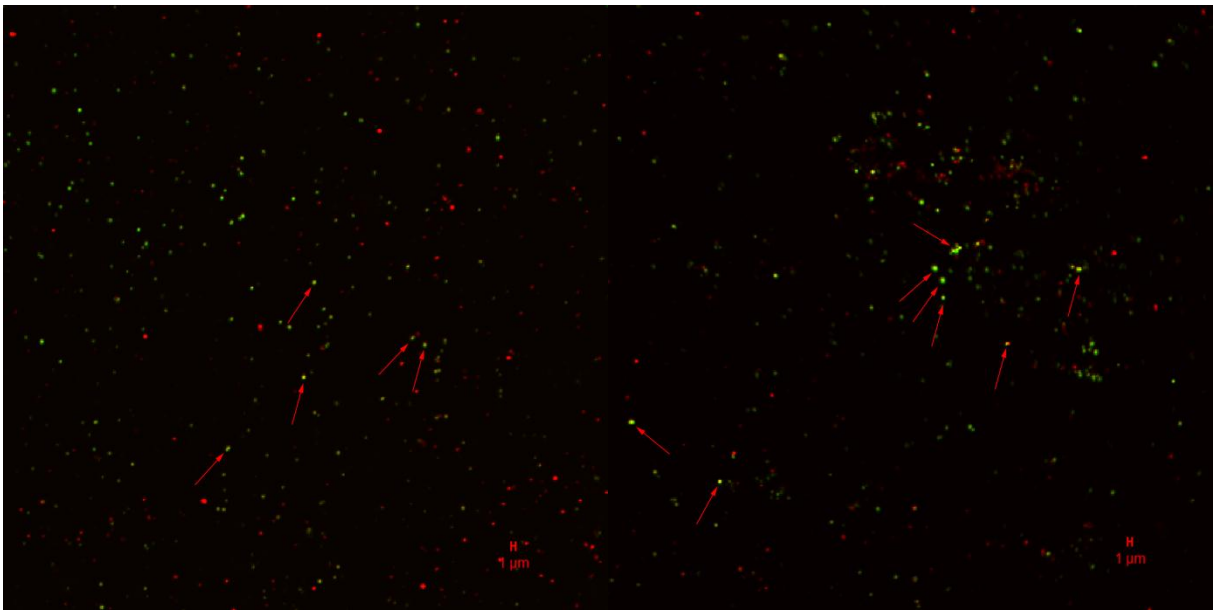

Figure 6.7: CLSM images of fusion enhancement by PEG 1500. Single labeled red and green mitochondria and mitochondria containing a mixture of GFP and RFP are visible as yellow dots. These fused mitochondria are indicated by red arrows.

The analysis of the fusion samples treated with PEG 1500 by TEM revealed fusion intermediates with fused outer and separated adjacent inner membranes (Figure 6.8 and Figure 6.9). Completely fused mitochondria with fused outer and inner membrane could not be detected with this transmission electron microscopy method. This TEM method also did not give evidence that mitochondrial fusion was enhanced by PEG 1500 but it revealed that the ultrastructure of mitochondria was still intact after the treatment with PEG 1500.

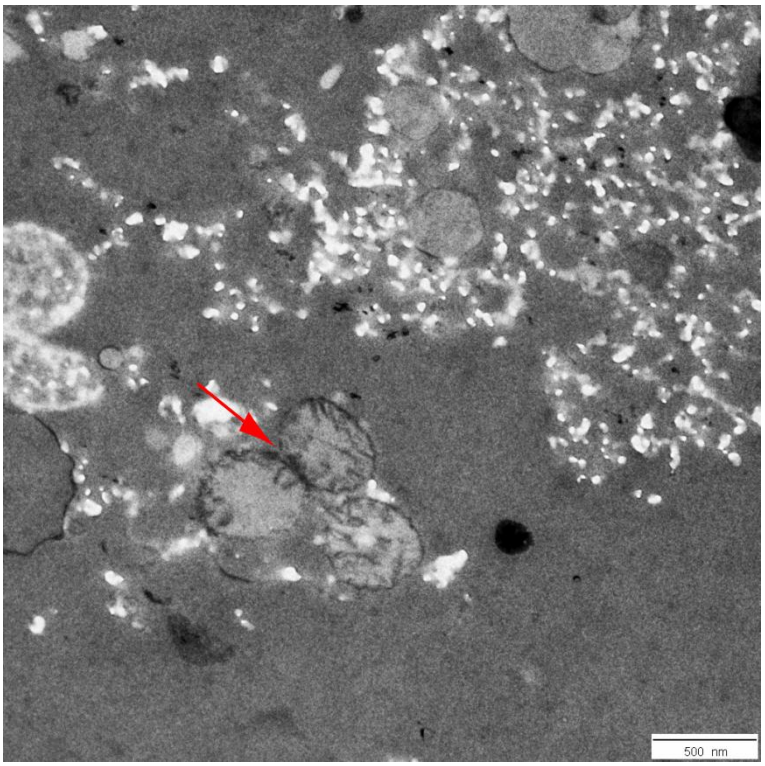

Figure 6.8: TEM image of fusion enhancement by PEG 1500, 12000x magnification. The fusion intermediate with separated inner membranes and fused outer membrane is indicated by a red arrow.

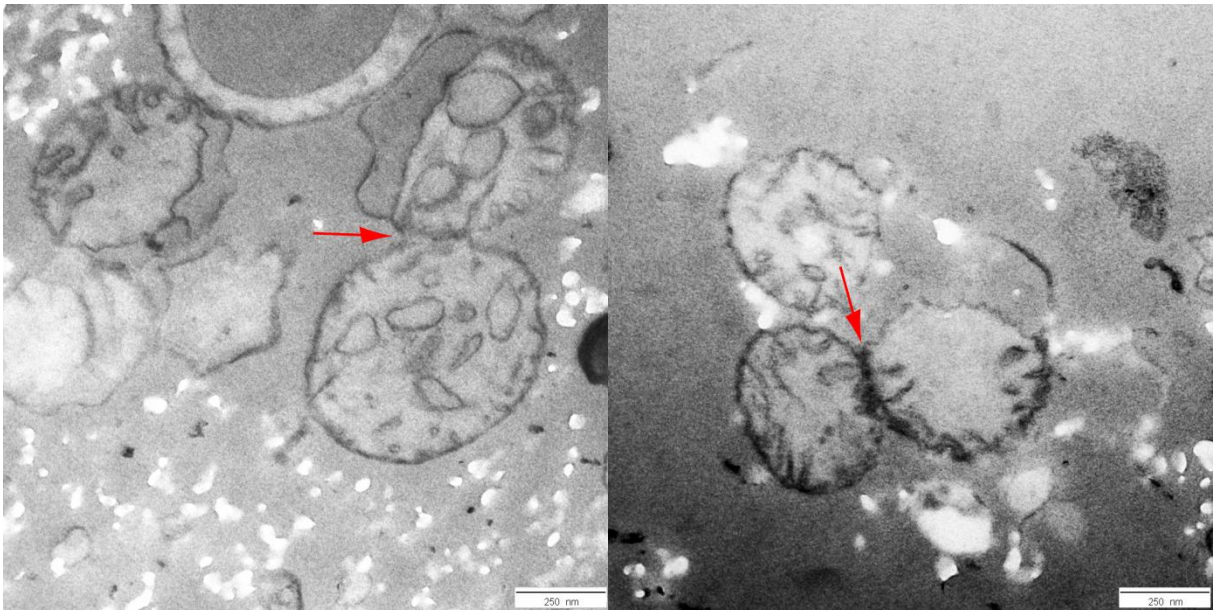

Figure 6.9: TEM images of fusion enhancement by PEG 1500, 30000x magnification. The fusion intermediates with separated inner membranes and fused outer membrane are indicated by red arrows.

The quantitative analysis of mitochondrial fusion efficiency after treatment with PEG 1500 by flow cytometry revealed that unspecific manipulation of mitochondrial fusion was successful (Figure 6.10).

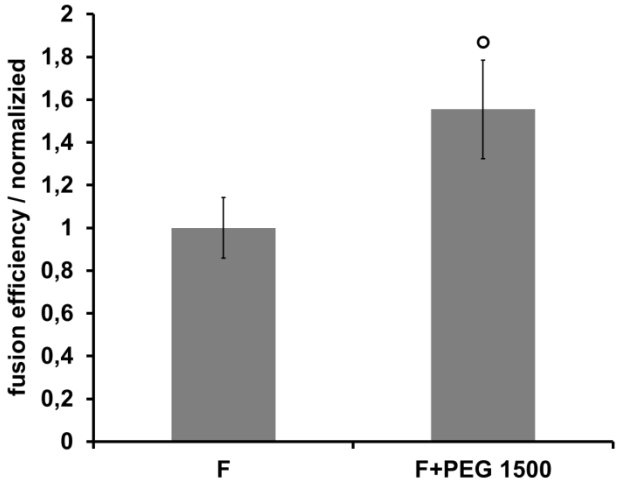

Figure 6.10: Unspecific enhancement of fusion efficiency with PEG 1500 50 %. Data are expressed as means of three measurements ± standard deviations (SD). Statistically significant differences are denoted by (°), $p < 0.05$.

Furthermore, the influence of 50 % PEG solutions with higher molecular weights of 4000 and 10000 Dalton compared to PEG 1500 was investigated (Figure 6.11). PEG 10000 also increased mitochondrial fusion efficiency unspecifically but it emerged that PEG 1500 was the most effective one among all investigated PEGs. PEG, thereby, must likely have dehydrated the samples [12] and brought mitochondria in close contact to facilitate mitochondrial fusion.

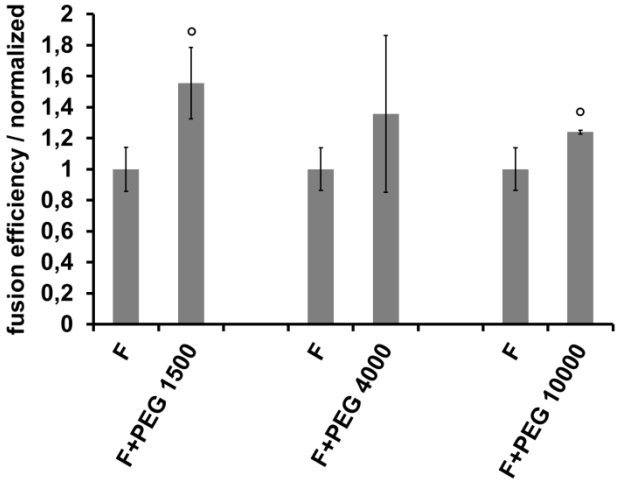

Figure 6.11: Unspecific manipulation of fusion efficiency with PEG 1500 50 % in comparison to PEG 4000 50 % and PEG 10000 50 %. Data are expressed as means of three measurements ± standard deviations (SD). Statistically significant differences are denoted by (°), $p < 0.05$.

The influence of lower concentrated PEG 1500 solutions was investigated in comparison to the 50 % solution that corresponded to 0.67 M. The concentrations 100 µM and 1 mM were chosen as modified polymers for specific manipulation, described later, were investigated at these concentrations. The lower concentrations of PEG 1500 had no influence on mitochondrial fusion efficiency (Figure 6.12). The effect of dehydration was apparently too low.

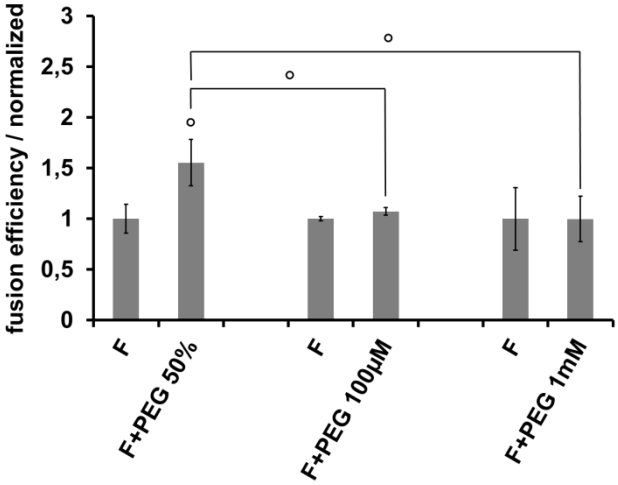

Figure 6.12: Unspecific manipulation of fusion efficiency with PEG 1500 50 % in comparison to PEG 1500 100 µM and 1 mM. Data are expressed as means of three measurements ± standard deviations (SD).Statistically significant differences are denoted by (°), $p < 0.05$.

The unspecific effects of highly concentrated 8arm PEGs, dendrimers and Jeffamine® that were used for the investigation of specific manipulation of mitochondrial fusion in vitro after modification with mitochondria specific peptides were also investigated. The 8arm PEGs showed toxicity due to the maleimide groups and the dendrimers showed toxicity due to the amine groups on the surface. Jeffamine® did not show toxicity but did also not enhance mitochondrial fusion unspecifically (Figure 6.13).

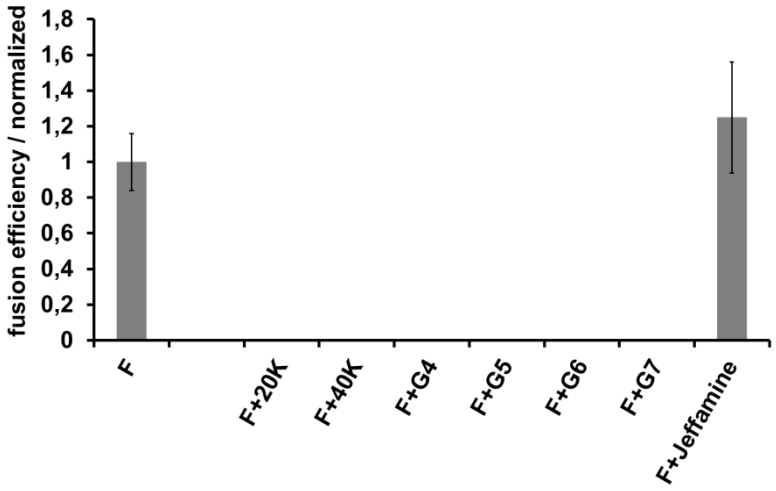

Figure 6.13: Unspecific manipulation of fusion efficiency with 8arm PEG 20 kDa 25 %, 8arm PEG 40 kDa 25 %, PAMAM dendrimers G4-G7 5 % and Jeffamine 50 %. Data are expressed as means of three measurements ± standard deviations (SD).

Specific manipulation of mitochondrial fusion in vitro

For specific manipulation of mitochondrial fusion in vitro, two 8armPEGs, 20 KDa and 40 kDa; four dendrimers, PAMAM-dendrimers generation 4, 5, 6 and 7 (G4-G7); a polyetheramine, Jeffamine® 2 kDa and quantum dots (Qdots) were chosen as carrier molecules.

These carrier molecules were modified with a natural mitochondrial targeting sequence (MLS) and a mitochondria penetrating peptide (MPP) that specifically recognized mitochondrial protein import pores. For comparison, the carrier molecules were also modified with β-mercaptoethanol and cysteine that should not be recognized by mitochondria. The influence of all modified carrier systems on mitochondrial fusion efficiency in vitro was

determined by flow cytometry. Furthermore, the influence of the carrier systems without modification was evaluated.

Modified 8arm PEGs added to a concentration of 100 µM did not influence mitochondrial fusion efficiency significantly (Figure 6.14).

A

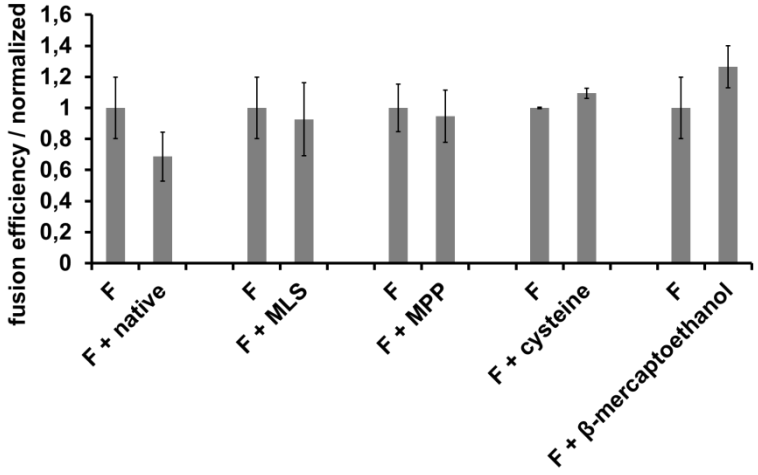

B

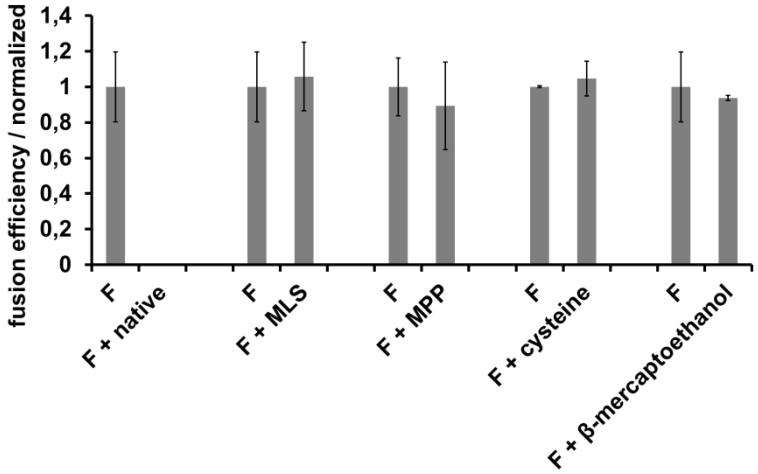

Figure 6.14: Specific manipulation of fusion efficiency with differently modified **8arm PEGs 20 kDa 100 µM** (A) and **8arm PEGs 40 kDa 100 µM** (B). Data are expressed as means of three measurements ± standard deviations (SD).

MPP-modified 8arm PEGs added at a concentration of 1 mM, significantly increased mitochondrial fusion efficiency. The MPP-modified 20 kDa 8arm PEG doubled mitochondrial fusion efficiency in vitro whereas the MPP-modified 40 kDa 8arm PEG increased mitochondrial fusion efficiency in vitro even to a twelvefold extent (Figure 6.15).

A

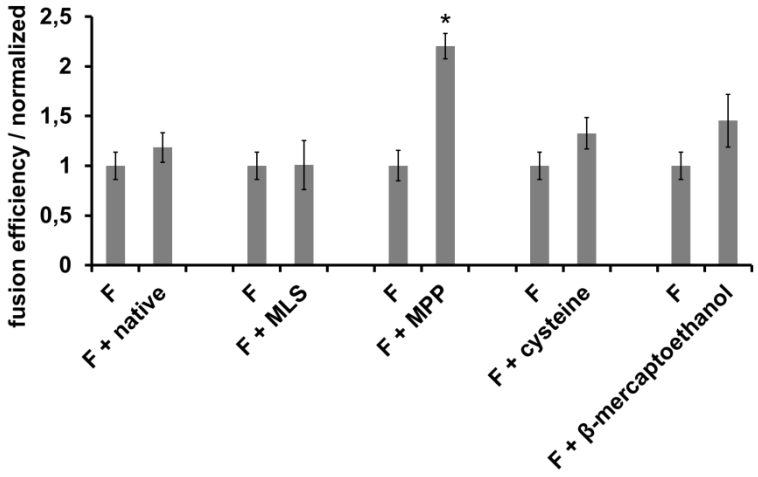

B

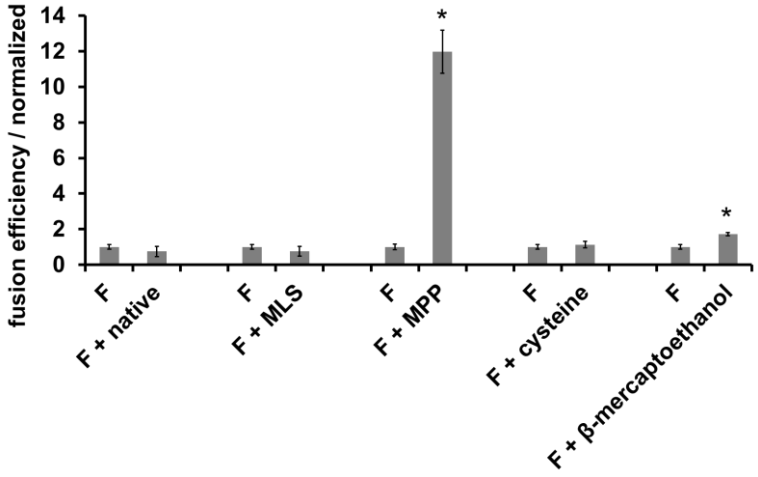

Figure 6.15: Specific manipulation of fusion efficiency with differently modified **8arm PEGs 20 kDa 1 mM** (A) and **8arm PEGs 40 kDa 1 mM** (B). Data are expressed as means of three measurements ± standard deviations (SD). Statistically significant differences are denoted by (*), $p < 0.01$.

To verify the results of the first batch of MPP-modified 8arm PEG 40 kDa, a second and a third batch were produced. They also increased mitochondrial fusion efficiency significantly but they only doubled mitochondrial fusion efficiency (Figure 6.16). The results of the second and third batch of the MPP-modified 40 kDa 8arm PEG were comparable to the results of the MPP-modified 20 kDa 8arm PEG.

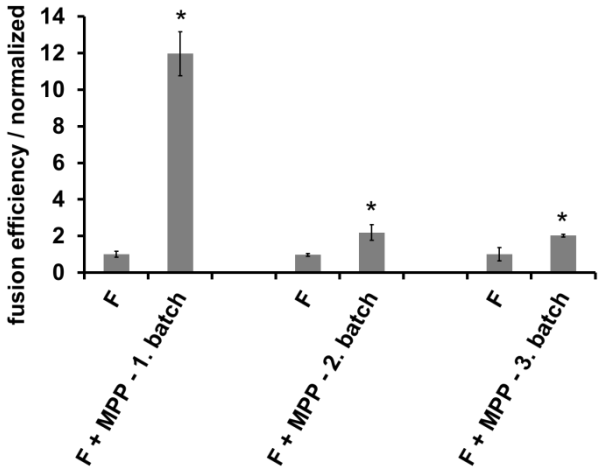

Figure 6.16: Specific manipulation of fusion efficiency with three batches of MPP-modified **8arm PEGs 40 kDa 1 mM**. Data are expressed as means of three or four measurements ± standard deviations (SD). Statistically significant differences are denoted by (*), $p < 0.01$.

The MPP-modified 8arm PEG was additionally labeled with the fluorescence dye BODIPY® to make it accessible for TEM analysis after photooxidation and to analyze where it accumulated, on the surface of mitochondria or inside mitochondria after it was eventually taken up. A mitochondrial fusion sample treated with a BODIPY®-labeled MPP-modified 40 kDa 8arm PEG (Figure 6.17) was analyzed in comparison to a sample treated with a BODIPY®-labeled β-mercaptoethanol-modified 40 kDa 8arm PEG (Figure 6.18) and a mitochondrial fusion sample without additional treatment (Figure 6.19). All TEM images showed fusion intermediates with fused outer mitochondrial membranes and adjacent but separated inner mitochondrial membranes. The black photooxidation product was not visible in Figure 6.17 and Figure 6.18 compared to Figure 6.19 that could not contain black photooxidation products. Eventually, the photooxidation products were distributed all over the samples and did not accumulate at specific sites.

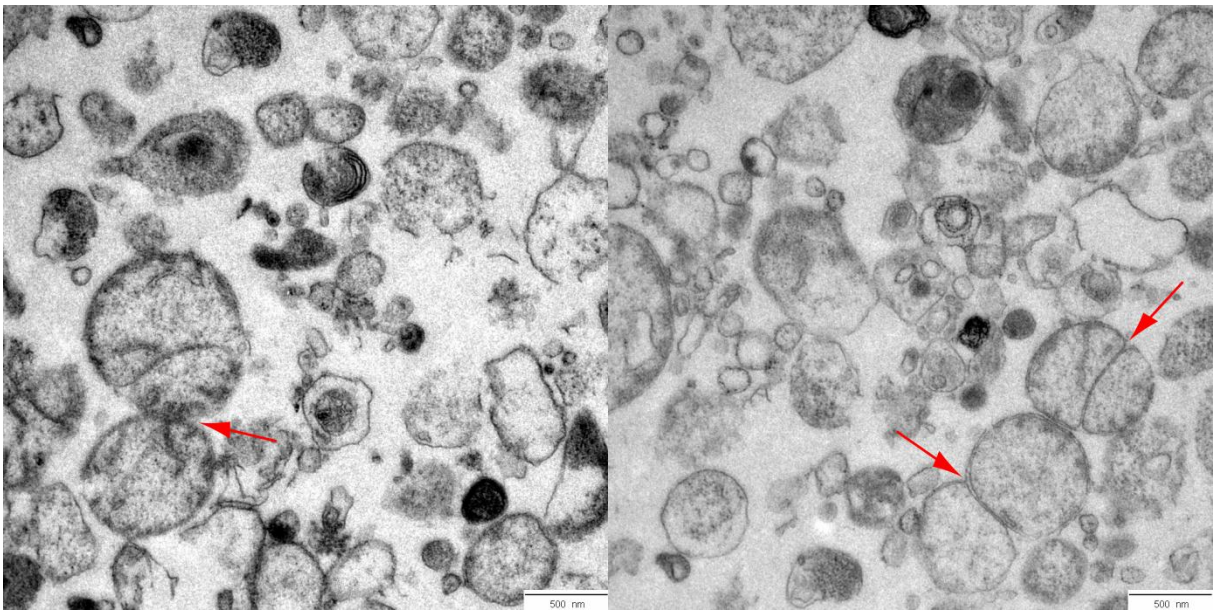

Figure 6.17: TEM images of fusion enhancement by MPP-conjugated 40 kDa 8arm PEG labeled with BODIPY® after photooxidation with DAB, 12000x magnification. The fusion intermediates with separated inner membranes and fused outer membrane are indicated by red arrows.

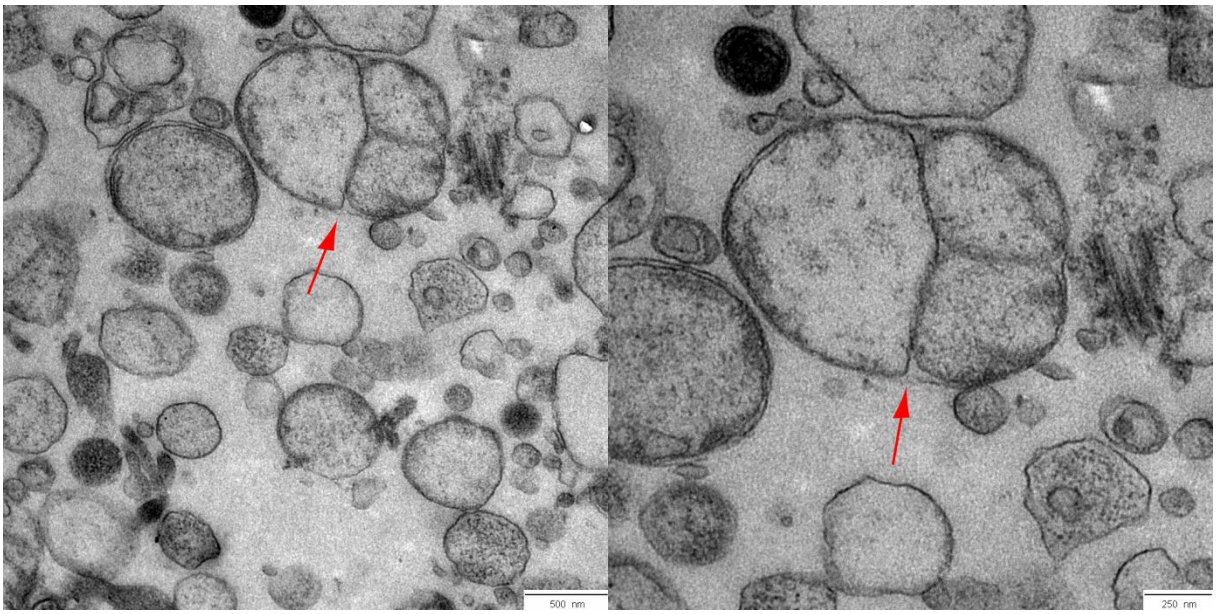

Figure 6.18: TEM images of fusion enhancement by β-mercaptoethanol-conjugated 40 kDa 8arm PEG labeled with BODIPY® after photooxidation with DAB, 12000x magnification on the left image and 20000x magnification on the right image. The fusion intermediates with separated inner membranes and fused outer membrane are indicated by a red arrows.

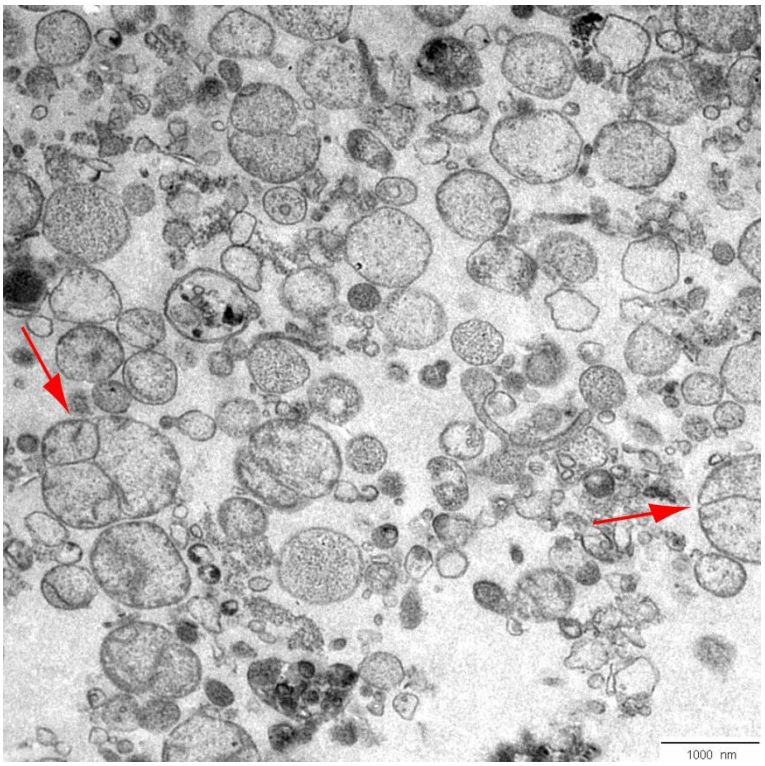

Figure 6.19: TEM images of mitochondrial fusion in vitro without manipulation and without BODIPY®. The fusion intermediates with separated inner membranes and fused outer membrane are indicated by red arrows.

MPP-modified generation 4, 5, 6 and 7 dendrimers slightly increased mitochondrial fusion efficiency in vitro at concentrations of 1 µM compared to fusion under normal conditions (Figure 6.20). Sometimes, also the control samples, that means dendrimers that were modified with cysteine or β-mercaptoethanol, slightly increased mitochondrial fusion efficiency.

A

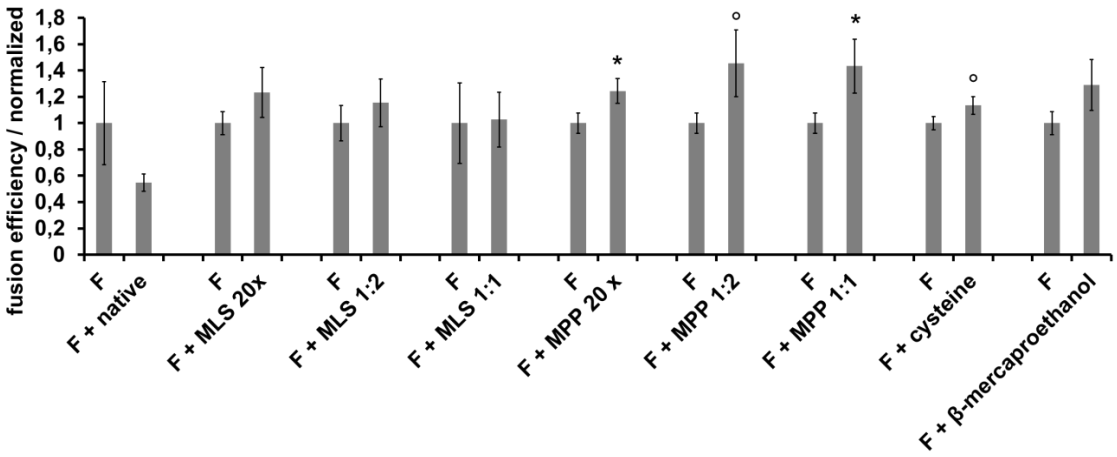

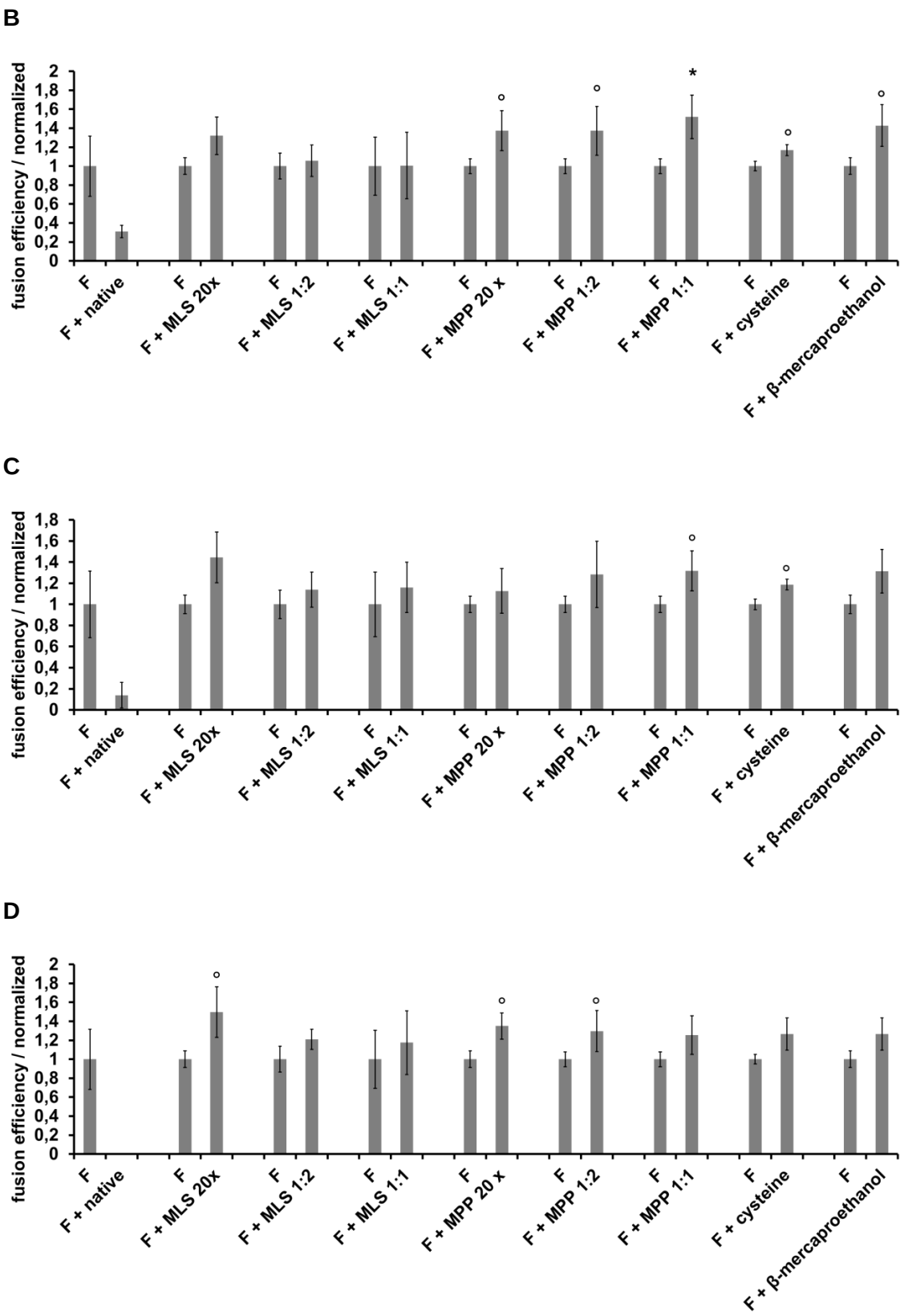

Figure 6.20: Specific manipulation of fusion efficiency with differently modified **PAMAM G4 dendrimers 1 µM** (A), **PAMAM G5 dendrimers 1 µM** (B), **PAMAM G6 dendrimers 1 µM** (C) **and PAMAM G7 dendrimers 1 µM** (D). Data are expressed as means of three or four measurements ± standard deviations (SD). Statistically significant differences are denoted by (°), $p < 0.05$ or by (*), $p < 0.01$.

Only the MLS-modified generation 7 dendrimer slightly increased mitochondrial fusion efficiency at a concentration of 1 µM (Figure 6.20 D).

The MPP-modified generation 4 and 5 dendrimers also increased mitochondrial fusion efficiency only slightly at concentrations of 100 µM (Figure 6.21). But the increase of carrier- and mitochondrial targeting peptide-concentration did not increase mitochondrial fusion efficiency.

A

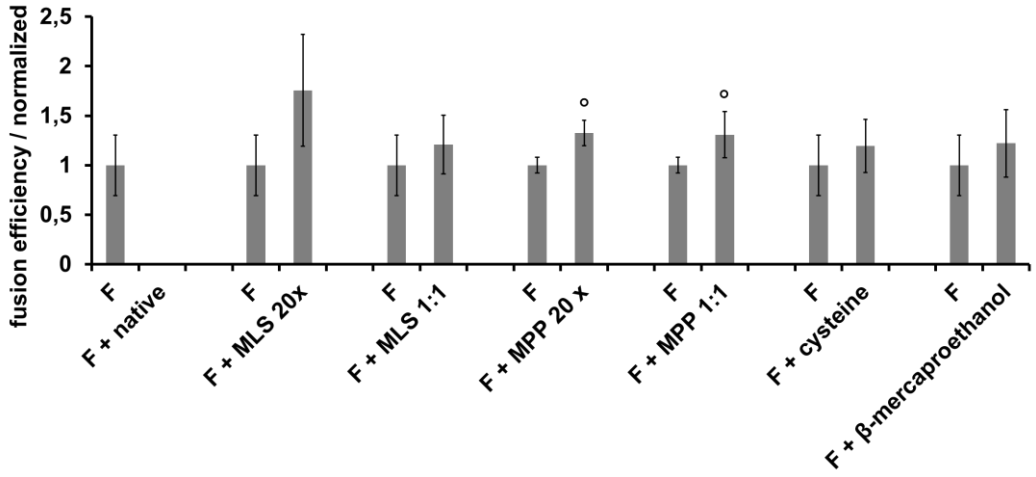

B

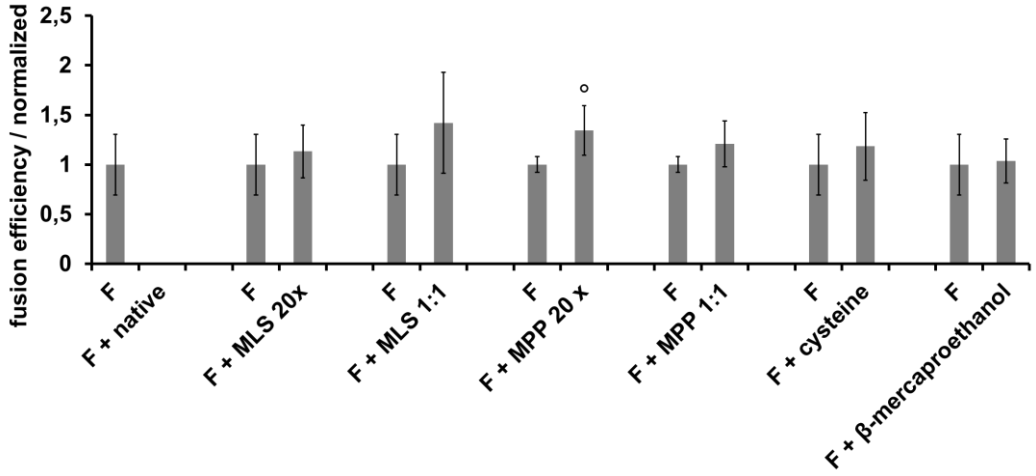

Figure 6.21: Specific manipulation of fusion efficiency with differently modified **PAMAM G4 dendrimers 100 µM** (A) and **PAMAM G5 dendrimers 100 µM** (B). Data are expressed as means of three or four measurements ± standard deviations (SD). Statistically significant differences are denoted by (°), $p < 0.05$.

Unmodified dendrimers were toxic for isolated mitochondria. The higher the generation with more amine groups on the surface, the more toxic was the dendrimer for isolated mitochondria (Figure 6.20).

Modified quantum dots did not show any influence on mitochondrial fusion efficiency in vitro (Figure 6.22). The concentrations of quantum dots (Qdots) that were investigated, 10 nM and 100 nM, were low compared to the concentrations of 8arm PEGs, eventually too low to influence mitochondrial fusion in vitro.

A

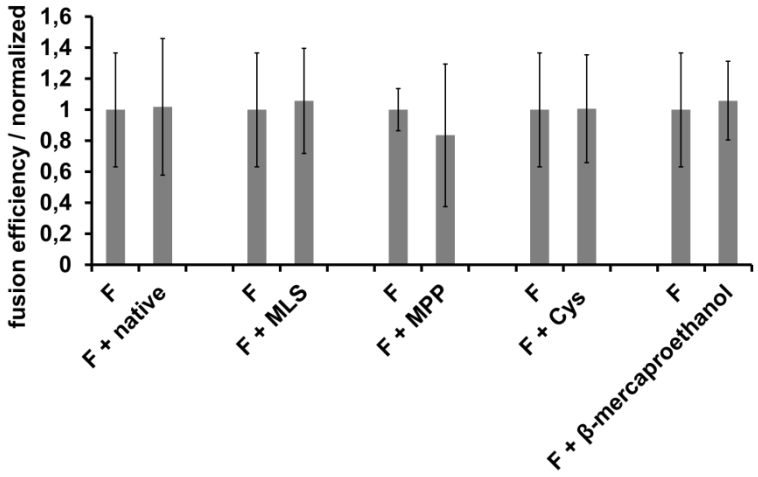

B

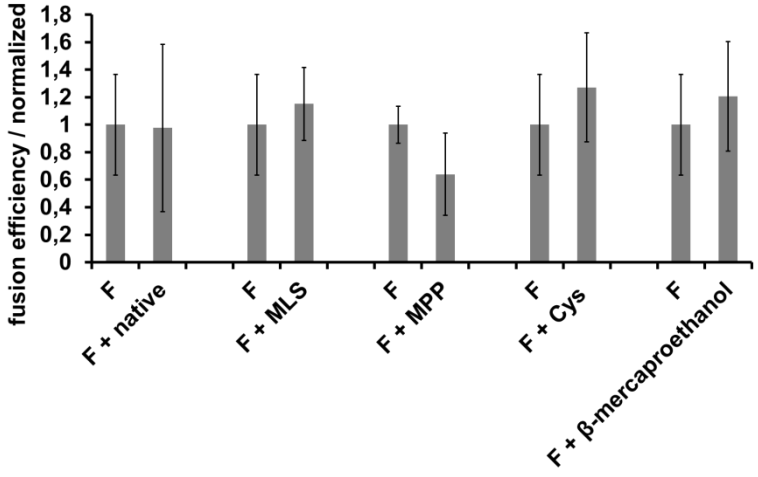

Figure 6.22: Specific manipulation of fusion efficiency with differently modified **Qdots 10 nM** (A) and **Qdots 100 nM** (B). Data are expressed as means of four measurements ± standard deviations (SD).

The MPP-modified polyetheramine Jeffamine® slightly increased mitochondrial fusion efficiency at a concentration of 100 µM and doubled mitochondrial fusion efficiency in vitro at a concentration of 1 mM (Figure 6.23). The investigated concentrations and observed effects were comparable to the 8arm PEGs.

A

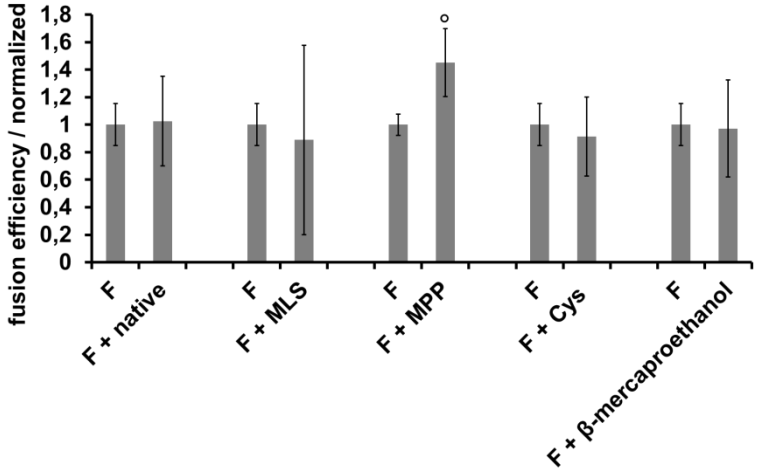

B

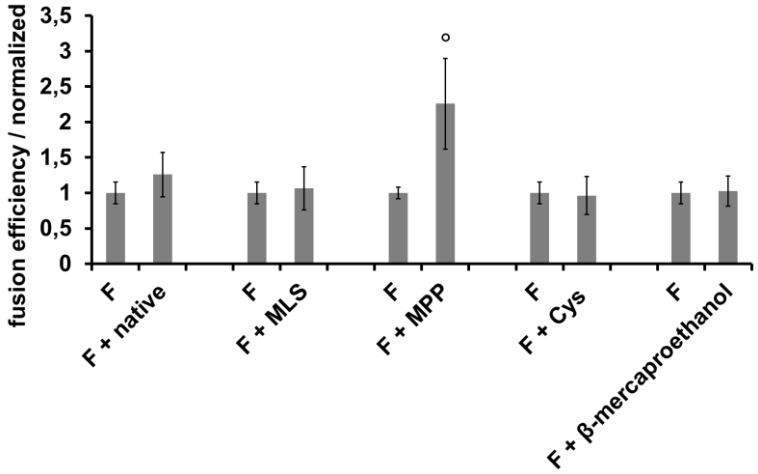

Figure 6.23: Specific manipulation of fusion efficiency with differently modified **Jeffamine 100 µM** (A) and **Jeffamine 1 mM** (B). Data are expressed as means of three or four measurements ± standard deviations (SD). Statistically significant differences are denoted by (°), $p < 0.05$.

MPP-modified Jeffamine®, dendrimers and 8arm PEGs enhanced mitochondrial fusion in vitro, in which the MPP modified 8arm PEGs were the most successful ones. Beside the influence of the targeting sequence, it seemed that the concentration of the carrier molecule

influenced on mitochondrial fusion efficiency in vitro. The higher concentrated MPP-modified 8arm PEGs and Jeffamine® enhanced mitochondrial fusion efficiency more than the lower concentrated MPP-modified dendrimers. The size or molecular weight of the carrier molecule and the amount of MPP molecules attached to the carrier did not influence on mitochondrial fusion efficiency as the results of the 20 kDa and 40 kDa 8arm PEGs with a maximum of eight MPP molecules at the surface and the 2 kDa Jeffamine® with a maximum of two MPP molecules at the surface were comparable at similar concentrations.

The targeting peptides MLS and MPP without carrier did not influence mitochondrial fusion efficiency in vitro significantly (Figure 6.24). High concentrations of 1 mM MLS and MPP were toxic for isolated mitochondria. A trend, that lower concentrations of peptide increase mitochondrial fusion efficiency more than higher concentrations, was observable. However, these results were difficult to reproduce.

A

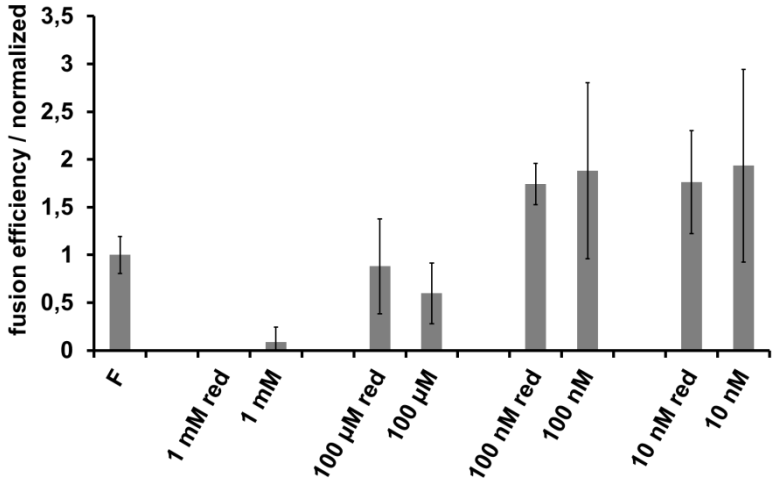

B

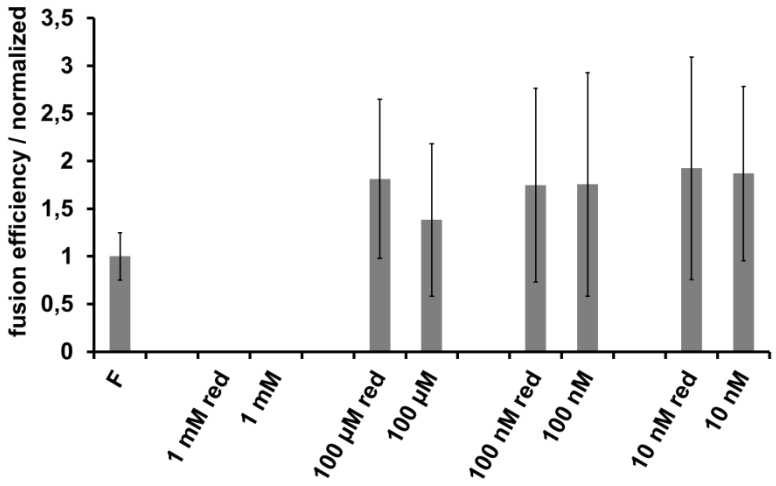

Figure 6.24: Specific manipulation of fusion efficiency with different concentrations of **MLS without carrier** (A) and **MPP without carrier** (B), reduced and not reduced. Data are expressed as means of three measurements ± standard deviations (SD).

6.4 Conclusions

It was shown that mitochondrial fusion could be enhanced by unspecific and specific approaches. PEG 1500 at a concentration of 50 % was the most effective additive for unspecific enhancement of mitochondrial fusion in vitro by dehydration. PEGs with higher molecular weights were not more effective. TEM studies revealed that the short term treatment with a highly concentrated PEG 1500 did not affect mitochondrial ultrastructure. The MPP modified 8arm PEGs, dendrimers and Jeffamine® were effective additives for specific enhancement of mitochondrial fusion in vitro. MPP modified 8arm PEGs at a concentration of 1 mM were the most effective enhancer of mitochondrial fusion in vitro. It emerged that carriers with the natural MLS did not enhance mitochondrial fusion efficiency. The successful conjugation of thiol containing molecules such as the targeting peptides MLS and MPP to maleimides was shown exemplarily in the conjugation of the 8arm PEGs to the model molecules β-mercaptoethanol and cysteine.

6.5 References

[1] S.A. Detmer, D.C. Chan, Functions and dysfunctions of mitochondrial dynamics, Nat Rev Mol Cell Biol 8 (2007) 870–879.

[2] H. Chen, M. Vermulst, Y.E. Wang, A. Chomyn, T.A. Prolla, J.M. McCaffery, D.C. Chan, Mitochondrial Fusion Is Required for mtDNA Stability in Skeletal Muscle and Tolerance of mtDNA Mutations, Cell 141 (2010) 280–289.

[3] D.C. Chan, Mitochondrial Fusion and Fission in Mammals, Annu. Rev. Cell Dev. Biol 22 (2006) 79–99.

[4] E.A. Schon, S. DiMauro, M. Hirano, R.W. Gilkerson, Therapeutic prospects for mitochondrial disease, Trends in Molecular Medicine 16 (2010) 268–276.

[5] V. Salnikov, Y. Lukyánenko, C. Frederick, W. Lederer, V. Lukyánenko, Probing the Outer Mitochondrial Membrane in Cardiac Mitochondria with Nanoparticles, Biophysical Journal 92 (2007) 1058–1071.

[6] M.P. Schwartz, A. Matouschek, The dimensions of the protein import channels in the outer and inner mitochondrial membranes, Proceedings of the National Academy of Sciences 96 (1999) 13086–13090.

[7] N. Pfanner, A. Geissler, Versatility of the mitochondrial protein import machinery, Nat. Rev. Mol. Cell Biol 2 (2001) 339–349.

[8] N. Pfanner, M. Meijer, Mitochondrial biogenesis: The Tom and Tim machine, Current Biology 7 (1997) R100–103.

[9] A. Heller, Chapter 5: Mitochondrial fusion in vitro, in: A. Heller (Ed.), Targeting mitochondria by mitochondrial fusion, mitochondria-specific peptides and nanotechnology: Dissertation.

[10] R.L. Davidson, K.A. O'Malley, T.B. Wheeler, Polyethylene glycol-induced mammalian cell hybridization: effect of polyethylene glycol molecular weight and concentration, Somatic Cell Genet 2 (1976) 271–280.

[11] J. Yang, M.H. Shen, Polyethylene glycol-mediated cell fusion, in: S. Pells (Ed.), Nuclear reprogramming: Methods and protocols, Humana Press, Totowa, N.J, 2006, pp. 59–66.

[12] J.W. Wojcieszyn, R.A. Schlegel, K. Lumley-Sapanski, K.A. Jacobson, Studies on the mechanism of polyethylene glycol-mediated cell fusion using fluorescent membrane and cytoplasmic probes, J. Cell Biol 96 (1983) 151–159.

[13] K.L. Horton, K.M. Stewart, S.B. Fonseca, Q. Guo, S.O. Kelley, Mitochondria-Penetrating Peptides, Chemistry & Biology 15 (2008) 375–382.

[14] L.F. Yousif, K.M. Stewart, K.L. Horton, S.O. Kelley, Mitochondria-Penetrating Peptides: Sequence Effects and Model Cargo Transport, ChemBioChem 10 (2009) 2081–2088.

[15] Y. Abe, T. Shodai, T. Muto, K. Mihara, H. Torii, S.-i. Nishikawa, T. Endo, D. Kohda, Structural Basis of Presequence Recognition by the Mitochondrial Protein Import Receptor Tom20, Cell 100 (2000) 551–560.

[16] J. Brix, K. Dietmeier, N. Pfanner, Differential Recognition of Preproteins by the Purified Cytosolic Domains of the Mitochondrial Import Receptors Tom20, Tom22, and Tom70, Journal of Biological Chemistry 272 (1997) 20730–20735.

[17] P. Rehling, N. Wiedemann, N. Pfanner, K.N. Truscott, The mitochondrial import machinery for preproteins, Crit. Rev. Biochem. Mol. Biol 36 (2001) 291–336.

[18] G.G.M. D'Souza, S.V. Boddapati, V. Weissig, Gene Therapy of the Other Genome: The Challenges of Treating Mitochondrial DNA Defects, Pharm Res 24 (2007) 228–238.

[19] S.H. Medina, M.E.H. El-Sayed, Dendrimers as Carriers for Delivery of Chemotherapeutic Agents, Chem. Rev 109 (2009) 3141–3157.

[20] G.G.M. D'Souza, V. Weissig, Subcellular targeting: a new frontier for drug-loaded pharmaceutical nanocarriers and the concept of the magic bullet, Expert Opin. Drug Deliv 6 (2009) 1135–1148.

[21] M. Labieniec, O. Ulicna, O. Vancova, J. Kucharska, T. Gabryelak, C. Watala, Effect of poly(amido)amine (PAMAM) G4 dendrimer on heart and liver mitochondria in an animal model of diabetes, Cell Biology Int 34 (2010) 89–97.

[22] M.M. Bradford, A rapid and sensitive method for the quantitation of microgram quantities of protein utilizing the principle of protein-dye binding, Analytical Biochemistry 72 (1976) 248–254.

[23] S. Meeusen, J.M. McCaffery, J. Nunnari, Mitochondrial Fusion Intermediates Revealed in Vitro, Science 305 (2004) 1747–1752.

Chapter 7

Binding behavior of mitochondrial targeting sequences to isolated mitochondria

Abstract

The binding properties of a natural mitochondrial targeting peptide (MLS) and a synthetic mitochondria penetrating peptide (MPP) to isolated mitochondria were evaluated. Quantum dots and fluorescent dyes were coupled to the mitochondrial targeting peptides to evaluate their binding affinity by flow cytometry whereas gold nanoparticles were used to investigate the binding affinity by transmission electron microscopy. Thereby, gold nanoparticles were successfully synthesized not by conventional exchange of citric acid but by a HEPES reduction method. Additionally, the binding behavior of MPP coupled to a BODIPY®-modified 8arm PEG was investigated by TEM analysis after photooxidation.

7.1 Introduction

Binding behavior and attraction of proteins to mitochondria are closely related to the affinity and properties of the targeting sequences. Beside this, the abundance of mitochondrial protein import pores that are targeted by these sequences also plays a role in achieving a sufficient binding and targeting to mitochondria. Mitochondria import more than a thousand different proteins, but a consensus in the amino acid sequence of the different mitochondrial targeting signals has not been identified [1]. Although they do not show amino acid sequence identity, the targeting signals have common characteristic physicochemical properties as they are enriched in positively charged, hydroxylated and hydrophobic residues with the ability to form an amphiphilic α-helix [1]. Protein translocation into mitochondria involves the targeting signal on the protein with a typical length of 15-50 amino acids [2], and a multiprotein translocator complex on the target membrane [3]. Interaction between these two components occurs due to the conformation of the targeting signal. The amphiphilic α-helix with hydrophobic residues on one side is able to interact with hydrophobic grooves of the translocator complex subunits in the mitochondrial outer membrane [3] and the positively charged surface on the other side of the α-helix is recognized by another subunit of the translocator complex [2]. Following to the interaction of targeting signal and translocator complexes, the membrane potential across the inner mitochondrial membrane directs the targeting sequences across this membrane, predominantly by an electrophoretic effect [1].

It is known that mitochondrial protein import is an efficient and rapid process as isolated mitochondria are able to import the majority of added protein within 30 seconds [4]. The mitochondrial targeting sequence (MLS) that has been examined in this study consists of 17 amino acids, derived from the targeting sequence of the saccharomyces cerevisiae protein cytochrome c oxidase subunit IV (CoxIV) plus an additional cysteine at the C-terminus for chemical reactions involving the thiol. This targeting sequence is well investigated and exhibits a high binding affinity to the translocator complexes in the mitochondrial membranes in comparison to other sequences [5–7]. Additionally, the binding behavior of a synthetic

mitochondria penetrating peptide (MPP) that consists of 6 amino acids, according to MPPs described by Horton et al. and Yousif et al. [8,9] has been investigated.

Beside the affinity of the targeting sequence to the protein import pores, the abundance of these translocator complexes in the mitochondrial membranes also play a crucial role in attaining a sufficient binding and targeting. It is difficult to define an exact number of protein pores on mitochondria as they are dynamic organelles that constantly change their size due to fusion and fission processes [10]. Only little is known about the distribution of the translocator complexes but there are approaches to define the density of protein import pores on mitochondria by special high resolution microscopy techniques [11]. It has been revealed that the density of the translocator proteins correlates to growth conditions and the mitochondrial membrane potential. It has also been detected that there is an intracellular gradient from perinuclear to the peripheral mitochondria [11]. The targeting sequence binding subunits of the protein import pores form clusters. Number, distribution and density are regulated and correlate with the activity of mitochondria and their position in the cell. The membrane potential of perinuclear mitochondria is higher than that of peripheral mitochondria and perinuclear mitochondria have a higher metabolic activity. This, in turn, correlates with a higher density of protein import pores on metabolic active perinuclear mitochondria. The molecular mechanisms that regulate the distribution of protein import pores are not known [11]. The density of protein import complexes also varies between different cell lines but an average number of approximately 100 translocator complex clusters per square micrometer has been determined [11].

For investigation of the affinity of the mitochondrial targeting sequence (MLS) and the mitochondria penetrating peptide (MPP) to mitochondria, it has been necessary to label the peptide sequence fluorescently to make it accessible to flow cytometry analysis. Therefore quantum dots as well as the fluorescent dyes tetramethylrhodamine (TAMRA) and BODIPY® have been conjugated to the MLS and the MPP.

To study the binding behavior of the MLS by transmission electron microscopy (TEM), MLS capped gold nanoparticles were synthesized. Several methods can be applied to cover and

stabilize gold nanoparticles with peptides. The success of which depends on the physicochemical properties of the peptide sequence. Peptide capped gold nanoparticles are conventionally synthesized by reducing tetrachloroaurate ions with citric acid. The addition of cysteine containing peptides results in the exchange of capping agents from citric acid to peptides. But it has been demonstrated that peptides that are abundant of basic amino acids lead to aggregation of gold nanoparticles during exchange reactions [12]. This may occur due to repulsion between adjacent peptides, resulting in less peptide molecules on the particle surface that stabilize the gold nanoparticle [12]. Therefore, a method that reduces tetrachloroaurate ions with HEPES under mild conditions (pH 7.2, ambient temperature) in the presence of a cysteine-terminal peptide [12,13] was applied to synthesize MLS-capped gold nanoparticles for TEM studies. Tetrachloroaurate ions are reduced due to oxidation of the piperazine ring of HEPES to an N-centered cationic free radical, producing gold nanoparticles in the presence of gold binding peptides [12]. Additionally, the binding behavior of the mitochondria penetrating peptide (MPP), conjugated to a fluorescently labeled 8arm PEG has been investigated by a photoconversion method in a transmission electron microscopy study.

7.2 Materials and methods

7.2.1 Materials

HAM F-12 nutrient mixture and fetal calf serum (FCS) were purchased from Sigma-Aldrich (Steinheim, Germany). Trypsin-EDTA 0.25 % was obtained from Gibco-Invitrogen (Karlsruhe, Germany). G418 was purchased from Sigma-Aldrich (Steinheim, Germany). Purified water was obtained by using a Milli-Q water purification system from Millipore (Schwalbach, Germany). All cell culture materials were purchased from Corning (Bodenheim, Germany).

Isolation buffer consisted of 250 mM sucrose (Merck, Darmstadt, Germany), 10 mM Tris (USB Corporation, Cleveland, OH USA), 10 mM KCl (Merck, Darmstadt, Germany), 1 mM Na_2EDTA (Merck, Darmstadt, Germany) and 0.1 % bovine serum albumin (BSA) (Sigma-Aldrich, Steinheim, Germany). MLS and MPP peptides were synthesized by GeneCust (Dudelange, Luxembourg). TCEP Reducing Gel was obtained from Thermo Fisher Scientific (Bonn, Germany) and TCEP was purchased from Sigma-Aldrich (Steinheim, Germany). Sodium phosphate/sodium chloride buffer consisted of 0.1 M disodium hydrogenphosphate dihydrate (Merck, Darmstadt, Germany) and 0.15 M sodium chloride (Merck, Darmstadt, Germany). The pH-value was adjusted to 7.2 by TitriPUR® 1 N hydrochloric acid (Merck, Darmstadt, Germany). Amicon® Ultra-4 centrifugal filter units 10 kDa (Millipore, Schwalbach, Germany) were used for purification by ultrafiltration.

Qdot 655 ITK amino (PEG) quantum dots were obtained from Invitrogen (Karlsruhe, Germany) and quantum dots eFluor 650 NC (amine) nanocrystals were purchased from eBioscience (Frankfurt, Germany). Sulfo-SMCC was obtained from Thermo Fisher Scientific (Bonn, Germany). β-mercaptoethanol and L-cysteine hydrochloride monohydrate were purchased from Sigma-Aldrich (Steinheim, Germany). TAMRA-maleimide was obtained from MoBiTec (Göttingen, Germany) and BODIPY® FL SE was purchased from Invitrogen (Karlsruhe, Germany). PD-10 columns filled with Sephadex G-25 medium were obtained from GE Healthcare (Freiburg, Germany). Gold(III)chloride trihydrate was obtained from Sigma-Aldrich (Steinheim, Germany) and HEPES was purchased from Merck (Darmstadt,

Germany). The pH-value of 0.1 M HEPES buffer was adjusted to 7.2 by TitriPUR® 1 N sodium hydroxide (Merck, Darmstadt, Germany). BODIPY® FL L-cystine was obtained from Invitrogen (Karlsruhe, Germany). The 8arm PEG-maleimide 40 kDa was purchased from Nanocs Inc. (New York, NY, USA). DPBS without calcium and magnesium was obtained from Gibco-Invitrogen (Karlsruhe, Germany).

0.1 M cacodylate fixation buffer consisted of 100 mM sodium cacodylate (Roth, Karlsruhe, Germany), 2 mM magnesium chloride hexahydrate (Merck, Darmstadt, Germany), 1 mM calcium chloride dihydrate (Merck, Darmstadt, Germany), 40 mM sodium chloride (Merck, Darmstadt, Germany) and 2 % glutaraldehyde (Serva, Heidelberg, Germany). 0.1 M cacodylate washing buffer consisted of 100 mM sodium cacodylate (Roth, Karlsruhe, Germany), 2 mM magnesium chloride hexahydrate (Merck, Darmstadt, Germany), 1 mM calcium chloride dihydrate (Merck, Darmstadt, Germany) and 40 mM sodium chloride (Merck, Darmstadt, Germany). Diaminobenzidine was purchased from Sigma-Aldrich (Steinheim, Germany) and agarose was obtained from Biozym (Hessisch Oldendorf, Germany). Osmium tetroxide (ScienceServices, Munich, Germany) was dissolved to 1 % in 0.1 M cacodylate buffer that consisted of 100 mM sodium cacodylate (Roth, Karlsruhe, Germany), 2 mM magnesium chloride hexahydrate (Merck, Darmstadt, Germany), 1 mM calcium chloride dihydrate (Merck, Darmstadt, Germany) and 40 mM sodium chloride (Merck, Darmstadt, Germany). Embedding in Epon was carried out with an Epoxy Embedding Medium Kit (Fluka by Sigma-Aldrich, Steinheim, Germany). Propylen oxide was purchased from Sigma-Aldrich (Steinheim, Germany).

7.2.2 Binding behavior of MLS- and MPP-modified Qdots to isolated mitochondria

Quantum dots from Invitrogen (Karlsruhe, Germany) and eBioscience (Frankfurt, Germany) were modified with the MLS, MPP, cysteine and β-mercaptoethanol as described in a previous study [14]. Long-time cultivation of a CHO-cell line that was stably transfected with mitochondria targeted green fluorescent protein (mtGFP) was carried out in selection medium HAM-F12 containing 10 % FCS and 400 µg/ml G418. The last cultivation step of

CHO-mtGFP cells before binding experiments was carried out in G418-free medium because the cells did not lose the plasmid within one week. Cells were cultured in HAM-F12 nutrient mixture with 10 % FCS in 150 cm^2 culture flasks until confluency, harvested by Trypsin-EDTA 0.25 % and washed with isolation buffer. The centrifugation steps for the washing steps of the cells were carried out in a GS-15R centrifuge (Beckman, Krefeld, Germany). Afterwards, mtGFP-containing cells from one culture flask were suspended in 250 µl isolation buffer. Then, cells from four flasks were pooled and the resulting one milliliter of cell suspension was transferred into a cooled 2-ml Dounce glass homogenizer (Sigma-Aldrich, Steinheim, Germany) where the cells were disrupted by 25 strokes. The suspension was transferred into a 2-ml safe-lock tube (Eppendorf, Hamburg, Germany) and centrifuged at 1500 g at 4 °C for 10 min a type 5415 R centrifuge (Eppendorf, Hamburg, Germany) to pelletize nuclei as well as remaining intact cells. The first supernatant was kept on ice, while the pellet was resuspended in isolation buffer and homogenized by 25 Dounce strokes for a second time to break remaining intact cells. A second centrifugation step at 1500 g at 4 °C for 10 min yielded a pellet that was the nuclei enriched fraction. The first and the second supernatant were mixed and centrifuged at 16000 g at 4 °C for 15 min to obtain a pellet enriched with mtGFP-containing isolated mitochondria. The amount of cells used for the isolation of mitochondria depended on the required amount for the different experiments. Mitochondrial protein concentration was determined by a Bradford-Assay [15].

Isolated mitochondria were mixed with unmodified, MLS-, MPP-, cysteine- and β-mercaptoethanol-modified quantum dots, in 10 nM and 100 nM concentrations. The mixture was either incubated on ice for 1 h or centrifuged at 16000 g, 4 °C for 10min and then incubated on ice for 1 h. After incubation, the pellets of the centrifuged samples were resuspended again. Analysis of the binding of quantum dots to isolated mitochondria was carried out by flow cytometry with a FACSCanto™ (BD Bioscience, Heidelberg, Germany). Therefore, the samples were diluted to not exceed the critical count rate of the flow cytometer. GFP was excited by a 488 nm blue laser and was detected at 515–545 nm. Quantum dots from Invitrogen (Karlsruhe, Germany) were excited by a 405 nm violet laser

and detected at 650–670 nm whereas quantum dots from eBioscience (Frankfurt, Germany) were excited by a 488 nm blue laser and detected with a 670 nm long pass filter. Plots that indicated fluorescence intensity of GFP on the x-axis and fluorescence intensity of quantum dots on the y-axis were created. GFP-labeled isolated mitochondria and non-fluorescent isolated mitochondria were used to define the quadrants of the plots as follows: the lower left quadrant (LL) indicated non fluorescent cell fragments, the upper left quadrant (UL) indicated quantum dots that bound non-specifically to non-fluorescent cell fragments as quantum dots in solution are too small to be detected by the flow cytometer, the lower right quadrant (LR) was determined by single-labeled GFP-mitochondria and the upper right quadrant (UR) was positive for quantum dots that bound to GFP-mitochondria (Figure 7.1).

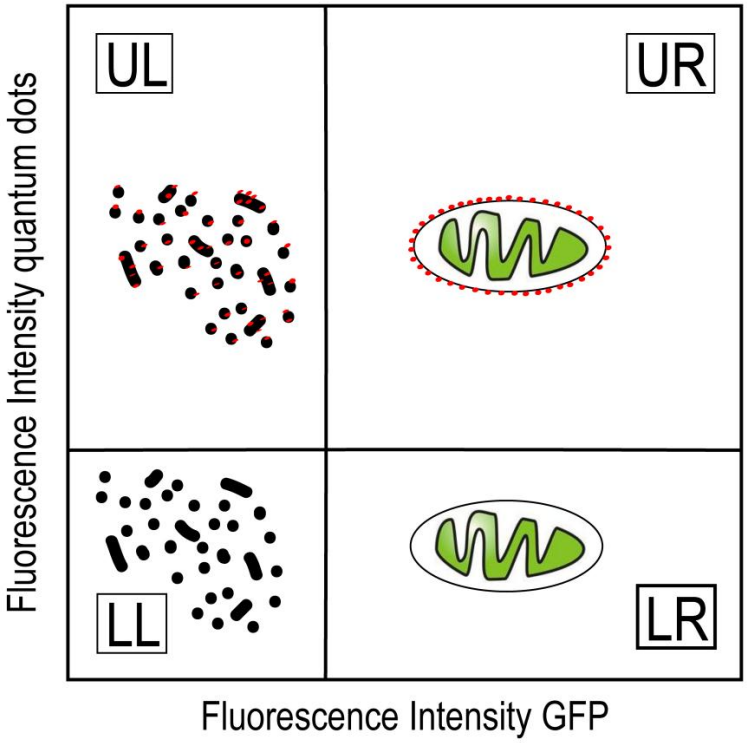

Figure 7.1: Flow cytometry plot for the analysis of the binding of quantum dots to mitochondria.

7.2.3 Binding behavior of MLS-modified TAMRA to isolated mitochondria

The MLS peptide was reduced by a TCEP-gel at room temperature in the dark for 1 h and modified with a tenfold molar excess of TAMRA-maleimide afterwards. Reactions were carried out at room temperature for 1-2 h. The conjugate was purified by a PD 10 desalting column and stored at -20 °C. Cells were cultured as described previously. The last cultivation

step of CHO-mtGFP cells before binding experiments was carried out in G418-free medium because the cells did not lose the plasmid within one week. Only long-time cultivation of CHO-GFP cells was carried out in selection medium containing 400 µg/ml G418. Mitochondria from CHO-mtGFP cells were isolated as described previously. Isolated mitochondria were mixed with unmodified or MLS-modified TAMRA, in 1 µM and 5 µM concentrations. The mixture was either incubated on ice for 1 h or centrifuged at 16000 g, at 4 °C for 10min and then incubated on ice for 1 h. After incubation, the pellets of the centrifuged samples were resuspended again.

Analysis of the binding of TAMRA-MLS to isolated mitochondria was carried out by flow cytometry with a FACSCanto™ (BD Bioscience, Heidelberg, Germany). Therefore, the samples were diluted to not exceed the critical count rate of the flow cytometer. GFP was excited by a 488 nm blue laser and detected at 515–545 nm. TAMRA was excited by a 488 nm blue laser and detected at 564–606 nm. Plots that indicated fluorescence of GFP on the x-axis and fluorescence of TAMRA on the y-axis were created. GFP-labeled isolated mitochondria and non-fluorescent isolated mitochondria were used to define the quadrants of the plots as follows: the lower left quadrant (LL) indicated non fluorescent cell fragments, the upper left quadrant (UL) indicated TAMRA that bound non-specifically to non-fluorescent cell fragments as TAMRA in solution could not be detected by the flow cytometer, the lower right quadrant (LR) was determined by single-labeled GFP-mitochondria and the upper right quadrant (UR) was positive for TAMRA that bound to GFP-mitochondria.

Intact cells, CHO and CHO-mtGFP cells were stained with the unconjugated TAMRA-maleimide dye in concentrations of 1 µM and 5 µM to determine the intracellular distribution of the dye. Analysis was carried out by confocal laser scanning microscopy (CLSM) with a Zeiss Axiovert LSM 510 (Carl Zeiss, Oberkochen, Germany) and an AxioCam HRc (Carl Zeiss, Oberkochen, Germany). Thereby, GFP was excited at 488 nm and detected at 505–530 nm whereas TAMRA was excited at 543 nm and detected at 560–615 nm.

7.2.4 Binding behavior of BODIPY® to isolated mitochondria

Before using BODIPY® FL SE as a dye to label the MLS, intact CHO and CHO-RFP cells were stained in concentrations of 10 nM and 100 nM to determine the intracellular distribution of the dye. Analysis was carried out by confocal laser scanning microscopy (CLSM) with a Zeiss Axiovert LSM 510 (Carl Zeiss, Oberkochen, Germany) and an AxioCam HRc (Carl Zeiss, Oberkochen, Germany). Thereby, RFP was excited at 488 nm and emission was detected at 560–615 nm whereas TAMRA was excited at 488 nm and emission was detected at 505–530 nm.

Afterwards, isolated mitochondria from CHO-cells containing a mitochondria targeted red fluorescent protein (mtRFP) were stained with BODIPY® FL SE to investigate the behavior of the dye in presence of isolated mitochondria. Therefore, cells were cultured as described previously. The last cultivation step of CHO-mtRFP cells before binding experiments was carried out in G418-free medium because the cells did not lose the plasmid within one week. Only long-time cultivation of CHO-mtRFP cells was carried out in selection medium containing 400 µg/ml G418. Mitochondria from CHO-RFP cells were isolated as described previously. The dye was added in 10 nM and 100 nM concentrations. The mixture was either incubated on ice for 1 h or centrifuged at 16000 g, at 4 °C for 10min and then incubated on ice for 1 h. After incubation, the pellets of the centrifuged samples were resuspended again.

Analysis of the binding of BODIPY® FL SE to isolated mitochondria was carried out by flow cytometry with a FACSCanto™ (BD Bioscience, Heidelberg, Germany). Therefore, the samples were diluted to not exceed the critical count rate of the flow cytometer. RFP was excited by a 488 nm blue laser and was detected at 564–606 nm. BODIPY® FL SE was excited by a 488 nm blue laser and was detected at 515–545 nm. Plots that indicate the fluorescence of RFP on the x-axis and the fluorescence of BODIPY® FL SE on the y-axis were created. RFP-labeled isolated mitochondria and non-fluorescent isolated mitochondria were used to define the quadrants of the plots as follows: the lower left quadrant (LL) indicated non fluorescent cell fragments, the upper left quadrant (UL) indicated BODIPY® FL SE that bound non-specifically to non-fluorescent cell fragments as BODIPY® FL SE in

solution could not be detected by the flow cytometer, the lower right quadrant (LR) was determined by single-labeled RFP-mitochondria and the upper right quadrant (UR) was positive for BODIPY® FL SE that bound to RFP-mitochondria.

7.2.5 Binding behavior of MLS-modified gold nanoparticles to isolated mitochondria

Gold nanoparticles capped by the targeting peptides MLS and MPP were synthesized using a HEPES reduction method according to Slocik et al. [13] and Serizawa et al. [12]. Thereby, the peptides were reduced on a TCEP-gel at room temperature in the dark for 1 h. The reduced peptides were added in 0.075 mM, 0.15 mM, 0.225, 0.3 mM, 0.45 mM, 0.6 mM or 0.75 mM concentrations to HEPES buffer 0.1 M in a glass vial. Tetrachloroauric acid was added to a 0.5 mM concentration. The mixture was stirred at room temperature for 42 h. Gold nanoparticles were purified by three centrifugation steps at 5000 g, 4 °C for 10 min in a type 5415 R centrifuge (Eppendorf, Hamburg, Germany) and resuspended in purified water. Characterization of the gold nanoparticles was carried out by UV-spectroscopy with a Kontron Instruments Uvikon 900 spectrophotometer (Goebel Instrumentelle Analytik, Hallertau, Germany). The size of the peptide capped gold nanoparticles was determined by photon correlation spectroscopy (PCS) with a Zetasizer nano ZS (Malvern, Herrenberg, Germany). The zetapotential of the peptide capped gold nanoparticles also was determined with a Zetasizer nano ZS (Malvern, Herrenberg, Germany). All measurements were carried at 25 °C in purified water and the concentration of the gold nanoparticles was determined according to Haiss et al. [16].

Cells were cultured and mitochondria were isolated as described previously. Gold nanoparticles were added to isolated mitochondria, incubated on ice for 1 h and analyzed by TEM. Therefore, samples were fixed in cacodylate fixation buffer at room temperature for 5 min and on ice overnight. Afterwards, mitochondria were washed by five washing steps, each of them in cacodylate washing buffer for 2 min. Then, isolated mitochondria were pelletized in a 1 % agarose solution that was heated to 40 °C. All centrifugation steps were carried out in a himac CT15RE (VWR Leuven, Belgium by Hitachi Koki Co. Ltd.). After

gelation of the agarose, the gel block was cut and fixed with osmium tetroxide solution overnight. Then, the samples were washed in DPBS four times for 15 min. Afterwards, the samples were dehydrated in a graded series of ethanol: 50 %, 70 %, 80 %, 90 % and 100 %. Each dehydration step was carried out two times for 15 min. Then, the samples were treated in an equal mixture of acetone or propylene oxide and ethanol for 20 min and two times in acetone or propylene oxide for 20 min. Afterwards, the samples were treated with a mixture of acetone or propylene oxide and Epon (2:1) for 2 h, then, in a mixture of acetone or propylene oxide and Epon (1:1) for 2 h and subsequently in a mixture of acetone or propylene oxide and Epon (1:2) in an open vial overnight. Then, the samples were embedded and hardened in Epon at room temperature for 1 h, at 30 °C for 2 h and at 60 °C for 2 days. Epon blocks were cut into sections of 50 nm with a microtome Leica EM UC6 (Leica, Vienna, Austria) and transferred to copper slot grids with a 1.5 % hyaloform foil. They were examined either unstained or stained with uranyl acetate and lead citrate in a transmission electron microscope Zeiss EM 902 (Carl Zeiss, Oberkochen, Germany), operating at 80kV. Digital images were recorded by a slow scan CCD camera (TRS Typ 7888, Serial No. 321/08).

7.2.6 Binding behavior of MPP-modified BODIPY®-labeled 40kDa 8arm PEG to isolated mitochondria

BODIPY® FL L-cystine and the MPP were reduced by a thirtyfold molar excess of TCEP in the dark for 30 min. The 8arm PEG-maleimid 40 kDa was modified with the reduced BODIPY® FL L-cystine in an equal molar ratio and with MPP or β-mercaptoethanol in a tenfold molar excess. Therefore, 8arm PEGs were dissolved in sodium phosphate/sodium chloride buffer to 1 mM and reduced BODIPY® FL L-cystine and MPP or β-mercaptoethanol were added to the 8arm PEG solutions. Reactions were carried out at 4 °C overnight. The modified 8arm PEGs were purified by six ultrafiltration steps in ultrafiltration units with a cut-off of 10 kDa and sodium phosphate/sodium chloride buffer.

Cells were cultured and mitochondria were isolated as described previously. The 8arm PEG modified with BODIPY® FL L-cystine and MPP or β-mercaptoethanol was added to isolated mitochondria, incubated on ice for 1 h and analyzed by TEM after photooxidation. Therefore, isolated mitochondria were fixed in cacodylate fixation buffer with glutaraldehyde at room temperature for 5 min and on ice overnight. Afterwards, mitochondria were washed by five washing steps, each of them in cacodylate washing buffer for 2 min. Then, the buffer solution was exchanged by diaminobenzide in cacodylate buffer 0.1 M and photooxidation was carried out at an Axiovert 200 (Carl Zeiss, Göttingen, Germany) with an excitation wave length of 488 nm and an emission wave length of 515 nm. Afterwards, the diaminobenzidine solution was exchange by cacodylate buffer 0.1 M. Then, isolated mitochondria were pelletized in a 1 % agarose solution that was heated up to 40 °C. All centrifugation steps were carried out in a himac CT15RE (VWR Leuven, Belgium by Hitachi Koki Co. Ltd.). After gelation of the agarose, the gel block was cut and fixed with osmium tetroxide solution overnight. The samples were washed in DPBS four times for 15 min. Afterwards, the samples were dehydrated in a graded series of ethanol: 50 %, 70 %, 80 %, 90 % and 100 %. Each dehydration step was carried out two times for 15 min. Then, the samples were treated in an equal mixture of acetone or propylene oxide and ethanol for 20 min and two times in acetone or propylene oxide for 20 min. Afterwards, the samples were treated with a mixture of acetone or propylene oxide and Epon (2:1) for 2 h, then, in a mixture of acetone or propylene oxide and Epon (1:1) for 2 h and subsequently in a mixture of acetone or propylene oxide and Epon (1:2) in an open vial overnight. Then, the samples were embedded and hardened in Epon at room temperature for 1 h, at 30 °C for 2 h and at 60 °C for 2 days. Epon blocks were cut into sections of 50 nm with a Leica EM UC6 microtome (Leica, Vienna, Austria) and transferred to copper slot grids with a 1.5 % hyaloform foil. They were examined either unstained or stained with uranyl acetate and lead citrate in a transmission electron microscope Zeiss EM 902 (Carl Zeiss, Oberkochen, Germany), operating at 80kV. Digital images were recorded by a slow scan CCD camera (TRS Typ 7888, Serial No. 321/08).

7.3 Results and discussion

The binding affinity of a natural mitochondrial targeting sequence (MLS) and a synthetic mitochondrial targeting peptide (MPP) to isolated mitochondria was investigated by flow cytometry. Therefore, the peptides were attached to red fluorescent quantum dots and the binding affinity to isolated mitochondria that carried green fluorescent proteins was evaluated in comparison to unmodified quantum dots and non-targeting quantum dots that were modified with cysteine or β-mercaptoethanol (Figure 7.2). Concentrations of 10 nM and 100 nM of quantum dots were investigated. Isolated mitochondria and quantum dots were either only mixed or centrifuged. The four quadrants of the flow cytometry plots in Figure 7.2 show non fluorescent cell fragments in the lower left quadrant, quantum dots that bound non-specifically to non-fluorescent cell fragments in the upper left quadrant, GFP-containing mitochondria in the lower right quadrant and quantum dots that bound to GFP-containing mitochondria in the upper right quadrant. Figure 7.2 shows that all kinds of unmodified and modified quantum dots bound to isolated mitochondria and cell fragments in the same manner. Unmodified and non-targeted quantum dots showed the same binding affinity to isolated mitochondria and cell fragments like targeted quantum dots that were modified with the MLS or the MPP. In turn, the targeted quantum dots showed the same binding affinity to cell fragments like the unmodified and non-targeting quantum dots. The higher the concentration of all modified and unmodified quantum dots was, the higher was the binding affinity to cell fragments and isolated mitochondria. Centrifugation also increased the binding affinity to cell fragments and isolated mitochondria.

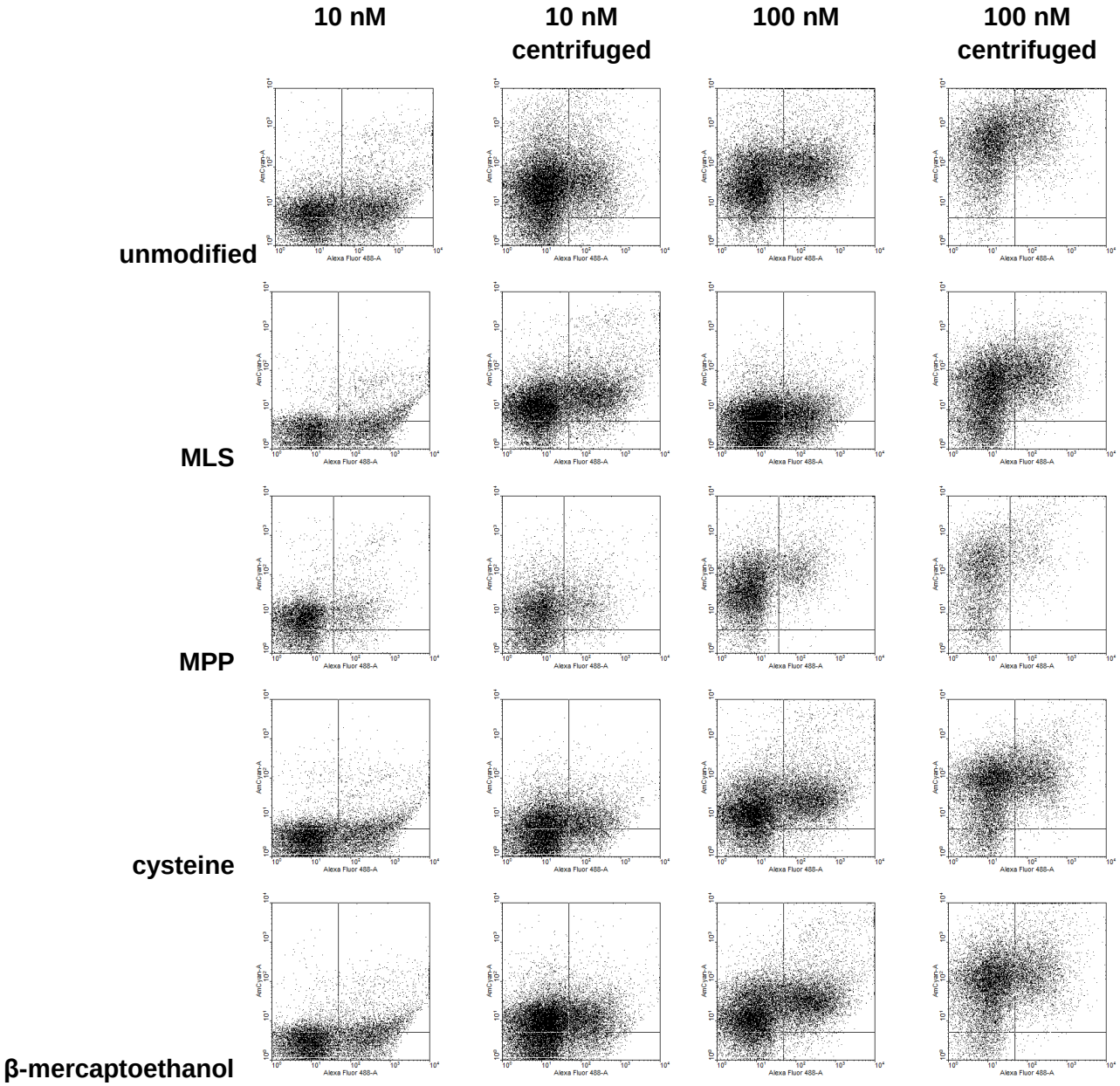

Figure 7.2: Flow cytometry plots showing the binding of unmodified, MLS-, MPP-, cysteine and β-mercaptoethanol-modified quantum dots to isolated mitochondria. The y-axis indicates red fluorescence intensity of the quantum dots whereas the x-axis indicates green fluorescence intensity of isolated mitochondria.

As quantum dots showed such a high non-specific binding affinity to isolated mitochondria and cell fragments, they were not considered useful for the investigation of the binding properties of mitochondrial targeting sequences. Therefore, the natural mitochondrial targeting sequence MLS was labeled with the red fluorescent dye TAMRA and the binding affinity to green fluorescent isolated mitochondria was investigated by flow cytometry in comparison to the binding properties of TAMRA without mitochondrial targeting sequence (Figure 7.3). The quadrants of the flow cytometry plots were defined as described previously.

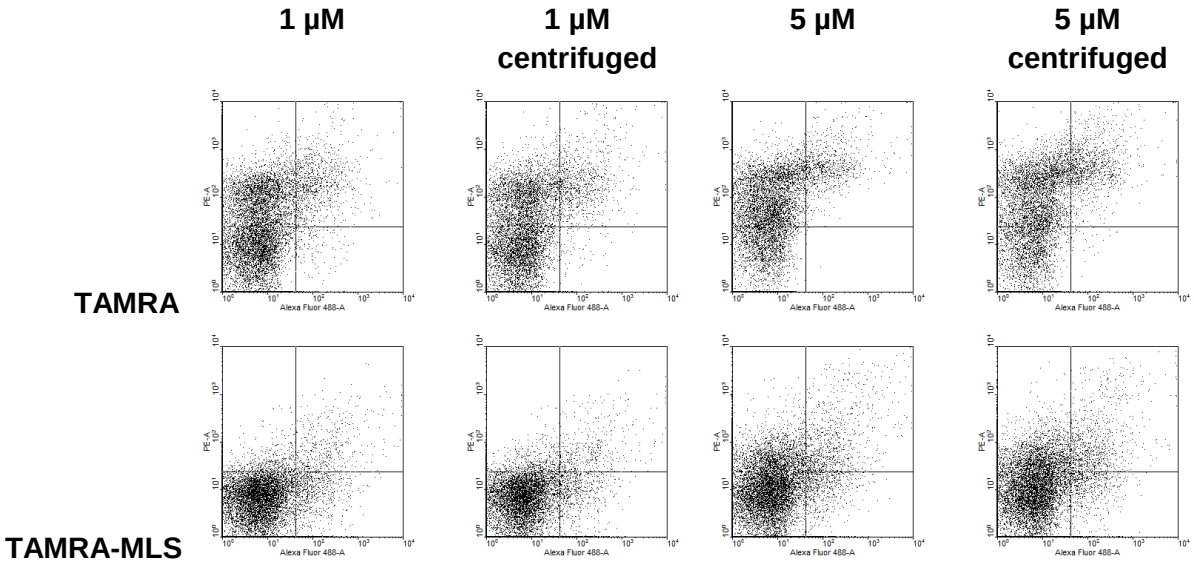

Figure 7.3: Flow cytometry plots showing the binding of TAMRA and MLS-modified TAMRA to isolated mitochondria.

Figure 7.3 shows that TAMRA as well as TAMRA-MLS stained cell fragments and isolated mitochondria. To evaluate where TAMRA accumulated in cells predominantly, intact cells containing mitochondrial targeted GFP were stained with unmodified TAMRA (Figure 7.4). The CLSM image showed that TAMRA accumulated in mitochondria due to the positive charge of the molecule that was attracted by the highly negative membrane potential of mitochondria [17]. Hence, TAMRA was not useful to study the binding properties of the MLS to mitochondria.

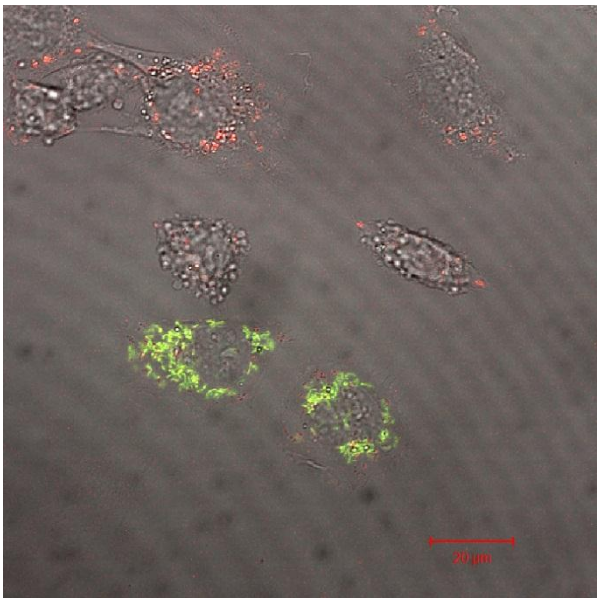

Figure 7.4: CLSM image of mitochondrial GFP containing cells stained with TAMRA 1 µM. The red fluorescence dye colocalized with GFP in mitochondria resulting in a yellow appearance. This panel shows a merge of both fluorescence images and the bright field image.

Based on these results, BODIPY® was chosen as an alternative dye as the molecule did not carry a charge. To evaluate where BODIPY® accumulated in cells, intact cells were stained with unmodified BODIPY®. Figure 7.5 showed that BODIPY® only stained the cytosol of cells and was not attracted to mitochondria.

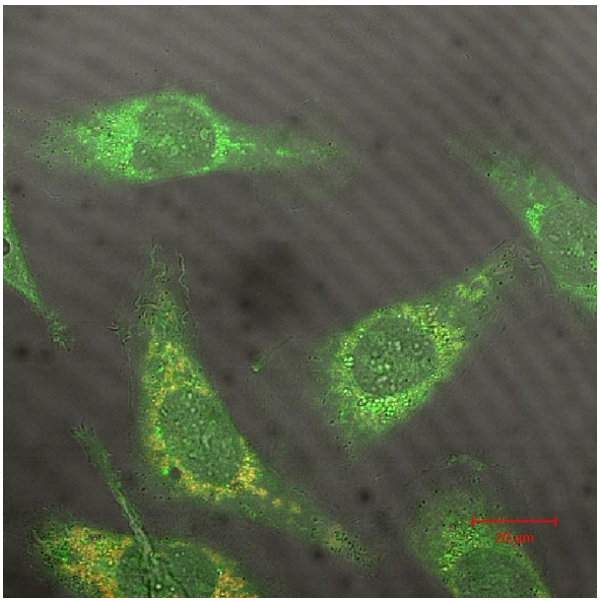

Figure 7.5: CLSM image of mitochondrial RFP containing cells stained with BODIPY® 100 nM. The green fluorescence dye localized in the cytosol and could be distinguished from the red fluorescence in mitochondria. This panel shows a merge of both fluorescence images and the bright field image.

To investigate how BODIPY® behaved when it was added to isolated mitochondria, the green fluorescent dye BODIPY® was mixed with a RFP-containing isolated mitochondria preparation and flow cytometry analysis was carried out. The four quadrants of the flow cytometry plots in Figure 7.6 showed non fluorescent cell fragments in the lower left quadrant, BODIPY® that stained non-specifically to non-fluorescent cell fragments in the upper left quadrant, RFP-containing mitochondria in the lower right quadrant and BODIPY® that stained to RFP-containing mitochondria in the upper right quadrant. Concentrations of 10 nM and 100 nM BODIPY® were investigated. Isolated mitochondria and BODIPY® were either only mixed or centrifuged.

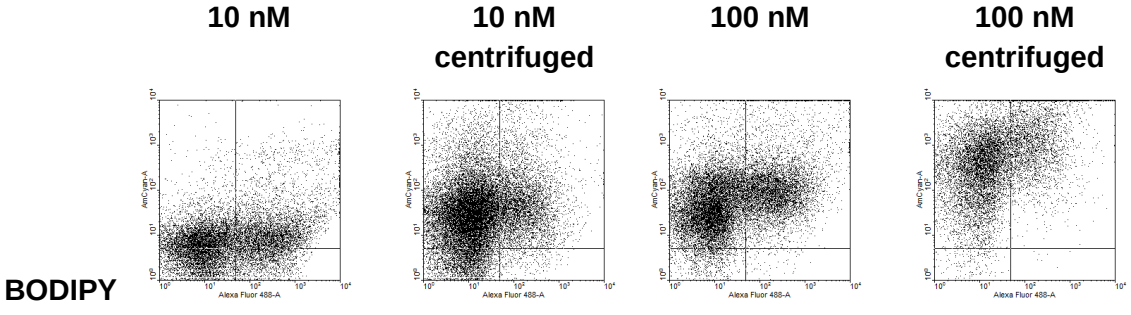

Figure 7.6: Flow cytometry plots showing the binding of BODIPY to isolated mitochondria.

Figure 7.6 showed that BODIPY® stained cell fragments as well as isolated mitochondria depending on concentration and additional centrifugation. Therefore, BODIPY® was also not suitable for the investigation of the binding properties of mitochondrial targeting peptides.

Finally, gold nanoparticles were capped with mitochondrial targeting peptides for investigation of the binding properties of mitochondrial targeting sequences by TEM. Gold nanoparticles that were synthesized by reducing tetrachloroaurate ions with citric acid and subsequent exchange by peptides showed aggregation. Aggregation occurred due to the physicochemical properties of the MLS and the MPP that were abundant of basic amino acids which could lead to aggregation of gold nanoparticles during exchange reactions [12]. Therefore, gold nanoparticles were synthesized by reduction of tetrachloroaurate ions with HEPES in the presence of the cysteine-containing MLS or MPP. Figure 7.7 showed preparations that contained different concentrations of the MLS. The solution without MLS appeared black which indicated that large gold aggregates were formed due to the absence of a stabilizer. Peptide containing solutions appeared violet which indicated that gold nanoparticles were present.

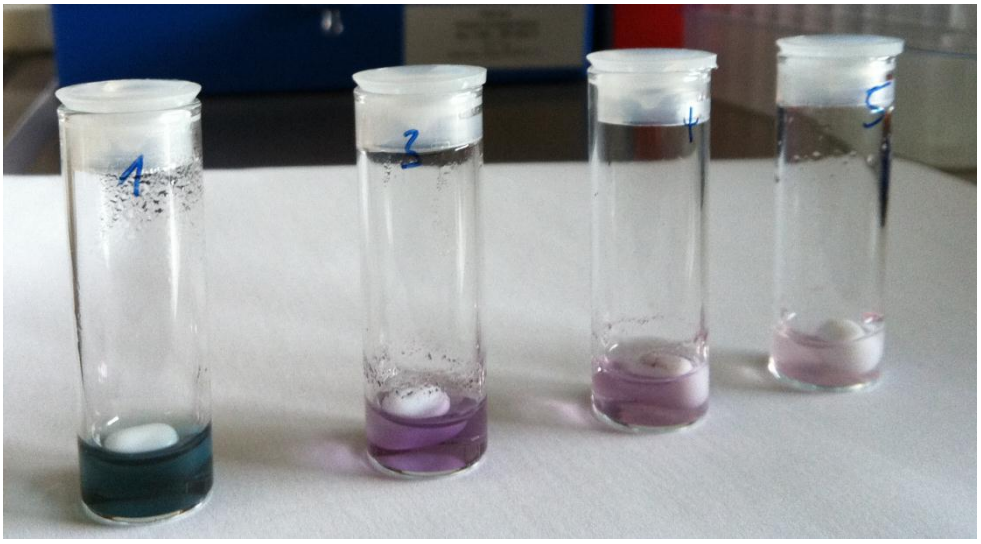

Figure 7.7: Gold nanoparticle solutions, 1 with 0 mM MLS, 3 with 0.45 mM MLS, 4 with 0.6 mM MLS and 5 with 0.75 mM MLS.

Figure 7.8 showed UV-spectra and PCS data of gold nanoparticles that were modified with 0.45 mM MLS. Only preparations that were modified with 0.45 mM or 0.6 mM MLS showed plasmon resonance in the UV-spectra and hence, formed gold nanoparticles. Concentrations of 0.075 mM, 0.15 mM, 0.225 mM and 0.3 mM were apparently too low whereas a concentration of 0.75 mM MLS was too high. These concentrations did not show the typical violet color and plasmon resonance in the UV-spectra. Figure 7.8 also showed that a longer incubation time did not lead to aggregation of the gold nanoparticles but rather led to a higher concentration of gold nanoparticles as reflected by a higher absorption compared to an incubation time of 18 h.

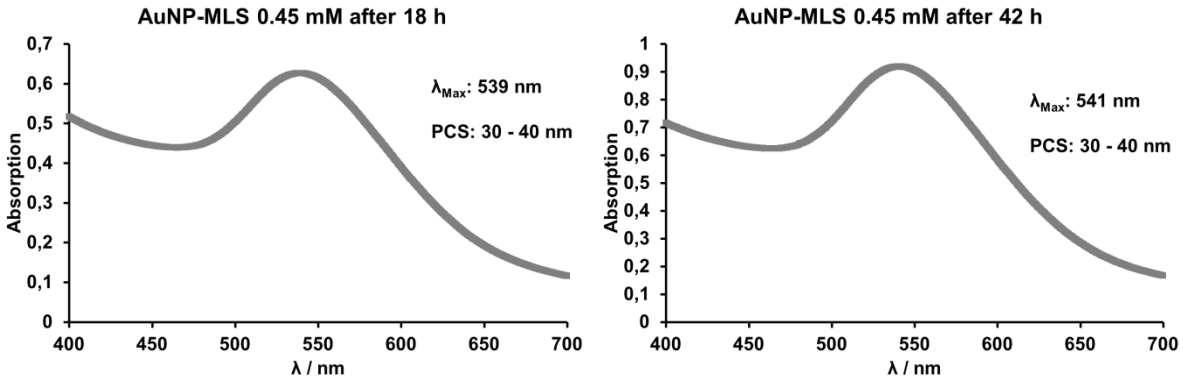

Figure 7.8: UV-spectra of MLS-conjugated gold nanoparticles (AuNP) with 0.45 mM MLS 18 h (left graph) and 42 h (right graph) after HEPES-reduction.

Figure 7.9 showed gold nanoparticles with 0.45 mM MLS after purification. The size of the gold nanoparticles increased to 40-50 nm but was stable over time.

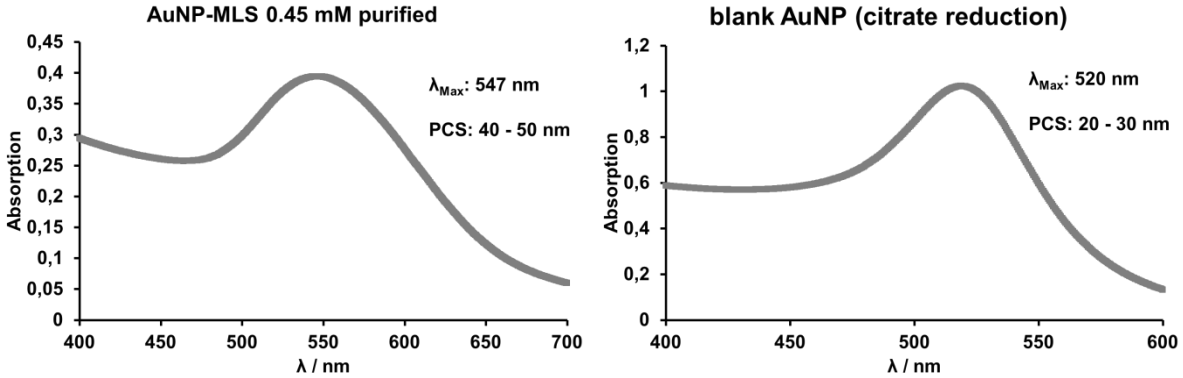

Figure 7.9: UV-spectra of purified MLS-conjugated gold nanoparticles (AuNP) with 0.45 mM MLS after HEPES-reduction (left graph) and citrate reduced blank gold nanoparticles (right graph).

The zetapotential of the MLS-modified gold nanoparticles was 47 mV compared to -40 mV of unmodified gold nanoparticles which indicated that the positively charged MLS capped the gold nanoparticles. Preparations with 0.6 mM MLS formed gold nanoparticles but showed aggregation over time. Hence, 0.45 mM MLS capped gold nanoparticles were used for TEM studies.

Preparations with 0.3 mM and 0.6 mM MPP formed larger gold nanoparticles that showed a plasmon resonance at higher wave lengths compared to MLS-modified gold nanoparticles. MPP-modified gold nanoparticles could not be purified and showed aggregation over time.

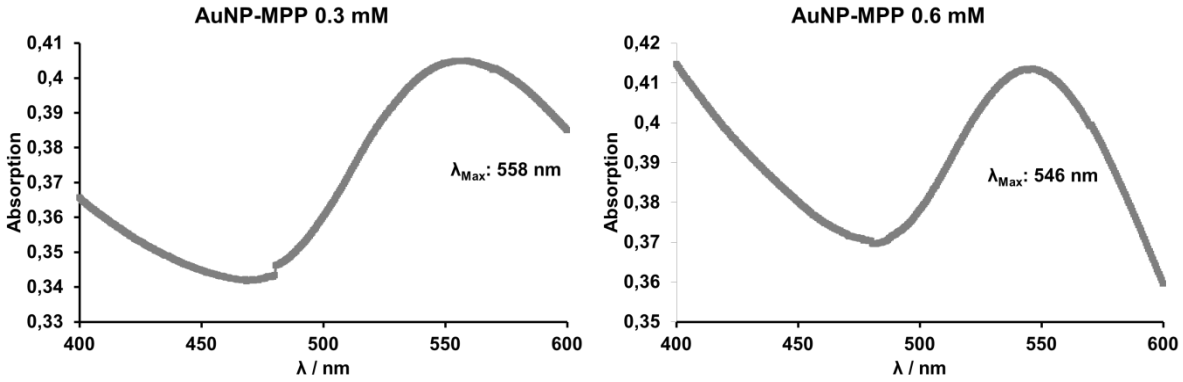

Figure 7.10: UV-spectra of MPP-conjugated gold nanoparticles (AuNP) with 0.3 mM MPP (left graph) and 0.6 mM MPP (right graph) after HEPES-reduction.

Therefore, only MLS-modified gold nanoparticles were investigated by TEM in comparison to unmodified gold nanoparticles that were synthesized by citric acid reduction (Figure 7.9). The concentration of gold nanoparticles that was used for the TEM studies was 3.34 pM, determined according to Haiss et al. [16].

Figure 7.11 showed gold nanoparticles modified with 0.45 mM MLS in mitochondria suspensions but they were not detected in proximity to isolated mitochondria.

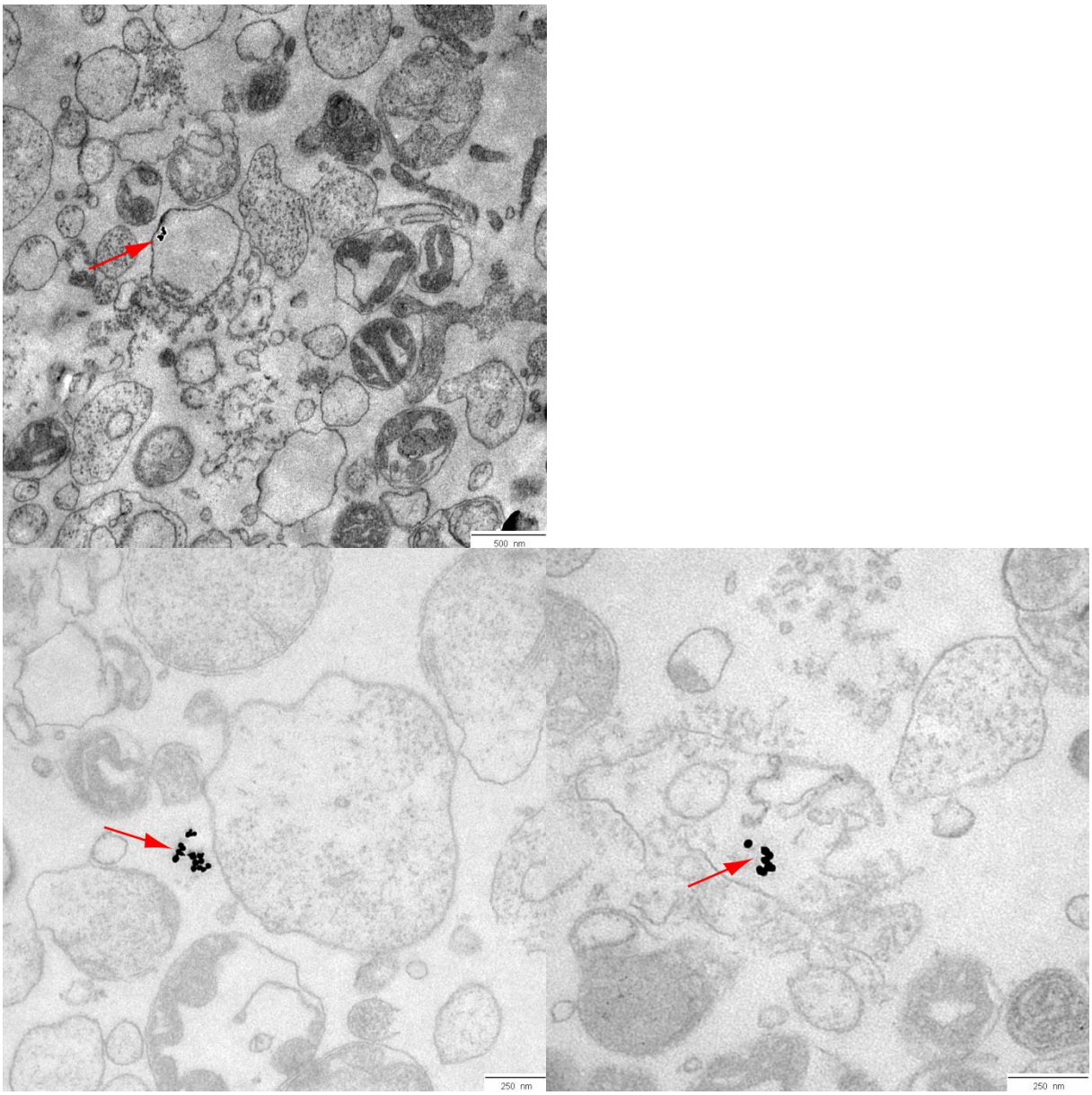

Figure 7.11: TEM images of the binding of MLS-modified gold nanoparticels to isolated mitochondria, 12000x magnification on the upper left image, 20000x magnification on the lower left image and 30000x magnification on the lower right image. MLS-modified gold nanoparticles are indicated by red arrows.

Figure 7.12 showed unmodified gold nanoparticles that were also not detected in proximity to isolated mitochondria.

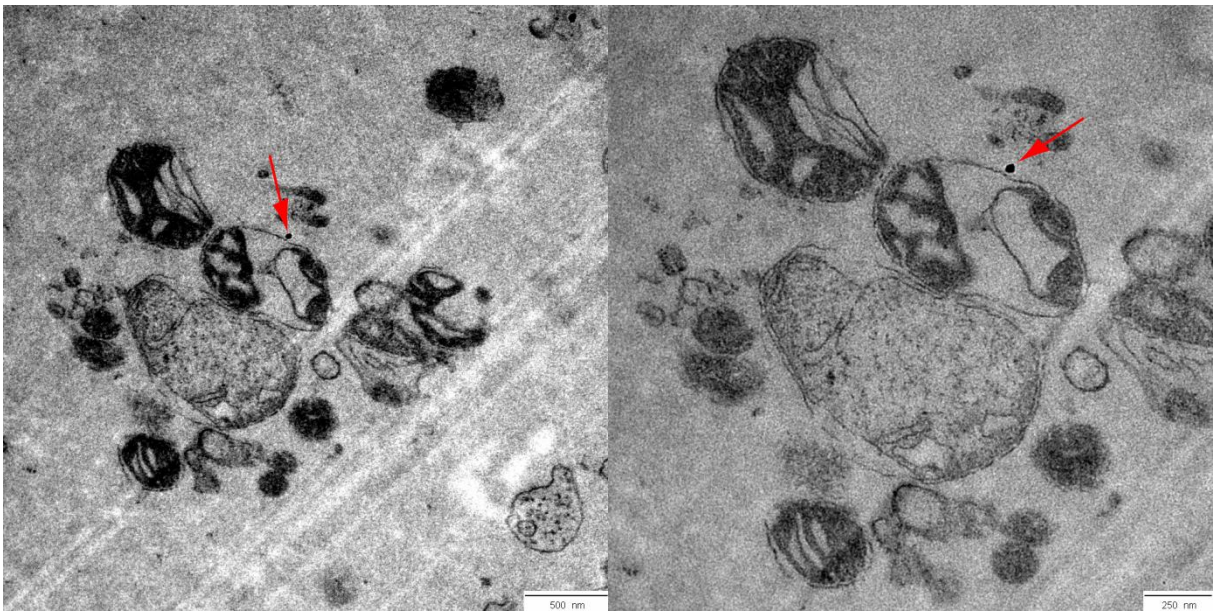

Figure 7.12: TEM images of the binding of unmodified gold nanoparticels to isolated mitochondria, 12000x magnification on the left image and 20000x magnification on the right image. Gold nanoparticles are indicated by red arrows.

As it was not possible to produce MPP-modified gold nanoparticles, the binding properties of a MPP modified 40 kDa 8arm PEG were investigated by additional labeling with BODIPY® that oxidized diaminobenzidine to an insoluble polymer in a photooxidation procedure. The insoluble polymer could be stained by osmium tetroxide and appeared in black in TEM analysis. Figure 7.13 showed a TEM images of an isolated mitochondria preparation that was mixed with the MPP- and BODIPY®-modified 8arm PEG. The black photooxidation product was not visible compared to images that did not contain black photooxidation products. Maybe the photooxidation products were distributed all over the samples and did not accumulate at specific sites.

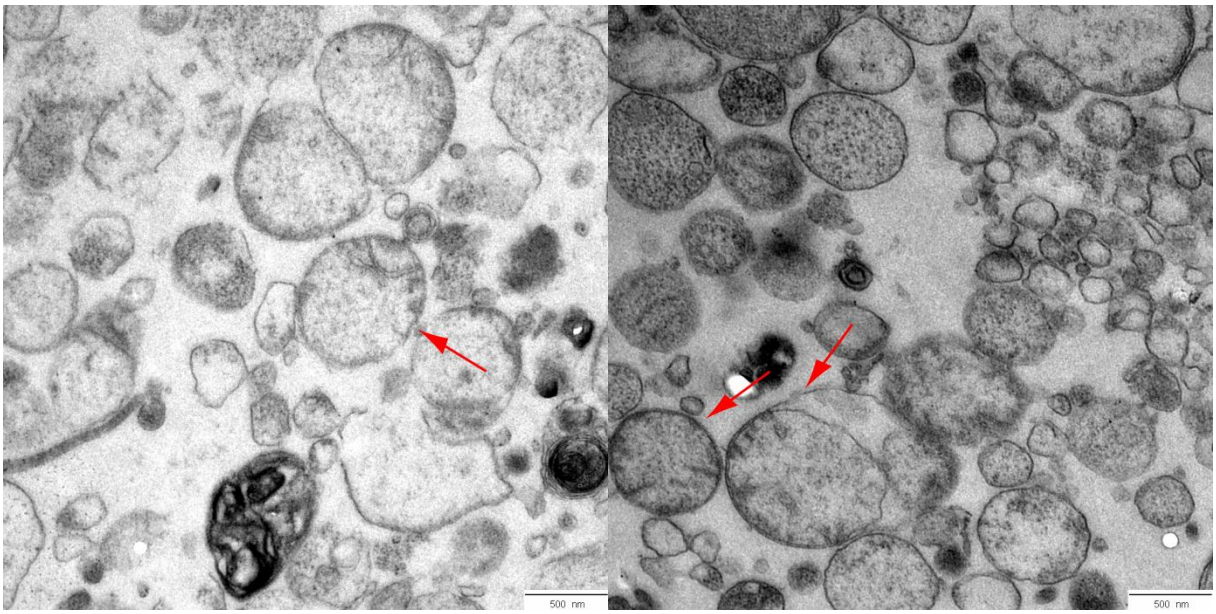

Figure 7.13: TEM images of the binding of MPP-conjugated 40 kDa 8arm PEG labeled with BODIPY® (left image) and β-mercaptoethanol-conjugated 40 kDa 8arm PEG labeled with BODIPY® (right image) to isolated mitochondria after photooxidation with DAB, 12000x magnification. Intact isolated mitochondria are indicated by red arrows.

7.4 Conclusions

It was not possible to evaluate the binding properties of the mitochondrial targeting peptides MLS and MPP by the applied methods. Quantum dots, modified and not modified, bound to cell fragments and isolated mitochondria, and it was not possible to distinguish between non-specific and specific binding mediated by mitochondrial targeting peptides. Fluorescent dyes were also not suitable: TAMRA accumulated in mitochondria even without modification due to the positive charge of the molecule and BODIPY® stained isolated mitochondria and cell fragments non-specifically without modification. MLS-modified gold nanoparticles were successfully synthesized by a HEPES reduction method but binding to isolated mitochondria could not be detected in a TEM study. The binding of a MPP- and BODIPY®-modified 8arm PEG could also not be detected by TEM after photooxidation.

7.5 References

[1] N. Pfanner, Protein sorting: recognizing mitochondrial presequences, Curr. Biol 10 (2000) R412-5.

[2] A. Chacinska, C.M. Koehler, D. Milenkovic, T. Lithgow, N. Pfanner, Importing Mitochondrial Proteins: Machineries and Mechanisms, Cell 138 (2009) 628–644.

[3] H. Yamamoto, N. Itoh, S. Kawano, Y.-i. Yatsukawa, T. Momose, T. Makio, M. Matsunaga, M. Yokota, M. Esaki, T. Shodai, D. Kohda, A.E. Aiken Hobbs, R.E. Jensen, T. Endo, Dual role of the receptor Tom20 in specificity and efficiency of protein import into mitochondria, Proceedings of the National Academy of Sciences 108 (2011) 91–96.

[4] J.M. Herrmann, W. Neupert, What fuels polypeptide translocation? An energetical view on mitochondrial protein sorting, Biochimica et Biophysica Acta (BBA) - Bioenergetics 1459 (2000) 331–338.

[5] Y. Abe, T. Shodai, T. Muto, K. Mihara, H. Torii, S.-i. Nishikawa, T. Endo, D. Kohda, Structural Basis of Presequence Recognition by the Mitochondrial Protein Import Receptor Tom20, Cell 100 (2000) 551–560.

[6] J. Brix, K. Dietmeier, N. Pfanner, Differential Recognition of Preproteins by the Purified Cytosolic Domains of the Mitochondrial Import Receptors Tom20, Tom22, and Tom70, Journal of Biological Chemistry 272 (1997) 20730–20735.

[7] P. Rehling, N. Wiedemann, N. Pfanner, K.N. Truscott, The mitochondrial import machinery for preproteins, Crit. Rev. Biochem. Mol. Biol 36 (2001) 291–336.

[8] K.L. Horton, K.M. Stewart, S.B. Fonseca, Q. Guo, S.O. Kelley, Mitochondria-Penetrating Peptides, Chemistry & Biology 15 (2008) 375–382.

[9] L.F. Yousif, K.M. Stewart, K.L. Horton, S.O. Kelley, Mitochondria-Penetrating Peptides: Sequence Effects and Model Cargo Transport, ChemBioChem 10 (2009) 2081–2088.

[10] S.A. Detmer, D.C. Chan, Functions and dysfunctions of mitochondrial dynamics, Nat Rev Mol Cell Biol 8 (2007) 870–879.

[11] C.A. Wurm, D. Neumann, M.A. Lauterbach, B. Harke, A. Egner, S.W. Hell, S. Jakobs, Nanoscale distribution of mitochondrial import receptor Tom20 is adjusted to cellular

conditions and exhibits an inner-cellular gradient, Proceedings of the National Academy of Sciences 108 (2011) 13546–13551.

[12] T. Serizawa, Y. Hirai, M. Aizawa, Novel Synthetic Route to Peptide-Capped Gold Nanoparticles, Langmuir 25 (2009) 12229–12234.

[13] J.M. Slocik, M.O. Stone, R.R. Naik, Synthesis of Gold Nanoparticles Using Multifunctional Peptides, Small 1 (2005) 1048–1052.

[14] A. Heller, Chapter 6: Affecting mitochondrial fusion efficiency in vitro, in: A. Heller (Ed.), Targeting mitochondria by mitochondrial fusion, mitochondria-specific peptides and nanotechnology: Dissertation.

[15] M.M. Bradford, A rapid and sensitive method for the quantitation of microgram quantities of protein utilizing the principle of protein-dye binding, Analytical Biochemistry 72 (1976) 248–254.

[16] W. Haiss, N.T.K. Thanh, J. Aveyard, D.G. Fernig, Determination of Size and Concentration of Gold Nanoparticles from UV−Vis Spectra, Anal. Chem. 79 (2007) 4215–4221.

[17] R.A.J. Smith, M.P. Murphy, Mitochondria-targeted antioxidants as therapies, Discov Med 11 (2011) 106–114.

Chapter 8

Summary and conclusions

This thesis was focused on mitochondria as an intracellular target for drug delivery by the reason that mitochondria are becoming of increasing interest in pharmaceutical and medical research due to their contribution to several diseases (Chapter 1).

A protocol for the quick isolation of mitochondria from cultured cells and several methods for the characterization of isolated mitochondria were established. Integrity and functionality of the mitochondrial preparations were demonstrated by a membrane integrity assay, the Cytochrome C Oxidase assay, by staining with a potential sensitive dye, JC-1, and by the analysis of mitochondrial ultrastructure by transmission electron microscopy (Chapter 2).

Additionally, a method for the monitoring of long time functionality of isolated mitochondria in terms of their oxygen consumption was established. Typical features of this method included the need of only a few microliters of isolated mitochondria and the possibility of using microplate sensor technology that allowed for the high throughput screening of large sample numbers (Chapter 3).

Furthermore, several methods to label isolated mitochondria were investigated. Labeling with fluorescent dyes was a quick and comfortable method but it was not applicable in further studies as the dyes washed out. Therefore, intact cells were transfected with mitochondria targeted green or red fluorescent proteins to label mitochondria permanently and to make them accessible for fluorescence based analytical methods (Chapter 4).

To approach the main idea of this thesis, the targeting of mitochondria with nanomaterials by utilization of the mitochondrial fusion process, protocols to accomplish and detect fusion of isolated mitochondria in vitro were established. Mitochondrial fusion in vitro was detected qualitatively by confocal laser scanning microscopy that revealed completely fused mitochondria with mixed matrices due to the merged colors of the fluorescent proteins and by transmission electron microscopy that revealed fusion intermediates of mitochondria with distinct inner membranes and fused outer membranes. Additionally, a protocol for the quantitative evaluation and calculation of mitochondrial fusion efficiency based on flow cytometry was established. Flow cytometry disclosed several advantages such as the capability for high throughput analysis, the possibility to analyze highly diluted samples that

did not consume large amounts of isolated mitochondria and an even higher number of mitochondria that could be investigated compared to microscopy techniques that would accompany with time consuming counting of a comparatively low number of mitochondria (Chapter 5).

One goal of this thesis was to combine targeting strategies by using specific mitochondrial targeting peptides and nanomaterials, and to utilize mitochondrial fusion to accomplish an uptake of these nanomaterials into mitochondria or to influence on mitochondrial fusion in vitro by these mitochondria targeted nanomaterials. To influence on mitochondrial fusion in vitro with nanomaterials and mitochondria-specific targeting peptides, several polymers such as 8arm PEGs and a polyetheramine, and nanocarriers such as dendrimers and quantum dots were conjugated to mitochondrial targeting peptides that were known to be recognized by mitochondria, in particular by recognition of the mitochondrial protein import pores. Mitochondrial fusion efficiency in vitro was determined by the previously described protocols based on confocal laser scanning microscopy, transmission electron microscopy and flow cytometry. Thereby, a natural mitochondrial targeting sequence (MLS) and a synthetic mitochondria penetrating peptide (MPP) were investigated. Additionally, mitochondrial fusion was affected unspecifically by highly concentrated polymer solutions. It was shown that mitochondrial fusion could be enhanced by unspecific and specific approaches. PEG 1500 at a concentration of 50 % was the most effective additive for unspecific enhancement of mitochondrial fusion in vitro by dehydration. PEGs with higher molecular weights were not more effective. The MPP modified 8arm PEGs, dendrimers and the polyetheramine Jeffamine® were effective additives for specific enhancement of mitochondrial fusion in vitro. MPP modified 8arm PEGs at a concentration of 1 mM were the most effective enhancer of mitochondrial fusion in vitro. It emerged that carriers with the natural MLS did not enhance mitochondrial fusion efficiency (Chapter 6).

Due to the results of affecting mitochondrial fusion efficiency in vitro, the binding behavior of the mitochondrial targeting peptides MLS and MPP to isolated mitochondria was investigated. Therefore, quantum dots and fluorescent dyes were coupled to the targeting

peptides and the binding to isolated mitochondria was determined by flow cytometry. It was not possible to evaluate the binding properties of the mitochondrial targeting peptides MLS and MPP as quantum dots, modified and not modified, bound to cell fragments and isolated mitochondria. Thereby, it was not possible to distinguish between non-specific and specific binding mediated by mitochondrial targeting peptides. The fluorescent dyes TAMRA and BODIPY®, coupled to the MLS, were also not suitable as TAMRA accumulated in mitochondria even without modification due to the positive charge of the molecule and BODIPY® stained isolated mitochondria and cell fragments non-specifically without modification. Therefore, MLS capped gold nanoparticles were synthesized for a transmission electron microscopy study. MLS-modified gold nanoparticles were successfully synthesized by a HEPES reduction method instead of the conventional method of citric acid exchange. The binding of these MLS-capped gold nanoparticles to isolated mitochondria could not be detected in a TEM study. The binding behavior of the MPP was determined by a photoconversion method in transmission electron microscopy using an 8armPEG modified with MPP and the fluorescent dye BODIPY®. The binding of the MPP- and BODIPY®-modified 8arm PEG to isolated mitochondria could also not be detected (Chapter 7).

Even due to the fact that mitochondria are of increasing interest in pharmaceutical and medical research as mitochondrial dysfunction contributes to several severe diseases and even though they exhibit a lot of potential targets, mitochondrial drug delivery and drug targeting is challenging and still at an early stage. Several barriers have to be crossed to achieve a selective targeting and accumulation in mitochondria and there is a need for suitable analytical methods to ensure that applied mitochondrial targeting strategies were successful. Then, it would eventually be possible to verify one goal of this thesis, the uptake of mitochondria targeted nanomaterials into mitochondria by mitochondrial fusion.

Appendix

Abbreviations

^{1}H-NMR ..... proton nuclear magnetic resonance

8arm PEG ..... 8arm poly(ethylene glycol)

ADP ..... adenosine diphoshate

AEQ ..... aequorin

ANOVA ..... analysis of variance

ATP ..... adenosine triphosphate

AuNP ..... gold nanoparticle

b-ME ..... β-mercaptoethanol

bp ..... base pair

BSA ..... bovine serum albumin

CcO ..... cytochrome c oxidase

CHO-K1 ..... chinese hamster ovarian cell line K1

CLSM ..... confocal laser scanning microscopy

CoxIV ..... cytochrome c oxidase subunit IV

CsA ..... cyclosporin A

CT ..... computed tomography

Cys ..... cysteine

DMSO ..... dimethyl sulfoxide

DNA ..... deoxyribonucleic acid

DOPE 1,2-dioleoyl-sn-glycero-3-phosphoethanolamine

DOTAP dioleoyl-1,2-diacyl-3-trimethylammoniumpropane

DQA ..... dequalinium

Drp1 ..... dynamin-related protein 1

dsRed ..... discosoma red fluorescent protein

E.coli ..... Escherichia coli

EDTA ..... ethylenediaminetetraacetic acid

EEG ..... electroencephalography

EMG ..... electromyography

EPR ..... enhanced permeability and retention effect

FCCP ..... carbonyl cyanide 4-(trifluoromethoxy)phenylhydrazone

FCS ..... fetal calf serum

Fe-S ..... iron-sulfide

FRAP ..... fluorescence recovery after photobleaching

FRET ..... Förster (fluorescence) resonance energy transfer

FS ..... freeze substitution

GFP ..... green fluorescent protein

GPCR ..... G-protein coupled receptor

GSH ..... glutathione

GSSG ..... glutathione disulfide

GTP ..... guanosine triphosphate

HEPES ..... 2-[4-(2-hydroxyethyl)-1-piperazinyl]ethanesulfonic acid

HPF ..... high pressure freezing

HR1, 2 ..... heptad repeat region 1, 2

JC-1 ..... 5,5′,6,6′-tetrachloro-1,1′,3,3′tetraethylbenzimidazolylcarbocyanine iodide

LL ..... lower left quadrant

LR ..... lower right quadrant

MCS ..... multiple cloning site

MEND ..... multifunctional envelope-type nano-device

Mfn 1, 2 ..... mitofusin 1, 2

mitoK_{ATP} ..... mitochondrial potassium channel

MLS ..... mitochondrial localization sequence

MPP ..... mitochondrial penetrating peptide

mPTPC ..... mitochondria permeability transition pore complex

MRI ..... magnetic resonance imaging

mRNA ..... messenger RNA

mtDNA ..... mitochondrial DNA

mtGFP..... mitochondrial green fluorescent protein

mtRFP..... mitochondrial red fluorescent protein

NAD^+ ..... nicotinamide adenine dinucleotide

NCV ..... nerve conduction velocity

nDNA ..... nuclear DNA

NO..... nitroxide

NPY..... neuropeptide Y

NSAID ..... non-steroidal anti-inflammatory drug

OPA1 ..... optic atrophy type 1

OXPHOS..... oxidative phosphorylation

PAMAM G4-G7 ..... poly(amidoamine) dendrimers generation 4-7

PEI ..... poly(ethyleneimine)

PBR..... peripheral benzodiazepine receptor

PBS..... phosphate buffered saline

PCR ..... polymerase chain reaction

PCS..... photon correlation spectroscopy

pDNA ..... plasmid DNA

PEG ..... poly(ethylene glycol)

pO_2..... oxygen partial pressure

Qdots ..... quantum dots

RES..... reticuloendothelial system

RFP..... red fluorescent protein

RNA ..... ribonucleic acid

ROS ..... reactive oxygen species

rRNA ..... ribosomal RNA

tRNA ..... transfer RNA

SD..... standard deviation

Sir ..... silent information regulator protein, sirtuin

siRNA ..... small interfering RNA

SOD ..... superoxidedismutase

SS-peptide ..... Szeto-Schiller-peptide

STPP ..... stearyl triphenyl phosponium

sulfo-SMCC ..... 4-(N-Maleimidomethyl)cyclohexane-1-carboxylic acid 3-sulfo-N-hydroxysuccinimide ester sodium salt

TAMRA ..... tetramethylrhodamine

TCEP ..... Tris(2-carboxyethyl)phosphine hydrochloride

TEM ..... transmission electron microscopy

TIM ..... translocase of the inner mitochondrial membrane

TOM ..... translocase of the outer mitochondrial membrane

TMAEC-Chol ..... trimethyl aminoethane carbamoyl cholesterol iodide

TPP ..... triphenylphosphonium

Tris ..... 2-Amino-2-(hydroxymethyl)-1,3-propanediol

tRNA ..... transfer RNA

UL ..... upper left quadrant

UR ..... upper right quadrant

UV ..... ultraviolett

VDAC ..... voltage dependent anion channel

X-ray ..... Röntgen radiation

Sequences and properties of MLS and MPP

MLS

NH_2-M-L-S-L-R-Q-S-I-R-F-F-K-P-A-T-R-T-C-COOH

M (Met, methionine)	→ hydrophobic
L (Leu, leucine)	→ hydrophobic
S (Ser, serine)	→ hydrophilic
L (Leu, leucine)	→ hydrophobic
R (Arg, arginine)	→ basic
Q (Gln, glutamine)	→ hydrophilic
S (Ser, serine)	→ hydrophilic
I (Ile, isoleucine)	→ hydrophobic
R (Arg, arginine)	→ basic
F (Phe, phenylalanine)	→ hydrophobic
F (Phe, phenylalanine)	→ hydrophobic
K (Lys, lysine)	→ basic
P (Pro, proline)	→ hydrophobic
A (Ala, alanine)	→ hydrophobic
T (Thr, threonine)	→ hydrophilic
R (Arg, arginine)	→ basic
T (Thr, threonine)	→ hydrophilic
C (Cys, cysteine)	→ nucleophilic

MPP

NH_2-L-Cha-dR-Cha-F-C-COOH

L (Lys, lysine) → hydrophobic

Cha (cyclohexylalanine) → hydrophobic

dR (D-Arg, arginine) → basic

Cha (cyclohexylalanine) → hydrophobic

F (Phe, phenylalanine) → hydrophobic

C (Cys, cysteine) → nucleophilic

Curriculum vitae

Personal information

Name	Anne Sabine Heller
Date of birth	April 16th, 1984
Place of birth	Erlabrunn/Erzgebirge
Nationality	German

Professional experience and internships

Since 05/2012	Manager Medical & Regulatory Affairs, Hexal AG, Holzkirchen
01/2008 – 03/2012	PhD student at the Department of Pharmaceutical Technology, University of Regensburg
11/2007 – 12/2007	Pharmacist, Neustädter Apotheke, Schwarzenberg
05/2007 – 10/2007	Pharmaceutical internship, Neustädter Apotheke, Schwarzenberg
11/2006 – 04/2007	Pharmaceutical internship, Merck KGaA, Darmstadt
08/2003, 02/2003	Pharmaceutical training, Neustädter Apotheke, Schwarzenberg

Education

11/2007	Acquisition of the license to practice as a Pharmacist
10/2002 – 10/2006	Study of Pharmacy at the Friedrich-Schiller-University, Jena
06/2002	Abitur
08/1994 – 06/2002	St.-Annen-Gymnasium Annaberg-Buchholz, Außenstelle Schlettau
09/1990 – 06/1994	Grundschule Markersbach

List of publications

Publications

A. Heller, G. Brockhoff, A. Göpferich, Targeting drugs to mitochondria, European Journal of Pharmaceutics and Biopharmaceutics 82 (2012) 1-18

A. Heller, L. H. Fischer, O. S. Wolfbeis, A. Göpferich, Long time monitoring of the respiratory activity of isolated mitochondria, Experimental Cell Research 318 (2012) 1667–1672

Conference Abstracts

A. Heller, A. Göpferich, Determination of mitochondrial fusion in vitro using flow cytometry, 7th World Meeting on Pharmaceutics, Biopharmaceutics and Pharmaceutical Technology, Valletta (Malta), 2010.

A. Heller, G. Brockhoff, A. Göpferich, Influence of biomaterials on mitochondrial fusion in vitro, DPhG Jahrestagung, Braunschweig, 2010.

A. Heller, L. H. Fischer, O. S. Wolfbeis, A. Göpferich, Long time monitoring of oxygen consumption in cell fractions with special respect to mitochondria, 1st World Congress on Targeting Mitochondria: Strategies, Innovations & Clinical Applications, Berlin, 2010.

Acknowledgments

An dieser Stelle möchte ich mich bei allen bedanken, die mich in den letzten Jahren begleitet, unterstützt und zum Gelingen dieser Arbeit beigetragen haben.

Mein besonderer Dank gilt:

Herrn Professor Göpferich vom Lehrstuhl für Pharmazeutische Technologie, der es mir ermöglichte, diese Arbeit an seinem Lehrstuhl anzufertigen und mich durch zahlreiche Gespräche bei der Bearbeitung des Themas unterstützt hat.

Herrn Professor Gero Brockhoff vom Labor für Durchflusszytometrie, Institut für Pathologie und Klinik für Frauenheilkunde und Geburtshilfe, Forschungs-AG Zytometrische und zelluläre Onkologie für die Ermöglichung der Durchflusszytometrie-Versuche und seine Hilfestellungen bei allen Fragen der Durchflusszytometrie. Weiterhin danke ich seinen Mitarbeitern Dr. Simone Diermeier-Daucher, Marietta Bock, Elisabeth Schmidt-Brücken und Gerhard Piendl für die immer freundliche Unterstützung.

Herrn Professor Wolfbeis vom Institut für Analytische Chemie, Chemo- und Biosensorik für die Zusammenarbeit bei den Sauerstoff-Messungen, Dr. Lorenz Fischer und Dr. Matthias Stich für die Unterstützung bei der praktischen Durchführung sowie Dr. Sarina Arain von PreSens für die Bereitstellung der OxoPlates®. Weiterhin danke ich Dr. Hans-Heiner Gorris für das Zurverfügungstellen eines Fluoreszenzfarbstoffes für die Photooxidation.

Herrn Professor Witzgall vom Lehrstuhl für Molekulare und Zelluläre Anatomie für die Unterstützung und Diskussionen bei den TEM-Versuchen sowie seinen technischen Assistentinnen Christine Meese und Helga Schmidt für die praktische Durchführung der Versuche.

Weiterhin danke ich:

- Herrn Professor Buschauer vom Lehrstuhl für Pharmazeutische und Medizinische Chemie II für das Zurverfügungstellen des FACSes, Herrn Professor Bernhardt für das Überlassen der Aequorin-Zelllinie und Dr. Nathalie Pop für die Unterstützung bei den Aequorin-Versuchen.
- Herrn Professor Schlossmann vom Lehrstuhl für Pharmakologie und Toxikologie für die hilfreichen Ratschläge zur Klonierung von DNA in Plasmide.
- Herrn Professor Dick vom Lehrstuhl für Physikalische Chemie, Dr. Kensy und Roger-Jan Kutta für die Einblicke in Fluoreszenz-Abklingkinetik-Messungen.
- Dr. Jörg Teßmar für die vielen kritischen Diskussionen, hilfreichen Ratschläge, praktische Unterstützung und die immer sehr gute Zusammenarbeit im „kleinen Praktikum“.
- Dr. Miriam Breunig und Professor Torsten Blunk für die wissenschaftlichen Diskussionen und praktischen Ratschläge.
- Dr. Andreas Sellmer für die Unterstützung bei den Refraktometrie-Messungen.
- Eva-Christina Wurster für das Zurverfügungstellen der citratreduzierten Goldnanopartikel.
- Elisabeth Doblinger für die Zusammenarbeit bei der Aufreinigung der Mitochondrienfraktion.
- Sonja Bauhuber für die Unterstützung bei allen NMR-Fragen.
- Klaus Pollinger für die Unterstützung bei der Arbeit mit den Quantenpunkten und die vielen wissenschaftlichen Diskussionen.
- Sadaf Taheri für das Korrekturlesen der Publikationen.
- Dr. Matthias Ferstl für die immer sehr gute Zusammenarbeit im Praktikum.
- Dr. Matthias Henke für viele praktische Ratschläge.
- Eva Esser für die Unterstützung bei den GFC-Versuchen.
- Meinen Laborkollegen Dr. Axel Ehmer, Dr. Christian Muhr, Andrea Lubich, Maria Baumann und Michael Backofen für die schöne gemeinsame Zeit im Labor.

- Den technischen Assistenten Renate Liebl, Andrea Blaimer, Angelika Berié, Stefan Kolb, Edith Schindler und den Sekretärinnen Eva Wrobel, Dominika Bilas, Liane Öttl und Lydia Frommer für sämtliche praktische, technische und organisatorische Unterstützung.
- Meinen Auszubildenden Sabine Hofmeister, Viktoria Meßmann und Alexandra Frimberger, meinen Praktikanten Philipp Merkl, Clement David, Julia Pickl und Uli Ohmayer sowie meinen Wahlpflichtfachstudenten Melina Erfany-Far und Lukas Stail für die fleißige Mitarbeit im Labor.
- Marta Torrente, Elena Groppa und Pelin Bulgurcu für ihre Freundschaft.
- Allen derzeitigen und ehemaligen Mitarbeitern des Lehrstuhls für das nette Arbeitsklima und die außeruniversitären Aktivitäten.
- Ganz besonders Christoph Luschmann für seine Unterstützung bei allen Uni-Angelegenheiten, die Hilfe bei der Erstellung der Grafiken für den Review, die tolle Zusammenarbeit im Praktikum und seine Freundschaft.

Mein ganz besonderer Dank gilt meinen Eltern und meinem Bruder Steffen, die es mir ermöglichen, meinen Weg zu gehen und mich dabei immer bestärken und unterstützen.

Erklärung

Hiermit erkläre ich, dass ich die vorliegende Arbeit selbst verfasst habe und keine anderen als die angegebenen Hilfsmittel verwendet habe.

Regensburg, den 21. Januar 2013

Anne Heller